# Application of the dorsal window chamber model to tumour vasculature manipulation studies.

A thesis submitted to The University of Manchester for the degree of Doctor of Philosophy in the Faculty of Medical and Human Sciences

2012

**BRIAN A. TELFER**

School of Pharmacy and Pharmaceutical Sciences

# Contents

**Word count: 47,596**

**ABBREVIATIONS**

| | |
|---|---|
| AA(s) | Antiangiogenic agent(s) |
| ANG | Angiopoietin |
| ASMase | Acid sphingomyelinase |
| ATP | Adenosine tri-phosphate |
| bd | Twice daily dose |
| BM | Bone marrow |
| BMCs | Bone marrow cells |
| BSA | Bovine serum albumin |
| CT | Chemotherapeutic |
| DWC | Dorsal window chamber |
| DSFC | Dorsal skin fold chamber |
| ECs | Endothelial cells |
| ECM | Extracellular matrix |
| ERK | Extracellular-signal-regulated kinase |
| FAK | Focal adhesion kinase |
| Fb | Background fluorescence |
| FITC | Fluorescein isothyocyanate |
| Fp | Initial plateau fluorescence |
| Fx | Time-lapse fluorescence data value |
| GD | Growth delay |
| Gy | Grays |
| $H_2O$ | Water molecule |
| HIF-1 | Hypoxia inducible factor -1 |
| HR | Homologous Recombination |
| HRE | Hypoxia responsive element |
| Hg | Mercury |
| i/d | Intradermal |
| IFP | Interstitial fluid pressure |
| IHC | Immunohistochemistry |
| iNOS | Inducible nitric oxide synthase |
| i/p | Intraperitoneal |

| | |
|---|---|
| i/v | Intravenous |
| IVM | Intravital microscopy |
| MEK | Mitogen-activated protein kinase (MEK in animals) |
| Min | Minute |
| MVD | Microvascular density |
| NA | Nicotinamide |
| NHEJ | Non-Homologous End Joining |
| NOS | Nitric oxide synthase |
| $O_2$ | Oxygen |
| PARP | Poly (ADP-ribose) polymerase |
| PBS (T) | Phosphate buffered saline (TWEEN) |
| PDGF | Platelet derived growth factor |
| PlGF | Placental growth factor |
| Raf | Rapidly accelerated fibrosarcoma oncogenes |
| Ras | Rat sarcoma oncogene |
| RFI | Relative fluorescence intensity |
| ROS | Reactive oxygen species |
| ROI | Region of interest |
| RT | Radiotherapy |
| µm | Micro-metre |
| s/c | Subcutaneous |
| SGD | Specific growth delay |
| SMCs | Smooth muscle cells |
| SRC | Sarcoma related tyrosine kinase family member |
| VDA(s) | vascular disrupting agents |
| VEGF | vascular endothelial growth factor |
| VSMCs | vascular smooth muscle cells |

**ABSTRACT**

Cancer, defined as the uncontrolled replication of cells remains one of the leading causes of death worldwide. In order to better understand the current status of cancer therapeutics this thesis set out to look at some key factors that influence our current understanding namely; the pre-clinical tumour models used, the tumour microenvironment and current targeting regimens.

As vascular delivery is the preferred route for current clinical chemotherapeutics, it is important that we develop models to understand effects on tumour vasculature post therapy. This thesis has applied and refined the Dorsal Window Chamber/Intra Vital Microscopy (DWC/IVM) model to study vascular responses to novel and existing drugs, allowing a more detailed study of tumour microenvironment and in particular angiogenesis and neo-vascularisation. The DWC/IVM model allows real time visualisation of events during therapy that cannot readily be achieved with conventional pre-clinical models or in the clinical setting.

In this study, the DWC/IVM model was used to study the angiogenesis inhibitor AZD2171 (Cediranib) and the MAP kinase signalling inhibitor AZD6244 (Selumetinib) using Calu-6 (lung) and HCT116 (colon) carcinoma cell lines, in combination with radiotherapy. Traditional murine xenograft models showed the growth delay benefits of combined drug and radiotherapy (RT) application showing a reduction in the tumour microvascular density as an additional mechanism of action that was confirmed using the DWC/IVM model.

Studies using PARP-1 DNA repair inhibitors AG14361 and AGO14699, structurally related to nicotinamide were also investigated and showed that, as well as having an effect on tumour growth when combined with RT, they provide us with mechanistic insights as to how they influence the perfusion characteristics both alone and in the presence of adjuvant modalities. As an investigative tool in ongoing studies looking at the influence of hypoxia inducible factor (HIF-1) and RT the DWC/IVM model confirms previous studies showing tumour vascular density and perfusion is influenced by the absence of HIF-1 function.

These results demonstrate that the DWC/IVM model is a powerful and versatile tool for evaluating cancer therapeutics and vascular response *in vivo*.

**DECLARATIONS**

No portion of the work referred to in the thesis has been submitted in support of an application for another degree or qualification of this or any other university or other institute of learning;

**COPYRIGHT STATEMENT**

**i.** The author of this thesis (including any appendices and/or schedules to this thesis) owns certain copyright or related rights in it (the "Copyright") and s/he has given The University of Manchester certain rights to use such Copyright, including for administrative purposes.

**ii.** Copies of this thesis, either in full or in extracts and whether in hard or electronic copy, may be made **only** in accordance with the Copyright, Designs and Patents Act 1988 (as amended) and regulations issued under it or, where appropriate, in accordance with licensing agreements which the University has from time to time. This page must form part of any such copies made.

**iii.** The ownership of certain Copyright, patents, designs, trademarks and other intellectual property (the "Intellectual Property") and any reproductions of copyright works in the thesis, for example graphs and tables ("Reproductions"), which may be described in this thesis, may not be owned by the author and may be owned by third parties. Such Intellectual Property and Reproductions cannot and must not be made available for use without the prior written permission of the owner(s) of the relevant Intellectual Property and/or Reproductions.

**iv.** Further information on the conditions under which disclosure, publication and commercialisation of this thesis, the Copyright and any Intellectual Property and/or Reproductions described in it may take place is available in the University IP Policy (see http://www.campus.manchester.ac.uk/medialibrary/policies/intellectual-property.pdf), in any relevant Thesis restriction declarations deposited in the University Library, The University Library's regulations (see http://www.manchester.ac.uk/library/aboutus/

## AUTHOR BIOGRAPHY

The author began his work at the University of Manchester in the Department of Anatomy and trained as a clinical therapy muscle biopsy histologist. After several years training and developing a novel digitised 3D reconstruction analysis programme, for serial sectioning of the crichopharangeal (throat) muscle he moved to the Manchester Immunology Group and developed a novel intracellular labelling technique for dual labelling of T helper cell subsets as well as studying *in vivo* murine transplant rejection models. The author worked with research clinicians to evaluate cytokine expression post delivery of the immunosuppressive drugs Tacrolimus (also *FK-506* or Fujimycin) and cyclosporin (cyclosporin A). After gaining an MSc the author was fortunate enough to be asked to be asked to develop a murine hind limb perfusion model to look at pharmacokinetic and pharmacodynamic modelling of drugs to add to the liver perfusion model data used by Professor Malcolm Rowland in the School of Pharmacy. The authors' next step was to be asked to join Professor Ian J Stratford's group in the Manchester Experimental Oncology Group looking at murine xenograft models investigating novel and existing chemotherapeutic and radiotherapeutic models for direct clinical application. Continuing work with this group involves the routine development and use of the dorsal window chamber model introduced to the group by Dr David Berk. The author has been fortunate the skills developed over the years has had such a direct influence on his work in the current field of investigating tumour microenvironment response to applied cancer therapeutics. Indeed the author has virtually completed a full circle of research work that now involves the investigation, by the group, into tracking immune cell recruitment into developing tumour vasculature.

**ACKNOWLEDGEMENTS**

I would like to thank all my friends and colleagues who have helped me over the years, not least my friends and supervisors Professor Ian J Stratford and Dr Kaye J Williams. Within our research group I have been fortunate enough to have met and worked with several researchers who have gone on to lead their own research groups. I would like to thank Professor David Clarke for his patience with a mature student and in particular Dr David Berk and Dr Sharon Sneddon and Muhammad Babur without whose help you wouldn't be reading this.

**DEDICATION**

I would like to dedicate this to my father Alistair Telfer who had a throat cancer (I finished it eventually Dad) and to my mother and my partner Justin and all my family. I would also like to dedicate this work to everyone who knew someone with cancer and those we have yet to know. We're getting there.

## CHAPTER - 1 INTRODUCTION

Although incorrectly attributed to President Richard Nixon, it was US Senator Edward M Kennedy who advocated the increase of the National Cancer Institute's research funding from $150 to $220 million in 1971 and the war on cancer began in earnest. Over 40 years on and $65 billion later we are still trying to decipher and understand the biological complexities of tumour microenvironment and signalling mechanisms.

The World Health Organisation (WHO) reported recently that cancer a leading cause of death worldwide and accounted for 7.4 million deaths in 2004. (World Health Organisation Report 2009). The hallmark of cancer is uncontrolled cell replication that can form a benign or malignant mass (tumour), or uncontrolled replication of bone marrow derived cells (BMCs) such as leukocytes resulting in wide ranging homeostatic imbalances in the host (Hanahan and Weinberg, 2000). Tumours or neoplastic tissues can best be described as clonally derived (although not exclusively) growing masses of excessively replicating cells with no real mechanism of regulation (Willis, 1967).

Improved early detection and intervention has had a marked effect in reducing the numbers of fatalities. But the fact still remains that despite a wealth of information from preclinical and clinical studies, the predicted therapeutic benefits often fail to materialise in the clinical setting. A major reason for this is our continuing lack of knowledge of the biological complexities occurring pre and post therapy intervention.

It is therefore essential that we continue to develop and refine biological models in order to maximise potential therapeutic strategies. The use of pre-clinical animal tumour models, though controversial in some areas, is still the best cost effective, representative,

reproducible and ethical research tool currently available. The use of immuno-compromised mice and human derived xenografts growth delay (GD) studies has been invaluable for studying novel and existing antitumour therapy strategies for translation into the clinic.

We know that in tumours structural and functional aberrations result as a consequence of cellular and molecular events. As such visualisation and quantitation of these processes are of particular interest when investigating tumour pathophysiological response to therapeutic intervention at a mechanistic level. For these reasons several non-invasive measuring research tools have been developed including, positron emission tomography (PET), computed topography (CT) (An and, Cowie, 2004), nuclear magnetic resonance (NMR) (Pham 1998, Kiessling 2003) and ultrasound (Laser Doppler) (Kiessling 2003, Hill 1996).

These non-invasive measuring tools have proved very useful in attempting to image the processes of tumour progression, but they currently do not have the desired spatial resolution required to monitor events at the cellular level and access, cost and complex analysis restricts their availability to bench-side researchers.

One affordable non-invasive research tool that allows resolution for temporal and spatial measurement of tumour tissue is the dorsal window chamber (DCW) tumour model (Jain 1999). The DWC tumour model allows chronic non-invasive measurement and visualisation of early tumour initiation and subsequent stromal development in situ and in 'real-time' under controlled conditions (Li et al 2000).

The DWC xenograft model (referred to as the DWC model hereafter) has definitively proved Judah Folkman's hypothesis in the 1970's that: angiogenesis (new vessel growth from existing host vasculature) plays a critical role in tumour nutrient supply and growth development beyond a 1-2mm$^3$ ball of cells and as such provides a therapeutic target (Folkman, 1971).

Greenblatt and Schubik proposed that nutrient demanding tumour cells might produce 'chemical messengers' to promote angiogenesis and we now know these messengers to have direct and specific angiogenic stimulating effects even at a pre-cancerous stage (Greenblatt and Schubik 1968, Li, et al. 2000).

In order to understand the significance of their work towards developing effective antitumour therapies it is necessary to look at some of major factors that are known to influence therapeutic response in the tumour microenvironment.

### 1.1 Tumour stroma.

Solid tumours principally consist of tumour cells, an interstitial matrix and vessels collectively known as tumour stroma.

Tumour stroma is thought to directly influence antitumour therapeutic outcome due to its heterogeneity between different tumour cell types, growth factor signals, chemokine signalling and the presence of adhesion molecules. Angiogenesis signalling factors that have direct influences on tumour response to therapies include reduced oxygen (hypoxia), pH gradient differences, interstitial fluid pressure (IFP), vascular endothelial growth factor (VEGF) and the degree of microvascular density (MVD).

### 1.1.1 Tumour vasculature.

The formation of blood vessels is controlled primarily by the process of vasculogenessis and angiogenesis (e.g. in the processes of wound healing, menstrual cycles and neonatal development), whereas in the tumour directed state the process is primarily via angiogenesis.

In adult healthy tissues the larger established vasculature is made up of closely packed endothelial cells (ECs) attached to a basement membrane surrounded by smooth muscle cells (SMCs). The medium-sized vasculature contains ECs, a basement membrane surrounded by pericytes, whereas the smaller vessels may consist only of ECs.

There are three main stages involved in vessel formation: vasculogenesis arising from various embryonic regions or from adult bone marrow (BM), angiogenesis and arteriogenesis. Stabilisation of newly formed vessels occurs via recruitment of vascular smooth muscle cells (VSMCs), pericytes, formation of an extra cellular matrix (ECM) and a basement membrane.

Pericytes extend along cytoplasmic processes on the albuminal surface of the ECs to form tight junctions that are essential for blood vessel stabilisation, remodelling and function (Nussenbaum and Herman, 2010) (Fig. 1.1).

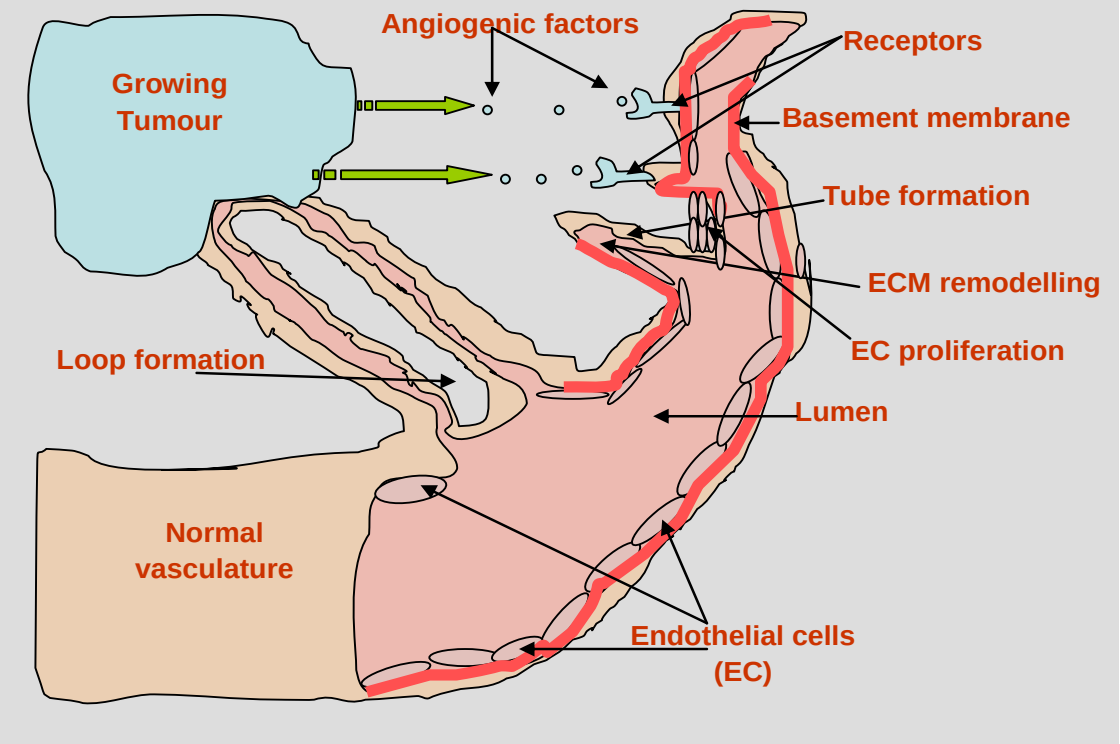


**Fig 1.1** Simplified diagram of tumour angiogenesis and vascular remodelling. The developing tumour mass initiates basement membrane breakdown via angiogenic signalling factors resulting in extracellular remodelling (ECM) resulting in a loop forming from the existing normal vasculature.

Tumour angiogenesis is multi-step process that depends on different tissue components:

- Production and release of angiogenic molecules such as VEGF in response to hypoxic cells or from circulating macrophages.
- Vascular destabilisation via detachment of pericytes.
- ECM degradation by endothelial proteases.
- Enhanced proliferation of ECs and migration towards the initiating site
- Tubule formation by ECs.
- Anastamosis of adjacent tubes to form perfused loops.
- Remodelling of the ECM.
- Re-attachment of the pericytes and vascular stabilisation.

In newly formed tumour vasculature the pericytes surrounding the tumour vessels are far fewer in number compared to that found in normal vasculature. ECs can form abnormal phenotypes and shapes and detach from the vessel basement membrane resulting in intercellular gaps (fenestrae), trans-endothelial cell pores, and vesiculo-vacuolar organelles (found in the cytoplasm of endothelial cells). As a result the vessels become hyper-permeable to circulating macromolecules and this increases the extravasation of plasma fluid and proteins (Graf et al. 2001, McDonald and Baluk, 2002) (Fig 1.2).

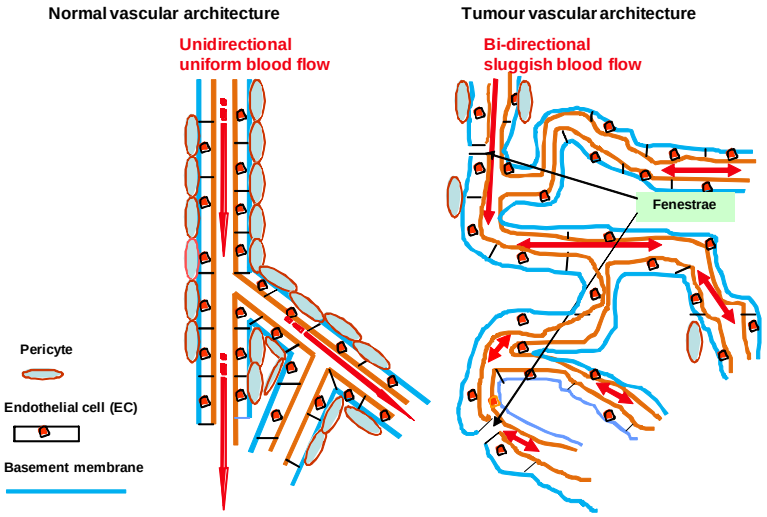


**Fig 1.2** Simplified diagram of normal vascular architecture versus tumour vascular architecture. Normal healthy tissue vessel architecture containing endothelial cells with tight junctions, a basement membrane and is encapsulated with pericytes. Blood flow is unidirectional with distinctive bifurcation vessel branching. Tumour vasculature architecture shows a reduction in or lack of pericytes and erratic vessel branching. The tumour vessels have thin walls and endothelial openings (*fenestrae*). The tumour vessel blood flow is chaotic sluggish often stopping and reversing direction.

Tumour vasculature is highly disorganised and tortuous with non-uniform diameters and has excessive branching and shunts. The net result is a blood supply that is chaotic, variable in directional flow, lacks lymphatic drainage and has microregional hypoxia with variant pH gradients due to an accumulation of necrotic tissues and metabolites (Pries et al. 2010, Kanthou and Tozer, 2009). As a direct consequence proangiogenic stimulators and inhibitors, normally found in balance, are tipped towards the proangiogenic state.

In the established tumour stroma 1-10% of its volume is made up by vasculature (Kuszyk et al. 2001). Fortunately most current chemotherapeutics do not have significant adverse effects on normal healthy host vasculature due to the fact that the ECs lining the vessels are normally quiescent and therefore less likely to develop drug resistance (Wu and Li, 2008). ECs in immature tumour vasculature however are actively replicating providing possible chemotherapeutic targeting (Bergers et al. 2003).

### 1.1.2 Angiogenesis.

Angiogenesis occurs relatively infrequently in healthy adult tissues where most vasculature is quiescent with only 0.1% of endothelial cells undergoing division at any one time. Angiogenesis is usually restricted to mammalian embryonic development, menstrual shedding and tissue wound repair, but can also include athletic exercise adaption (Kraus et al. 2004). However in non-healthy adult tissues angiogenesis is active in several pathologies including diabetic retinopathy, arthritis, atherosclerosis, psoriasis, neovascularisation and in age-related macular degeneration as well as cancer (Buysschaert et al. 2007).

Hypoxia mediated angiogenesis can be triggered by physiological parameters including low glucose status and stromal pH gradient changes which are associated with vascular insufficiency. As neo-vasculature establishes in the growing tumour mass it may often lag in its ability to meet the increase in nutrient demand. This can lead to the establishment of a self perpetuating autocrine feedback loop resulting in further angiogenesis activity.

## 1.2 Tumour hypoxia.

Oxygen ($O_2$) and nutrients are essential maintenance of homeostasis in mammals. In tumour tissue however $O_2$ concentration can fall below 10mmHg and become hypoxic. This has significant implications for antitumour directed therapies such as chemotherapy and radiotherapy (RT) either alone or in combination (chemoradiation).

Thomlinson and Gray, in the 1950's and 60's, established that tumour resistance to radiation was directly influenced by the level of hypoxic tissue present. (Thomlinson et al. 1965). Aerobic respiration is the primary mechanism mammalian tissues use to obtain energy from organic nutrients such as glucose in order to maintain a vast range of essential metabolic processes. In the presence of oxygen the breakdown of glucose and subsequent energy release results in the storage of this 'energy currency' in the form of Adenosine Tri-Phosphate (ATP). If however the level of oxygen availability decreases then tissues adaption mechanisms are induced to increase $O_2$ availability including haemoglobin synthesis or they can switch to a secondary less efficient glycolytic process in order to generate ATP. However tumours preferentially use the less efficient glycolytic process perhaps as an adaptive mechanism to the accelerated cellular proliferation in order to cope with the energy demands (Gatenby and Gilles, 2004).

In tumours two types of hypoxia have been described; the first is rapid intermediate or 'acute hypoxia' and can occur as a direct response to intermittent perfusion caused by temporary opening and closing of vessels, whilst the second 'chronic hypoxia' occurs as a result of sustained oxygen deprivation.

Chronic hypoxia is an oxygen diffusion-limited process where cells are found at distances of over 140μm from the nearest perfused vessel or in regions of necrotic tissue (Fig. 1.3).

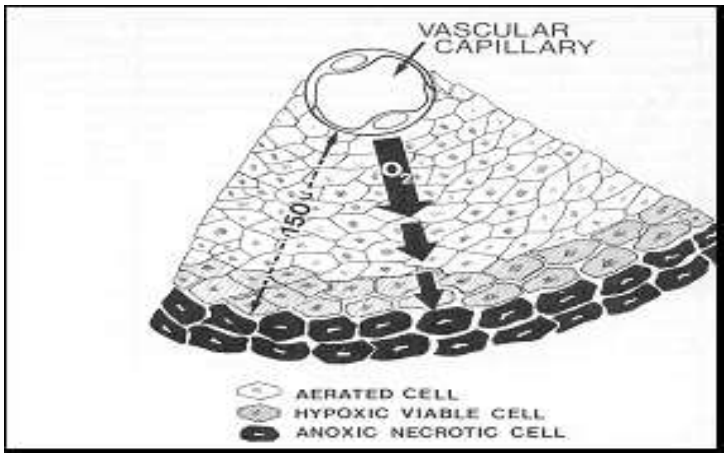


**Fig 1.3** Chronic tissue hypoxia. As the distance from the vascular capillary increases the diffusing oxygen concentration decreases resulting in hypoxic regions and/or anoxic necrotic regions.

The significance of tumour hypoxia, in relation to tumour therapy response failure, is borne out by findings that nearly 50 % of locally advanced breast cancers exhibit hypoxic and/or oxygenated areas that are heterogeneously distributed within the tumour mass (Vaupel, 2008).

Vaupel et al described tumour hypoxia as having a 'Janus Face' effect where tumour cells reduce their proliferation rates, increase the rate of tumour cell differentiation, induce apoptosis and increase necrosis or alternatively can result in tumour cell genetic adaptive processes resulting in the development of clones with aggressive phenotypes that result in local and distant spread.

Wouters and Brown proposed that hypoxia plays a more significant role in determining the outcome of fractionated RT. They cautioned that it was necessary to characterize tumour hypoxia in relation to all the tumour cells present and not just on the ones most resistant to RT (Wouters and Brown, 1997).

## 1.3 The role of HIF-1 in tumours.

It is widely accepted that all nucleated cells in the human body can 'sense' oxygen concentration fluctuations and that hypoxic tissues can activate an oxygen sensitive transcription hypoxia inducible factor-1 (HIF-1) to initiate adaptive responses to cope with decreased oxygen availability. Detection and adaption to hypoxia via HIF-1 leads to the transcriptional induction of a series of genes that are involved with promoting angiogenesis. One principle protein HIF-1 induces is vascular endothelial growth factor (VEGF) as well as inducing increased iron metabolism, activating glucose metabolism and inducing cell proliferation and survival (Semenza, 2003).

HIF-1 is also accepted as having a significant role in the pathology of several major causes of mortality such as cancer, cerebral and myocardial ischemia and chronic heart and lung diseases (Semenza, 2002). HIF-1 is also influences enzymes that control vascular tone e.g. inducible nitric oxide synthase (iNOS), vasodilator proteins such as adrenomedullin (ADM) and inflammatory cytokines such as interleukin-8 (IL-8) (Hickey and Simon, 2006). HIF-1 is a heterodimer consisting of the hypoxia response factor HIF-1α and constitutively expressed HIF-1β (also referred to as ARNT aryl hydrocarbon receptor nuclear translocator).

In oxygenated tissue ubiquitin dependent proteasomal-mediated degradation of HIF-1α occurs via the actions of the von Hippel-Lindau (pVHL) ubiquitin E3 ligase complex (Srinivas et al. 1999).

In renal cell carcinomas (RCCs) that have lost the tumour suppressor pVHL complex HIF-1α is not degraded resulting in elevated levels of HIF-1 being present (Maxwell et al. 1999) (Fig.1.4).

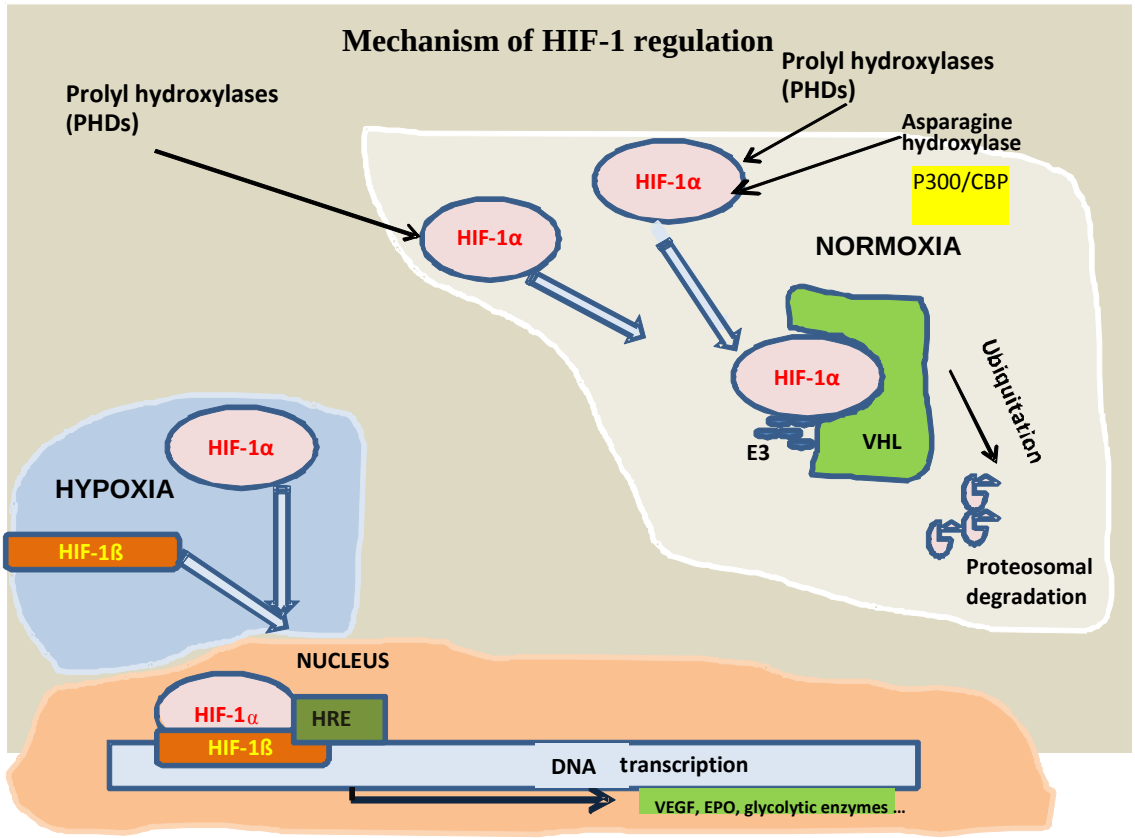


**Fig. 1.4** In the presence of sufficient oxygen the HIF-1 α subunit (through interaction with PHDs and ARD1 acetyl transferase) results in the presentation of HIF-1α to the von Hippel Lindau (VHL) protein in the presence of Elongin 3 (E3 ubiquitin ligase) resulting in ubiquitation and proteasomal degradation of the HIF-1α. In the oxygen deficient state the HIF-1α sub-unit moves to the nucleus to pair up with the HIF-1β sub-unit. This complex then initiates activation of the hypoxia responsive element (HRE) gene to initiate transcription of angiogenic stimuli proteins such as VEGF. Co-activating HIF-1proteins (P300/CBP). DNA transcription can result in VEGF, EPO, Glycolytic enzymes etc.

HIF-1α is also inhibited, by hydroxylation of an asparagine residue in C-TAD, from any transcriptional activity via binding to CBP/p300 (Lando et al. 2002). Under hypoxic conditions HIF-1α is stabilised and translocates from the cytoplasm to the nucleus where it dimerises with HIF-1β forming the HIF-1 complex. The HIF-1 complex then associates with hypoxic response elements (HREs) in the regulatory regions of target genes to induce gene expression.

There are a large number of downstream genes that HIF-1 can activate such as vascular endothelial factor (VEGF) and its receptors VEGFRs, glycolytic enzymes, erythropoietin (EPO), matrix metalloproteinases (MMPs), and Insulin growth factor-2 (IGF-2).

Over expression of HIF-1α is associated with poor prognosis and resistance to therapy in high as well as low grade tumours (Aebersold et al. 2001, Birner et al. 2001, and Bos et al. 2003). As such, targeting HIF-1 mediated pathways by inhibiting HIF-1 stability, transactivation, or inhibiting different steps in the signalling pathway downstream from HIF-1 could lead to the development of more HIF-1 targeted strategies (Yeo et al. 2004).
Loss or inactivation of tumour suppressor genes or proteins also provides a mechanism for the up regulation of HIF-1α. Several oncogenes and tumour suppressor gene products can act to stabilise HIF-1 or conversely increase its activity. These include; Src (sarcoma) oncogene, H-ras (Harvey **r**at **s**arcoma, also known as transforming protein p21), phosphatidylionisotol 3 kinase (PI3K), VHL, SDH (succinate dehydrogenase) and FH (fumarate hydratase) mutations.

Many of the known oncogenic pathways and hypoxia induced signalling pathways overlap resulting in cross talk between the oncogenic and hypoxic response pathways. HIF-1 is known to increase the activity of PI3K, a downstream mediator of tyrosine kinase signalling, involved in cell proliferation and suppression of apoptosis. PI3K is inhibited by PTEN (phosphatase and tensin protein) and mutations in the PTEN gene enhance HIF-1 responses as well as interacting with the oncogenic Ras (**Ra**t **s**arcoma) signalling pathway.
HIF-1 can also interact with p53 tumour suppressors to promote p53 dependant apoptosis via transcription of p53 leading to pro-apoptotic proteins such as BAX in mitochondrial membranes.

Hypoxia is also known to promote p53 dependant apoptosis mediated through APAF-1 and caspase-9.Mandriota et al. found that HIF-1 activity is present very early in tumour development (Mandriota et al. 2002).

All these studies suggested that HIF-1 could be a potential therapeutic target for antiangiogenic (AA) based therapeutic intervention in the clinic. A secondary influential factor is HIF-2α which also dimerises with HIF-1β in hypoxic environments also binds to HREs in the promoter regions of many genes involved in hypoxia adaptation (Tian et al. 1997, Qingdong Ke and Max Costa, 2006). Interestingly HIF-2α has been shown to be expressed in tumour vascular cells, parenchymal cells, and infiltrating macrophages (Leek et al. 2002, Onita et al. 2002) indicating that HIF-2α may play a major role in a broad range of cells in addition to ECs in tumourigenesis ( Chen-Jung et al. 2003).

Immuno-histochemical analysis of many tumours has detected high levels of HIF-1α proteins in benign tumours, malignant tumours and in metastases (Zhong et al 1999, Harris et al. 2002). The elevated levels of HIF-1α detected in many tumours are thought to be as a direct result of the loss of function of several factors including the VHL gene, succinate dehydrogenase complex -B (SDH-B), SDH-C, SDH-D or FH ( fumarate hydratase) and subsequent the cessation of ubiquitination.

The first cell lines used by our group to investigate the role of HIF-1 were derived from the murine hepatoma line Hepa-1 wild type (Hepa-1wt that are HIF-1β competent), Hepa-1c4 (HIF-1β deficient sub clone) and revertant Hepa-1c4 (Rc4, HIF-1β had been re-introduced) these were used in murine syngeneic subcutaneous (s/c) xenograft tumour models.

These early studies further indicated not only the importance of HIF-1 levels in tumour development, but also its potential as a therapeutic target (Dachs et al. 1997).

### 1.3.1 Targeting HIF-1.

Many novel agents targeting signal transduction pathways have been shown to block HIF-1 as well as having antiangiogenic effects (Harris, 2002). These include Herceptin, and ZD-1839(Iressa); BAY 43-9006; calphostin C (protein kinase C inhibitor); an inhibitor of MAPK(mitogen activated phosphate kinase) PD98095 and wortmannin (inhibitor of phosphatidylionisotol 3-kinase PI3K), or act as direct inhibitors of HIF-1 activity (reducing HIF-1α levels) such as YC-1, 2MEZ, 17-AAG, the DNA damaging drug Camptothecin and Topotecan (a topoisomerase-1 inhibitor) as well as the newly identified 2-methoxyestradiol (a tumour microtubule disruptor)(Kimbro and Simons 2006).

Although the exact mechanisms of action of these drugs have still to be determined i.e. they may be non-specific, it is encouraging that some levels of HIF-1 activity have the capability of being modified and therefore offer a potential therapeutic targeting rationale not only for cancer therapeutic strategies, but also for a range of human diseases.

There have been many novel therapeutic agents developed to target signal transduction pathways including anti-HIF-1 function blockers that also mediate antiangiogenic effects (Harris, 2002). Examples of these include Herceptin (trastuzumab) and Iressa (gefitinib); calphostin C (an inhibitor of protein kinase C); rapamycin (inhibitor of an FKB12-rapamycin-associated protein); diphenylene iodonium (redox signalling blocker) and mannoheptulose (inhibitor of a glucokinase) (Table 1.1).

**Table 1.1 HIF-1 activity targeted drugs**

| Drug | Target |
|---|---|
| **Trastuzumab** | Mab against $HER2^{neu}$ |
| **Imatinib mesylate STI-571** | Bcr-Abl inhibitor |
| **NS398, celecoxib, ibuprofin** | COX-2 inhibitors |
| **17-Allyl-amino-geldanamycin** | Hsp90 inhibitor |
| **Rapamycin, CCI-779, RAD-001** | mTOR inhibitors |
| **PD98059** | MEK/ERK inhibitor |
| **Endostatin** | Angiogenesis inhibitors |
| **Topotecan** | Topoisomerase I inhibitor |
| **2-Methoxyestradiol** | Microtubule disruption |
| **Chetomin** | p300 inhibitor |
| **PX-478** | HIF-1α degradation |
| **YC-1** | HIF-1α degradation |
| **Echinomycin** | Inhibit DNA binding |
| **Flavopiridol** | HIF-1α degradation |
| **Genistein** | Tyrosine kinase inhibitor |
| **GL331** | HIF-1α mRNA inhibitor |

HIF-1 transcriptional activation pathways can also be blocked using small molecular inhibitors reducing HIF-1 production and as a consequence modify VEGF expression impairing tumour growth, vascularisation and angiogenesis (Rapisarda et al. 2002). These include YC-1 3-(5'-hydroxymethyl-2'-furyl)-1-benzylindazole, potential HIF-1α inhibitor)), 17-allyl-aminogeldanamycin (inhibitor of the 90-kDa heat shock protein); thioredoxin-1 (redox regulator inhibitor) and 2-methoxyestradiol (tumour microtubule disruptor). A relatively new anti-HIF-1 drug PX-478 has been shown to suppress HIF-1α

synthesis and to a lesser extent increase HIF-1α ubiquitination (Koh et al. 2008). *In vitro* studies have shown the enhancing effect PX-478 has on prostate carcinoma cell response to radiation under hypoxic and normoxic conditions and the potentiation of radiotherapy (RT) through inhibition of HIF-1 signalling in glioma xenografts (Schwartz et al. 2009).

### 1.4 Tumour stroma and radiotherapy (RT).

The principle action of RT in antitumour therapies is that it causes DNA damage to rapidly dividing tumour cells via the generation of an ion radical [$H_2O + \gamma \rightarrow H_2O^+ + e^-$]. The ion radical reacts immediately with other water molecules to produce a hydronium ion and a hydroxyl radical [$H_2O^+ + H_2O \rightarrow H_3O^+ OH\bullet$]. It is these hydroxyl radicals that induce DNA single strand breaks (SSBs) or double-strand breaks (DSBs), base pair damage or cross-link damage. The resultant effect of the DNA damage is to push the cell into programmed cell death (apoptosis) unless rescued by the repair enzyme poly-ADP-ribose-polymerase (PARP) which assists in base excision repair (BER) of SSBs.

Non-surgical cancer therapeutic strategies have classically focussed on direct killing of cancer cells by chemotherapy and or radiation therapy. However it is becoming evident that the efficacy of these therapies can be significantly influenced by the tumour microenvironment. The contribution of a vascular component, in tumour response to RT, has been an area of debate for many years (Garcia-Barros et al. 2010, Gerweck et al 2006) Radiation impacts on both tumour cells as well as normal tissue stromal cells (e.g. endothelium, connective tissue). It has proved difficult to determine the overall contribution each component has in tumour growth delay post chemoradiation therapy.

Budach et al. addressed the question of radiation impact on the two compartments making up the tumour stroma by studying severe combined immune deficient mice (SCID), that have a germline mutation in the DNA-dependent protein kinase (DNA-PK) gene associated with a deficiency in DNA DSB repair, to distinguish between the host stromal cell responses and the effects on the tumour clonogenic cells (Budach et al. 1993). He reasoned that if SCID host stroma contributed to the radiation response of the tumours then a greater overall response would be seen compared to tumours established in hosts that were DNA-PK gene competent (wild type mice). Budach implanted SCID, C3H (wild type, wt) and athymic nude mice with five different murine lines and showed that the SCID host phenotype did not influence the overall tumour response to radiation. Gerweck et al. agreed with Budach's hypothesis that it was the clonogenic cells that responded to radiation based on studies using isogenic tumour xenografts in NCr (nu/nu) hosts that differed only in the activation of DNA-PKcs (Gerweck et al. 2006) . Further Gerweck et al. found that tumour vasculature was similar in tumours that exhibited markedly different responses to radiation and that the vascular response to radiation could differ even for the same tumour types (Gerweck et al. 2006).

Conflicting with Budach and Gerweck's sole clonogenic radiosensitivity hypothesis Garcia-Barros and Paris found that radiation increased the rate of stromal vascular ECs apoptosis concluding that this was an important contributory factor in the overall tumour response (Garcia-Barros and Paris, 2001). Garcia-Barros implanted tumours into mice that had a mutation for the enzyme acid sphingomyelinase (ASMase) (an essential enzyme involved in cell apoptosis) and found that tumours irradiated in the ASMase $^{-/-}$ knockout mice responded much less than was found in the wt mice (ASMase $^{+/+}$ ). Garcia-Barros et al. found that the ASMase$^{-/-}$ ECs were more resistant to radiation induced apoptosis

compared to wild type mice (Garcia-Barros et al. 2003). These studies inferred that the vascular component of the tumour had a much more prominent role in effecting a tumour radiation response.

More recently Garcia-Barros has once again re-challenged the notion by Gerweck and others that host stroma endothelial compartment has little or no influence on tumour cure by testing the hypothesis that acid sphingomyelinase (ASMase)-mediated endothelial cell apoptosis, which results from plasma membrane alterations, not DNA damage is a crucial element in the cure of tumours in SCID mice (Garcia-Barros et al.,. 2010). In recent studies they have shown that endothelium in MCA/129 fibrosarcomas and B16 melanomas exhibit a wild-type apoptotic phenotype in SCID mice that is abrogated in SCID ASMase-/- littermates that also acquire resistance to single dose radiotherapy (SDRT). Their studies showed that cell membrane ASMase mediated microvascular dysfunction, rather than the DNA damage-mediated endothelial clonogenic lethality, plays a significant role in the complex mechanisms of tumour cure post radiation treatment (Garcia-Barros et al. 2010). The debates continues, however the role of ASMase and in particular its response to radiotherapy warrants further investigation in order to more fully understand the influence of the tumour microenvironment on tumour response to radiotherapy.

### 1.4.1 Ceramide.

Until recently DNA damage has been the main focus describing tumour chemoradiation responses at the cellular level leading to cellular apoptosis (programmed cell death). However chemoradiation also impacts on the protein components of cellular damage response networks by activation of signal transduction cascades initiated through in the plasma membrane, the cytoplasm and the nucleus in response to induced biological stress.

This offers up a potential tumour target since many of the survival attributes of tumour cells are determined by proteins involved in antiapoptosis (cell survival), cell cycle regulation and damage repair.

Chemoradiation regimens induce apoptosis via receptor-mediated and non-receptor mediated processes through the activation of effector caspases (proteases responsible for cell disassembly) and both processes use ceramide as an intracellular signalling molecule. Ceramide has been shown to have a central role in both apoptotic and mitogenic pathways *in vitro* where it was seen to influence drug resistance. Ceramide is generated in response to chemoradiation via hydrolysis of sphingomyelin by acid sphingomyelinase (ASMase) resulting in the release of ceramide rich membrane platforms involved in apoptosis (Kolesnick et al. 2000, Grassmé et al. 2003.

PI3K forms part of the apoptosis signalling pathway PI3K/AKT/mTOR and its activity is down-regulated by stress-induced ceramide in a dose-dependent manner. Ceramide inhibition or down regulation of PI3K is dependent on ASMase and results in inhibition of the kinase Akt and decreased phosphorylation of the death effector Bad. Therefore ceramide levels may act as a general apoptotic rheostat controlling cell survival by regulating PI3K signalling. This has important implications in antitumour therapies since HIF-1 is also involved in many cancers and is regulated by hypoxia, PI3K and MAPK signalling pathways affecting chemoradiation responses (McCubrey et al. 2006).

### 1.5 VEGF and tumour angiogenesis.

VEGF is a potent mitogen for micro and macro vascular ECs that line the arteries, veins and lymphatic vessels in mammals and doesn't seem to demonstrate mitogenic activity on

other cell types (Ferrara et al. 2005). It has also been found to induce angiogenesis in a variety of *in vivo* models including chick chorioallantoic membrane (CAM) (Leung et al. 1989), rabbit cornea (Philips et al. 1994) and rabbit bone (Connolly et al. 1989).

VEGF has also been reported as having regulatory effects on certain blood cells influencing monocyte chemotaxis and granulocyte-macrophage progenitor cells (Clauss et al. 1990, Broxmeyer et al. 1995).

Originally described as vascular permeability factor (VPF) (Sieger et al. 1983), five distinct ligands of VEGF have been identified including VEGF(s) A, B, C, D and E as well as placental growth factor (PlGF) making up a 'family' of VEGF ligands that have distinct roles in the development of tumour stroma . VEGF is known to have a critical role in embryonic vascular (vasculogenesis) lymphatic development (lymphogenesis) as well as in tumour angiogenesis being found at elevated levels over a wide range of tumour types with pivotal influences on the augmentation of secondary tumours at distant sites (metastases) often resulting in a poor prognosis for many tumour hosts in the clinical setting (Ellis and Hicklin, 2008). For these reasons targeting VEGF and its signalling pathways presents an exploitable antitumour targeting strategy. Several monoclonal antibodies (Mabs) and small-molecule inhibitors have been developed over the last few decades and progressed to clinical trials targeting cancer characteristics such as cell growth, survival, angiogenesis, and metastasis improving patient cure rates, quality of life and disease prevention.

Bevacizumab (Avastin®), a monoclonal antibody against vascular VEGF, was the first U.S. Food and Drug Administration (FDA)-approved biological therapy for the treatment of tumours. Avastin began Phase III clinical trials in 2004 showing benefit in first-line treatment of metastatic colorectal cancer when the drug was combined with standard

chemotherapy (Hurwitz et al. 2004). However, as with many newly introduced therapies there has to be caution. Avastin has recently been removed from the FDA-approved therapeutic drug list for breast cancer due to unsatisfactory results and questions over its safety and efficacy (www.medscape.com/viewarticle/753862).

### 1.5.1 VEGF receptors.

As homodimeric glycoproteins VEGFs affect responses through interaction with three different, but overlapping, structurally related VEGF receptors (VEGFRs) with tyrosine kinase (TK) domains in the endothelial cytoplasm via receptor tyrosine kinases (RTKs) (Fig. 1.5).

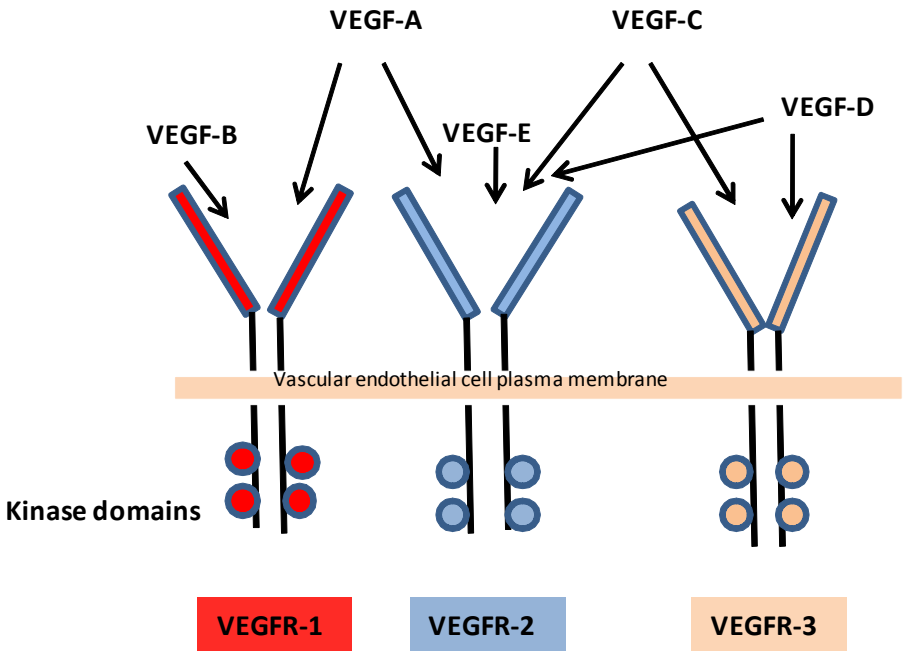


**Fig.1.5** VEGF signalling proteins and their receptors. VEGFR-1 binds the mitogenic ligands VEGF A and B whereas VEGFR2 binds VEGF A, C and D and VEGFR-3 binds VEGF-C and D.

VEGFR-2 is a type III transmembrane tyrosine kinase receptor composed of 1,356 amino acids in humans and has been identified as the principle mediator of several physiological

and pathological effects via its activation by VEGF-A ( referred to as VEGF hereafter unless distinction is needed between the ligands) including EC proliferation, migration, survival and vascular permeability (Ferrara et al. 2005).

Binding of VEGF to the VEGFR-2 receptor induces dimerisation and autophosphorylation of specific intracellular residues resulting in the initiation of several intracellular signalling pathways (Fig. 1.6).

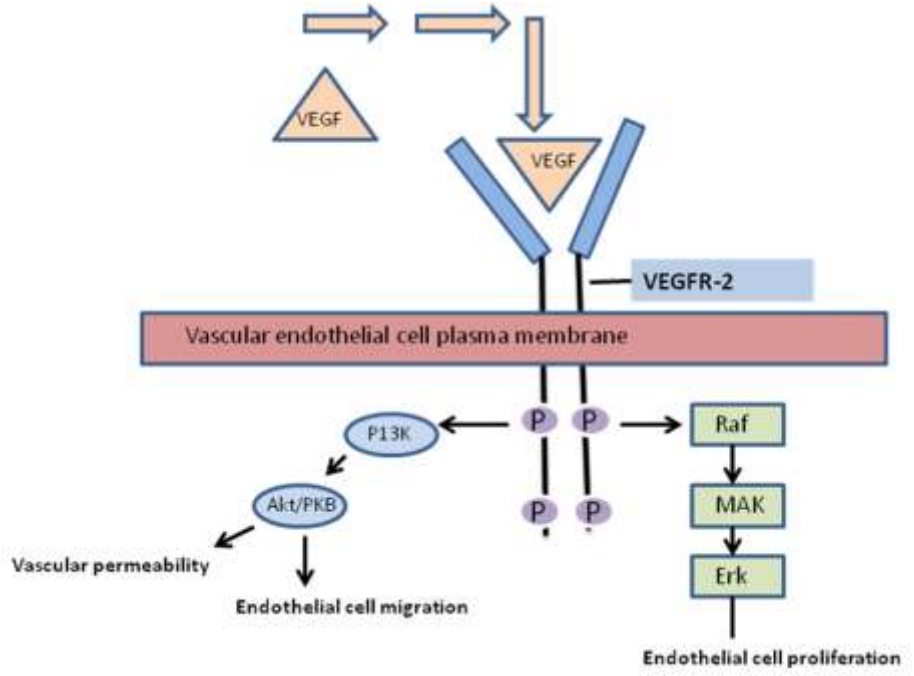


**Fig. 1.6** PI3K/Akt and Raf/MAPK/ERK pathway signalling via VEGFR-2. A simplified representation of the downstream cellular effects post activation of the VEGFR-2 receptor found on the surface of endothelial cell plasma membranes. The result of the activation of the receptor is the initiation of the PI3K/Akt pathway that can lead to the increased vascular permeability and endothelial cell migration and the Raf/MAPK/ERK signalling pathway leading to endothelial cell proliferation and survival.

However unlike other representative TKRs using the Ras signalling pathway VEGFR2 principally uses the Phospholipase- C gamma-Protein kinase-C pathway to activate the mitogen-activated phosphate kinase (MAPK) signalling pathway and DNA synthesis. VEGFR2 is a direct signal transducer for pathological angiogenesis including cancer and

diabetic retinopathy and its signalling pathways appear to be critical targets for the suppression of these diseases.

VEGFR1 can have a negative role in angiogenesis in the embryo by trapping VEGF and a positive role in adulthood in a tyrosine kinase-dependent manner. VEGFR1 is expressed not only in ECs but also in macrophage-lineage cells, promoting tumour growth, metastasis, and inflammation. VEGFR-1 activation may also have a role in active recruitment of bone marrow derived cells (BMDs), monocytes and in haemopoesis influencing the vasculogenessis process in developing tumours as well as influencing matrix metalloproteinases (MMPs) and EC paracrine release of growth factors (Hiratsuka et al. 2008). VEGFR2 is expressed primarily on activated ECs and is believed to be a key driver of mitogenic responses stimulating tumour angiogenesis, while VEGFR-1 is expressed on multiple cell types (Plate et al. 1993, Fisher et al. 2008). Although VEGFR-2 has been the most extensively studied of the three receptors it is thought that VEGFR-1 activity may involve a role as a 'decoy' for the VEGFR-2 receptor by 'mopping' up excess VEGF and by doing so regulate the activation rate of the VEGFR-2 receptor (Ferrara et al. 2005). VEGFR-3 (via VEGF-C ligand interaction) initiates lymphanogenesis by promoting lymphatic proliferation and migration and has been implicated in lymph node metastasis (Su et al. 2006, He et al. 2005). Expression of VEGFR-3 has also been reported to be significantly correlated with the different stages of cervical carcinogenesis (Van Trappen et al. 2003) as well as colorectal adenocarcinoma (Witte et al. 2003).

### 1.5.2 VEGF signalling.

VEGF has been also been identified as a potent survival factor for ECs *in vitro* and has been shown to inhibit apoptosis via activation of the PI3K –Akt (serine/threonine kinase) /PKB(protein kinase-B) signalling pathway (Fig. 1.7).

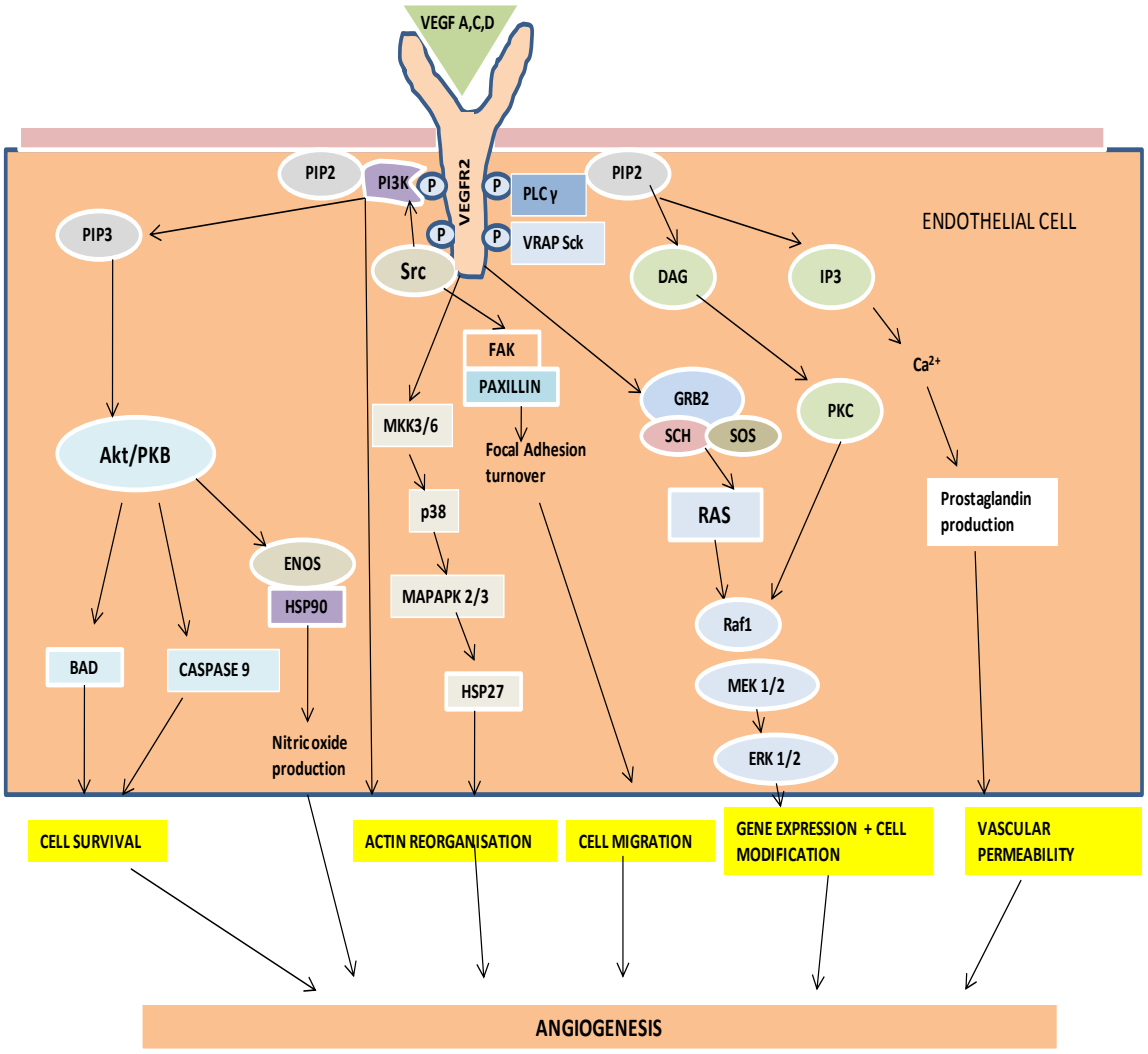


**Fig. 1.7** Major signalling cascade pathways post VEGFR-2 activation. Dimerisation and autophosphorylation of VEGFR2 in the endothelial cell by VEGF A, C or D results in several SH2 (**S**rc **H**omology 2 a conserved protein contained within the Src oncoprotein domain containing signal transduction molecules being directly activated by Phospholipase C-gamma (PLC-γ) signal transduction, VEGF Receptor-Associated Protein (VRAP), and Sck, or indirectly via Src and PI3K. Protein Kinase-C (PKC) activation via VEGFA mitogenic signalling stimulates the Raf1-MEK-ERK pathway. Cell survival signals are mainly mediated through PI3K-mediated activation of Akt/PKB (Protein Kinase-B). PI3K activation results in elevated levels of Phosphatidylinositol-3, 4, 5-Trisphosphate (PIP3) mediating membrane targeting and phosphorylation of Akt/PKB. Downstream targets for the Akt/PKB pathway include the proapototic protein BAD, FKHR1 (Forkhead Transcription Factor-1), and Caspase-9 whose phosphorylation inhibits apoptosis. PLC-γ catalyzes the hydrolysis of Phosphatidylinositol-4, 5-Bisphosphate (PIP2), creating Inositol Trisphosphate (IP3) and Diacylglycerol (DAG), causing release of stored $Ca2^{+}$ and activation of PKC. VEGF-A-induced $Ca2^{+}$ results in prostaglandin production via nitric oxide concentration increases. SHC phosphorylation promotes formation of SHC-GRB2 (Growth Factor Receptor-Bound Protein-2)-SOS (son of sevenless) complexes inducing PKC-dependent and Ras-independent induction of the Raf1-MEK-ERK1/2 pathway. VEGFA signalling via the p38 pathway leads to Actin cytoskeleton reorganisation influencing endothelial cell migration by modulating the activation of MAP Kinase Activated Protein Kinase-2/3 (MAPKAPK2/3), phosphorylation of the F-Actin polymerization modulator and Heat Shock Protein-27 (HSP27) as well as via Focal Adhesion Kinase (FAK) and Paxillin.

The PI3K/Akt pathway is critical to the regulation of cell proliferation survival and migration VEGF has also been shown to up regulate anti-apoptotic proteins such as bcl-2 (Gerber et al. 1988).

VEGF signalling inhibits caspases through pro-survival signalling and up regulates members of the inhibitors of apoptosis (IAP) family including survivin and XI AP in addition to activating focal adhesion kinase (FAK) and associated proteins influencing EC survival (Fig 1.7) and VEGF has been shown to enhance PI3K enzymic activity via promotion of p85 phosphorylation (a regulatory subunit) probably via association with Src kinases b-catenin and vascular endothelial cahedrin. This pathway activates cellular prosurvival transcription factors, such as nuclear factor κB ($NF_{\kappa}B$). Akt also suppresses proapototic proteins of the Forkhead transcription factor family and Bad (Jiang and Liu et al. 2008) as well as suppressing PTEN (phosphate and tensin homolog that acts as a tumour suppressor gene) as well as angiogenesis induction via.

There are several strategies being developed to inhibit VEGF and VEGFR signalling including monoclonal antibodies, VEGF-trap, VEGF aptamers, small molecule inhibitors of TKRs as well as the development of antisense and VEGF/VEGFR siRNA targeting (Fig. 1.8).

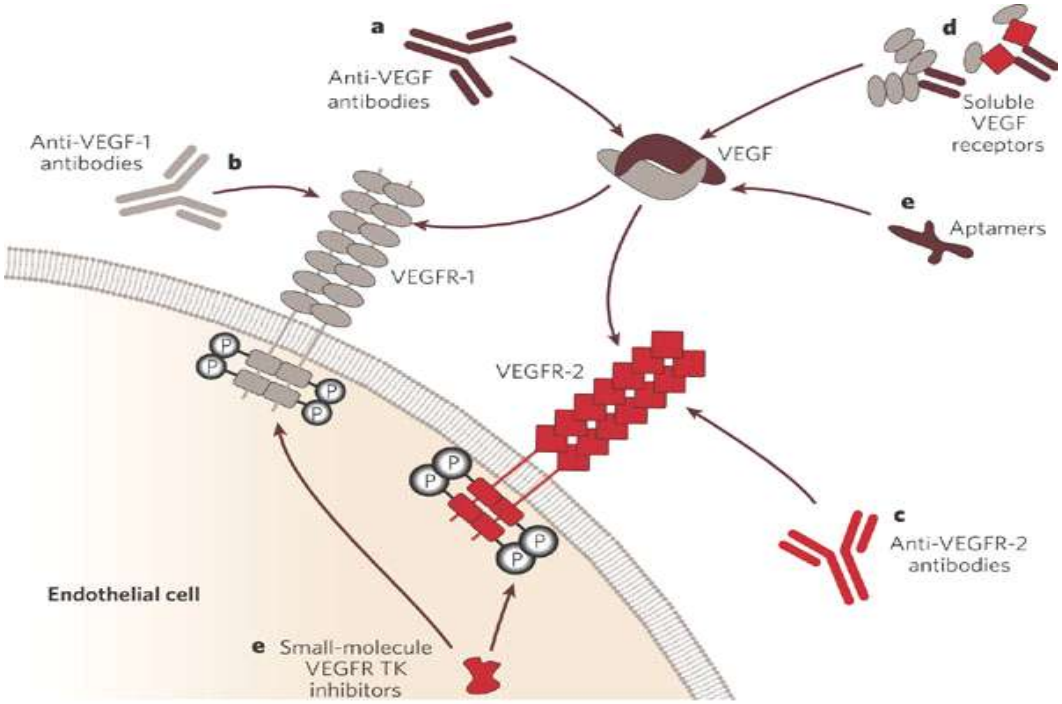


**Fig. 1.8** Strategies being developed to inhibit VEGF and VEGFR in pre-clinical and clinical studies. VEGF targeting strategies currently being studied include; monoclonal antibodies targeting VEGF-A (**a**) or the VEGF receptors (**b**, **c**), **d**, soluble receptors such as the 'VEGF-trap', **e** extracellular targeted aptamers , small-molecule RTK inhibitors as well as antisense and siRNA targeting VEGF-A or its receptors. (Adapted from Ferrara and Kerbel 2005).

Since tumour vasculature is characterised by the reduced presence or contact between pericytes and ECs this may contribute to the selective vulnerability of tumour blood vessels to the use of VEGF inhibitors. Another potential target is the disruption of the gene that codes for platelet derived growth factor-B (PDGF-B) which is involved in the recruitment of pericytes to immature blood vessels.

Recent focus has looked the effects of genetically engineered fusion proteins that function as 'traps' for VEGF. Aflibercept is an example of a recent VEGF-Trap that binds both VEGF and PlGF with high affinity (Teng et al. 2010).

Many TRKs in association with G proteins are known to activate intracellular protein serine/threonine kinases, termed mitogen-activated protein kinases (MAPKs). Of the various families of MAPKs and their extracellular signal-related kinases ERKs, the first to be characterised were ERK1 and ERK2 (ERK1/2). These two kinases were found to be linked to a variety of extracellular signals such as growth factors, hormones and adhesion factors as well as cytoplasmic and nuclear factors. Numerous solid tumours are known to constitutively express phosphorylated ERK1 and 2 and activation of ERK is critical for a large number of Ras-induced cellular responses (Fig 1.5) via the Ras/Raf/MAPK signalling pathway. Two components of the Ras/Raf/MAPK pathway are the Ras and Raf proto-oncogenes (genes that encode proteins able to transform cells in culture or to induce cancer in mammals). Ras genes encode small guanosine tri-phosphate proteins (GTPs) that regulate cellular differentiation, cytoskeletal organisation, and protein trafficking as well as tumour angiogenesis. Mutations in Ras/Raf leads to aberrant activation of downstream targets such as MAPK/ERK1/2 (or MEK1/2) signal transduction and as such provide potential antitumour therapeutic drug targeting.

One of the earliest TKI drugs was SU 5416, which was found to be a potent inhibitor of the kinase activities of both VEGFR and platelet derived growth factor receptor (PDGFR) leading to the development of a number of antiangiogenic agents that are currently undergoing clinical phase trials (Table 1.2).

**Table 1.2 Antiangiogenic (AA) tyrosine kinase inhibitors in clinical development.**

| Drug | AA target | Clinical cancer target | Clinical Phase |
|---|---|---|---|
| **Sunitinib (SU11248; Sutent)** | VEGFR-1,2, 3, PDGFR, KIT, FLT3, CSF-1R, RET | Kidney, breast, prostate, lung, liver, ovarian, colorectal, thyroid, head and neck, gastric, bladder, cervical and pancreatic cancer, GIST, melanoma, glioblastoma, myeloma, lymphoma | Approved kidney cancer and GIST, phase II or III for other cancers |
| **Sorafenib (BAY439006; Nexavar)** | VEGFR-2,3, PDGFR, Raf, KIT | Kidney, liver, breast, prostate, lung, ovarian, colorectal, thyroid, head and neck, gastric and pancreatic cancer, GIST, melanoma, glioblastoma, lymphoma, leukaemia | Approved kidney and liver cancer, phase II or III for other cancers |
| **Pazopanib Votrient)** | VEGFR-1,2,3, PDGFR, KIT | Kidney, breast, lung, cervical, liver, thyroid, prostate and colorectal cancer, melanoma, glioblastoma | Approved kidney cancer, phase II or III for other cancers |
| **Vandetanib (ZD6474; Zactima)** | VEGFR-2, EGFR, KIT, RET | Lung, kidney, thyroid, head and neck, prostate, ovarian, breast and colorectal cancer, glioma, neuroblastoma | Phase II or III |
| **Axitinib AG01373)** | VEGFR-1,2 3, PDGFR-β,KIT | Kidney, lung, thyroid, pancreatic, colorectal and breast cancer, melanoma | Phase II or III |
| **Cediranib (AZD2171; Recentin)** | VEGFR-1,2,3, PDGFR-β, KIT | Kidney, breast, lung, liver, ovarian, head and neck, prostate and colorectal cancer, GIST, glioblastoma, melanoma | Phase II |
| **Vatalanib (PTK787; ZK222584** | VEGFR-1, -2, -3, PDGFR-β, KIT | Prostate, colorectal, kidney and pancreatic cancer, melanoma, lymphoma, leukaemia | Phase II or III |
| **Motesanib (AMG706)** | VEGFR-1, -2, -3, PDGFR, KIT, RET | Lung, thyroid, gallbladder, breast and colorectal cancer, GIST | Phase II or III |

CSF-1R colony stimulating factor-1 receptor, EGFR epidermal growth factor receptor, FLT3 fms-related tyrosine kinase 3, GIST gastro-intestinal stromal tumour, PDGFR platelet-derived growth factor receptor, VEGFR vascular endothelial growth factor receptor (source www.clinicaltrials.gov)

Later inhibitors were developed including Sunitinib and Sorafenib which were found to target primarily VEGFR-2 resulting in beneficial responses in patients over a range of cancers including renal cancer (Plate et al. 1994, Choueiri et al. 2008).

Sunitinib has been approved for treatment of gastro-intestinal stromal tumours (GISTs) and Sorafenib inhibits RAF serine kinase as well and has been approved for treatment of hepatocellular and renal cancers (Lovet et al. 2007).

Many AAs such as the small molecule TKIs have multi-targeted capabilities involving several signalling pathways and therefore possess a broader efficacy than singular-targeted inhibitors. The VEGF and PDGF signalling pathways play important roles in tumour angiogenesis and effecting multi-targeted kinase inhibition may reduce the need for higher toxic singular inhibitory doses in order to achieve a beneficial response. They may also have active targeting capabilities on tumour vessels.

### 1.6 Antiangiogenic therapeutic approaches.

Despite the promising potential of some AA directed therapies in pre-clinical studies these often don't translate into the clinical setting. The reason for this is primarily due to an incomplete knowledge of their mechanisms of action. *S*ome agents, that were thought to specifically target tumour cells, may also have secondary effects such as seen in the case of Herceptin (HER-2 specific antibody) which causes not only a decrease in the expression of endogenous angiogenic inhibitors such as thrombospondin-1, but also induces and increases the expression of VEGF in the surrounding stromal cells. Additionally AAs can produce adaptive (evasive) tumour cell resistance by initiating the up regulation of secondary proangiogenic signalling pathways. The treatment of tumour angiogenesis using anti-VEGF drugs can also result in the up regulation of fibroblast growth factor (FGF) dependent re-vascularisation such as that seen with the VEGFR-1,2 and 3 inhibitor AZD2171(Cediranib) (Williams et al. 2005).

Drugs targeting the tumour stroma may also affect other pro-angiogenesis stimuli such as circulating vascular progenitor cells and monocytes modifying recruitment of heterogeneous populations particularly if stromal hypoxia is present. Endothelial and pericyte progenitor cells differentiate to form the walls of neo-vasculature as well as

protecting the tumour vessels from destruction by enveloping the vasculature retrospectively (a prosurvival mechanism). As well as pro-survival adaptive processes, tumour drug resistance (TDR) occurs naturally i.e. the drug doesn't reach the intended cells at sufficient concentrations to affect them and subsequent dosing leads to desensitisation and reduction in efficacy. The net effect is the emergence of sub-populations of cells that can re-populate between treatments resulting in the re-establishment of tumour growth.

Teicher et al. proposed that combining AAs with chemoradiation could result in a greater antitumour effect compared to than singular modalities (Teicher et al. 1996). Teicher proposed for example that the net effect of AAs and radiotherapy (RT) could lead to an increase in tumour stroma oxygenation and hence an increase in tumour response to radiation (Teicher et al. 1996). Mauceri et al. targeted tumour vasculature using combined angiostatin (specific inhibitor of endothelial proliferation and a potent angiogenesis inhibitor) with radiation resulting in an improved antitumour effect using clinically relevant RT doses for four distinct tumour types (Mauceri et al. 1998). Gorski et al. used VEGF neutralising antibodies combined with RT that also resulted in increased antitumour effects (Gorski et al. 1999).

Moeller et al. showed that the first response of the tumour vascularity to RT was to increase the activation of HIF-1 demonstrating that by blocking the elevated levels of HIF-1 tumour vascular radiosensitisation could be achieved. They realised that it was necessary to block HIF-1, thereby reducing the effects of downstream activated EC protective cytokines, in order to achieve increased tumour radiosensitivity and enhanced vascular destruction (Moeller et al. 2004).

These studies highlight the validity of using AAs in multimodal therapy regimens to improve chemotherapeutic strategies. However they also highlight the need to improve our understanding of tumour stromal responses to AAs and combined therapies in order to more fully understand how they affect the whole tumour microenvironment if we are to improve therapeutic outcome in the clinical setting.

### 1.7 Tumour vascular disrupting agents (VDAs).

The effects of VDAs will not be discussed here other than to distinguish them from other antiangiogenic agents. Introduction of VDAs into established tumour vasculature causes catastrophic vessel shutdown resulting in tumour stroma nutrient deficiency and ultimately tumour regression.

The mechanisms of action of the VDAs on tumour vasculature have recently been extensively reviewed elsewhere (Kanthou and Tozer, 2009). AAs are primarily involved in the disruption of the angiogenesis signalling pathways that initiate neo, and therefore immature vasculature. VDAs act primarily on more established/mature tumour vasculature.

### 1.8 Combining antitumour therapeutic regimens.

Solid tumours account for over 85% of cancer mortality (Jain et al. 2005). Folkman rationalised that if we could limit the nutrient supply to the tumour we might be able to either destroy the tumour or at least push it into stasis. By identifying the signals that 'switched on' the angiogenesis process it was hoped to develop specific AAs that would starve the tumour mass of essential nutrients and induce apoptosis. AA drug development using pre-clinical models lead to their introduction into the clinic initially as monotherapies.

However the beneficial effects of many of the subsequent AA clinical trials resulted in only modest short term survival benefits for patients (Yang et al. 2003, Cobleigh et al. 2003, Mayer, 2004). These findings were in contrast to clinical trials that used combined chemoradiation therapies and AAs as first alluded to by Teicher et al. 1996. Teicher proposed that a combination regimen approach should yield a better therapeutic outcome principally because they would target several components of the tumour stroma at the same time. This resulted in combined modality studies to investigate which combinations would work maximally and in which order they should be applied.

In essence this was the realisation that tailored antitumour strategies were needed due to the heterogeneic responses that might present between different tumour types.

### 1.9 Factors affecting drug delivery to the tumour stroma.

If cytotoxic agents cannot gain access to their targets then it stands to reason their effectiveness will be at best compromised or at worst negligible. In order to be effective a drug must be able to achieve an effective concentration at the desired site for a period of time preferably without causing significant local or systemic tissue toxicity.

Tumour stromal physiochemical and physiological barriers often result in heterogeneous accumulation of various therapeutic molecules, particles, and cells in solid tumours (Minchinton and Tannock, 2006).

In order for a chemotherapeutic to gain access to the tumour stroma several barriers need to be surmounted before it can have an effect. One primary barrier is the heterogeneity of tumour vasculature and the presence of intermittent chaotic blood flow.

Tumour vasculature has been described as hyperpermeable to proteins which should in theory aid drug delivery into stromal tissues however this permeability can exhibit significant spatial as well as temporal heterogeneity within the tumour as well.

Additional barriers are the physiochemical properties of the stroma itself where intermittent blood flow results in areas of acute (short duration) or chronic (long lasting) hypoxia, tumour cell necrosis, nutrient waste accumulation and pH concentration gradients (Bussink, 2000).

If a therapeutic drug manages to overcome the previous barriers it then has to deal with the interstitial compartment if it is reliant on diffusion through the tumour tissue. As a rule the diffusion coefficient of a drug (D) decreases with the increase in the molecular weight of the drug. Larger drugs or molecules diffuse at a much slower rate allowing more time for a drug to bind to relatively immobile molecules and thus hinder any further movement across the tumour stroma. The effect of drug convection is negligible in tumours except in the periphery where there may be steep pressure gradients (Griffon-Etienne et al. 1999).
The tumour cell membrane and cytoplasm present additional barriers as well as tumour interstitial fluid pressure (IFP) being higher than that within the blood vessels supplying it (Znati et al. 1996).

The resultant variances in the concentrations of therapeutic drugs within the tumour stroma poses the additional problem of cells evading the therapeutic agent and therefore having the ability to re-populate as resistant cells capable of further angiogenesis at a later stage.

## 1.10 Tumour vascular 'normalisation'.

Ide et al. and Algire et al. highlighted the importance of the abundant blood supply for sustaining tumour growth (Ide et al. 1939, Algire et al. 1945). Systemic antiangiogenic therapy was developed after the hypothesis from Judah Folkman that inhibiting blood vessel formation would result in either dormancy or death of the tumour (Folkman, 1971). Tumour antiangiogenic therapy has been applied for several years now however the precise mechanisms of action are still poorly understood in the intact tumour. The chaotic appearance of tumour vasculature is closely associated with uneven perfusion, hypoxia and increased interstitial fluid pressure (IFP) and as such presents both physiological and physiochemical barriers to effective delivery of cytotoxic drugs (Tannock et al. 2002). Unlike the microvasculature of normal tissues, tumour vasculature is characterised by areas of high and low microvascular density (MVD). At the cellular level the ECs lining the vessel walls have an irregular disorganised morphology often lacking support from pericytes that help maintain the structure of the vessel wall. The use of antiangiogenic directed therapies in combination with traditional antitumour therapies have been proposed to take advantage of a process called vascular normalisation.

Yuan et al. studying pre-clinical human xenograft models described the tortuous vasculature as being re-modelled post introduction of an antiangiogenic VEGF inhibitor resulting in increased vessel permeability and that this re-modelling might also influence malignant cell migration into lymph vessels as well as reducing stromal nutrient and oxygen diffusion (Yuan et al. 1996). Winkler et al. established that cytotoxic therapy proved more effective when given 'during' the re-modelling phase when combining a VEFGR2 blocker with radiation (Wrinkler et al. 2004).

These findings were counterintuitive to the original concept of how AA therapies worked. The central dogma had been that AAs act by shutting down tumour vessels resulting in tumour nutrient starvation, not to improve perfusion. Rakesh Jain addressed this paradox by introducing the concept of vascular normalisation in 2001(Jain et al. 2001).

Previous clinical studies had shown that singularly applied AAs therapy (monotherapy) had at best only a limited effect on reducing tumour growth. Jain et al. hypothesised AAs may in fact normalise the chaotic blood flow by pruning smaller vessels thus increasing the nutrient and oxygen flow in the larger more mature vessels. The normalisation process also reduced areas of hypoxia and acidosis thereby improving radiotherapy response and the delivery of a cytotoxic drugs as well as reducing the conditions thought to aid metastatic disease development. Normalisation resulted in the re-modelling of the existing vessels by modifying leaky endothelial cell junctions resulting in a drop in intratumoural IFP, reduced oedema and induced pericyte recruitment to stabilise existing tumour vessel walls resulting in the development of a more normal vasculature. Jain proposed that a 'therapeutic window' had been created that could be exploited for cytotoxic cell kill. (Jain et al. 2005). Both pre-clinical and clinical studies have added strength to the concept of vascular normalisation post AA treatment (Table(s) 1.3-1.5).

**Table 1.3 Studies reporting improved therapeutic drug delivery**

| Therapeutic compound | Normalisation Strategy | Tumour model | Tumour stromal Delivery | Study |
|---|---|---|---|---|
| **Cytotoxics** | | | | |
| Irrinotecan | A4.6.1 | Colon carcinoma | ↑ | Wildiers et al. 2003 |
| Temozolamide | Sunitinib | Glioma | ↑ | Zhou et al. 2009 |
| Cyclophosphamide | Thalidomide | Liver carcinoma | ↑ | Segers et al. 2006 |
| Temozolamide | TNP-470 | Glioma | ↓ | Ma et al. 2001 |

## Table 1.4 Studies reporting improved oxygenation post AA therapy

| Antiangiogenic (AA) therapy | Tumour model | Effect on oxygenation | Time window of improved oxygenation (days post introduction) | |
|---|---|---|---|---|
| **Antibody therapy** | | | | |
| Avastin | Melanoma, breast carcinoma, ovarian carcinoma | ↑ | 2-4 | Dings et al. 2007 |
| **Small molecule targeting therapies** | | | | |
| Sunitinib | Squamous carcinoma | ↑ | 4 | Batra et al. 2009 |
| Gefitinib | Fibrosarcoma, squamous carcinoma | ↑ | 10 | Qayum et al. 2009 |
| FTIs (Ras inhibitors) | Glioblasoma | ↑ | 35-40 | Bemsen et al. 1999 |
| | Prostate carcinoma | ↑ | | |
| | Bladder carcinoma | ↑ | 7-10 | Cohen-Jonathan et al. 2001 |
| | squamous carcinomas | | 7-10 | Delmas et al. 2003 |
| | Liver carcinoma | ↑ | 7-10 | Wong et al. 2010 |
| **Other therapies** | | ↑ | | |
| Thalidomide | | | 2-3 | Segers et al. 2006 |

**Table 1.5 Clinical studies demonstrating vascular normalisation in humans**

| Tumour type | Ant-angiogenic therapy | Vessel structure change | Vessel function change | Clinical observation |
|---|---|---|---|---|
| **Primary tumours** | | | | |
| Rectal carcinomas | Bevacizumab | Decrease in density, increased perivascular cell coverage | ↓tumour blood flow, ↓IFP, improved FDG delivery | Tumours became pale. Willet et al. 2004 |
| Glioblastoma | Cediranib | Decrease in vessel size | ↓ permeability | Decrease in tumour associated oedema Batchelor et al. 2010 |
| High-grade glioma | Bevacizumab | Decrease arcades and glomeruloid vessels | | Fischer et al. 2008 |
| Prostate carcinoma | Androgen ablation | Immature vessels pruning, increase in perivascular cell coverage | | Benjamin et al. 1999 |
| **Metastatic disease** | | | | |
| HER2+ breast cancer brain metastases | Lapatinib | Decrease in density | | Bullit et al. 2007 |

It has been however limited in the clinical setting due to the difficulties and ethics of repeated biopsy acquisition. Clinical data should improve with the ongoing development of non-invasive imaging systems such as magnetic resonance imaging (MRI) and positron emission topography (PET).

Particular interest in pre-clinical model studies of vascular normalisation has emerged using models that allow direct visualisation of the normalisation process in-situ in response

to AAs and chemoradiation strategies using the non-invasive dorsal window chamber (DWC) model.

Using the DWC murine xenograft model in pre-clinical studies others have confirmed and visualised in 'real-time' the vessel normalisation effects of the small molecular inhibitor of VEGF signalling such as AZD2171 (Cediranib; Recentin) (Williams et al. 2005). In this study Cediranib caused vessel pruning and a normalising of blood flow to the tumour in DWC model xenografts. This helped explain the reduced tumour growth rate seen in complementary conventional tumour growth delay (GD) studies. The improved nutrient flow, in particular oxygen, helped reduce the degree of radioresistance often seen in tumour growth studies and in the clinic. This study demonstrated AAs can complement antitumour strategies such as chemoradiation resulting in the ability to beneficially exploit a 'window' of vascular normalisation (Jain et al. 2001).

### 1.11 Nicotinamide (NA).

NA is one of the two principal forms of the B-complex vitamin niacin. NA, via its major metabolite nicotinamide adenine dinucleotide ($NAD^+$) is involved in a wide range of biological processes including energy production, fatty acid synthesis, signal transduction and maintenance of the integrity of the genome. It is also known to vasodilate cutaneous blood vessels in humans resulting ('niacin flush'). NA has also been shown to reduce arterial blood pressure in rodents suggesting that a vascular component may be part of its mechanism of action (Hirst, 1994).

Studies involving NA and related benzamine analogs suggest a potential role for NA when combined with either single or fractionated radiation regimens by enhancing murine xenograft growth delay (GD).

The enhancement of the tumour GD effects was primarily thought to be due its inhibition of the tumour cells DNA repair mechanisms via its actions as a weak poly (ADP-ribose) polymerase (PARP) inhibitor; however this did not explain its effects on reducing measured hypoxia within the tumours.

This reduction in hypoxia led to the proposal that NA may also have a modifying effect on tumour blood flow. It was proposed that NA was modulating the normally chaotic, bi-directional, sluggish, cessant blood flows to form a more uniform normal flow resulting in improved oxygen delivery and hence radiosensitisation of the tumour stroma. These studies resulted in NA incorporation onto RT regimens and formed the basis of ARCON (**A**ccelerated **R**adiotherapy with **C**arb**O**gen (95% oxygen + 5% carbon dioxide) and **n**icotinamide) treatments to reduce to reduce tumour radioresistance (Kaanders et al. 2002). Phase l and phase II trials were carried out resulting in promising results for head, neck and bladder cancers although some degrees of normal tissue toxicity presented. Later clinical trials involving ARCON necessitated the reduction in the concentration of NA (Janssens et al. 2011).

Radiation causes cellular damage via the production of hydroxyl radicals that induce DNA single-strand/double-strand breaks (SSBs/DSBs), base pair damage or cross-linking damage. Of the two strand breaks types the DSBs are more lethal, but SSBs are approximately 25-fold more numerous. In non-dividing cells PARP inhibition causes a delay in SSBs repairs, but doesn't impact significantly on DSBs. In rapidly dividing cells however, such as tumour cells, the effects of non-repaired SSBs can lead to potentially lethal DSBs (Dungey et al. 2008).

## 1.12 Poly (ADP-ribose) polymerase (PARP).

PARP has been found to play a crucial role in normal cellular functions, in particular the mechanisms involving DNA repair, replication, differentiation and genomic integrity. PARP is a nuclear enzyme which detects damaged DNA where it binds to DNA single or double strand breaks and then uses nicotine adenine diphosphate ($NAD^+$ ) as a substrate to form nicotinamide and ADP ribose. It is an important protein in DNA repair processes that involve base excision repair (BER). If BER is impaired in damaged cells in the presence of PARP inhibition single strand breaks (SSBs) can accumulate and result in DNA double strand breaks (DSBs). As a result the damaged cells try to find alternative repair mechanisms such as homologous recombination (HR) and non-homologous end joining.

Interest has recently focussed on tumours that express homozygous mutations in both the BRCA1 and BRCA2 breast cancer genes. BRCA1 is expressed in the cells of breast and other tissues, where it helps repair damaged DNA, or destroy cells if DNA cannot be repaired. If BRCA1or BRCA2 itself is damaged, damaged DNA is not repaired properly and this increases risks of cancer development (Venkitaraman et al. 2009).

The BRCA1 gene has been found to be very sensitive to PARP inhibition (Farmer et al. 2005, Bryant et al. 2005). In addition BRAC1 and BRAC2 were identified as having a role homologous (HR) and non-homologous end joining (NHEJ) DNA repair processes and that continuous subsequent exposure of the cycling cells to the PARP inhibitors resulted in the accumulation of lethal DNA DSBs.

Some breast-ovarian tumour patients with defective HR are found to have hereditary BRCA gene mutations resulting in ‘hereditary breast-ovarian cancer syndrome’ making them more susceptible to base excision repair (BER) pathway impairment.

Despite the fact that a great deal of data regarding the toxic effects of PARP inhibitors on tumour cells (Mendeleyev et al. 1995, Curtin et al. 2007) has been reported more recent studies have focussed on the potential role of PARP inhibitors as potentiators of alkylating agents or ionisation radiation therapies in antitumour directed therapies.

### 1.12 PARP inhibitors and antitumour therapy.

In the presence of DNA damage PARP functions to enhance repair and mitigate the effects of damage between sites on the strands. However by activating and increasing the activity of PARP the availability of $NAD^+$ is markedly reduced.

This could lead to the initiation of cellular apoptosis as well as triggering an inflammatory response due to the presence of cellular necrosis and cell lysis products. The cytotoxic effects of DNA damaging agents have been shown to reduce cellular $NAD^+$ levels by up to 80% and therefore reduce the level of ATP production needed to effect repairs in DNA strands. In the context of a potential antitumour therapy the impact of PARP inhibition on DNA repair seems to be of greater significance than the effect of $NAD^+$ depletion.

Natural endogenous inhibitors of PARP include Nicotinamide (NA) and 3-aminobenzamide have limited cellular uptake and cellular residence time often exerting non-specific effects such as acting as an antioxidant (Szabo and Dawson, 1998a).

The effects of PARP inhibition can vary according to the cellular environment and in particular the presence of DNA damage and/or metabolic stress (Tentori et al. 2002). Additional studies have shown the consummate relationship between the effects of radiation and PARP activity using cell lines and knockout mice (generated to lack PARP expression) supporting the potential use of PARP as a target for radiopotentiation (Wang et al. 1998, de Murcia et al. 1994 ).

In addition to the direct effects on DNA-repair some PARP inhibitors have been identified as mediating a secondary tumour radiation response via their vasomodulatory effects on tumour vessels (Calabrese et al. 2004). Studies have shown that PARP inhibition can enhance the effects of a range of cytotoxic agents in both pre-clinical *in vitro* and *in vivo* models (reviewed Plummer and Calvert, 2007, Tentori et al., 2005). Briefly; some PARP inhibitors (that largely fall into the categories of monoaryl amides and bi- tri or tetracyclic lactams) have been shown to enhance the cytotoxic effects of alkylating agents such Temozolomide (TMZ) and topoisomerase I poisons such as Irrinotecan (IRR) without the need to use drug concentrations that would normally result in systemic tissue toxicity.

Several PARP inhibitors are currently being evaluated in pre-clinical and clinical studies with a view to using them as adjuvants to current chemoradiation regimens although the precise mechanisms have yet to be fully elucidated (Table 1.6).

**Table 1.6 PARP inhibitors and combined therapies.**

| PARP inhibitor | Cytotoxic agent | Model | Tumour | Effect | Reference |
|---|---|---|---|---|---|
| **AGO14699** | TMZ | Human | Malignant melanoma | Encouraging response rates | Plummer(2005) |
| **AG14361** | TMZ, IRR | Mouse xenograft | Colorectal SW620/LoVo | Enhanced growth delay | Calabrese(2004) |
| **AZD2281** | TMZ | Mouse xenograft | Colorectal SW620 | Enhanced growth delay | Calabrese(2004) |
| **CEP-8983** | TMZ | Mouse xenograft | Colorectal HT29, rat glioma RG2 | Enhanced growth delay | Miknyoczk(2007) |

In recent studies the PARP inhibitor AZD2281 caused growth arrest and shrinkage of BRCA1-deficient tumours in mice without toxic side effects (Underhill et al. 2011).

It was also found that removal of AZD2281 resulted in the regrowth of these tumours, but when challenged a second time after having reached their original treatment size, then AZD2281 did not produce tumour growth delay (GD)(Underhill et al.,. 2011). AZD2281 has also been used in studies as an adjuvant to chemotherapies in the presence of cisplatin and carboplatin resulting in a transient increase in murine xenograft GD (Rottenberg et al. 2008).

Pre-clinical studies also indicate a potential role for PARP inhibitors as radiosensitisers. Murine SW620 (human colon) xenografts in combination with AG14361 and RT produced increased tumour GD (Calabrese et al. 2004) also seen in colorectal and lung cancer xenografts treated with ABT-888 (Donawho et al. 2007, Albert et al. 2007). Numerous groups are currently carrying out studies to identify not only the tumour types that are most susceptible to PARP inhibition, but also to determine the possible modes of action particularly if they have the same modulatory effects seen with NA.

### 1.13 Developing models for studying tumour vasculature.

The science of developing pre-clinical models to investigate the effects of anticancer therapies established itself after the derivation of some basic ground rules and experimental endpoints first set up by Howard Skipper in the 1960s. Through extensive work both *in vitro* and *in vivo* Skipper and co-workers went on to develop very sensitive and reasonably quantitative *in vivo* bioassays that allowed anatomical distribution and rate of proliferation of the leukaemic cell line P388 to be measured (Skipper et al. 1974 ).

These studies allowed the effects of drug dosing to be more clearly understood (Skipper, 1974, Simpson-Herren, 2006). Later solid tumour models were developed and the appropriate end-points were expressed as tumour growth delay (GD) or tumour control.

Tumour GD is the time it takes a tumour to reach a given volume (measured usually in days) post manipulation with a modifying therapy or agent compared to the time measured growth rate profile in the absence of any potentially influencing factors i.e. its normal growth rate profile .

The basis of these models was to test therapy doses that produced an effect on the tumour growth with the minimal toxicity to surrounding tissues. Tumour growth inhibition studies were described as studies where the treatment agent was given at the same time as the initiation/inoculation of the tumour cells and tumour GD was described as commencement of a treatment post establishment of a tumour mass at 50-200$mm^3$.

Although often not appreciated enough the establishment of reproducible *in vivo* model protocols with defined endpoints and measurable parameters is the fundamental basis of good tumour model research.

The use of animal models, though controversial in some areas, is the only method currently available that can be measured in a cost effective reproducible ethical manner. The use of immuno-compromised mice and xenografts implants as a model to study human tumour cell lines has been invaluable in the study of tumour initiation and growth (Gitler, Monks et al. 2003, Kelland, 2004).

However the influence of mouse/human tumour stroma and the contribution of subcutaneous ectopic sites currently used have raised questions as to whether we are seeing non-characteristic stroma responses to applied therapeutic regimens for a specific tumour type.

As a direct result there is a move to develop orthotropic tumour xenograft models where the tumour cell line is grown in its tissue of origin and hence a more 'natural' series of tumour dynamics should present (Bibby, 2004). Continued development and refinement of current xenograft models has resulted in the development of new tools where tumour cells have been labelled with green fluorescent proteins (GFPs), red fluorescent proteins (RFPs) or firefly luciferase (Cao et al 2005, Hoffman et al. 2006, Amoh et al. 2008).

The continuing development of tools such as these will significantly impact on our understanding of how tumour masses respond to therapy *in vivo* and allow us to study the tumour microenvironment as a whole. There are now developments aiming to look at some of these tumour models *in vivo* in real-time and non-invasively.

The advantages of these advances are self evident in that we are moving closer to being able to measure *in situ* tumour physiological responses to applied therapies as they modulate the tumour microenvironment.

Although some currently available 'tools' are available to image tumour microenvironment response to applied therapies such as positron emission tomography (PET) (Ren et al. 2009, Benchaou et al. 1996) computed topography (CT) (Pickhardt et al. 2005, Choquet et al. 2007) ultrasound (Laser Doppler) (Gee et al. 2005, Palmowski et al. 2008) and magnetic resonance imaging (MRI) (Nelson et al. 2003) they currently do not have the desired spatial resolution required to monitor events at the cellular level.

One non-invasive method that allows both temporal and spatial studies to be carried out on tumour physiological parameters is the dorsal window chamber intravital microscopy (DWC/IVM) model (Papenfuss et al. 1979, Dewhirst et al. 2002).

The DWC/IVM model has allowed researchers to measure, both directly and continuously, the process of tumour vessel growth and its response to therapy manipulation.

Through continuous modification of the DWC and development of IVM technology and software analysis it is now possible to study tumour growth from a few tumour cells up to a 100mm$^3$ volume using the DWC under controlled conditions (Dewhirst et al. 2002).

### 1.14 The dorsal window chamber (DWC) xenograft model.

Studies by Folkman and co-workers investigating tumour angiogenesis relied on *in vivo* assays models, such as the chicken chorioallantoic membrane (CAM) and the rabbit corneal models (Folkman et al. 1971).

Most other studies involved the use of *in vitro* models to measure tumour proliferation, cell migration and differentiation of vascular cells such as human umbilical cord vein endothelial cells (HUVEC), human microvascular endothelial cells (HMVEC) and smooth muscle cells (SMCs) evolving into more complex angiogenesis assays such as the tumour spheroid model in which the co culture of two or more cell types were used to study the pharmacodynamics of applied therapeutics. Although these models produced some pharmacokinetic and pharmacodynamic information with regard to the angiogenic signalling transduction pathways, they cannot, with any real accuracy, mimic the 'truer' microenvironment of an *in situ* tumour. *In vitro* assay models lack the ability to represent the complex interplay between the surrounding tumour stroma and the host's vasculature.

Histology provides a detailed insight into tumour tissue pathology, but these tissues have to be removed from their original site, processed and stained before a 'snapshot assessment' is possible. It was thought that it would be advantageous if a cost effective *in vivo* model

could be developed allowing non-invasive *in-situ* 'real-time' chronic tumour vascular responses to be measured without the need for complex biochemical tissue processing. This resulted in the development of the dorsal window chamber (DWC) xenograft model.

The study of microvasculature *in vivo* using chamber models is not new. As early as 1924 Sandison used early preparations to view the microvasculature of the rabbit ear (Sandison, 1924). Since then there have been repeated modifications depending on the species, materials available and improvements in surgical techniques. Algire in the early 1940's adapted the chamber so that it he could observe the microcirculation of murine subcutaneous skin (Algire et al. 1943). Endrich et al. 1980 adapted the DWC (Fig. 1.9) and introduced tumour pieces into the chamber in order to measure tumour oxygen concentrations using phosphorescent dyes.

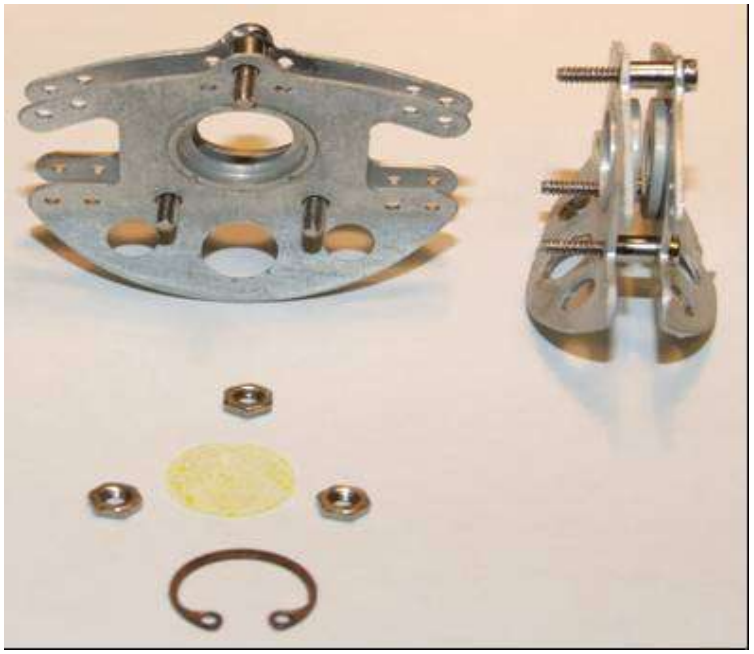

**Fig. 1.9** Fabrication of the dorsal window chamber (DWC). The DWC consists of two aluminium frames that marry together to form a saddle on the back of the mouse and is attached using spacers, bolts and fastening nuts. A glass coverslip covers the area created by the 8mm diameter resected dorsal skin and is held in place using a 'C' clip.

Further adaptations and modifications led to its use for studying microvasculature (Kerger et al. 1995), wound healing (Devoisselle et al. 2001), interstitial tumour pressure gradients (Jain and Ward-Hartley, 1987), fluid transport in tumours and the penetration of chemotherapeutics into tumour stroma (Leung et al. 1989, Hak et al. 2010). The DWC model allowed chronic and repeated visualisation and measurement of tumour stroma pathophysiological parameters to be made for up to 3-4 weeks using the same preparation.

### 1.14.1 Fluorescent markers for tumour pathophysiological measurements.

The quality and quantity of information gained from DWC intravital microscopy (IVM) tumour vasculature studies has improved markedly over the past few years with the introduction of fluorescent dyes and labelled proteins (Shaner et al. 2007).

Early IVM brightfield trans-illumination provided tumour vessel morphological information such as vessel length, diameter, branching patterns and blood flow (Endirch et al. 1980).

Although a great deal of information was obtained in these early studies it has been the introduction of fluorescently labelled molecules that has provided us with even more insight into the tumour microenvironment, its pathophysiological functions and how it responds to manipulation. The development of synthetic dyes such as the Alexa fluor dyes (Alexa® 350, 488, 549, 647 etc) conjugated with bovine serum albumin (BSA) to form a spectral range of AlexaBSAs has resulted in their use as potential markers mirroring tumour vascular blood flow and permeability for therapeutic modulation studies (Shannon et al. 2009, Tozer et al. 2008, Williams et al. 2007, 2008).

The AlexaBSAs have helped to overcome previously encountered problems using fluorescein isothyocyanate (FITC) organic dyes. FITC based fluorophores are prone to photobleaching (Berk et al. 1993), whereas AlexaBSAs are more stable and hence allow greater duration of different parameter measurements.

Through the continuing development and increased commercial availability of live green, blue, yellow, red and far red fluorescent proteins (GFP, BFP, CYP, YFP, DsRed and HcRed, respectively) it is now possible to study several parameters at the same time within the tumour stroma (Lunt et al. 2011). By creating transgenic cell lines and animals that constitutively express GFP or its spectral variants under the control of the promoter genes of interest, it is also possible to measure multiple tumour stromal parameters in the same preparation at the same time (Fukumura, 1998, 2001).

### 1.14.2 Intravital microscopy (IVM).

In the past we have had to rely on invasive techniques when measuring either genetic function or physiological and anatomical responses in tumour tissues post modulation. This had limited us to studying tumour responses *ex vivo* and subsequently we could not determine the temporal dynamics of an applied therapy. Recently advances in optical equipment have significantly improved imaging quality up to a 1000-fold magnification using trans and epi-illumination (Menger and Lehr, 1993). Combining IVM with time-lapse video recording and computer software analysis has allowed sophisticated off-line analysis of complex dynamic microcirculatory processes (Lehr et al. 1993).

These capabilities have lead to the use of IVM technology to study a large range of tissues *in-situ* with the minimum of influence from post surgical manipulation and include for example brain (Unterberg et al. 1984), heart (Kong et al. 2001), lung (Kuhlne et al. 1993)

kidney (Steinhausen et al. 1976) in different laboratory animal species. Coupled with the advances in the production of fluorescent markers, mentioned before, we now have a measuring 'tool' that is minimally invasive and minimally impacts on macro- and micro-haemodynamic parameters allowing us a clearer picture of vascular, cellular and molecular functional responses to therapeutic manipulation. Through the development of a model that allows tumour vasculature to be imaged in real-time and *in situ* previous limitations have been overcome. It is now possible to measure physiological changes in tumour microvasculature, to measure pH change (Martin and Jain, 1993), oxygen gradients (Helmlinger et al. 1997) and tumour vessel cell recruitment (Nickerson et al. 2009).

### 1.15 Aims and objectives.

The introduction presents the case for molecular targeted therapy of cancer and identified approaches such as PARP, MAPK and VEGF inhibitors and their potential roles as beneficially effective therapeutic modulators. Identifying and targeting targets, thought to be associated with tumour stromal cells and their responses to different applied therapy regimens within such a complex system as that found in tumour host tissue, is exceptionally difficult to predict. Anti-angiogenic or anti-vascular therapies are controversially linked to the effectiveness of other therapies such that, evaluation of combination therapies is even more difficult to decipher. For this reason *in vivo* research models are indispensible in the study of the development of novel classes of drugs (more so than for 'conventional' drugs) and the effects of monotherapeutic or combined therapeutic strategies. The DWC xenograft model can provide additional valuable information/insight regarding the mechanisms of action of applied therapeutics at the microenvironment level to add to the information gleaned from conventional murine tumour xenograft growth delay studies.

Using the DWC model a time-lapse stromal response to a therapy can be qualitatively and quantitatively assessed in real-time without the need for large numbers of tumour bearing mice, large number of time-point sampling and costly additional histological analysis. The DWC model also gives us an insight into the stromal responses to therapy regimens that cannot readily be achieved in the clinical setting.

The work presented in this thesis was conducted as part of a series of ongoing collaborative studies that examined the complex *in vivo* activity of experimental ant-angiogenic drugs either alone or in combination with complementary therapeutics. In addition to performing standard *in vivo* measurements (tumour growth delay, histological analysis etc.) the role of this author was to develop the DWC model to complement these methods and provide insight into the vascular permeability to macromolecules, or on a longer timescale changes to vascular architecture changes that may be separate from other ant-tumour effects. As such this work is presented from the perspective of assessing/measuring vascular changes in solid tumours, primarily measured through the use of intravital microscopy (IVM). To understand the specific aim of each results chapter (3, 4, 5, 6 and 7) it is necessary to understand how the DWC/IVM studies contribute to the overall aims of each chapter:

- **In Chapter 3** the aim was to develop and apply the DWC model to characterise the growth characteristics of selected tumour cell lines to be used in parallel with *in vivo* and *in vitro* studies. The objectives included measurement of growth timescales and definition of suitable measurement time-points for vascular manipulation studies.
- **In Chapter 4** the DWC/IVM model was applied in the context of a wider study of the radiosensitisation effects of PARP-1 inhibitors (AG14361 and AG14699) and the structurally similar molecule Nicotinamide (NA). The aim in this chapter was to

develop a fluorescence IVM method to quantify some vascular effects of these agents. It was hypothesised that novel agents like NA would exhibit vascular effects independent of the primary mode of action (inhibition of DNA repair following radiation damage).

- **In Chapter 5** the aim was to study the effects of AZD2171 (Cediranib), a highly potent orally available inhibitor of VEGF receptor tyrosine kinase activity in combination with radiation in Calu-6 lung xenografts. We hypothesised that VEGFR inhibition would enhance radiation response in pre-clinical models and provide a rationale to develop Cediranib in combination with radiotherapy in the clinical setting. In addition we aimed to apply the DWC/IVM model to determine whether it had a direct effect on tumour microvascular function alone or in combination with radiotherapy to complement conventional murine xenograft growth delay (GD) studies and histological analysis.
- **In Chapter 6** the aim was to look at the potential benefit of combining AZD6244 (a small molecular inhibitor of the MAPK signaling pathway) with fractionated radiotherapy using Calu-6 (human lung cancer) to determine whether it had an effect on inhibiting tumour hypoxia response reducing the number of surviving clonogenic cells. In addition we aimed to include the DWC/IVM model to visualise the tumour vascular response hypothesizing the response could be due to compromised functionality.
- **In Chapter** 7 a HIF-1 deficient tumour cell line was developed to investigate the whether the variant would exhibit a different vascular response to radiotherapy from the wild type HIF-1 competent cell line. HIF-1 is known to influence tumour response to radiation therefore we aimed to determine the growth characteristics of HIF-1 deficient cell lines pre- and post radiotherapy. As one of the range of

measurement methods the DWC/IVM model was applied to test the hypothesis that HIF-1 deficient tumour vasculature responds differently from the wt competent vasculature in growth characteristics and post radiotherapy.

# CHAPTER 2 - METHODS AND MATERIALS

## 2.1 Tumour cell preparation.

All tumour cell lines were grown in Roswell Park Memorial Institute medium (RPMI) (GIBCO Invitrogen Ltd., Paisley Scotland) supplemented with 10% foetal calf serum (FCS) (Biosera, UK) and supplemented with 2 mM glutamine (GIBCO Invitrogen Ltd., Paisley Scotland). The cell cultures were maintained in 95% air, 5 % $CO_2$ in a humid environment at 37$^{o}$C. The cells were routinely screened for Mycoplasma contamination (Mycotect® Invitrogen Ltd www.invitrogen.com) and prepared using aseptic procedures.

For tumour inoculation, cells were harvested in the exponential phase of growth. Following trypsinisation and resuspension in 10ml RPMI, a 10µl aliquot was removed and loaded onto a Neubauer Improved haemacytometer (www.labtech.com ). The cells in the four corner squares and the central square were then counted excluding non-viable cells. Cells overlapping the top and left-hand edges were included and overlapping the bottom and right-hand edges excluded. The total number of cells for the five squares were then averaged and multiplied by a factor of $10^4$ to give the number of cells/ml in suspension.

Where a support matrix is required, as for Calu-6 tumour cells, these were made up in a final volume of a 1:1 mix of serum free RPMI and Matrigel™ (phenol red-free BD Biosciences UK). The tumour xenograft cell line origin and cell inoculation concentrations (unless otherwise stated) were summarized (Table 2.1).

**Table 2.1 Tumour cell line origin and inoculation concentrations.**

| Cell Line | Origin | Inoculation conc. cells/ml | Source |
|---|---|---|---|
| **HT29** | Human colon carcinoma | $5x10^7$ | ATCC atcc@gstandards.com |
| **Hepa-1wt** | Murine hepatoma (HIF-1β competent) | $5x10^6$ | Wellcome Trust Centre for Human Genetics, Oxford |
| **Hepa-1c4** | Murine hepatoma (HIF-1β deficient) | $5x10^6$ | Wellcome Trust Centre for Human Genetics, Oxford |
| **SW620** | Human colorectal adenocarcinoma | $1x10^7$ | ATCC atcc@gstandards.com |
| **HCT116** | Human colon | $5x10^7$ | ATCC atcc@gstandards.com |
| **Calu-6** | Human pulmonary adenocarcinoma | $2x10^7$ | ATCC atcc@gstandards.com |
| **LoVo** | Human colorectal adenocarcinoma | $5x10^7$ | ATCC atcc@gstandards.com |

## 2.2 Tumour xenograft models.

All xenograft studies used adult (8 weeks $^+$) female nude (immuno-compromised) mice. The mice were housed using an individually ventilated caging system (IVC) and supplied with sterile feed and water *ad libitum* and subjected to alternate 12 hour light and dark cycles. All procedures employed in this study were approved by the UK Home Office Inspectorate, the supervised by the designated named animal care welfare officer (NACWO) and The University of Manchester Ethics Care Committee. All *in vivo* procedures and techniques followed Guidelines for the welfare and use of animals in cancer research (Workman et al. 2010).

### 2.2.1 Tumour cell implant.

Cells were implanted into the aseptically prepared skin layer via the intradermal route (i/d) on the mouse dorsal midline 1 cm from the tail base in a 0.1ml volume (standard adopted volume for injection of cells). The weights and condition of the mice were monitored and recorded at least three times weekly, but more frequently when a treatment commenced. Developing tumours were measured using callipers and volumes recorded up to three times per week or more frequently if required. The xenograft tumour volumes were calculated using the formula length (l) x breadth (b) x height (h). For DWC xenografts a 20-30µl volume of cell stock solution was introduced into the chamber using a 27G syringe needle (Table 2.1) (unless otherwise stated). The volume of the DWC tumours was calculated using an oblate spheroid formula $V=4/3 \times \pi \times r^2 \times t$ (where t = the thickness of the protruding DWC tumour, measured by callipers) and for vascular studies a range of 50-100 $mm^3$ was used.

### 2.2.2 Tumour xenograft irradiation.

Non-anaesthetised tumour bearing mice were restrained in specifically designed jigs before each localised radiotherapy (RT) X-ray dose (Fig. 2.1). The X-ray dose rate was calibrated to produce 2Gy per minute with tumour bearing mice being turned round halfway through a dose to ensure even tissue exposure. The X-ray room had adjustable temperature control and was maintained at 23-25°C throughout.


**Fig. 2.1** Tumour irradiation apparatus. The image on the left shows a side-view of the MXR-320/36 X-ray apparatus with a tumour bearing mouse (X-rays were delivered in the horizontal plane). The image on the right shows a tumour bearing nude mouse in a polyvinyl restraining jig (black) with lead shielding (grey) with maximal exposure of the tumour to the X-rays and minimal exposure to other tissues.

A fabricated ventilated lead shielded jig was used obviating the need for sedation. Variable X-rays doses were delivered via a metal-ceramic X-ray tube assembly MXR-320/36 (Comet AG, Switzerland 320kV).

## 2.3 Drug concentrations and delivery routes.

All drugs were prepared on the day of use using either the intraperitoneal (i/p) route or the oral route for delivery (Table 2.1). The Alexa594 or 647 dyes conjugated with bovine serum albumin (Alexa594BSA or Alexa647 BSA) and Hoechst were the only compounds injected via the tail vein intravenous route (i/v) (Table 2.2).

**Table 2.2 Drug concentrations and delivery routes for xenograft and DWC studies.**

| Drug | Dose (per kg) | Carrier concentration | Source | Dose frequency | Route |
|---|---|---|---|---|---|
| **Nicotinamide** | 1g | 0.9% saline | Sigma Aldrich | Single | i/p |
| **AZD2171 (Recentin)** | 3mg or 6mg | 1% Polysorbate | AstraZeneca | Single | oral |
| **AZD6244** (**Selumetinib**) | 25mg | 0.5% hydroxypropyl methyl cellulose + 0.1% polysorbate | AstraZeneca | Split dose (8h between doses) | oral |
| **AG14361** | 5-15 mg | 0.9% saline | Pfizer Oncology | Single | i/p |
| **AGO14699** | 1-10 mg | 0.9% saline | Pfizer Oncology | Single | i/p |

## 2.2 The attached dorsal window chamber (DWC).

The chamber was made up of two separate aluminium plates (total weight 2.5g) that 'marry' together to form a unit that saddles the dorsal midline skin of the mouse (Fig. 2.2).

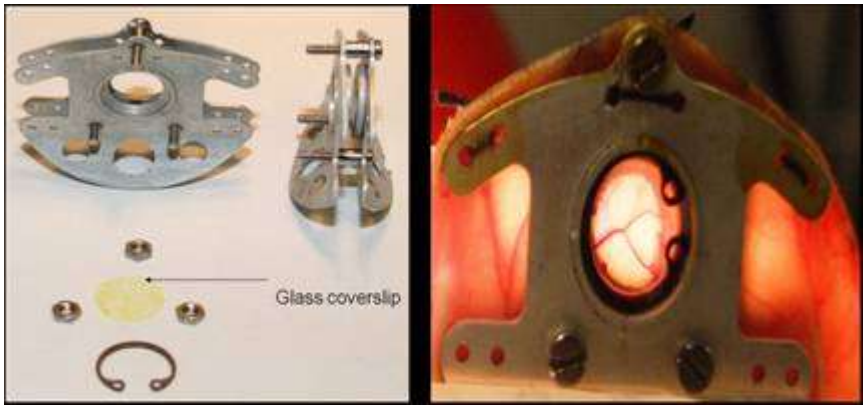


**Fig. 2.2** Machined anodized aluminium sections, spacers, nuts, glass coverslip and fastening 'C' clip. When attached with additional sutures, the opposing fascia of the attached dorsal window is translucent containing clearly visible flowing vessels when viewed using brightfield trans-illumination intravital microscopy (IVM).

Preparation of the mouse dorsal skin fold chamber allows for the removal of an 8mm diameter piece of skin (made up of an epidermal layer, dermal layer, subcutaneous fat, muscle layer, connective tissue and fat) in one surgical procedure leaving the opposing fascia layer and vessels intact. Spacers between the two halves of the saddle ensure

uninterrupted blood flow in the opposing fascia. A ‘chamber’ was formed after a transparent glass coverslip was placed onto the attached saddle covering the exposed fascia containing vessels and secured using a sterile removable ‘C’ clip (Fig. 2.2).

Visualisation of the intact opposing skin vasculature was achieved by placing the DWC on a specially designed heated microscope stage (Fig. 2.3) and using brightfield trans-illumination or fluorescence excitation epi-illumination for perfusion studies. The newly formed chamber allowed for the introduction of tumour cell suspensions, typically 20-30µl volumes using a 25G 5/8” sterile syringe (BD Microlance™, BD Drogheda, Ireland).

The transparency of the opposing fascia layers allowed brightfield illumination of the opposing skin vasculature and subsequent repeated imaging. Labelled fluorescent perfusion markers were also imaged using epi- fluorescence illuminations (ε-F) and intravital microscopy (IVM) (Fig. 2.3, Table 2.2).

## 2.4 Preparation of the window chamber hardware.

Surgical instruments were cleaned using the enzymatic tissue digester Endozyme (Ruhof NY USA www.ruhof.com ) before being triple washed in distilled water and, together with all glassware, autoclaved immediately prior to surgery. Aseptic surgical procedures were carried out throughout DWC attachment.

For surgical attachment adult nude female mice were anaesthetised using a combination of Ketamine/Xylazine 100mg/ kg + 10mg /kg i/p respectively (Pfizer Ltd, Kent, UK) giving good surgical anaesthesia for 30-40 minutes (Flecknell, 1996). Mice also received an analgesic Buprenorphine (Vetergesic® http://www.alstoe.co.uk/ ) at 0.1mg/kg via sub-cutaneous(s/c) injection immediately before surgery and post operatively if necessary.

### 2.4.1. Surgical attachment of the (DWC).

The dorsal skin area was first swabbed with Betadine® antiseptic solution (Sefton Healthcare Group Plc, Oldham UK) and then twice with 70% ethanol. Firstly the dorsal skin was drawn up into a tall thin fold that extended caudally along an ink marked mid-line drawn using a sterile pen (Viomedex www.viohealthcare.com ). The drawn up skin was then attached using 2-0 gauge Ethicon Mersilk (Johnson & Johnson Intl, Belgium) sutures to a supporting 'C' frame bridge plate allowing the dorsal skin to be 'fanned' out. Once supported, an 8mm diameter disc of skin was cut away from the middle of the fold on one side leaving the opposing fascia with associated vasculature intact.

Three hole punches were made to correspond to the three spacer bolts that connect the male and the female saddle sections (Fig. 2.2). Once the chamber was fixed in place the exposed inner subcutaneous tissue was washed in 0.9% saline and covered using a fitted glass cover-slip which was held in place using a retaining 'C'ring. Additional sutures were added to further secure the chamber (3-0 gauge Ethicon Mersilk, Johnson & Johnson Intl, Belgium). The supporting 'C' frame bridge plate was then removed and all suture wounds swabbed with antiseptic Betadine® solution. To avoid possible mouse dehydration post surgery, a 1ml volume of 0.9% saline was given (i/p).

The DWC mice were allowed to recover for 2-3 hours in an incubator at $32^{o}$ C with 35% humidity before being returned to an individually ventilated cage experiment rack.

The DWC surgical attachment wounds were allowed to rest for 48-72h. Immediately before inoculation with the desired cell line the DWC was assessed for flowing vasculature using IVM brightfield trans-illumination. If no flowing vessels were present the DWC protocol was stopped.

Tumour cells were introduced into the window chamber from the opposing side to the glass cover-slip using 25G needles (BD Microlance™ Becton Dickinson Ltd., UK). The DWC was assessed daily and the condition and weight of the mice recorded.

## 2.5 IVM apparatus data acquisition and analysis.

### 2.5.1 Protocol for DWC mouse IVM imaging.

Animal movements have to be minimised for successful long term imaging (e.g. $60^{+}$ minutes), and therefore DWC mice were anaesthetised using a 2-3% isofluorane mixture (initiating dose) reduced to a 1.5% mixture (maintenance dose) (www.**baxter**.com/ ). Isoflurane was the anaesthetic of choice since it has been shown to have minimal influence on the blood vessel vasoconstriction, hypotension and hence blood flow when used for long periods (Baudelet and Gallez, 2004). The DWC mouse was placed on a specially adapted heated stage and the temperature of the IVM room was maintained at $28^{o}$C. The mouse body temperature was monitored during surgery using an infrared thermometer (TECPEL 512, Taiwan) and a rectal thermometer (TES 1319 K-Type, Taiwan).

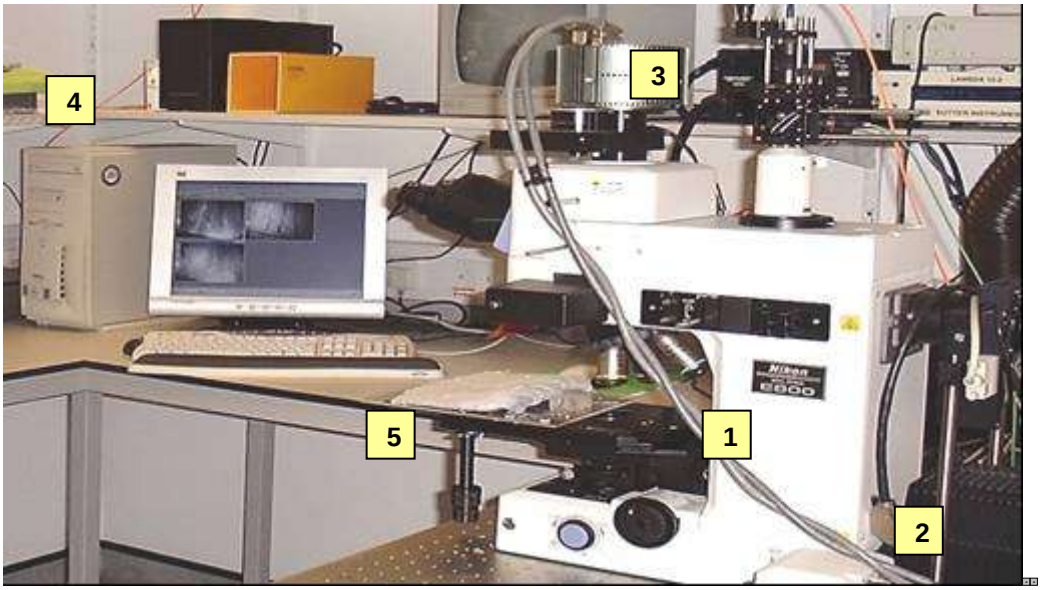


**Fig. 2.3** Basic components of the IVM time-lapse acquisition apparatus in a temperature controlled room, (1) Nikon E800 upright compound microscope, (2) fluorescence excitation source (mercury arc lamp and filters for epi-illumination) and halogen lamp for brightfield trans-illumination, (3) digital camera in-line with interchangeable fluorescence wavelength filters, (4) imaging storage and software package MetaMorph®, (5) adjustable heated fabricated microscope stage.

Images of the tumour vasculature in the window chambers were captured with a mounted scientific grade CCD camera with an intensity resolution of 12 bits (0-4095 grey levels). The image exposure time was adjustable over a range of 10ms to several seconds.

Time-lapse images could be acquired at a video rate of ~ 25 images per second, but were typically acquired a slower rate of 1 image every 10 seconds or later at 1 image per minute for longer time-lapse studies. The Micro-Max monochrome digital camera (RS Roper Scientific Tucson AZ USA http://www.roperscientific.com/) was linked to a large capacity storage hard drive (Fig 2.3). The Meta-Morph® software package (version 6.0/6.1) was used for off-line time-lapse imaging and quantitative brightfield image acquired measurement analysis.

### 2.5.2 IVM time-lapse imaging analysis.

The IVM fluorescent time-lapse data logs were transferred to Microsoft Excel spreadsheets and analysed. Background fluorescence (Fb) was recorded for each time-lapse session. The DWC mice were prepared for IVM and injected i/v with either Alexa549BSA or Alexa647BSA as described earlier. Equilibrated tumour vasculature perfusion of the Alexa BSA plasma protein was observed as a fluorescence intensity plateau (Fp) after 5-10 minutes post i/v injection (Section 2.8). The Fp values for the Alexa BSA perfusion marker during in the first 5-10 minutes can be used as a baseline measure of how open/perfused the tumour vessels were between IVM time-lapse sessions.

The plateau value of Fp-Fb may vary between sequential time-lapse measurements using AlexaBSA, i.e. from day 1 to day 5, indicating a change in how open the tumour vessels were at that time-point. The values for Fp-Fb were used as a measure of the status of the vessels at the initial introduction of the AlexaBSA showing measurable values for how perfused the vasculature was between successive IVM time-lapse measurements. Time-lapse data was normalised to derive a relative fluorescence increase value (RFI) using the following formula where; Fx is the average fluorescence intensity value from the raw data plot (Fig. 2.4) between successive 1 minute interval time-lapse intensity values: **RFI= (Fx-Fb)/(Fp-Fb)** as shown in Fig. 2.5. The RFI values can then be tabulated for different vascular modulating treatments.

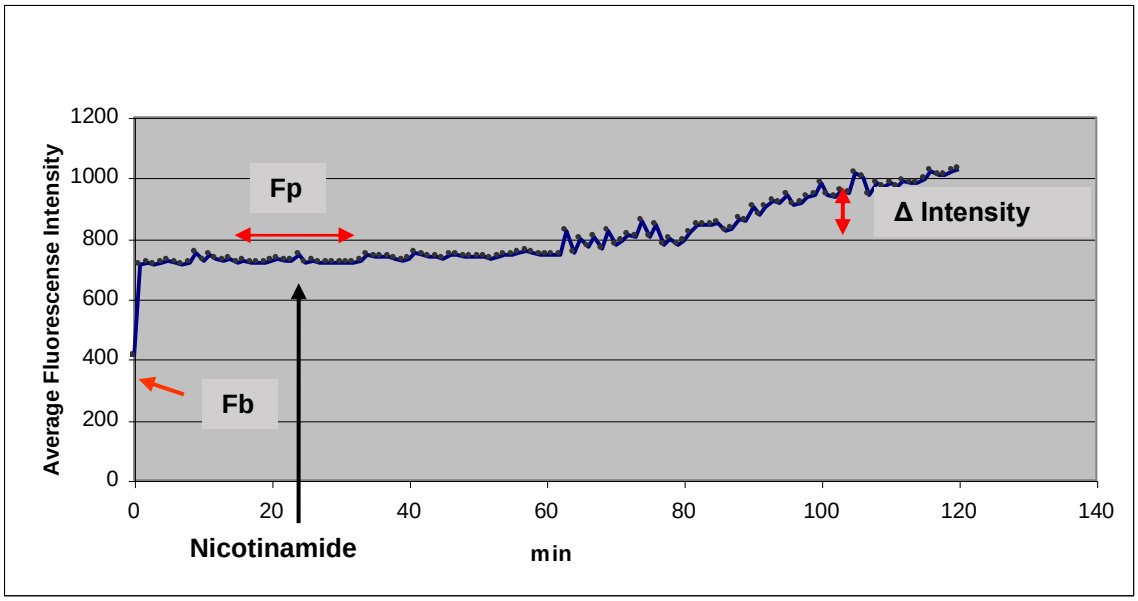


**Fig. 2.4** Effects of NA on HT29 tumour vessels. Time-lapse IVM fluorescence data for HT29 tumour vessels perfused with AlexaBSA conjugate. Background average fluorescence units (Fb) =400. Fp= perfusion plateau average fluorescence values at 1 minute intervals. Nicotinamide (1g/kg i/p) injected at t=23 minutes. Δ=Increase in average fluorescence intensity from initial plateau (Fp).

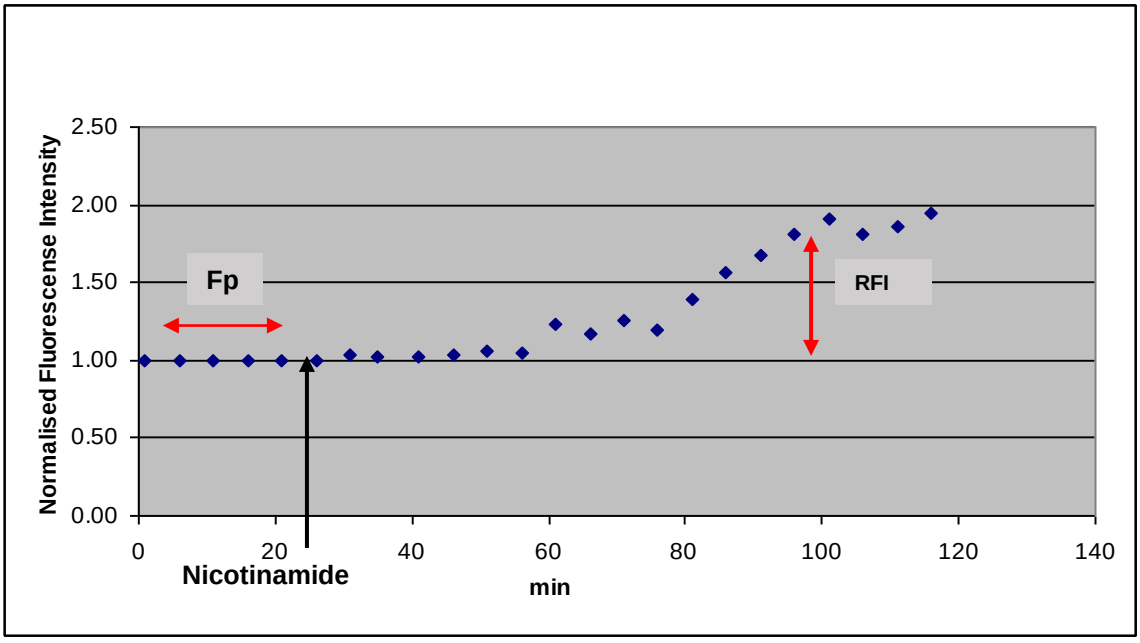


**Fig. 2.5** Relative Fluorescence Intensity (RFI) data for Fig.2.4 showing a twofold increase in measured AlexaBSA fluorescence in the HT29 DWC tumour stroma.

## 2.6 Tumour microvascular density (MVD) analysis method.

Tumour MVD values were calculated using brightfield images of the DWC tumour vasculature and the imaging software package ImageJ by Rasband WS et al. at www.macbiophotonics.ca/ The MVD value was expressed as the percentage thresholded pixilated area within the region of interest (see Fig. 2.6 for worked example).

ImageJ is a Java-based image processing program that can edit, analyse and process 8-bit, 16-bit and 32-bit images including .tif, .gif and jpeg images. It is a public domain program developed at the National Institutes of Health in the USA. Another affiliated site, more suited to vascular imaging studies was www.macbiophotonics.ca/imagej/ ImageJ calculates area and pixel value statistics of regions of interest (ROI) and intensity 'thresholded' IVM 'stack' images.

The image is loaded into the ImageJ program (in a .tiff format) and where the illumination level or background brightness level varies i.e. is non-uniform especially towards the edge of the image, some degree of distortion and also some difference in photon loss needs to be corrected for before additional analysis. By using the image overlay 'flatten' function in ImageJ we corrected for this. Next (after changing the image to an 8 bit format) the image was passed through a broadband pass filter (FFT). The FFT filtering removes the slowly varying gray level pixel information to produce an image that was then thresholded for pixel intensity. The pixel intensity thresholded image was used to create a binary image of black vessels on a white background. The vascular (black) fraction of the image for the region of interest (ROI) occupies a fraction of the total recorded image and as such can be expressed a percentage of the total area i.e. MVD%.

The image was then saved in a binary image format for later display. A worked example is given in Fig. 2.6.

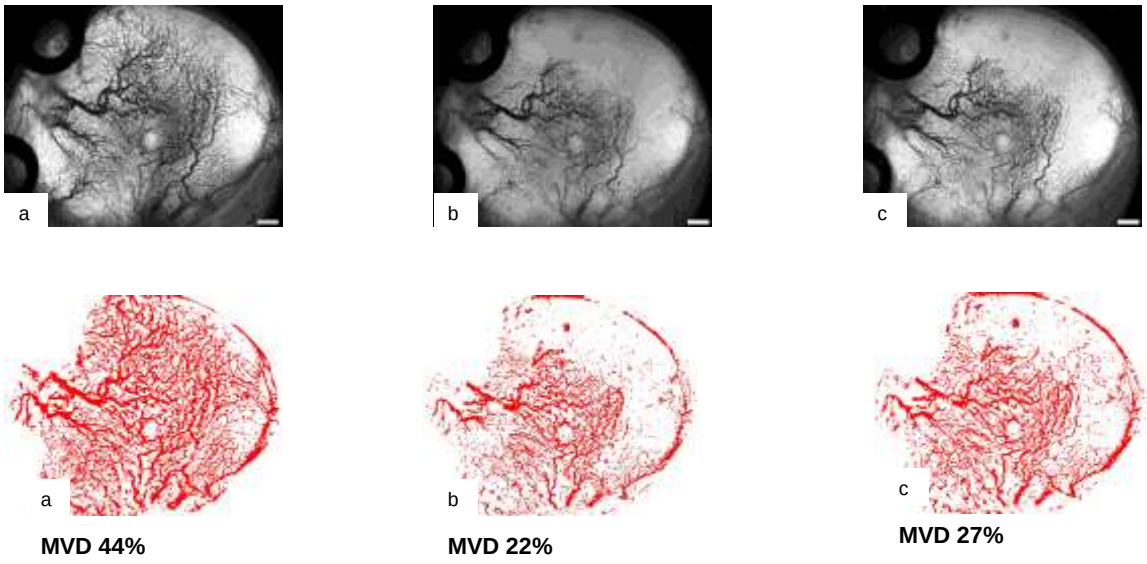


**Fig. 2.6** Worked example of microvascular vessel density (MVD) measurement**.** a) Brightfield IVM image of DWC xenograft day15 vasculature and measured MVD%, b) MVD % value 30 minutes after introduction of drug X, c) MVD% 60 minutes post drug X introduction.(Scale bar 500μm).

## 2.7 Tumour vascular perfusion markers for DWC tumours.

Alexa594®BSA and Alexa647®BSA (Molecular Probes, Invitrogen, Oregon, USA) were chosen due to good separation of their emission spectra epi-fluorescence excitation and to avoid absorption by haemoglobin of the emitted fluorescence (Table 2.3). The AlexaBSA Fluorophores were made up into stock solutions using sterile 0.9% saline at 1mg/ ml and injected i/v in a 0.1ml volume via the tail vein when time-lapse studies were initiated. Either AlexaBSA perfusion marker could be used for DWC/IVM tumour vascular time-lapse studies as the molecular weight for both is 66 kD). The AlexaBSA perfusion markers allowed good spectra epi-fluorescence separation using the corresponding filters to measure optimal peak emission (Table 2.3).

**Table 2.3 Properties of Alexa bovine serum albumin (BSA).**

| Albumin Conjugated Fluorophore | Absorbance wavelength (nm) | Molecular weight (kD) | Emission wavelength (nm) |
|---|---|---|---|
| **Alexa594®BSA** | 590 | 66 | 617 |
| **Alexa647®BSA** | 650 | 66 | 668 |

| Fluorescence filter | Excitation (nm) | Dichroic mirror cut-off (nm) | Barrier (nm) |
|---|---|---|---|
| **Texas Red** | 540-580 | 595 | 600-660 |
| **Cy5** | 590-650 | 660 | 670-730 |

## 2.8 Tumour harvesting.

Harvested tumours were bisected with one half snap frozen in liquid nitrogen ($LN_2$) and stored at -80$^{o}$C, before subsequent cryostat sectioning for immuno histochemical (IHC) staining. The cryostat preparation of the snap frozen tumour pieces involved placing onto cork discs and embedding in OCT®-mounting matrix (CellPath UK) and the tumours sectioned at 5-10 µm thick slices onto glass slides and stored at -20$^{o}$C.

## 2.9 Tumour pathophysiological markers.

### 2.9.1 Pimonidazole (Hypoxyprobe-1®) staining.

Pimonidazole (Hypoxyprobe-1, Chemicon Ltd,) is a bioreductive agent (lipophilic 2-nitromidazole compound) that binds to hypoxic cells via a thiol group that forms adducts at low oxygen partial pressures (<10mmHg). It allows direct visualisation of hypoxic tumour regions post immuno histochemical (IHC) staining. Pimonidazole was prepared at 10mg/ml in saline (0.9%) and given i/p (0.2ml/ mouse) 2 hours before tumour harvest.

Pre-cut cryosections (5-10μm) on glass slides were removed from -80° C storage and allowed air dry for 10 minutes. The sections were then fixed using 4°C acetone for 10 minutes before air drying further a further 30 minutes and a DAKO immuno-edge pen used to draw around the section (creating a shallow well).The non specific antibody sites in the tumour section were then blocked using 10% horse serum in phosphate buffered solution (PBS) containing 0.1% Tween20 (PBST) for 15 minutes at room temperature.

The slides were then washed twice with PBST supplemented with 0.1% BSA. The antibodies were made up using PBST supplemented with 0.1% BSA. The Hypoxyprobe antibody was made up at 1:50 in PBST. The primary antibody was added to the well containing the tumour section (~ 100μl volume) and incubated overnight at 4°C in a humidified chamber. The next stage involved triple washes of the sections for 2 minutes in PBS before applying the secondary antibody (a FITC labelled rabbit anti-mouse) at 1:100 dilution in PBST containing 0.1% BSA and leaving at room temperature in the dark for 60 minutes. The sections were triple washed again for in PBS before being mounted with coverslips using DAKO fluorescent mounting medium. The slides could then be viewed using a fluorescence microscope and analysed.

### 2.9.2 Hoechst 33342 vessel perfusion staining.

Hoechst 33342 (Hoechst) (bis-Benzamide, Sigma Aldrich, UK) is a fluorescent dye (Abs/Em = 350/461 nm) that labels cells immediately adjacent to perfused vasculature. Histological fluorescent images were scored using IVM epi-fluorescence using a DAPI filter (340-380nm excitation, 400nm Dichroic Mirror Cut-off with a 435-485 Barrier) and quantitatively analysed to give a value for the tumour vessel density per $mm^2$.

Hoechst was prepared at 6mg/ml using sterile saline (0.9%) and injected i/v (0.1ml) 1 minute before tumour harvest. Prepared Hoechst labelled tumour cryo-sections were imaged prior to any subsequent staining (double or triple) to avoid loss of fluorescence due to IHC processing. The captured images could then be overlaid (using MetaMorph® software) with later images of the same section stained with additional fluorescently labelled antibodies e.g. for dual staining of endothelial cells (EC) and/or regions of tumour hypoxia or other pathophysiological parameters.

### 2.9.3 CD31 endothelial cell marker staining.

CD31 (also known as PECAM-1 for **P**latelet **E**ndothelial **C**ell **A**dhesion **M**olecule) is a glycoprotein expressed on endothelial cells and in platelets. It is known to be involved in cell signalling and cell adhesion. Antibodies to CD31 are often used in the study of benign and malignant vascular tumours. Tumour microvasculature staining involved incubating the prepared cryosections overnight at 4°C with a rat anti-mouse CD31 (PECAM) antibody (Pharmingen, BD Biosciences) made up at 1:250 in PBST-0.1% BSA. The secondary antibody, goat-anti-rat Texas red isothyocyanate (TRITC) labelled antibody (Molecular Probes, Invitrogen), was made up at 1:150 in PBST-0.1% BSA and then applied to the sections for 60 minutes at room temperature in the dark. Subsequent washes and coverslip mounting has been described before (Section 2.9.1)

## 2.10 Statistical analysis used throughout these studies.

In order to determine if there was a statistical difference in between only two groups of data of equal size and normally distributed e.g. number of vessels in one tumour versus the number of vessels in a second tumour type an independent paired two-tailed test' was

carried out where a probability factor (P) value $\leq 0.05$ was considered to represent a statistically significant difference between the two groups.

When statistical comparison was needed between two treatment groups of differing sample size the Mann-Whitney U test was used in place of an unpaired t-test. Although it is a non-parametric test it does assume that the two distributions are similar in shape. Statistical analysis was computed using the Analyse-it for Microsoft Excel package (Analyse-it Software, Ltd, Leeds, UK).

When statistical comparisons were needed to determine if tumour growth delay data were different across three or more groups an ANOVA followed by a least significant difference *post hoc test* was carried out. If however there was a need to compare groups, defined by two independent variables (e.g. treatment type and tumour type) then a two way ANOVA was carried out using a SigmaStat analysis package www.systat.com/.

# CHAPTER 3 - OPTIMISING THE DORSAL WINDOW CHAMBER MODEL.

## 3.1 Introduction.

In order to add to our understanding of the processes involved in tumour angiogenesis and neovasculature development it is essential that more qualitative and quantitative *in vivo* models are developed and refined that allow the least invasive means of making pathophysiological measurement of any applied manipulation.

Observation chambers as research 'tools' to investigate cellular and vascular development are not new and have contributed greatly to our understanding of how vessels develop and respond to manipulation in tumours (Tozer et al. 2005 Dewhirst et al. 2002) and has many other non-invasive applications (Makele et al. 2005). Continuous development and optimisation of materials, animal species, surgical techniques and microscopy has resulted in the current use of the mouse dorsal skinfold chamber as a very effective tool for investigating tumour vasculature response to applied manipulations *in situ*.

Modifications of the dorsal window chamber/intravital microscopy model (DWC/IVM), adapted by Algire in the early 1940's, now allow us to carry out non-invasive, non-destructive imaging of tumour vasculature development *in vivo* and in real-time (Algire, 1949). With the advent of laser-scanning confocal and multiphoton microscopy, fluorescently labelled markers and nanoparticle technology, it is now possible to track the development of tumour margins, the interactions between individual cells, local blood vessels as well as the effects of applying antitumour therapies (Lunt et al. 2008, 2011).

### 3.1.1 Objectives.

The main objectives of this of part of the work were to:

- optimise and the surgical attachment protocol for DWC
- determine the period of tolerance for the DWC
- obtain vascular growth characteristics for xenografts established in DWCs

These objectives would allow future application of the DWC/IVM model tumour to provide additional complementary data to conventional murine sub-cutaneous tumour growth delay studies involving applied therapeutic modalities. Tumour vascular response studies using antiangiogenic agents (AAs) and vascular disrupting agents (VDAs) have been carried out alone and in combination using this model. Tozer et al. demonstrated the effects of the VDA Combrestatin –A- phosphate (CA-4-P) measuring a reduction in tumour microvascular density (MVD), tumour vessel length and blood flow rates using DWC xenografts (Tozer et al. 2001). Additional DWC xenograft therapeutic combination using AZD2171 (broad VEGFR tyrosine kinase inhibitor acting on several receptor sites) and radiotherapy produced a reduction in MVD and provided additional information about the benefits of scheduling pre-treatment RT on overall vessel response (Williams et al. 2007). In addition the effects of VEGR blocking by Tong et al. showed improved drug penetration and visualisation of the vascular normalisation effect that resulted (Tong et al. 2004).

The DWC/IVM model allows chronic real-time measurements of the tumour microenvironment responses *in situ* without the need to excise the xenograft. Studies using the DWC/IVM model would also allow an insight into the mechanistic effects of applied modalities. In addition we would be able to assess both qualitatively and quantitatively the effects of these modalities that is currently not available in the clinical setting without multiple biopsy material and associated labour intensive tissue modifying histology.

The volume of data produced from only a few DWC xenografts would also mean a reduction in the numbers of mice, the associated tumour processing cost, as well as providing a 'truer' picture of how a particular therapy affected the tumour microenvironment.

## 3.2 Characterising DWC xenograft tumour vasculature.

A series of DWCs were attached to adult female nude mice and inoculated with several types of tumour cell lines in exponential phase of growth as described earlier (Chapter 2.5.2 and 2.2.1). Briefly a series of DWCs were inoculated with cellular suspensions of HT29, Calu-6, SW620, Hepa-1wt or Hepa-1c4. Subsequent tumour vasculature development was then imaged using IVM. The tumour vessel growth characteristics for each tumour were then recorded. Serial chronic imaging was carried out to detect angiogenesis initiation and vascular development with the limitation of DWC tumour volumes reaching ~ 100mm$^3$ (Project License permitted tumour volume maximum).

Observations, regarding the surgical attachment procedure, anaesthesia, analgesia, recovery etc., were also routinely recorded in order to evaluate and refine the DWC murine model procedure. Brightfield IVM images of the opposing vasculature and facia in the attached DWCs were routinely imaged ensuring integrity of the proposed implant site and to verify opposing facia vascular perfusion before implanting with different tumour cells.

## 3.3 Results.

Most mice tolerated the DWC well however the technical expertise required and the complexity lead to an initial 30% DWC exclusion rate. Initial studies were carried out to determine an optimal time-period, post DWC attachment, for surgical implant site

recovery. Several studies established that a 48-72h post DWC attachment was a suitable time period in order to determine if the DWC experiment could continue.

The complications that led to an initial high exclusion rate included; loss of mouse condition post-surgery, occlusion of flowing blood vessels resulting in tissue necrosis and or infection inside the chamber; mice exhibiting an agitated state when handled; failure of the tumour cells to establish; or obscured IVM images due to skin slippage during the attachment period or due to incomplete removal the opposing skin facia at the attachment stage. Improved host tolerance of the DWC was achieved via the introduction of newly fabricated aluminium DWCs that were up to 1g lighter than the original titanium DWCs. The introduction of the aluminium frames reduced the incidence of DWC 'tilting' or 'flopping over' which occurred more frequently using titanium DWCs.

The effect of the titanium DWCs flopping over did not interfere with the ability to image vascular blood flow when the chamber was righted back to an upright position. Maintaining an upright DWC position was the preferred sate as well as proving less of a discomfort to the mouse. Adhesive tape was introduced under the metal saddle reducing the incidence of skin pressure sores.

IVM imaging images were recorded from around day 4 for most tumour vessel development studies achieving a volume of ~ 60$mm^3$although some tumour cell lines did not produce distinguishable vessels until a few days later (Table 3.1).

**Table 3.1 Characteristics of DWC xenografts**

| Tumour cell line (number of DWCs) | Concentration cells/ml | Detectable DWC vessels (days) | % MVD of tumours at 60mm$^3$ | Optimal time period for time-lapse studies (days) | Time to reach 100mm$^3$ volume (days) |
|---|---|---|---|---|---|
| **HT29 (n=7)** | 5 x10$^7$ | 5-6 | 20-30 | 9 - 18 | ~ 17-18 |
| **Hepa (wt) (n=5)** | 5 x10$^6$ | 7-10 | 20-30 | 10 - 18 | ~ 18-20 |
| **Hepa (c4) (n=8)** | 5x10$^6$ | 10-12 | 20-30 | 12 - 20 | ~ 20-22 |
| **SW620 (n=5)** | 1x10$^7$ | 6-7 | 30-40 | 7 - 15 | ~ 15-16 |
| **Calu-6 (n=8)** | 5x10$^7$* | 8-12 | 16-30 | 10 - 17 | ~ 17-18 |
| **MDA 231 (n=8)** | 2x10$^7$ | 10-12 | 20-30 | 12 - 20 | ~ 20-22 |

* Matrigel support matrix used (1:1 volume ratio).

To optimise tumour vascular visualisation and active blood flow therein, a fluorescein isothyocyanate (FITC) filter was used during IVM, due to haemoglobin light absorbance in this wavelength range that resulted in clearer distinction of smaller vessel blood flow that would normally appear various shades of red to pale pink when viewed by the naked eye using IVM.

Changes to the surgical attachment of DWC protocol included; the replacement of the initial surgical anaesthetic mixture of Hypnorm/Midazolam with a Ketamine/Xylazine mixture and allowing the mice to fully recover in a ventilated, temperature (32$^o$C) and humidity (60%) controlled recovery incubator for a minimum of 3 hours post surgery. This improved the overall condition and tolerance of the DWC by the murine host. Revising the aseptic surgical preparation and the time to complete the attachment procedure, as well as verifying continuous blood flow before returning the mice to a ventilated cage, all contributed to the reproducibility of the DWC model success rates.

In addition to the above findings the elasticity/tonicity of the dorsal skin supporting the DWC improved when Hypnorm/Midazolam anaesthesia was replaced after introducing the Ketamine/Xylazine combination.

Pre-implantation DWC brightfield images allowed visualisation of the host venous and arterial vessels supply, but not the detection of lymphatic vessels. The appearance of the pre-existing vasculature within the DWC however changed markedly when imaged a few days post inoculation (Fig. 3.1).

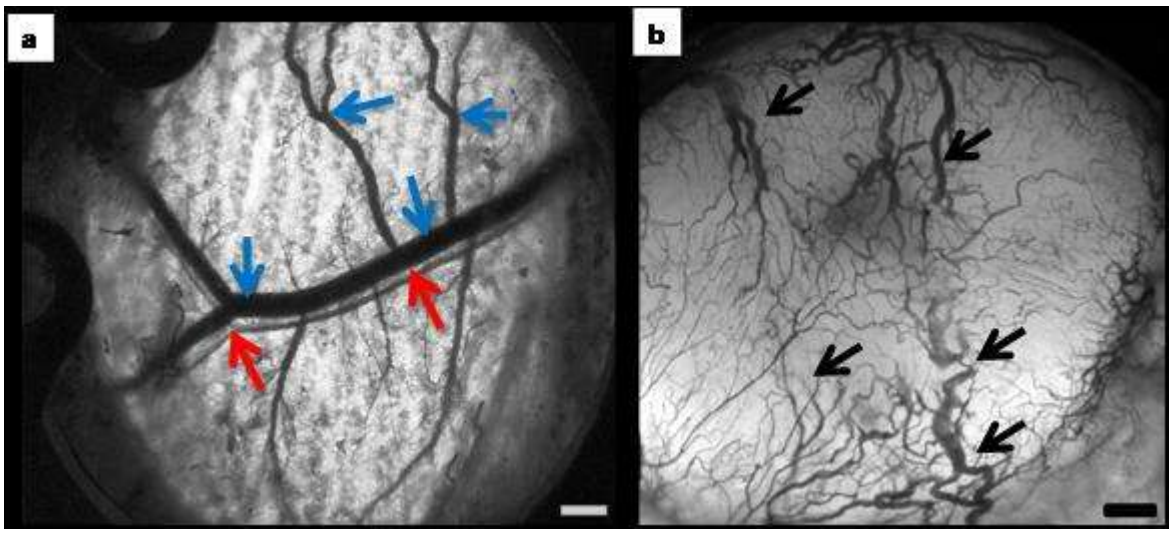


**Fig. 3.1** Optically clear brightfield IVM images of: a) the opposing DWC murine skin fascia vasculature pre SW620 cell inoculation. The majority of the vessels appear uniform with bifurcation of both arterial (red arrows) and venous (blue arrows) vessels and b) SW620 tumour vasculature day 12 post cell inoculation showing irregular chaotic, looped and blunt end (shunted) vessels (black arrows) (Scale bar 500µm).

A refinement to the DWC model included changing the method used for introducing cell inoculants via the opposing dorsal skin as carried out by others (Dewhirst et al. 2002, Tozer et al. 2008, and Fukumura et al. 2010). The inoculants were introduced routinely between the two saddle halves through the sandwiched skin and directly into the chamber avoiding unnecessary excess DWC manipulation via 'C' circlip, coverslip removal and subsequent replacement.

Established tumour vessels appeared tortuous, irregular in length and diameter often ending at abrupt points (shunts) with some emerging and disappearing into the tumour(verified visually as blood flow disappearing into the tumour) stroma at these shunt points. At higher magnification the blood flow in some of the tumour vessels ceased for a few seconds before surging forward and occasionally backwards.

IVM images for x20, x40 and x 100 magnifications were recorded before choosing an optimal x40 magnified region of interest (ROI) with good vessel resolution properties for subsequent tumour vessel studies (Fig 3.2).

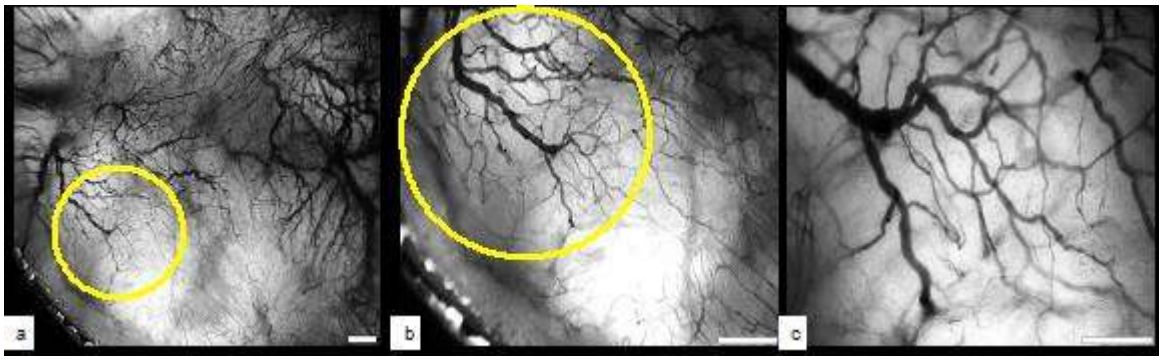


**Fig. 3.2** Brightfield IVM images of SW620 tumour vasculature at; a) x20 chosen region of interest (ROI), b) x40 and c) x100 magnification fields of view (Scale bar 500µm)

The xenograft vasculature appeared heterogeneous within the same tumour and between different tumour cell types. Visual observations showed that angiogenesis appeared to initiate from the existing opposing mouse skin fascia vasculature as if it was being 'robbed out' and the components used to build the new vessels. Dark cell deposit areas were typically visualised pre-neovascular initiation in most inoculated DWCs followed by a progression to more distinguishable vessels before forming into irregular chaotic larger vessels (Fig 3.3).

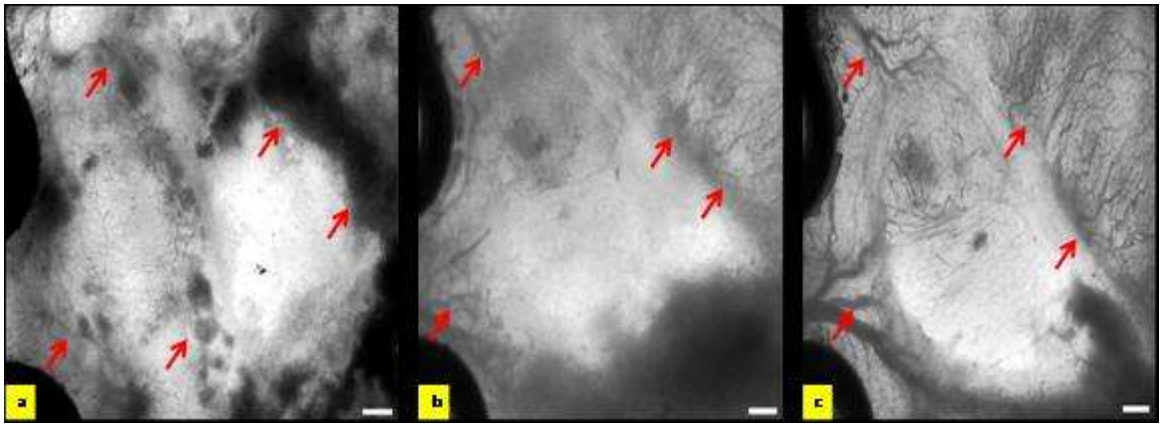


**Fig. 3.3** Typical brightfield images of Hepa-1wt DWCs stromal development a) Darker dense areas of tissue appeared 4 days after inoculation (indicated by red arrows), that appear to be the origins of neovasculature 2 days later b) before becoming more established by day 10 c). (Scale bar 500µm).

A common feature to all the initial DWC vasculature imaged was the gradual disappearance of the pre-existing vasculature and the development of vasculature from the advancing tumour periphery. Once tumour vasculature reached a measurable MVD the tumour volumes were typically ~ 50-60mm$^3$ The rate of development of Hepa-1wt and c4 tumour however vasculature was slower reaching a comparable level of MVD around 10-11 days and 12-14 days respectively compared to SW620 and HT29 tumours.

Tumour neovasculature varied between tumour cell types. HT29 and Hepa-1 wt neovasculature were visible from day(s) 5-6, whereas Calu-6 had a similar degree of vessel development around day 13 post inoculation (Fig 3.4).

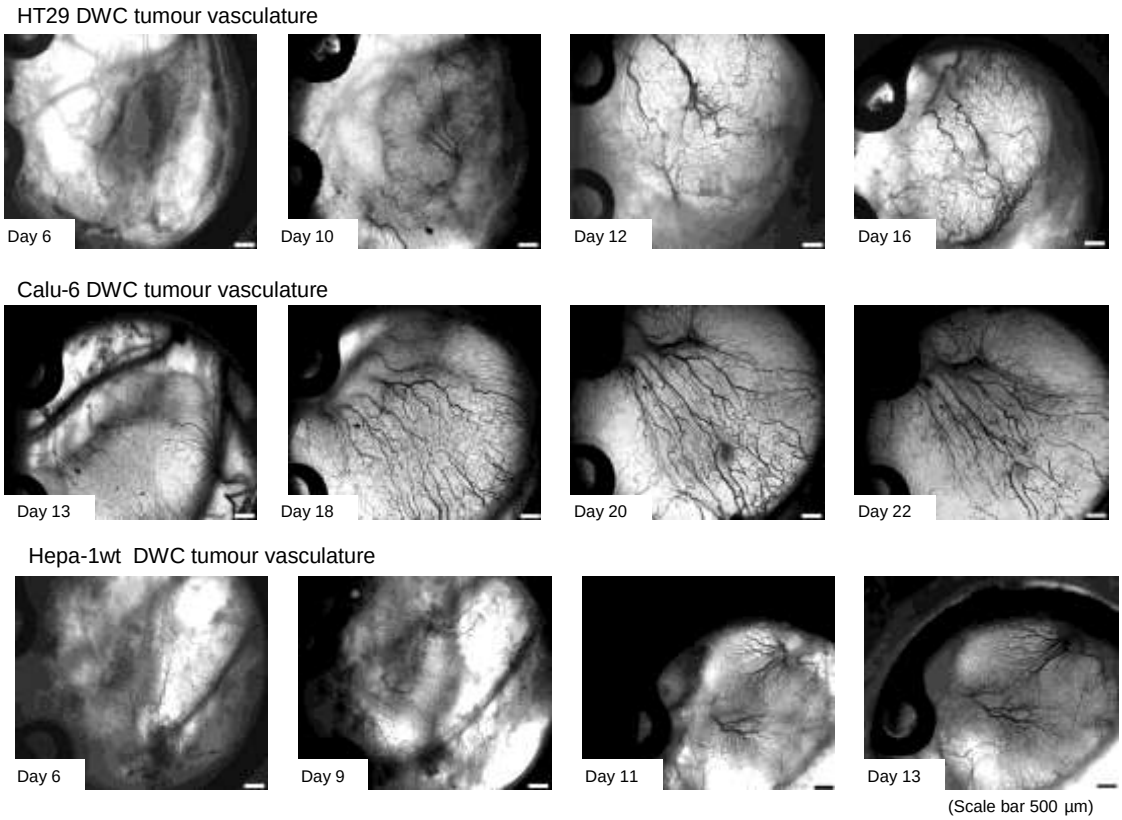


**Fig. 3.4** Brightfield IVM images of HT29 tumour vasculature development from day (s) 6-16 post HT29 cell implant, day (s) 13-22 for Calu-6 and day (s) 6-13Hepa-1 wt.(Scale bar 500um).

## 3.4 Discussion.

The development of tumour vasculature has been established as an essential component of tumour growth and as such we need try to measure its responses to antitumour therapies (Folkman et al. 1971). In order to achieve this it is essential we continue to develop and refine non-invasive measurement models such as the DWC in order to 'see' their in situ effects and translate these findings into the clinical setting.

The DWC model allows repeated spatial and temporal tumour vasculature measurements to be recorded for days to weeks without the need for multiple histological biopsies in order to evaluate stromal responses to manipulation.

The modifications to the original DWC protocol resulted in a tolerance that allowed chronic imaging for up to 30 days. After 30 days the stability of the upright window deteriorated with resulting flopping over and ethically it was decided that this was a suitable endpoint to the studies. A more limiting factor to the duration of the study was the tumour reaching 100mm$^3$ volumes before the 30 day time-point). Once the tumour reached these volumes it resulted in skin tears appearing at the perimeter of the tumours on the opposing side to the window glass. This would result in fluid leakage and subsequent crystallisation and the development of necrotic skin tissue. In addition we had to consider the terms of the project license where we were limited to tumours of this size.

Frequent IVM observations allowed the DWC mouse to become accustomed to the imaging protocol and this helped reduce the time required to obtain clear images for later off-line analysis. The brevity of some of the imaging protocols meant that no anaesthesia was needed and the mouse sat calmly in the purpose built microscope stage holder allowing rapid brightfield (1-2 minute duration) imaging of the ROI without visual distortion of the tumour vascularity. Analgesics (Buprenorphine) were initially used for pre- DWC attachment and 24-48 hours later however, the additional stress and agitated state that resulted from the i/p injection led to them being used typically only once after 24h resulting in a reduction in the agitated state and a better response to handling. It is not known whether the procedure of injection or the analgesic itself caused this heightened agitated behaviour.

It was also of note that the rate of growth for some tumours seemed to depend on whether there were ‘good’ opposing host fascia perfused vascular vessels present immediately pre-cell implant. If there was only one vessel or a ‘feeble’ vessel present, either from the deep

circumflex iliac artery/vein (DCIA/DCIV) or the lateral thoracic artery/veins (LTA/LTV) (the major vessels feeding the dorsal skin attachment area), the MVD did not develop to the same extent often taking a few days longer to achieve a useable IVM MVD for time-lapse studies.

The basis of the effect on the tonicity of the skin supporting the DWC, as a result of switching the anaesthesia cocktail from Hypnorm/Midazolam to Ketamine/Xylazine, is not clear. However it may be that the muscle relaxant action of the Hypnorm/Midazolam anaesthesia also changes the tonicity of the dorsal skin such that post surgical stretching causes it to lose its ability to return to its original tension pre-attachment. In some cases additional adjustments were needed to the tension of the nuts and bolts of the DWC saddle an hour or so after surgery to reduce the incidence of vessel occlusion pressure. Additional vascular perfusion checks could be carried out serially without the need for anaesthesia by using approved jigs in order to verify vascular blood flow immediately pre inoculation of cells into the DWC.

The procedure for introducing tumour inoculants into the DWC chamber (a ‘between the plates’ injection) was modified from the method used by previous groups. The previous method was refined due to concerns about cell/fluid escape through the injection point and the introduction of a needle puncture point on opposing fascia skin surface. This to the author’s knowledge this is a novel method for the DWC model studies.

A second option that had been considered was the removal of the glass coverslip and the deposit of a cell pellet or piece of tumour also described by others (Papenfaus et al. 1979. Huang et al. 1999).

However although attempted a few times by the author it was thought that, by removing the glass coverslip to introduce either a cell pellet or a $1mm^3$ piece of donor tumour xenograft there was an increased chance of infection introduction. Not only was there added technical complexity of the procedure, there was a likelihood of removing some already adherent facia tissue that may have attached during the 72h post attachment recovery period. This might be an important consideration if we don't want to introduce an additional influencing factor to the first stages of xenograft angiogenesis i.e. removing an establishing support matrix adhering to the underside of the glass coverslip. By changing this we may affect primary remodelling of pre-existing vasculature via intussusceptions also influence the characteristics of secondary metastasis although these studies have yet to be carried out in detail.

There was also the concern that by using non characterised tumour pieces we would not be able to accurately determine how many cells we were introducing or the influence of a preformed stroma matrix from the donor xenograft. Cell suspensions would allow a better monitoring of developing tumour cell morphological change and tumour host interactions to be characterised. These factors could affect the overall growth characteristics of the developing tumour and introduce a degree of non-uniformity in growth characteristics and composition (although comparison studies have not been carried out as yet).

Care had to be taken when initially selecting a mouse with regard to age, weight and the amount of loose skin on its back. Choosing 10-14 week adult female mice weighing 23 ± 2g and selecting mice with lower, but not least, subcutaneous dorsal skin fat also improved DWC tolerance and duration. Indeed choosing mice with thin backed skin often results in skin slippage within the DWC when viewed under IVM and resulting reduced tonicity.

There was no clear distinction between veins or arteries and no evidence of a lymphatic system when visualising the developing vasculature at high magnification (x100) despite good vessel resolution. Another interesting observation was the detection of circulating white cells (supposed white blood cells) in most DWCs in the larger more established vessels. By visualising the movement of the circulating white blood cells this further confirmed the observations by others that blood flow through tumour vasculature was chaotic and erratic.

Additional refinements involved the introduction of isofluorane anaesthesia for IVM imaging rather than an initial Ketamine/Xylazine combination resulting in a better maintenance of murine core temperature and resulting in a much shorter recovery period (3-5 minutes compared to 50-60 minutes respectively). The overall condition of the mouse, post IVM imaging, improved dramatically with the introduction of isofluorane anaesthesia and was therefore adopted as a standard protocol method.

As shown in Fig. 3.3 there were differences between the growth rates for some tumours, although the concentrations of the Hepa-1 inoculants were a factor of 10 less than the HT29, SW620 and MDA231, but this may due to the fact that Hepa-1 is a syngeneic tumour cell line where the others were human in origin. This may also an important consideration when characterising vascular responses to therapies using DWC models and translating results to the clinic. The ‘norm’, as found by others was to find angiogenesis initiation around day 3 post cell implant with discernable vasculature appearing around day(s) 5 and 6 (Tozer et al. 2005). Some cell lines such as SW620 require a matrix support for initiation for growth and did not typically establish vasculature until days 8-10 post cell inoculants.

However this delay was also seen in the human mammary adenocarcinoma cell line MDA231 where no support matrix was used included and where vascular development often didn't present until days 10- 12 post inoculation. This highlights the importance of tumour heterogeneity consideration and that before using new cell lines for tumour manipulation studies using the DWC model it must be routine to characterize them first.

### 3.5 Conclusions.

The DWC optimization studies confirmed that xenograft tumour cell lines could be grown in the DWCs successfully using immunodeficient mice and that tumour vasculature could be imaged from as early as day 5 confirming studies by others. Tumour vessels established typically from days 5-7 in the DWC and repeated IVM imaging of the developing vasculature was possible for an additional l4 days without loss of condition of the mouse.

This allows the DWC/IVM model to be used as an additional investigative tool to murine subcutaneous xenograft growth delay therapeutic manipulation studies. The additional benefits will be the ability to see and quantify different stromal parameters in real-time. These studies highlighted the fact that not all DWC tumours have the same rate of vascular growth and hence the importance of carrying out pre-characterisation studies.

It also is worth noting that these xenografts established in a pseudo-ectopic site i.e. in the dorsal skin facia supporting in the DWC. This may result in differing growth characteristics compared to those found in its natural setting (native or orthotropic site) and is an important consideration. Although the importance for developing relevant orthotropic models has been realised the technical and financial costs limit their use at the moment.

Non-invasive whole-body imaging systems are now being evaluated to study orthotropic fluorescently tagged tumour responses to manipulation and are producing increased interest in the field of pre-clinical oncology (http://www.caliperls.com/ ) however spatial resolution still presents some challenges.

The continued development of the DWC model also drastically reduces the need for multiple time-points involving large numbers of mice and time consuming histological analysis. We can use the DWC model to study tumour microenvironmental responses to therapeutic manipulations and translate these to the clinical setting. Recent advances now include the development of lighter polyethylene plastic DWC chamber which will allow tumour stromal development to be studied up to a 200 $mm^3$ volume and will also be suitable for complementary DWC murine Magnetic Resonance Imaging (MRI) studies.

# CHAPTER 4 - DWC XENOGRAFT STROMA MODULATION STUDIES.

## 4.1 Introduction.

Conventional approaches to antitumour therapy have been designed to attack the tumour cells directly using radiation and chemotherapy as single modalities or in combination (chemoradiation). After the seminal hypothesis proposed by Judah Folkman that tumours could not grow without initiating neovascularisation, attention began to focus also on targeting the tumour vasculature (Folkman et al. 1971).

The ability to study tumour vessels and surrounding microenvironment in situ in response to an applied therapy, using non-invasive methods such as the DWC/IVM model has resulted in a wealth of information about tumour stromal responses to existing and novel therapeutic drugs and how they affect overall tumour responses.

Through the development of fluorescence imaging technologies (Chapter 1) researchers are now able to observe and measure complex biological systems such as tumour stroma in far greater detail. Imaging fluorescence using "intravital" preparations now allows us to study tumour development from a suspension of cells through to large complex vascularised masses and to determine some of the myriad biological processes occurring within the surrounding stroma. Perhaps more importantly, with regard to Folkman's hypothesis, we can use now use the dorsal window chamber (DWC) model to determine the mechanisms of actions of existing and novel antitumour therapy regimens within intact tumour stroma.

The aim of these studies was to determine whether fluorescently labelled bovine serum albumin (BSA) could act as a marker of perfused tumour vasculature and, as such, how tumour vasculature responds to potential modulators.

In addition to establishing fluorescent BSA as a marker it was decided to look at the effects of nicotinamide (NA) and two novel analogues AG14361 and AGO14699 originally studied for their inhibitory ploy (ADP-ribose) phosphate (PARP) DNA repair activity and subsequent tumour radiosensitisation responses (Chapter 1).

The structure of the novel analogues AG14361 and AGO14699 are similar to NA. Since NA is thought to have vasomodulatory effects it may be that AG14361 and AGO14699 produce similar vessel modulation effects in the tumour stroma resulting in a secondary mode of action.

### 4.1.1 Objectives.

Having established the DWC xenograft model previously (Chapter 3) the first objective was to:

- Characterise AlexaBSA in DWC xenografts vasculature
- Measure the effects of NA, AG14361 and AGO14699 on DWC xenograft vasculature
- Measure the effects of AG14361 and radiation on tumour growth delay(GD)

## 4.2 Measuring AlexaBSA in DWC xenograft stroma.

The first objective was to determine whether two fluorescently labelled albumin conjugates, Alexa594BSA and Alexa674BSA (chemically and structurally similar 64kD

compounds with differing spectral emission properties), produce measurable stromal fluorescence data for different DWC xenograft cell types using intravital microscopy (IVM) time-lapse imaging studies.

A series of DWCs containing different tumour cell lines were initiated to detect and measure AlexaBSA within established tumour stroma. Briefly, a series of DWCs were prepared and inoculated with tumour cells (Chapter 2.2.1). At around a 50-60mm$^3$ tumour volume and the development of a 'reasonable' degree of vasculature, the DWC xenografts were prepared for IVM time-lapse imaging and injected with either AlexaBSA594 or 647 (1mg/ml 0.1ml tail i/v)( Chapter 2.6.1).

Identifiable regions of interest (ROIs) were selected, based on 'reasonable' areas of vessel development within the DWC field of view, and then imaged, using both brightfield and epifluorescence illumination, for subsequent off-line measurement using MetaMorph® image analysis software. The MetaMorph acquisition programme also allowed real-time visualisation of the changes in stromal accumulation of AlexaBSA via simultaneous graphing of the acquired fluorescence intensity values data points. Background autofluorescence measurements were taken before commencing each time-lapse study. Typically images were recorded for the first few seconds post introduction of the AlexaBSA and at minute intervals thereafter.

Quantitation of the AlexaBSA fluorescence was carried out using arbitrary fluorescence units (FU) (Chapter 2.6.2). Recorded time-lapse data was used to compare the AlexaBSA values for a series of different tumour cell-line types. As a control check, to discount any potential effects of introducing drugs by either the intravenous (i/v) route or the

intraperitoneal (i/p) route, physiological saline injections studies were carried out during AlexaBSA time-lapse studies involving 0.1ml i/v or 0.3ml i/p volumes.

These studies were carried out to determine if subsequent volume injections i.e. after tail vein AlexaBSA impacted on the fluorescence being measured during continuous time-lapse series.

### 4.2.1 Results.

Qualitative visualisation assessments of the accumulation of AlexaBSA in the tumour stroma showed in 'real-time' the measurable fluorescence intensities of the AlexaBSA within the tumour vessels and the surrounding tumour stoma (Fig. 4.1). AlexaBSA fluorescence was clearly distinguishable within larger established vessels and locally around smaller vessel tips (Fig 4.1).

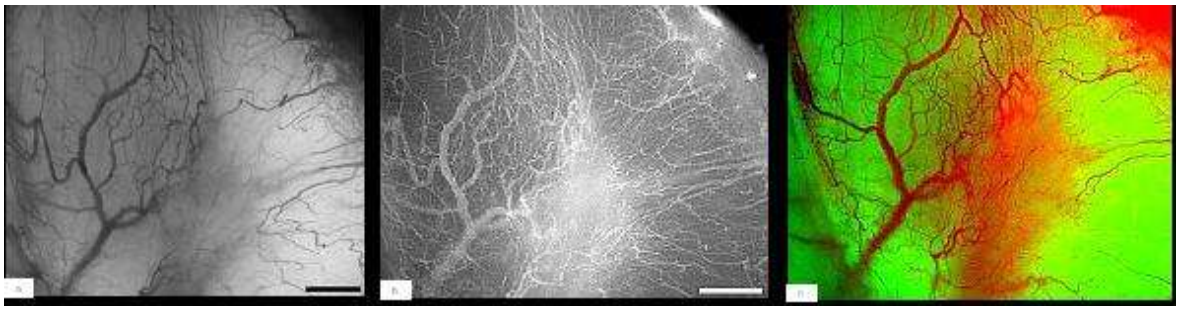

**Fig 4.1** Time-lapse grabbed images of HT29 tumour vessels perfused with AlexaBSA. Image taken 10 minutes post AlexaBSA 1mg/ml 0.1ml i/v tail vein a) brightfield illumination of HT29 DWC tumour vasculature on day 10 post cell implant, b) epi-fluorescence illumination of the HT29 DWC tumour vasculature post AlexaBSA and c) overlay of a) and b) where tumour stroma is shown in green and the presence of AlexaBSA in red (Scale bar 500μm).

Overlaid brightfield and epi-illumination images showed that it was possible to use AlexaBSA to distinguish between the perfused vascular regions of the tumour stroma and the non-vascularised regions. IVM time-lapse data showed the rapid appearance of AlexaBSA within the tumour vessels, after an initial spike of fluorescence before a more

constant level of fluorescence was seen between 2-10 minutes. Time-lapse studies showed that AlexaBSA fluorescence could be measured within the DWC for periods in excess of 60 minutes without loss of fluorescence intensity.

A plateauing of AlexaBSA fluorescence intensity developed between 8-10 minutes post introduction of AlexaBSA when the data was plotted (Fig 4.2).

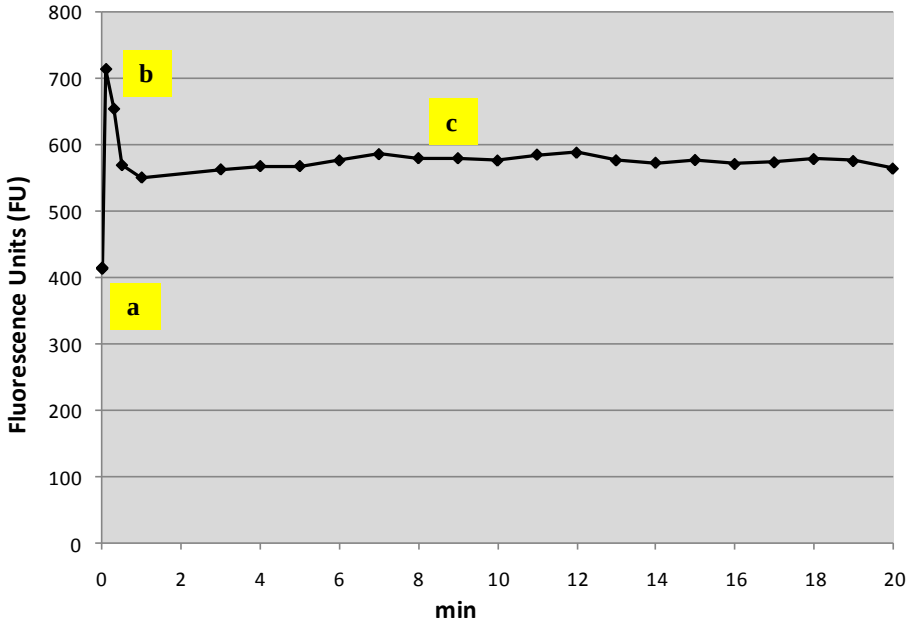


**Fig 4.2** Typical fluorescence intensity data profile for AlexaBSA (1mg/ml 0.1ml i/v) using an HT29 DWC xenograft a) background fluorescence, b) an AlexaBSA fluorescence spike occurred in the first few seconds before c) fluorescence intensity reached a uniform intensity (fluorescence plateau).

Saline volume control studies confirmed that the additional volumes injected via i/v (0.1ml) or i/p (0.3ml) routes did not markedly affect the AlexaBSA fluorescence data during the time-lapse studies for three different tumour types (Fig 4.3).

Repeat injections 20-30 minutes later, using the same preparation, also did not markedly impact on the time-lapse AlexaBSA fluorescence values during acquisition.

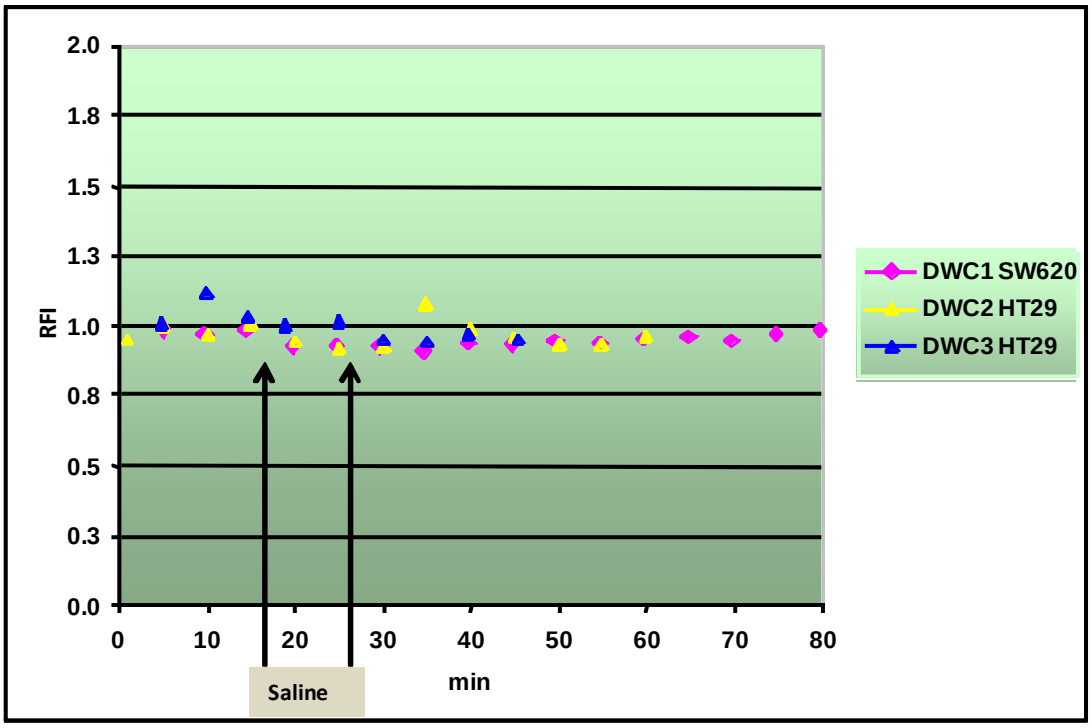


**Fig 4.3** Relative fluorescence intensity (RFI) profile for AlexaBSA (1mg/ml) in HT29 (n=2) and SW620 (n=1) DWC tumour stroma. Saline injections between 10-15 minutes (i/v) post AlexaBSA plateau and after 25-30 minutes i/p.

## 4.3 Effects of NA on DWC xenograft stroma

The preparation and attachment of the DWC and cell inoculants have been described earlier (Chapter 2.1, 2.2.1). Briefly, a series of DWCs were set up and inoculated with either HT29 or SW620 tumour cells. Once the tumour vasculature had established the DWC xenograft stroma was imaged using IVM brightfield illumination and epi-illumination for time-lapse studies.

AlexaBSA (1mg/ml 0.1ml i/v) was injected and time-lapse images recorded at minute intervals until a plateau of fluorescence intensity was achieved.

NA (1mg/kg 0.3ml i/p) was introduced and continuous time-lapse images recorded at minute intervals (Chapter 2.6). The data was then plotted as fluorescence units versus time before being converted to normalised plots of relative fluorescence intensity (RFI) and the data for each DWC tumour type tabulated.

### 4.3.1 Results.

NA increased the RFI within the tumour stroma of HT29 DWC xenografts post i/p injection. Plotted time-lapse image fluorescence intensity data showed a sustained level of fluorescence was attained from 2-10 minutes post AlexaBSA injection (Fp). The effect of the NA injected after Fp was achieved was to increase the amount of fluorescence detected within the DWC for the next 30-40 minutes before a second fluorescence plateau developed (Fp2) (Fig 4.4)

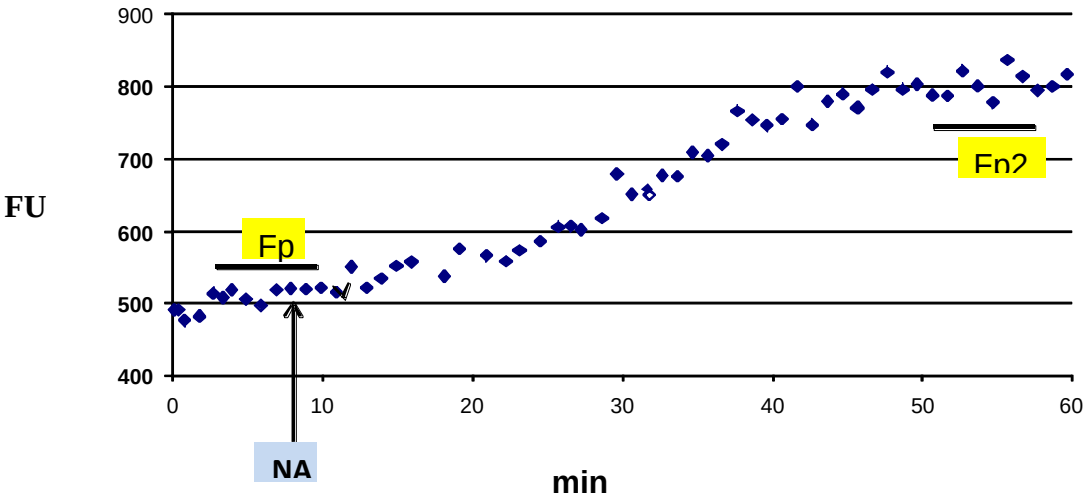


**Fig. 4.4** DWC/IVM time-lapse data for AlexaBSA (1mg/ml 0.1ml i/v) HT29 tumour stroma. Nicotinamide (NA 1g/kg 0.3ml i/p) introduced after 10 minutes. Fluorescence intensity increased (FU) until levelling out forming a second fluorescence plateau (Fp2) between 50-60 minutes of time-lapse measurements.

AlexaBSA time-lapse fluorescence profiles were obtained in repeat studies for HT29 and SW620 DWC stroma (example of time-lapse fluorescence profile for SW620 DWC Fig.4.5 and normalised time-lapse fluorescence Fig 4.6).

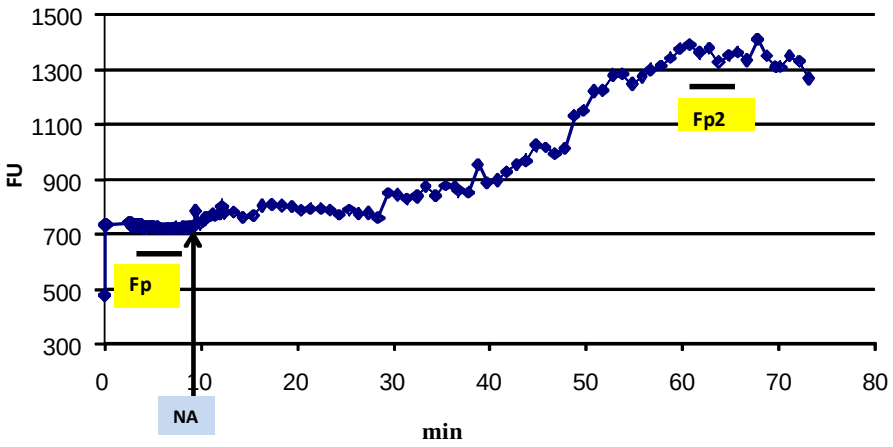


**Fig. 4.5** DWC/IVM time-lapse data for AlexaBSA (1mg/ml 0.1ml i/v) SW620 tumour stroma (n=1). Nicotinamide (NA 1g/kg 0.3ml i/p) introduced after 10 minutes. Fluorescence intensity increased (FU) until levelling out forming a second fluorescence plateau (Fp2) between 50-60 minutes of time-lapse measurements.

Similar to the HT29 time-lapse studies a plateau (Fp) of AlexaBSA fluorescence intensity was achieved at around 10 minutes. The introduction of NA at this time point resulted in a gradual increase in measured AlexaBSA fluorescence intensity 20 minutes later continuing for a further 20-30 minutes before a characteristic second plateau of fluorescence (Fp2) presented (Fig(s) 4.5, 4.6).

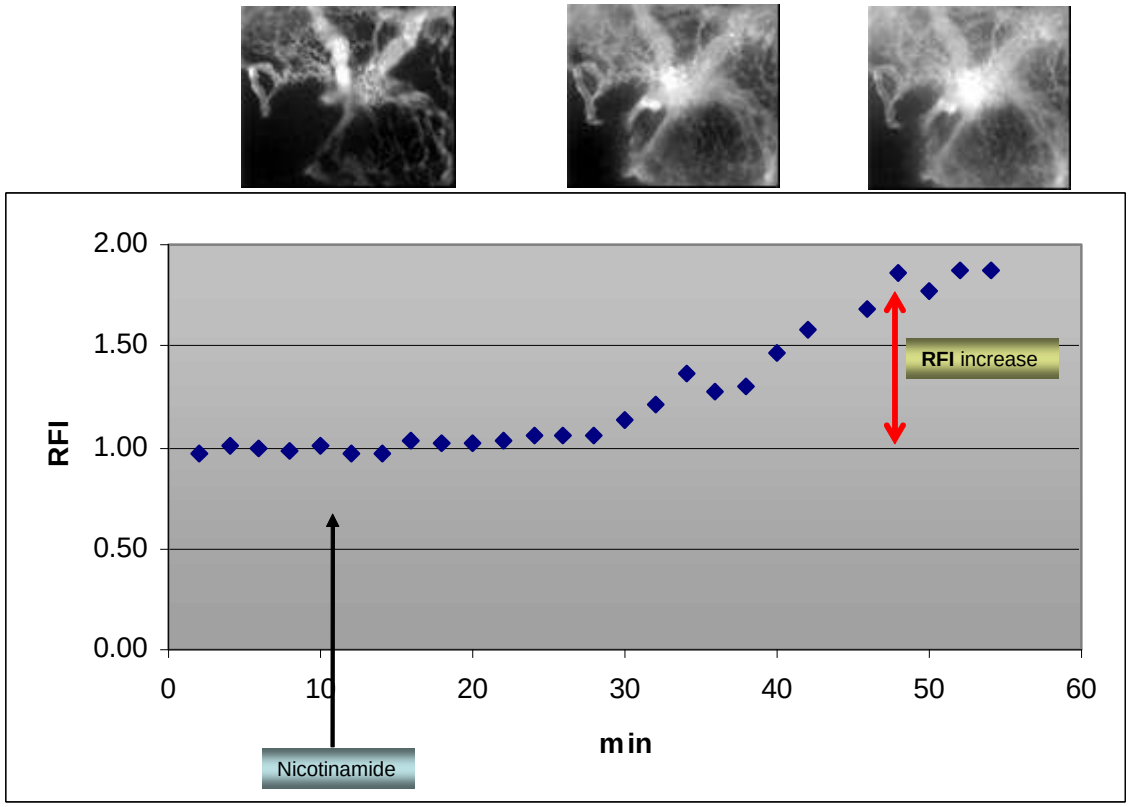


**Fig 4.6** Relative fluorescence intensity (RFI) data plot showing SW620 DWC stroma (n=1) accumulation of AlexaBSA (1mg/ml 0.1ml i/v). Nicotinamide (1g/kg 0.3ml i/p) injected after a 10 minutes. AlexaBSA fluorescence increased from a primary plateau after 20 minutes before forming a second fluorescence plateau around 50-60 minutes of the time-lapse study. Corresponding epi-fluorescent time-lapse images are shown for the 10, 30 and 50 minutes time-points above.

Time-lapse images of one AlexaBSA treated SW620 DWC xenograft showed a new vessel being perfused by the circulating AlexaBSA after 2 minutes post introduction.

This vessel remained open throughout the time-lapse study (Fig 4.7).

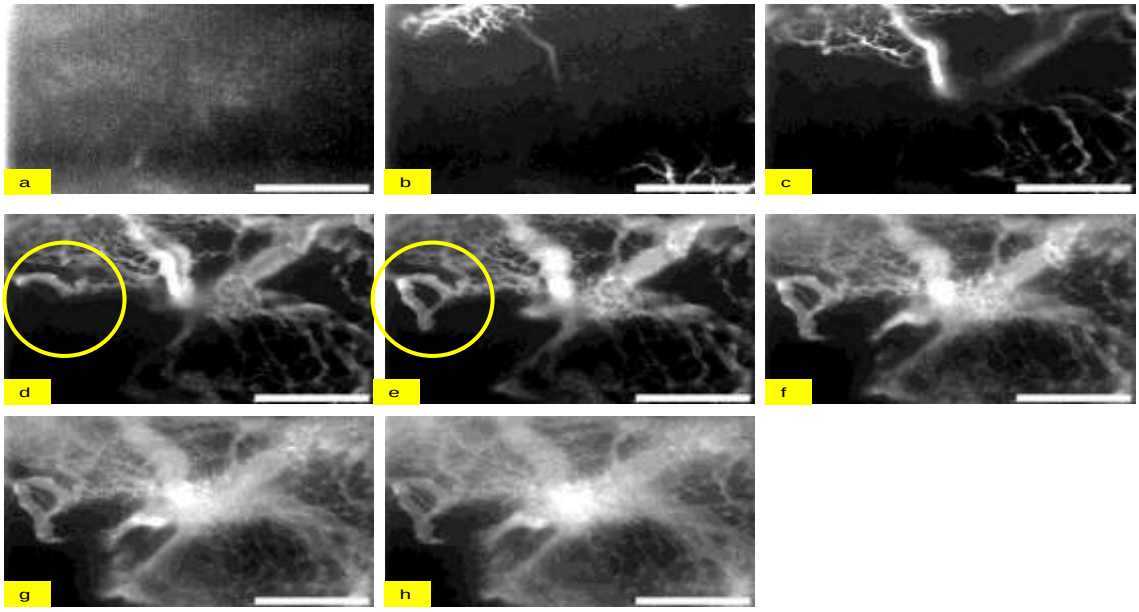


**Fig 4.7** DWC/IVM sequential epifluorescence time-lapse images of AlexaBSA (1mg/ml 0.1ml i/v) perfusing SW620 tumour vessels. a) Pre AlexaBSA injection (background fluorescence Fb), b) 2 second later, c) 4 seconds, d) 2 minutes and e) 10 minutes. Na (1mg/ml 0.3ml i/p) was introduced after 10 minutes and time-lapse images taken at f) 20 minutes, g) 40 minutes and h) 60 minutes. (Scale bar 500µm). Note the opening of a vessel between d) 2 minutes and e) 10 minutes.

The effects of NA on the SW260 DWC/IVM time-lapse studies (n=2) showed that NA produced 1.6 - 1.8 fold increases in the stromal accumulation of AlexaBSA for 40 minutes before reaching of a second stable fluorescence plateau (Fp2) (Fig 4.8). Similar results were seen for the HT29 DWC stromal time-lapse data where 1.7 – 2.0 fold increases were obtained (Fig 4.8). The normalised data for a total of n=3 for each tumour type was then tabulated (Table 4.1).

**Table 4.1 Effects of NA on HT29 and SW620 DWC AlexaBSA fluorescence intensity**

| DWC/IVM study | Tumour xenograft | RFI |
|---|---|---|
| 1 | HT29 | 2.0 |
| 2 | HT29 | 1.75 |
| 3 | HT29 | 1.7 |
| 4 | SW620 | 1.75 |
| 5 | SW620 | 1.8 |
| 6 | SW620 | 1.6 |

### 4.4 Vascular effects of PARP inhibitors.

Since AG14361 and AGO14699 have similar chemical structures to NA (Fig 4.8) it was hypothesised that they may also have similar vasomodulatiory effects on tumour vasculature.

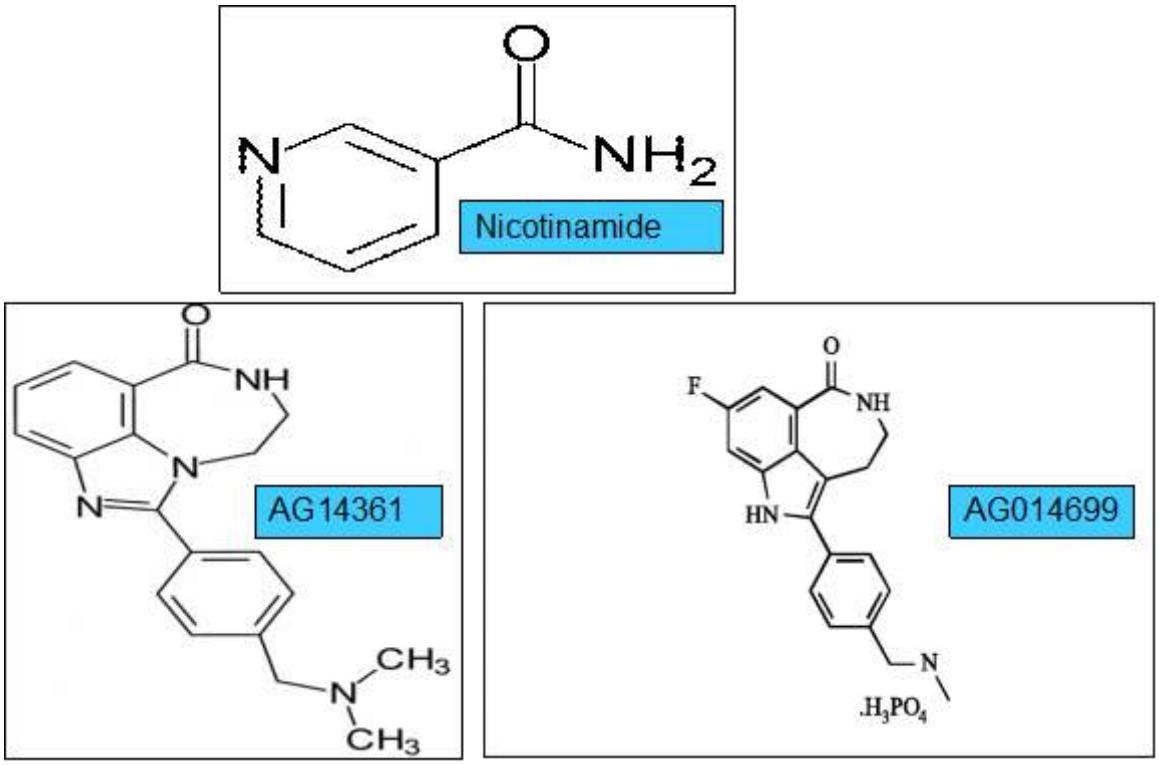


**Fig 4.8** Chemical structures of Nicotinamide, AG14361 and AGO14699.

A series of DWC xenografts were set up using HT29 and SW620 tumour cell lines (Chapter 2.2.1, 2.5.1). Once tumour vasculature had established DWC/IVM time-lapse studies were carried out to measure the effects of AG14361 (10mg/kg 0.3ml i/p) and AG14699 (1mg/kg 0.1ml i/p) on AlexaBSA fluorescence intensity using the same procedure as for NA and the data plotted.

### 4.4.1 Results.

The effects of AG14361, using HT29 (n=4) and SW620 DWC xenografts (n=3) on AlexaBSA fluorescence intensity levels, showed that the AlexaBSA fluorescence intensities formed plateaus (Fps) typically between 8-10 minutes post introduction. Injection of the AG14361(10mg/kg 0.3ml i/p) at the 10 minute time-lapse time-point resulted in an increase in fluorescence intensity around 20 minutes later continuing for another 20 minutes before effectuating a second fluorescence intensity plateau (Fp2) (Figs. 4.9, 4.10 and normalised cumulative data plots in Fig.4.11).

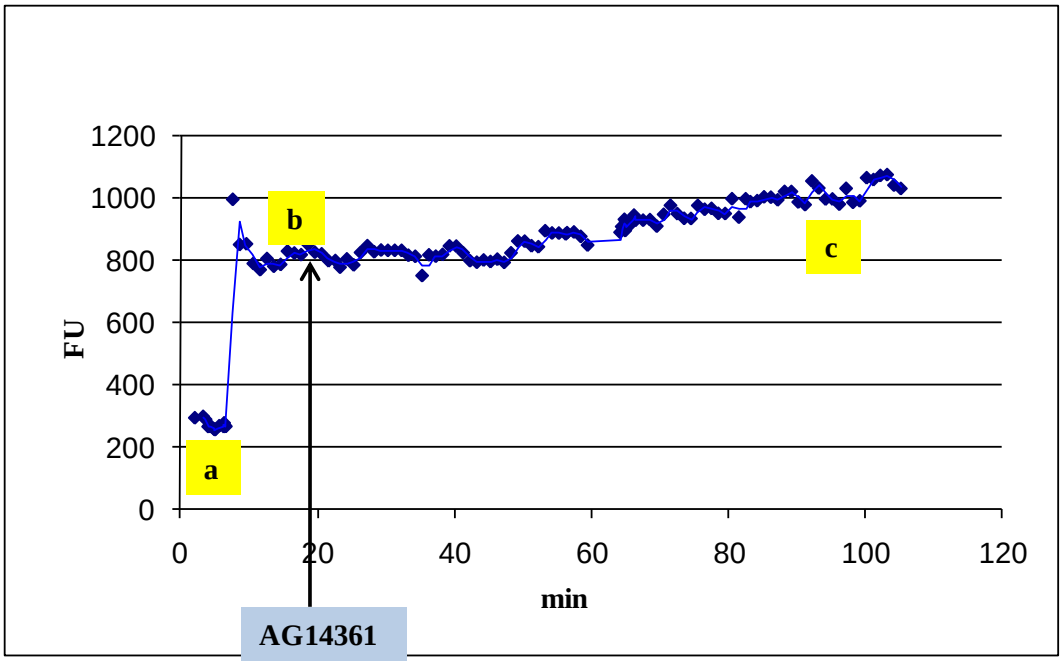


**Fig 4.9** AlexaBSA (1mg/kg 0.1ml i/v) time-lapse fluorescence data for SW620 DWC stroma (n=1) treated with AG14361 (10mg/kg i/p). Background fluorescence (a), AlexaBSA fluorescence plateau (Fp) (b) and second fluorescence plateau (c) (Fp2). Fluorescence units (FU).

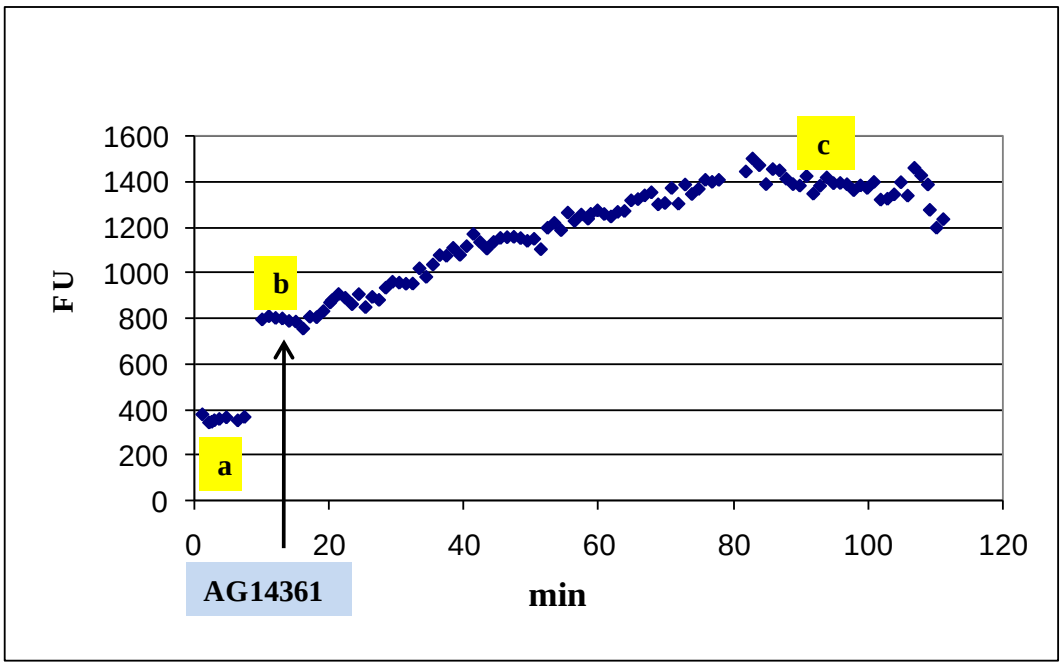


**Fig 4.10** AlexaBSA (1mg/kg 0.1ml i/v) time-lapse fluorescence data for HT29 DWC stroma (n=1) treated with AG14361 (10mg/kg i/p). Background fluorescence (a), AlexaBSA fluorescence plateau (Fp) (b) and second fluorescence plateau (c) (Fp2). Fluorescence units (FU).

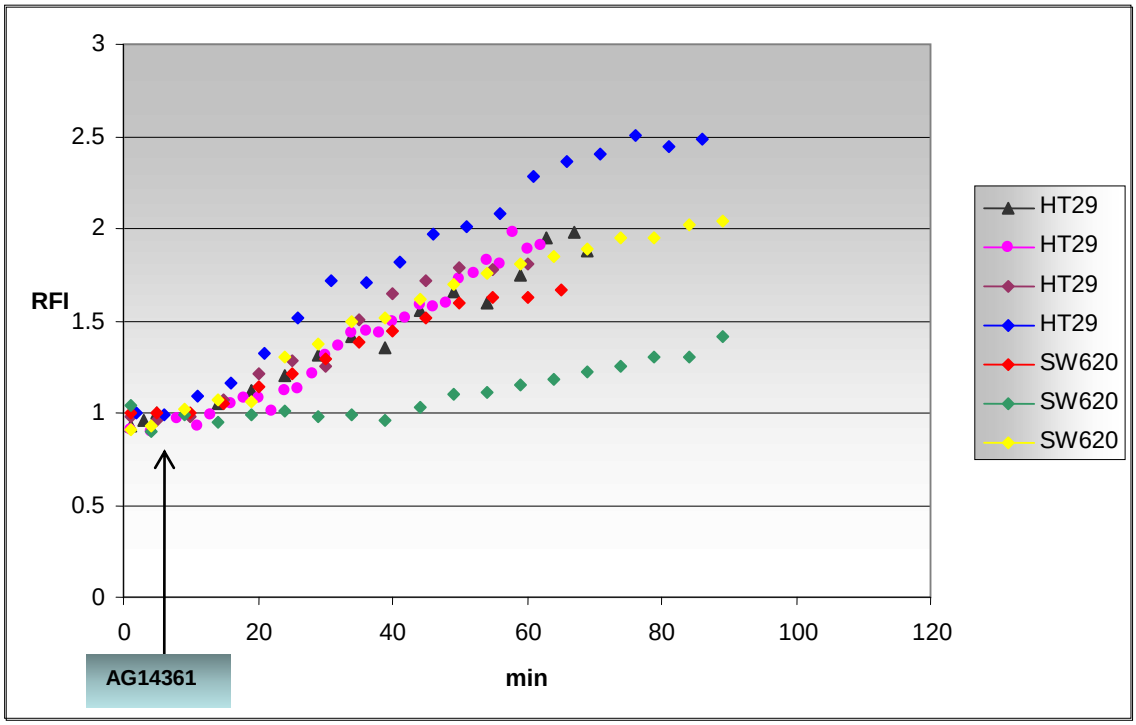


**Fig. 4.11** RFI DWC/IVM time-lapse data for HT29 (n=4) and SW620 (n=3) stromal accumulation of AlexaBSA (1mg/ml) post introduction of AG14361 (10mg/kg i/p).

Data from AGO14699 DWC/IVM time-lapse studies using both the HT29 and SW620 tumour stroma accumulation of AlexaBSA produced quantifiable results (Fig 4.12).

Saline control studies using HT29 and SW620 DWC xenografts and AGO14699) confirmed earlier findings in that no marked changes in stromal fluorescence intensity resulted from the additional volumes (0.3ml) being introduced via the i/p routes during the time-lapse acquisition studies (Fig. 4.12).

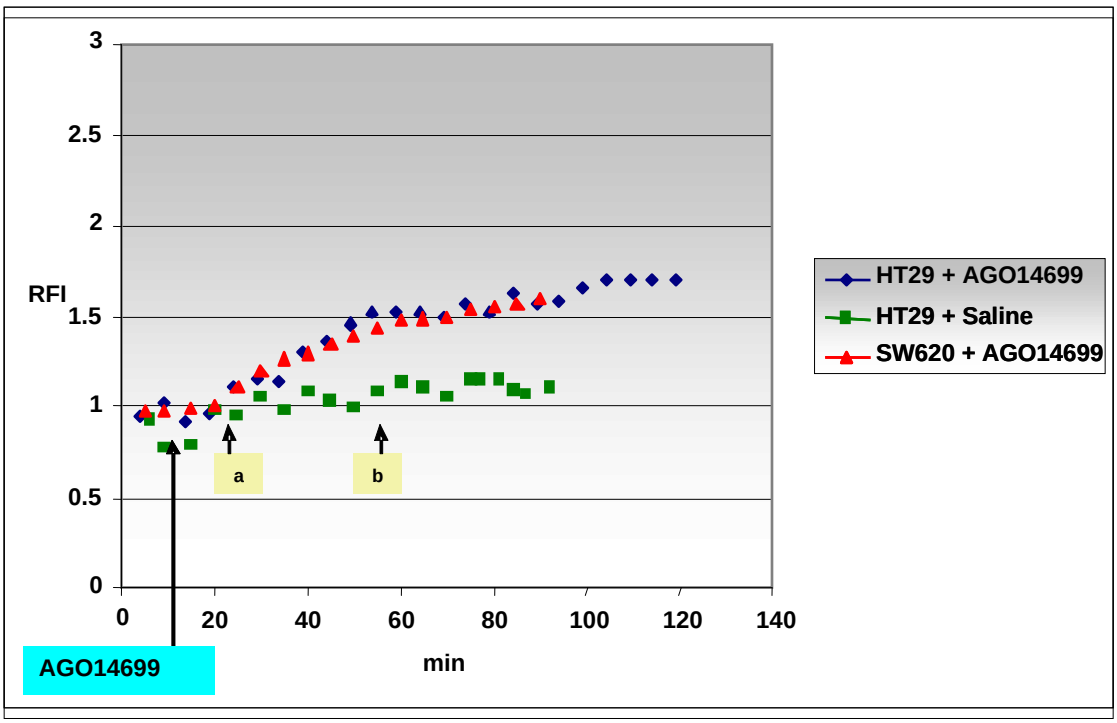


**Fig.4.12** AlexaBSA fluorescence normalised time-lapse data for HT29 (n=1) and SW620 DWC (n=1) post AGO14699 (1mg/kg 0.3ml i/p) introduction. Physiological saline (0.3ml i/p) introduced at a) 25 minute and b) 55 minute time-points during the HT29 DWC time-lapse study.

The AlexaBSA fluorescence intensity values for the HT29 DWC (n=1) and SW620 DWC (n=1) time-lapse studies using AG14361, AGO14699 and NA were calculated and collectively tabulated (Table 4.2). The time taken for AlexaBSA to reach a second fluorescence intensity plateau (Fp2) for NA, AG14361 and AGO14699 was around 20 minutes post introduction.

**Table 4.2 RFI data for HT29 and SW620 DWC stroma post drug**

| DWC Cell line | AG14361 (10mg/kg) RFI | AGO14699 (10mg/kg) RFI | AGO14699 (1mg/kg) RFI | Nicotinamide (1g/kg) RFI |
|---|---|---|---|---|
| **HT29 (n=12)** | 2.5<br>2.0<br>1.8<br>1.7 | 1.8<br>1.8<br>1.7 | 1.7<br>1.3 | 2.0<br>1.7<br>1.7 |
| **SW620 (n=11)** | 2.0<br>1.6<br>1.4 | 1.2 | 1.6<br>1.5<br>1.3 | 1.8<br>1.7<br>1.6<br>1.4 |

NA introduction produced increased Alexa BSA intensities of 1.7 - 2.0 fold for HT29 DWC stroma when compared to the Fp plateau values, whereas it produced 1.4 -1.8 fold increases in the SW620 DWC stroma (Table 4.3). AG14361(10mg/kg) produced 1.7 to 2.5 folds increases in fluorescence intensity in the HT29 DWC stroma compared to 1.4 – 2.0 in the SW620 DWC stroma. The effect of AGO14699 (10mg/kg) on the fluorescence intensity in the HT29 tumour stroma ranged from 1.7 – 1.8 similar to that seen for NA for this tumour type. The effect of the lower dose of AGO14699 on both the HT29 and the SW620 DWC was similar in that a 1.3 – 1.7 and a 1.3 – 1.6 folds increase was measured respectively.

Qualitative assessment of the fluorescence intensity images for AGO14699 (1mg/kg) for SW620 tumour stroma showed that the AlexaBSA (and therefore by inference plasma proteins) had accumulated at higher concentrations in the central region of the stroma, but less so in the periphery. The increased fluorescence appeared to be highest in areas containing smaller less distinct vessels. (Fig.4.13). The intensity images showed that AlexaBSA was not accumulating in the stroma in a uniform manner and that some regions were not being perfused by blood vessels.

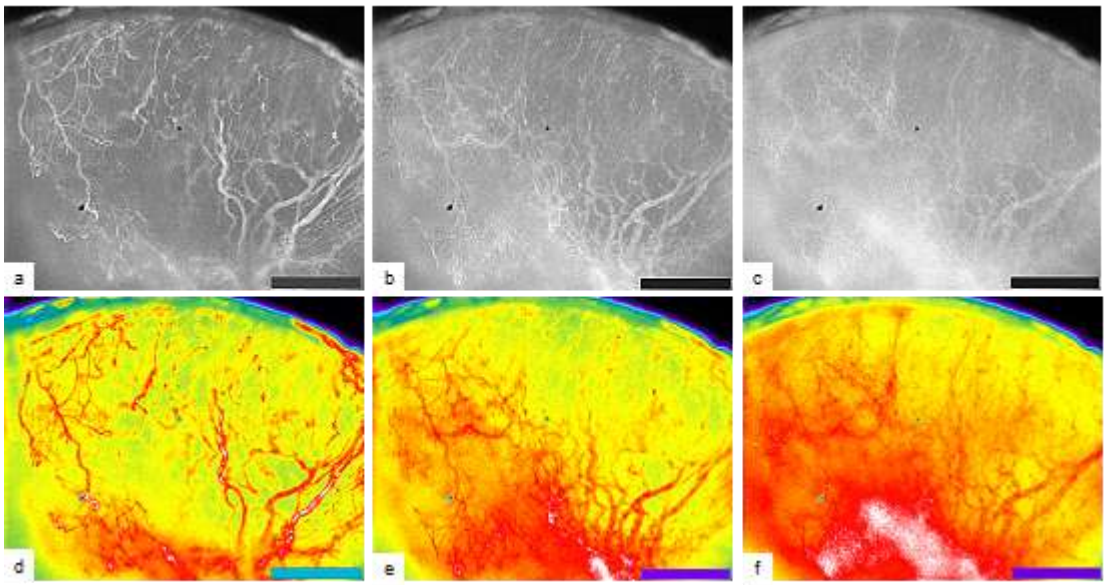


**Fig. 4.13** Alexa647BSA(1mg/ml i/v) epi-fluorescence time-lapse images of SW620 DWC stroma post AGO14699 (1mg/kg i/p) introduction at a) 7 minutes, b) 20 minutes, and c) 80 minutes using MetaMorph® pixel intensity analysis d), e) and f) below. The intensity images d), e) and f) show the range from the higher fluorescence intensities (shown in white) to lower (shown in red) for AlexaBSA (1mg/kg 0.1ml i/v) and non vascular areas (shown in yellow).(Scale bar 500µm).

## 4.5 AG14361 as an adjuvant to radiotherapy (RT).

In collaboration with other researchers the potential radiopotentiation of the PARP-1 inhibitor AG14361 was investigated using murine subcutaneous xenograft growth delay studies. Previous studies by others had investigated the chemo and radiation responses of LoVo and SW620 tumour cell lines *in vitro* as well as well as gene expression effects *in vivo*. We aimed to contribute by investigating whether AG14361 had radiopotentiation effects using SW620 subcutaneous xenograft growth delay studies using clinically relevant radiotherapy (RT) regimens.

The preparation and implantation of the SW620 tumour cell line has been described earlier (Chapter 2.1, 2.2.1, 2.2.2). Briefly tumours were grown in immunodeficient female adult mice until they reached a treatment size of 200-220mm$^3$ and randomly assigned into treatment groups as follows ( n=5 mice per group):

- Vehicle alone for 5 days i/p
- AG14361 (15mg/kg i/p) daily for 5 days
- Fractionated 10Gy radiation (2Gy daily fractions + vehicle i/p for 5 days)
- AG14361 (15mg/kg i/p) daily for 5 days + fractionated 10Gy (2Gy daily fractions for 5 days) (Chapter 2)

Tumour volumes were recorded up to three times per week and the GD values calculated for each group (based on the time taken to achieve a relative quadrupling of the treatment size, RTV4).

### 4.5.1 Results.

Data from two separate experiments, studying the combined effects of AG14361 + fractionated RT, were combined to assess the potential tumour radiosensitising effect of AG14361.

The groups receiving RT alone induced a GD of 28.1 days (± 1.9 SEM) (using $RTV4_{\text{treatment group data}} - RTV4_{\text{vehicle alone control data}}$). The effect of combining 10Gy RT and AG14361 was to significantly increase ($p=0.001$) the GD to 37.3 days (± 2.8 SEM) whereas there was no real difference in GD seen in the groups receiving vehicle alone or AG14361 alone. The results clearly showed that combining AG14361 and fractionated RT had increased the GD for the SW620 xenografts (Fig 4.14).

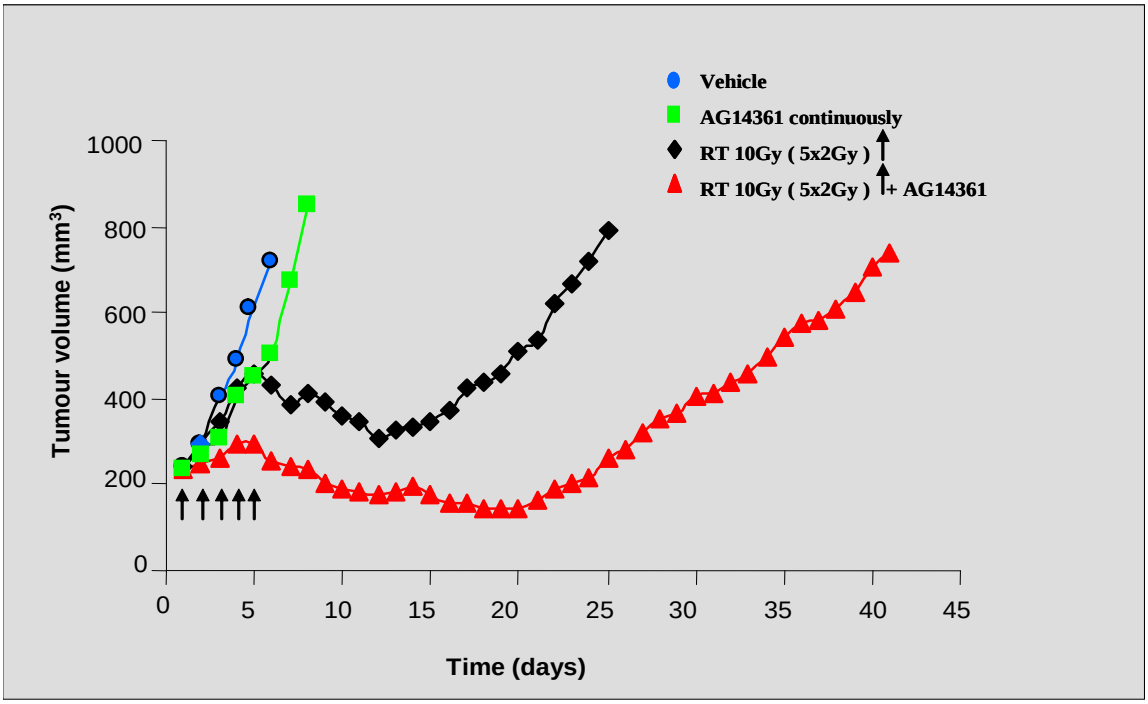


**Fig. 4.14** Effects of AG14361 (15mg/kg i/p) alone and in combination with fractionated 10Gy (2Gy daily for 5 days) radiation on the growth delay (GD) profile for SW620 xenografts (Adapted from Calabrese et al. 2004).

## 4.6 Discussion.

Tumour vasculature is known to be highly permeable to macromolecules compared to normal vasculature due to the absence of basement membranes, a lack of enveloping pericytes and loosely packed endothelial cells (ECs) causing fenestrae or changes in EC tight-junctions in tumour vascular walls. It is therefore surprising that some drugs don't diffuse or extravasate across the tumour stroma more easily resulting in better drug access to the stroma and subsequent tumour cytotoxic cell kill (Tannock et al. 2002). One barrier to drug penetration may be the presence high interstitial fluid pressure (IFP) within the developing stromal tissue. It has been reported that uniformly high intratumoural pressure decreases sharply towards the tumour's periphery or in the peritumour region (Stylianopoulos and Jain, 2010).

This may result in lower fluid extravasation across the vessel walls especially where osmotic and hydrostatic pressures are in equivalence between the intravascular and extravascular spaces.

Transvascular transport of drugs, in normal tissues occurs primarily by convection and as a result convective transport of drugs in the centre of tumours may be less than in the tumour periphery (Lunt, 2008). The studies using AG14361 in combination with radiation had shown that it did result in a radiopotentiation effect *in vivo* when the xenograft growth delay model was used. Coupled with the finding by our collaborators that AG14361 had chemopotentiation affects, it was decided to employ a model that would allow a visualisation of the drug's effects at the stromal level in order to describe its possible mechanisms of action.

Studies, using the AlexaBSA as a marker of stromal accumulation, showed that equilibrium between extravasation and re-absorption occurred reproducibly in the two tumour types studied i.e. HT29 and SW620 between a 2-10 minutes post introduction.

The DWC/IVM time-lapse studies also provided information about the degree of perfused vessels open at the start of a study by subtracting the stromal autofluorescence (background fluorescence (Fb) values from the initial AlexaBSA fluorescence intensity plateau (Fp) (Chapter 2). This information is useful for repeat studies using the same DWC tumours chambers and clinically relevant dosing regimens for direct comparison with conventional histological 'mis-match' studies using the pathophysiological markers Hoechst and Carbocyanine to determine the amount of vessels open and perfused at a particular time-point. This comparative observation has not previously been alluded to by others to the author's knowledge.

Being able to determine *in situ* whether vessels are open at the time of treatment initiation or closed could have important implications when introducing antiangiogenic agents such as vascular disrupting agents (VDAs) and trying to deliver a cytotoxic chemotherapeutic drug. If the vessels are shutdown due to the primary modality of the VDAs (vessel shutdown or collapse) then subsequent chemotherapeutics would fail to reach the tumour stroma resulting in reduced cytotoxic cell death i.e. prevent the chemotherapeutic from ever getting into the tumour in therapeutic doses. The reverse is also true in that if a cytotoxic agent is allowed to gain access to the tumour and VDAs are given immediately after then the cytotoxic agent is trapped within the tumour stroma.

Likewise the ability to determine whether a modality increases or decreases stroma blood perfusion could impact on the effectiveness of an RT regimen where oxygenated tumour cells produce a greater response to radiation cytotoxic kill and hypoxic cells offer up resistance.

This may prove an additional parameter that needs to be considered when describing possible mechanistic modes of action. We currently accept vessels close or are shutdown, indicated by MVD measurement data, but it may be that these vessels can be manipulated to open and close to enhance particular therapeutic strategies such as stromal cytotoxic drug accumulation. It is worth bearing in mind that some vessels will randomly open or close independently of any applied modality due to the heterogeneity of tumour vascular perfusion resulting in regional variances. But it does highlight the need to look at as many parameters as possible, in real-time using a model such as the DWC, in contrast to manipulative artificial histological evaluation. Being able to measure stromal responses, particularly the vasculature responses to optimise the timing of an applied multimodal therapy regimen would be of great importance when designing ‘tailored’ antitumour therapies.

The images from the DWC model highlighted the heterogeneity of vessel formation for different tumours types as described by others (Dewhirst et al 2002, Jain et al. 2002, Tozer et al. 2005, Fukumura and Jain 2007).

Since the molecular weight of the Alexa/BSAs is around 64kD it also provided information about which parts of the vessels had pore sizes (fenestrae, EC tight junction gaps) that allowed molecules of this size to gain access to the stroma. In these studies the newer less developed advancing angiogenic vessels (sprouting vessels) proved more permeable than the larger established vasculature. This is an important factor when the delivery of larger drug molecules is being considered such as cytotoxic Doxorubicin enveloped liposomes or small molecular weight antibody fragments (Tang et al. 2007). It is also important with regard to establishing if an AA acts more as a VDA than an antiangiogenic agent or has whether it has dual activity.

Although detailed measurements of vascular pore sizes (endothelial cell junction gaps or fenestrae), could have been included in these studies, using dextrans with known molecular sizes (Lunt et al. 2009), The principle aim was to try to determine whether AlexaBSA could provide additional information about the proposed secondary effects of known PARP-1 inhibitors in situ using the DWC xenograft model. Tentori et al. established that PARP-1 inhibition produced antiangiogenic effects using PARP-1 knockout mice and Ruddock and Hirst have shown that NA causes relaxation of pre-constricted normal and tumour arteries using ex-vivo rat studies (Tentori et al 2002, Ruddock et al. 2000). Ruddock proposed that the relaxant effects of NA are mediated through myosin light chain (MLC20) action found in vessel walls and that this could be exploited as a potential

therapeutic via the development of similar oxygenator compounds to enhance tumour chemoradiation response.

Our novel findings showed real-time in situ measurable tumour vasculature modulation responses occurred after treatment with NA or the structurally similar PARP-1 inhibitors AG14361 and AGO14699 resulting in an increase in stromal accumulation of AlexaBSA. To the authors' knowledge this had not been shown before.

The DWC model can also provide additional information about the biological events in the tumour stroma via the incorporation of pressure transducer adapted or oxygen sensor adapted DWCs to determine more clearly if a reduction in interstitial fluid pressure occurs (IFP) or if it induced acute or chronic hypoxia (Makale et al. 2005). Additional pathophysiological markers now include the fluorescently labelled apoptotic cell marker agent FLIVO™ Polycaspase (Invitrogen) allowing multiple parameter measurements within the tumour stromal tissue at the same time.

Before interpreting the AlexaBSA time-lapse data from these studies however several potential erroneous factors need to be considered:

- The injection of tail vein AlexaBSA must be achieved cleanly. Failure to inject cleanly results in a reservoir of AlexaBSA (cuffing) resulting in a slow drift of fluorescence intensity time-lapse data before a primary plateau is achieved.
- The haemodynamic effects of adding later drugs via i/v or i/p routes must be discounted using saline control injections during any time-lapse study. Control saline injection volumes must be carried out for each DWC xenograft type as a standard protocol.

- This validates the fluorescence plateau (Fp) data for the AlexaBSA marker as a true reflection of the haemodynamic function within the tumour stromal and that any changes must be due to a therapeutic intervention. This to the authors' knowledge has not been carried out before.
- The ROI must be clearly identifiable for repeat IVM time-lapse studies.

Indeed one of the key aims of establishing this model was to study the stromal response to manipulations over a period of days.

The results produced a typical RFI increases of 50% to 100% after administration of PARP inhibitors compared to a negligible change after control saline administration only) clearly shows a vascular response. The substantial increase in quantity of the vascular marker (AlexaBSA) can be explained by two mechanisms: 1) an increase in vascular volume and / or 2) the extravasation of plasma proteins and accumulation within the interstitial space. The possible mechanism(s) would be that it has a modulatory effect on vascularity, possibly by influencing endothelial cell (EC) junction gaps or by altering the tonicity of the vessels leading to increased perfusion volumes or by altering the stromal interstitial fluid pressure as described by Hirst et al. (Hirst et al. 1994). The data from the NA, AG14361 and AGO14699 time-lapse studies did not address parameters such as increased vascular perfusion to the stroma although this may be possible via re-analysis of vessel diameters in the stored images as carried out by others (Lunt et al. 2009). However the development of diffuse fluorescence and loss of contrast is strongly suggestive of extravasation.

Although the ability to measure vessel volume changes was outside the capability of the author there were concerns about the actual benefits of using these parameters without the ability to reconstruct 3D vascular maps showing the sizes and directions of the vessels.

However the wealth of data accumulated using this model meant that it can be re-visited at a later date once newly available software analysis software becomes available such as that being developed currently by other groups at The University of Sheffield (CAIMAN : CAncer IMage Analysis http://caiman.group.shef.ac.uk/caiman/).

Investigating whether AG14361 has similar vasoactive properties to those seen for NA, the DWC/IVM tumour vascular studies showed AG14316 increased AlexaBSA tumour fluorescence in both HT29 and SW620 xenografts confirming collaborative studies by others using vessel mis-match studies (Calebrese et al. 2004). Even though the exact mechanism(s) for the measured increase in tumour stroma accumulation cannot be fully explained it is most likely a combination of increased blood flow, increased permeability and a reduction in IFP.

The studies evaluating AG14361 as a potential radiosensitiser proved quite clearly that combining AG14361 and RT has a dramatic effect on radiosensitising LoVo tumours as shown by the tumour growth delay data (Fig. 4.10). The DWC studies showed that oxygenated blood would be able to access the stroma more readily if NA was introduced before a radiation treatment, but the DWC data also provided information on how long the NA, AG14361 and AGO14699 needed to be in the host before inducing a vasomodulatiory effect i.e. 20 minutes in most studies. This also shows that this group of compounds produce similar effects on similar tumour vascular types. We also determined, using the DWC model, that AGO14699 could produce similar vasomodulatory effects at 100 fold reductions in concentration (Table 4.2). This would have a direct impact on reducing the potential systemic side effects previously seen in the clinical setting.

These studies have shown a duality of action for PARP-1 inhibitors; however PARP-1 inhibitors may produce multiple effects within the stroma such as influencing HIF-1 responses at the cellular level thus modulating VEGF signalling and in turn vascular EC functional responses (Peralta-Leal et al. 2009).

PARP-1 inhibitors are receiving a great deal of attention at the moment due to their potential to enhance a number of antitumour DNA-damaging effects (Curtin et al. 2005). Additional studies by collaborating groups found that the effects of AG14699 were minimal on sensitising SW620 tumour cells to the cytotoxic chemotherapeutic drug Temozolomide (TMZ) *in vitro*, but had marked effects when combined *in vivo*; implying a different mode of action may exist in the tumour stroma microenvironment. Curtin et al. , looking at xenograft growth delay (GD) using AGO14699 and TMZ, showed that RTV4 values of 60, 63, and 100 days were achieved in the presence of AGO14699 compared to control data (Curtin et al. 2005). The AGO14699 DWC/IVM time-lapse data indicates that one of its mechanisms of action may be to increase TMZ concentration in the tumour stroma via modulating tumour vessel perfusion (Ali et al. 2009). The benefit of including AGO14699 in a TMZ chemotherapeutic regimen could be increasing tumour cell kill without the need to increase TMZ concentrations to achieve the same effect, thus reducing the chances of systemic toxicity.

Using PARP-1 inhibitors as adjuvants for RT and/or chemotherapy, further adds to the beliefs that multi-modal regimens need to be devised and that we need to consider the whole tumour stroma when developing antitumour strategies.

# CHAPTER 5 – THERAPY COMBINATION STUDIES USING AZD2171 AND RT

## 5.1 Introduction.

The importance of radiotherapy (RT) in the treatment of cancer patients is borne out by the fact that nearly 50% of solid tumours still involve its use (Steel 1997), but a major factor still affecting overall beneficial antitumour response is tumour radioresistance. By reducing tumour radioresistance even by a small amount the effects could translate to highly significant benefits in the clinical setting. In recent years there has been a great deal of interest in reducing radioresistance through the use of antiangiogenic (AA) therapies. Although AAs theoretically have the potential to increase tumour hypoxia by reducing nutrient supply via the shutdown of its vascular supply (thereby increasing radioresistance) it may be that AAs may operate via different mechanisms. Jain et al. hypothesised that AAs may in fact cause a transient vascular 'normalisation' effect on the chaotic tumour vessels that would a 'window' of opportunity during which a cytotoxic therapy might be more effectively delivered and increase oxygen delivery to the stroma increasing cytotoxic kill by chemoradiation strategies (Jain et al., 2001, 2005). Jain's explanation of vessel normalisation was that rather than destroying tumour vessels the AAs may work by pruning weaker immature neovascular vessels, reduce vessel permeability and lower interstitial fluid pressure (IFP) as well as increasing the recruitment of pericytes stabilising more mature intact vessels (Jain, 2005).

Targeting specific VEGF signalling pathways can result in enhancing antitumour responses to RT and or CT (Wachsberger et al. 2003, Gorski et al. 1999, Geng et al. 2001). One area of intense focus is the VEGF family of ligands and their cellular transmembrane receptors VEGFR(s) 1, 2 and 3, but primarily VEGFR-2 (Chapter 1), where their inclusion as therapeutic adjuvants has reinforced the significant role VEGF has in enhancing tumour endothelial cell (EC) survival post RT ( Geng et al. 2001).

There has been a great deal of interest in the importance of scheduling when designing combined AAs and RT treatments. The timing of the introduction of a vascular targeting agent in combined regimens concurrently (at the same time) with a neo-adjuvant or sequentially (post RT) may significantly influence the overall tumour response. There have been a number of studies carried out where AA and RT in combination have improved therapeutic response either using a conconcurrent schedule; Angiostatin + RT (Maureci et al. 1998), anti-VEGFR-2 antibody DC101 continued dosing post RT (Kozin et al. 2001), AZD2171 (Cediranib) + RT (Cao et al. 2006, Williams et al. 2007) or sequentially; TNP-470 + RT (Murata et al. 1997), PTK787/ZK222584 (VEGFR Tyrosine Kinase Inhibitor) + RT (Zips et al.2003), AZD2171 (Cediranib) + RT (Williams et al. 2007).

In pre-clinical murine xenograft model GD studies Williams et al. demonstrated that the therapeutic benefit of administering AZD6474 (Vandetanib®, small molecule inhibitor of VEGFR-2) post RT (sequential scheduling) was markedly greater than that seen when the drug was administered before each RT fraction (concurrent scheduling) (Williams et al. 2004). The authors demonstrated that the concurrent drug only schedule lead to an decrease in tumour vascular perfusion improving tumour reoxygenation between RT fractions thereby increasing tumour cell radiosensitivity (Williams et al. 2004). From these and other studies (Zips et al. 2003) it is becoming apparent that scheduling strategies involving combined modalities such as antiangiogenics with radiation could hold greater promise for future clinical development if their mechanisms of action are better understood.

### 5.1.1 Aims.

The main aim of this study was to look at the efficacy of AZD2171 (a small molecule inhibitor of the VEGF signalling pathway) in combination with radiation using both sequential and concurrent dosing regimens and the murine xenograft growth delay (GD) model as well as to apply DWC/IVM imaging approaches to determine the tumour microvascular responses in real-time. Wedge and co-workers showed that once daily administration of AZD2171 (≥ 1.5 mg/kg) had a significant impact on the growth rates of a selection of human tumour xenografts GDs including Calu-6 and LoVo tumour cell types which prompted its later consideration for clinical development and in our studies to investigate whether the sequence regimens for RT is important in improving its antitumour effects (Wedge et al 2005).

## 5.2 Effects of AZD2171 and radiotherapy on tumour xenograft growth delay.

Adult female nude mice were prepared and inoculated with Calu-6 tumour cells (Chapter 2.2, 2.21, 2.2.2). When tumours reached a treatment volume of 250-280$mm^3$ they were randomly assigned into the following treatment groups (n=5-7) and dosed continuously with vehicle or drug AZD2171 (3mg/kg) throughout:

- Vehicle alone
- AZD2171 alone
- RT 6Gy (3 daily doses of 2Gy) + vehicle
- RT 10Gy (5 daily doses of 2Gy) + vehicle
- AZD2171 (3mg/kg) + fractionated 6Gy (concurrent dosing)
- AZD2171 (3mg/kg) + fractionated 6Gy(sequential regimen)
- AZD2171 (3mg/kg) + 10Gy (concurrent regimen)
- AZD2171 (3mg/kg) + 10Gy (sequential regimen)

Tumour volumes were measured up to 3 times per week and the RTV4 (time taken for the tumours to reach 4 x treatment size volume) and the tumour volume doubling times (DT) calculated for each treatment group. All tumours were harvested for histological analysis (Chapter 2.9, 2.10).

### 5.3 Effects of AZD2171 and RT on Calu-6 and LoVo xenograft growth delay.

Nude female mice were prepared and inoculated with Calu-6 tumours (2 $x10^7$ cells/ml in a 1:1 mix with Matrigel) or LoVo cells (5 $x10^7$ cells/ml (Chapter 2.2, 2.21, 2.2.2). When tumours reached a treatment volume of 250-280$mm^3$ they were randomly assigned into the following groups (n=5-7):

- Vehicle daily
- AZD2171 (6mg/kg oral daily)
- Fractionated 10Gy (5 daily doses of 2Gy) RT + vehicle
- Fractionated 10Gy (5 daily doses of 2Gy) RT + AZD2171for 28 days (concurrent regimen)
- Fractionated 10Gy (5 daily doses of 2Gy) followed by 28 days of AZD2171 (sequential regimen)

Tumour volumes were measured up to 3 times per week and the RTV4 (time taken for the tumours to reach 4 x treatment size volume) and the tumour volume doubling times (DT) calculated for each treatment group. All tumours were harvested for histological analysis (Chapter 2.9, 2.10).

## 5.4 Application of the DWC model to AZD2171 and RT xenograft studies.

In order to visualise in situ and non-invasively the effects of AZD2171 and RT on the tumour vasculature DWCs were set up (n=6) (Chapter 2.5) and inoculated with Calu-6 (1 $x10^7$ cells in a 1:1 ration with Matrigel®). The DWC/IVM xenografts were then put into treatment groups receiving:

- Vehicle alone for 3 days (n=2)
- AZD2171 (3mg/kg) daily for 3 days (n=2)
- Fractionated 6Gy (3 daily 2Gy doses) followed by 3 daily doses ofAZD2171 (3mg/kg) (n=2).

Brightfield IVM images were recorded for each DWC treatment group pre-treatment start (day 0) and on day(s) 3 and 6 and used to assess qualitative changes to the tumour microvasculature. In some cases fluorescently labelled AlexaBSA (1mg/ml 0.1ml i/v) was included to image perfused vasculature using IVM 5-10 minute time-lapse measurements (Chapter 2.8).

## 5.5 Results.

The effects on Calu-6 xenograft using AZD2171 (3mg/kg) and fractionated 6Gy, either concurrently or sequentially, showed a significant decrease in GDs in tumours receiving the combined therapies compared to those receiving single modalities (Fig 5.1, Table 5.1). AZD2171 alone and RT alone treatments produced GDs of 12 ± 2 and 17 ± 2 days respectively when compared to the vehicle alone. The combined regimen of AZD2171 and RT both concurrently and sequentially regimens produced a significant increase in the GDs for each combined treatment group; 34 ± 5 (sequential schedule) and 35 ± 5 days

(concurrent schedule) compared to vehicle control ($P < 0.001$) and a significant increase GD increase compared to RT or drug alone ($P < 0.05$) (Table 5.1).

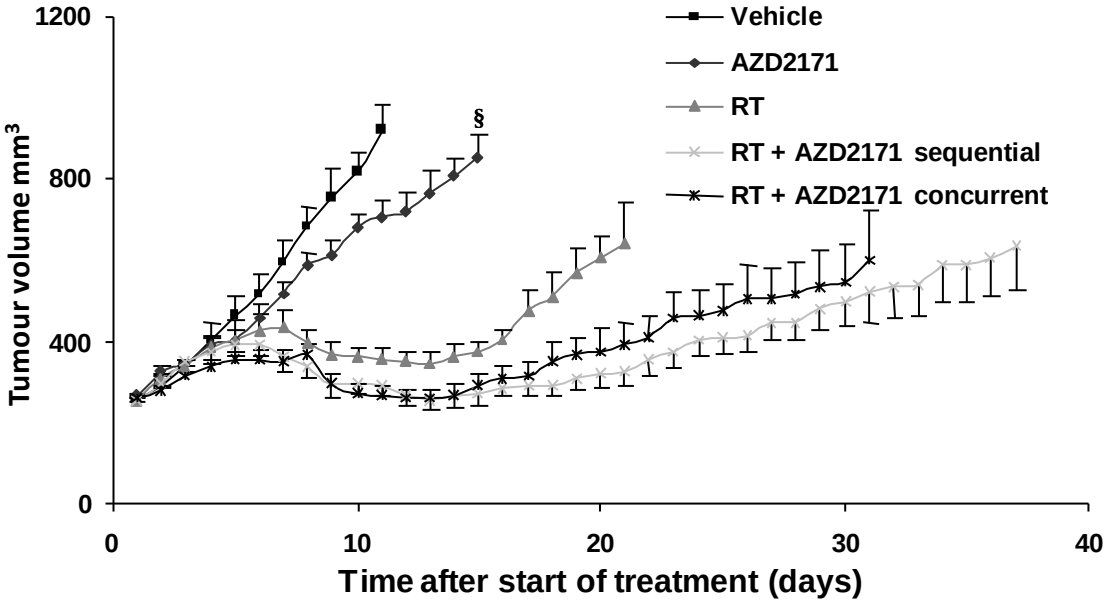


**Fig 5.1** Calu-6 tumour growth delay (± SEM bars) post AZD2171 (3mg/kg daily oral dose) ± fractionated 10Gy RT. Data points plotted from treatments size until first tumour within the group reached RTV4. (§ one tumour regressed completely and was removed from the group). (Adapted from Williams et al. 2007).

The effects of 10Gy combined with AZD2171 (3mg/kg) produced Calu-6 tumour GD values of 21 ± 2 days for 10Gy alone, 37 ± 3 days (sequential schedule) and 41 ± 6 days (concurrent) being significantly greater than for RT alone (Table 5.1)

**Table 5.1 AZD2171 (3mg/kg) enhances Calu-6 xenograft GD usinig 6 and 10 Gy RT.**

| Treatment | RTV4 (days) | DT (Days) | Growth delay (days) |
|---|---|---|---|
| Vehicle | 11 ± 0.5 | 5 ± 0.2 | NA |
| AZD2171 § | 23 ± 2 | 12 ± 2** | 12 ± 2 |
| 3 x 2 Gy IR | | | |
| IR | 28 ± 2 | 9 ± 2** | 17 ± 2 |
| IR + AZD2171 sequential | 45 ± 5* | 17 ± 3* | 34 ± 5* |
| IR + AZD2171 concomitant | 46 ± 5* | 16 ± 1* | 35 ± 5* |
| 5 x 2 Gy IR | | | |
| IR | 32 ± 2 | 8 ± 0.5** | 21 ± 2 |
| IR + AZD2171 sequential | 48 ± 3* | 16 ± 2* | 37 ± 3* |
| RT + AZD2171 concurrent | 52 ± 6* | 17 ± 3* | 41 ± 6* |

**^ Tumours treated daily with AZD2171 until RTV4**
**DT: tumour volume doubling**
**§ One tumour treated with chronic 3 mg/kg AZD2171 regressed**
**•*P* < 0.05 compared with radiation or AZD2171 alone; ** *P* < 0.001 versus vehicle control; Mann Whitney**

(Taken from Williams et al. 2007)

Increasing the dose of AZD2171 to 6mg/kg combined with fractionated 10Gy RT in Calu-6 and LoVo xenograft GD studies for sequential or concurrent scheduling showed similar GD profiles to those seen for the Calu-6 AZD2171(3mg/kg) + 10Gy RT studies. During the course of the combined concurrent schedule the Calu-6 tumours volume were significantly reduced (8 ± 7 $mm^3$) compared to RT alone treated tumours (125 ± 25$mm^3$) ($p$ = 0.003).

There was a significant difference in tumour volumes recorded for LoVo tumours during the combined AZD2171 + RT concurrent schedule compared to those recorded in the RT alone group -38 ± 20$mm^3$ and 60 ± 21 $mm^3$ respectively ( $p$ = 0.04) (Fig. 5.2).

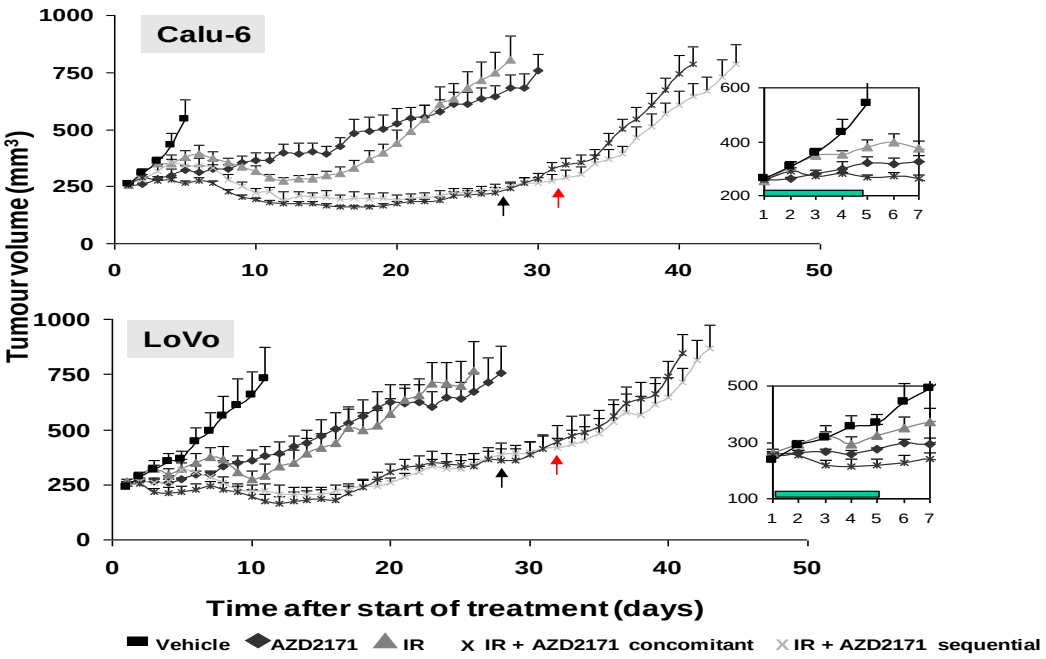


**Fig. 5.2** Calu-6 and LoVo tumour growth delay (GD) data for vehicle alone duration of the study, AZD2171 (3mg/kg p/o daily for 28 days ( black arrows), fractionated 10 Gy (5 x 2Gy), concomitant fractionated 10 Gy with AZD2171 (3mg/kg) 2h prior to each 2Gy then drug for 28 days ( red arrow) and sequential dosing post fractionated 10GyRT of AZD2171 (3mg/kg) commencing after last 2Gy fraction and dosed for 28 days thereafter. Average values from all the tumours in each group; bars, SE (n = 6 for AZD2171 alone and n = 7 for others). (Taken from Williams et al. 2007).

The RTV4, doubling times and nadir (the lowest tumour volumes reached during a treatment) volumes for the tumours was then summarized for each treatment group where the nadir volumes reached by the groups receiving combined modalities were significantly different compared to RT alone (Table 5.2).

**Table 5.2 Effects of AZD2171 (6 mg/kg) on Calu-6 and LoVo tumour growth post RT**

| Treatment | RTV4 (days) | DT (days) | nadir volume ($mm^3$) [day] |
|---|---|---|---|
| Calu-6 | | | |
| Vehicle | 11 ± 0.5 | 5 ± 0.2 | |
| AZD2171 | 36 ± 2 | 17 ± 1 | |
| RT | 32 ± 2 | 8 ± 0.5 | 311 ± 18 [12] |
| RT + AZD2171 (seq) | 50 ± 4** | 7 ± 0.4* | 191 ± 23 [20]*** |
| RT + AZD2171 (con) | 48 ± 3** | 7 ± 0.3* | 161 ± 7 [17]*** |
| LoVo | | | |
| Vehicle | 12 ± 1 | 6 ± 0.7 | |
| AZD2171 | 35 ± 3 | 16 ± 2 | |
| RT | 31 ± 1 | 9 ± 0.5 | 275 ± 36 [10] |
| RT + AZD2171 (seq) | 47 ± 2*** | 9 ± 1* | 204 ± 36 [13]** |
| RT + AZD2171 (con) | 44 ± 1*** | 9 ± 0.5* | 164 ± 34 [12]** |

*Doubling time after removal of AZD2171
**p<0.05 compared with radiation alone
***p<0.001 compared with radiation alone

Sequential (seq), Concurrent (con) (Taken from Williams *et al*. 2007)

On cessation of AZD2171 drug both Calu-6 and LoVo xenografts began to grow at rates similar to those seen for the RT alone group. The Calu-6 DWC xenograft % MVD studies showed that vehicle alone had little or no effect on the over the 6 day period (data not included). The overall change in MVD was calculated from subtracting the final %MVD measured by MetaMorph® on day 6 from the initial %MVD measured pre-treatment on day 0 expressed as a percentage change (Fig 5.3).

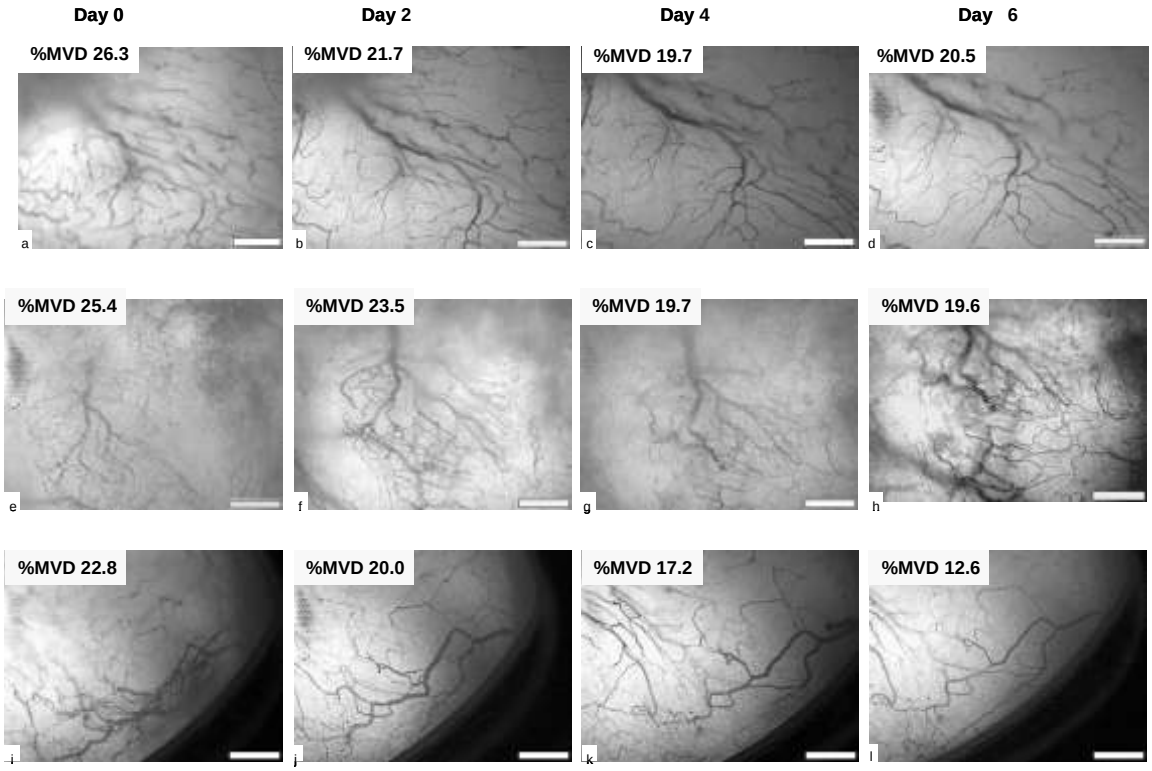


**Fig. 5.3** Examples of brightfield IVM images of Calu-6 dorsal window chambers vessels (DWCs n=1 per treatment group) and % MVDs for a-d) AZD2171 (3mg/kg oral) dose alone given on day 0 for 3 days, e-h) RT 6Gy (3x2Gy), i-l) AZD2171 (3mg/kg oral) given after 6Gy (3x2Gy) (sequential regimen) (Scale bar 500μm).

The effects of AZD2171 alone resulted in a %MDV of -22% compared to the pre-treatment %MVD measured on day 0. Fractionated RT produced a similar reduction in %MVD of -22% by day 6. However the effects of sequential AZD2171 and fractionated 6Gy resulted in a %MVD of -44% by day 6 compared to the pre-treatment values (Fig 5.3). Qualitatively the DWC vasculature treated with the combined RT and AZD2171 sequential regimen showed a change from a multi-branched appearance (Figs 5.4 (a, a1) to fewer branching vessels 48h later (Fig 5.4 (b, b1). This change continued with some vessels either closing or disappearing over successive imaging days resulting in smoother vessel appearance compared to that seen on treatment day 0 (Figs 5.4 (a1 – d1)).

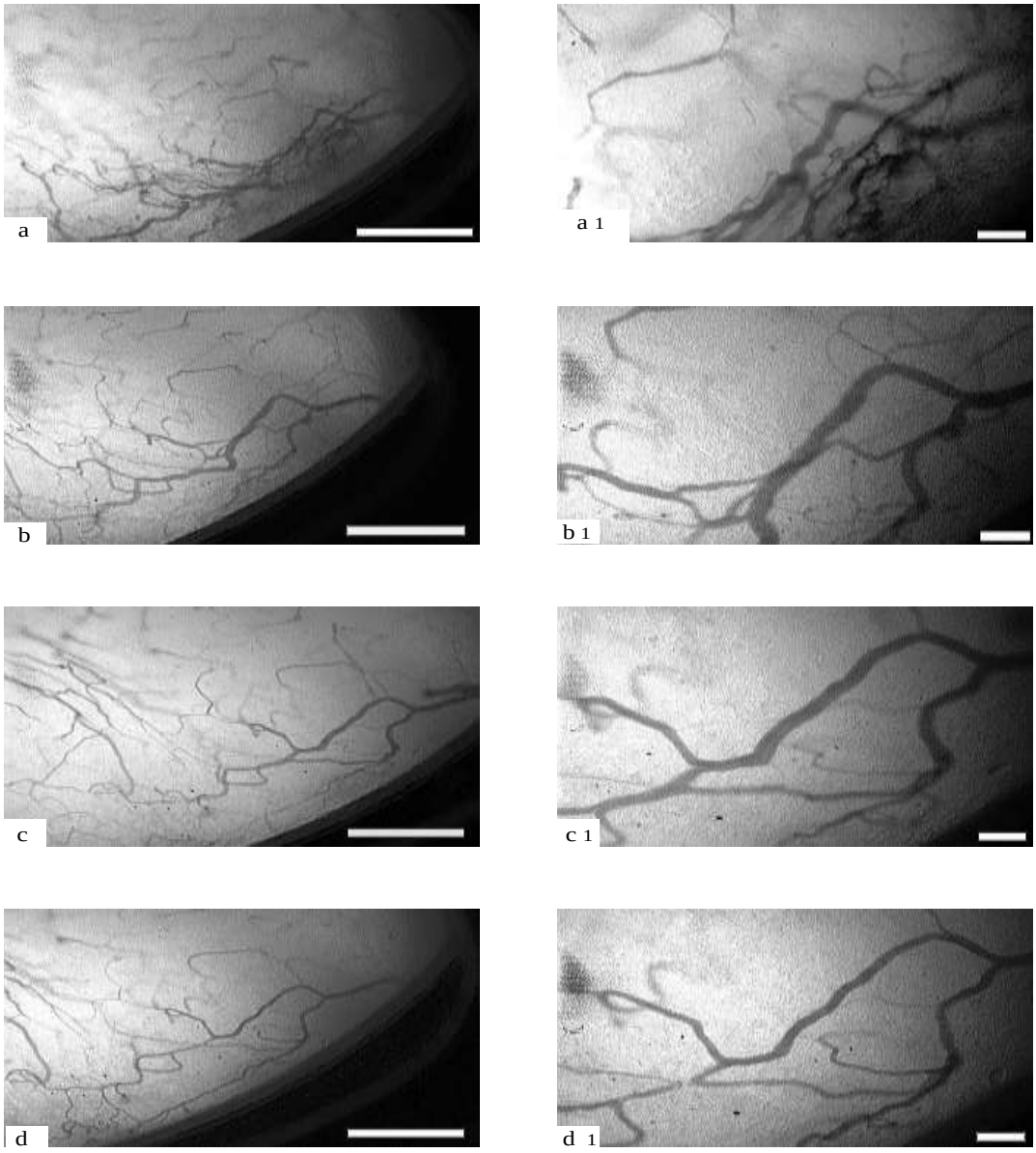


**Fig 5.4** IVM brightfield illumination images of Calu-6 DWC vasculature a) last day of the fractionated 6Gy (3x2Gy) schedule, b) 48h post AZD2171 (3mg/kg) , c) 96h day post AZD2171and d) 144h post AZD2171 (Scale bar 500µm for a- d and 250µm for a1- d1).

## 5.6 Discussion.

A number of different proposals have been put forward for the mechanism of action for the small molecular inhibitors of VEGFR tyrosine kinases (VEGFRs -1, -2, and -3) in combination with RT. AZD2171 has previously been shown to inhibit VEGF signalling responses in EC cells at sub nanomolar concentrations resulting in angiogenesis inhibition *in vivo* (Wedge et al. 2005). There are two principle modes of action proposed for the effects seen when combining AZD2171 and RT; the first is that it interferes with the VEGF signalling pathway such that it leads to direct radiosensitisation of the ECs of the tumour vasculature (Gorski et al. 1999); secondly it induces vascular normalisation and hence improved vessel perfusion (Winkler et al. 2004).

One potential anomaly might be that by using VEGFR targeted strategies concomitantly with RT, the reduction in MVD should result in increased tumour hypoxia thereby increasing the radioresistance of the tumour cells (Franco et al. 2006). An alternative approach might be to use a sequential dosing regimen where the anti VEGF treatment is given after RT. The latter regimen has proved successful in pre-clinical trials with additional studies supporting the belief that tumour vasculature may be specifically sensitized to an applied VEGF targeting agent (Zips et al. 2005, Cao et al. 2006).

In this study we looked at the effects of combining AZD2171 and RT using both conventional mouse tumour xenograft GD studies and non-invasively using the DWC xenograft model.

These studies showed that AZD2171, whether given as a concomitant or sequential regimen were equally effective in enhancing radiotherapy outcome using subcutaneous murine xenograft models.

The effects in the subcutaneous xenograft were to reduce MVD by 50% and in the DWC by 44%. Histological analysis of tumours treated using a similar sequential schedule to that used for the DWC studies carried out by Dr Kaye Williams in our group, showed that a marked vessel loss resulting in a MVD of 6 ± 0.4 vessels per $mm^2$ after combined treatment and that this was significantly lower than the RT alone group or the drug alone group being ($p = 0.04$) and $p = 0.03$ respectively (Table 5.3). The results from the DWC studies were complementary to those found after histological analysis when the same regimens were used.

**Table 5.3 Effects of AZD2171 and 10Gy RT on Calu-6 xenografts.**

| **Treatment** | **MVD ($mm^2$)** Total | **MVD ($mm^2$)** Perfused | **Perfused Fraction (%)** | **Hypoxic Fraction (%)** |
|---|---|---|---|---|
| **Vehicle** | 21 ± 5 | 12 ±3 | 64 ± 24 | 9 ± 5 |
| **RT** | 10 ± 2 | 4 ± 1[a] | 40 ± 9 | 10 ± 2 |
| **AZD2171 (3mg/kg)** | 11 ± 2 | 8 ± 1 | 80 ± 6 | 13 ± 4 |
| **AZD2171 + 10Gy RT concomitant** | 8 ± 1[a] | 4 ± 1[a] | 51 ± 15 | 24 ± 5[a] |
| **AZD2171 + 10 Gy RT sequential** | 6 ± 0[b] | 2 ± 0[b] | 40 ± 3 | 1 ± 1 |

[a] $p < 0.05$ and [b] $p < 0.005$
Compared to vehicle.
Average values ± SE

The change in MVDs for the drug alone or RT alone DWCs was not as marked as that seen found in the histological measured tumours however we need to remember we were measuring MVDs in DWCs tumour that were on average one third of the volume.

It may be that in more developed tumours the rates of angiogenesis may be greater than that of initiating tumour volume sizes within the DWCs. The ability to resolve this apparent difference is currently being investigated with the introduction of polyethylene DWCs that permit tumour volumes of up to 200mm$^3$ and to carry out vascular studies in subcutaneous xenografts at 100mm$^{3.}$

Histological analysis showed that the MVDs for the treated groups was lower than the untreated tumours, but that the proportion of perfused vessels in the AZD2171 alone treated tumours was higher than the RT alone group or the drug + RT group. This could indicate a possible mechanism of action for ADZ2171 is to reduce the number of vessels, but make them perfuse more efficiently. This may indicate that normalisation of the vessels was occurring as seen in DWC model where pruning of vessels was evident (normalisation) as early as 48h post AZD2171 introduction. In the DWC model the pruning of vessels continued before eventually beginning to close by day 6. It could be interpreted than the initial effect of AZD2171 is to cause transient normalisation, but after a period of time the RT eventually causes vessel shutdown. Studies are warranted to verify this in the DWC model using vessel diameter measurement software analysis or by using perfusion markers as carried out by others (Iga et al. 2006, Tozer et al. 2005, Yuan et al. 1996).

In addition to the pruning of vessels it was evident that we may be seeing transient acute hypoxia taking place since areas around the larger vessels were no being fed by perfusing vessel. This transient state might be confirmed if we were able to continue time-lapse imaging for several days longer than we could in these studies.

It would be interesting to see if the disappearing or closed vessels re-opened at a later time-point to allowing angiogenesis to re-establish. This may have been what was seen when the drug was removed after 28 days dosing of sequential and concurrent regimens using the LoVo and Calu-6 xenograft GD studies. Dr Williams showed there was an increase in hypoxia (measured by Pimonidazole) in the drug alone treated tumours suggesting that the transient normalisation of the vasculature might assist in the formation of acute regions of hypoxia (Fig 5.5).

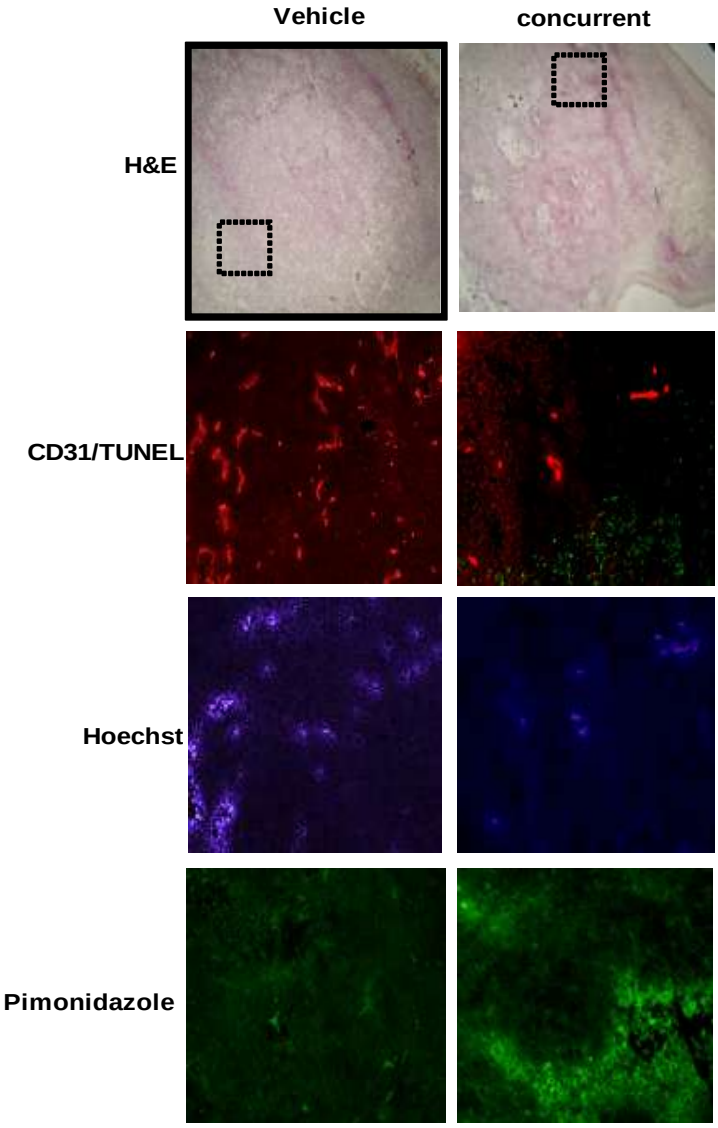


**Fig 5.5** Representative histology images of vessel distribution, perfusion and hypoxia in a vascular hot spot (indicated by the boxes) of vehicle treated Calu-6 tumour compared to a combined AZD2171 (6mg/kg) + 10Gy tumour. Overlay of vessels (CD31; red) and apoptosis (TUNNEL; green, vessel perfusion (Hoechst; blue and hypoxia (Pimonidazole binding; green). Boxes, relative position of the ROIs on the Haematoxylin and Eosin (H&E) stained sections (Reproduced with permission from Dr Kaye Williams).

Histological analysis of the combined treatment tumours showed a reduction in vascular endothelial cells, a reduction in perfusion and an increase in hypoxia as well as necrosis and apoptosis (Fig 5.9). This indicates a whole chain of events occurs when RT and AZD2171 are used in combination resulting in enhanced anti tumour responses (Fig 5.9). The question as to whether AZD2171 causes decreased or increased stromal oxygenation could be partially answered if studies had been carried out using DWCs equipped with oxygen sensors (Dewhirst Yuan).

Although concurrent scheduling, using AZD2171(6mg/kg), did produce a slightly more enhanced tumour GD response than the lower dose (3mg/kg), it did not improve the extent of tumour regression observed post RT compared to the sequential regimen for Calu-6 tumours. Since hypoxic cells are known to confer both chemotherapy and RT resistance it is important that this drug is studied in relation to whether it acts specifically on one type of target i.e. tyrosine kinase receptors or if it has additional effects on secondary angiogenesis signalling pathways such as endothelial growth factor receptor EGFR signalling. The inducible hypoxia resulting from combined AZD2171 and RT may result in a reduction in the efficacy of an additional therapy allowing re-population of the tumour stroma with more resistant cells. The results from these studies might also imply also there might be a finite number of vessels that are susceptible to AZD2171 and as such only a limited response to AZD2171 is possible and that increasing the concentration will not enhance its activity.

However when AZD2171 was stopped after 28 days in the combined RT regimens tumours growth resumed implying that AZD2171 had constrained the tumour growth rate indicating a possible novel use where it is essential to try and limit tumour growth during a therapy strategy allowing more time for additional therapies to act.

The DWC xenograft model allowed us to 'see' what was happening to the vasculature immediately the dosing regimen was started and to follow it for several days. To the authors knowledge this has not been shown before for either these cell types or for this molecular inhibitor of VEGFR.

Although an insight into the possible mechanisms of action has been possible through comparative studies between tumour growth delay and DWC models it is important to note we were comparing tumours of different sizes. One disadvantage of the DWC model was being limited to a 100mm$^3$ tumour volume not an RTV3 or 4 volumes of 700mm-1100mm$^3$ and that the stroma make-up may differ for larger tumours where necrotic tissues as well as interstitial pressure variances may influence our interpretations.

### 5.6.1 Summary.

The mechanism of action of AZD2171 could be partially described in that; normalisation was clearly evident as a primary response to the combined sequential scheduling of AZD2171 and RT using the DWC model (Figs 5.8 i-l) confirming the vessel normalisation hypothesis described by others (Jain et al. 2005). It is particularly important we look at combined therapies in relation to vascular changes in order we don't adversely affect a potential window of opportunistic therapeutic benefit.

The use of the DWC model has already been used to understand the effects of antiangiogenic agents such as the vascular disrupting agent (VDA) Combrestatin (Kanthou et al. 2002.)

It may also prove useful for determining whether an antiangiogenic agent works on the tips of developing vessels (angiogenesis sprouts) or on the more established larger vessels which may be important if we are to develop tailored antitumour therapies.

The development of structural and functional tumour vasculature markers, as well as imaging technologies, should lead to a better understanding of what cytotoxic drugs work well with which RT dosing schedule and for which particular tumour type. Here we have shown that AZD2171 enhanced tumour radiation response as well as impacting on the tumour stroma. The inclusion of the DWC model allowed us to measure MVD changes; however additional work involving vascular perfusion markers such as fluorescently conjugated AlexaBSA would provide a more detailed interpretation of the mechanisms of action of AZD217).

The usefulness of the DWC model in developmental antitumour therapy regimen studies has several beneficial aspects since it allows real-time imaging of an applied dosing regimen that is not readably available in the clinical setting. It may be useful to use the DWC model to re-visit some chemotherapeutic strategies that have been discontinued due to a lack of efficacy or toxicity in the clinic and offer new perspectives on why they failed in the clinical setting. Additionally the DWC model could be developed as a tumour therapy screening tool to determine how best to implement a proposed scheduling regimen therapy strategy.

# CHAPTER 6 - THERAPY COMBINATION STUDIES USING AZD6244 AND RT.

In complex biological systems the processes of cell proliferation, differentiation and survival are regulated by a number of extracellular hormones and growth factors as well as cellular signalling molecules. In cancer cells cellular dysregulation may occur via the mutation and or overexpression of proto-oncogenes. One such proto-oncogene is Ras. The Ras (**Ra**t **s**arcoma) genes were first identified as transforming oncogenes that synthesize Ras protein to act as binary molecular switches controlling many cytoplasmic kinase signalling cascades. One of the most studied and best characterised biological signal transduction pathways is the Ras/Raf/ mitogen-activated protein kinase (MAPK) /extracellular signal-regulated kinase (ERK) pathway (MAPK/ERK also is known as MEK1/2). The MAPK/ERK signalling pathway responds to a vast number of extracellular signals via ERK1/2 proteins that control several aspects of cellular biology. These include DNA synthesis, cell cycling, growth, division, differentiation and apoptosis (Brunet et al. 1999, Yoon et al. 2006), as well as influencing actin cytoskeleton integrity, cell adhesion, integrin cell migration signalling and cell migration (Mavria et al. 2006).

The importance of Ras was noted in cancers when mutated forms of Ras were found in approximately 30% of all human cancers resulting in the realisation that this G protein could be an important target for the development of anti-cancer drugs. This has been comprehensively reviewed by others (Bos et al. 1989, Adjei et al. 2001).

Oncogenic Ras mutations have also been implicated in tumour metastasis and angiogenesis. The Ras oncogene has also been reported to confer resistance to radiation ionisation (Sklar 1988, McKenna et al. 1990) and as such modifying this resistance could

improve applied therapy regimens of radiotherapy combined with Ras knockdown treatments. The realisation that the Ras to MAPK pathway has an influence on tumour radioresistance has been shown through work carried out by Kasid et al. who transfected a truncated constitutively active Raf gene into a human squamous cell carcinoma line which led to increased cell survival post radiation (Kasid et al. 1989). They also showed that down-regulation of Raf through antisense c-raf-1 also reduced the radioresistance of human cells implying that the Raf-MEK-MAPK pathway was linked to radiosensitivity (Kasid et al. 1989, Gorkhale et al. 1999).

Studies from two laboratories provided evidence that radioresistance of Ras-mutated cells is most likely the result of a constitutively activated autocrine loop of endothelial growth factor receptor (EGFR)-ligand production and receptor stimulation (Toulany et al. 2005, Cengel et al. 2007). It has been established for a while now that the constitutive activity of mutated Ras-protein, especially K-Ras, leads to an increase in the production of EGFR-ligands, such as tumour growth factor alpha (TGFα) and amphiregulin (Ganggarosa et al. 1997, Sizemore et al. 1999). These ligands can in turn bind to the EGFR in an autocrine manner leading to the activation of this receptor and subsequent downstream signalling cascades. Toulany et al., found that the autocrine loop preferentially simulates EGFR signalling through the P13K-AKT pathway. P13K-AKT activity results in the activation of DNA protein kinase catalytic subunit (DNA-PKcs) (Toulaney et al. 2007). The radiosensitisation of tumour cells is thought to be as a consequence of an impaired repair of DNA double strand breaks (DNA-DSB) mediated through blockade of EGFR signalling events (Dittmann et al. 2005a, 2005b, Toulany et al. 2005a, 2005b, 2006).

In irradiated cells a reduction of DNA-phosphokinase (DNA-PK) activity leads to a reduced autophosphorylation of DNA-PK which is essential for the non-homologous end joining (NHEJ) repair of DNA-DSBs. Chen et al., further showed the importance of low levels of DNA-PK and resulting increase in cellular sensitivity to ionisation energy resulting from impaired DNA-DSB repair by measuring enhanced residual DNA-DSBs 24h post irradiation (Chen et al. 2007).

The largest clinical study carried out looking at one of the family of Ras mutations (K-Ras mutation) demonstrated that the detection of this mutation in non-small-cell lung cancer in 1413 patients was a poor prognostic indicator (Samowitz et al. 2000).

The high percentage of human tumours having Ras mutations has led researchers to try and develop drugs that can interfere with the Ras-signalling pathway by either inhibiting Ras protein expression through ribozymes, antisense oligonucleotides or RNAs, the prevention of membrane localisation of Ras and or trying to inhibit downstream effectors of Ras function (Golding et al. 2007).

Oncogenic transformation of cells can cause constitutive activation of cell signalling pathways such as MEK1/2 resulting in excessive expression of growth factors or mutations of intermediate components of the pathway causing the normally balanced processes to remain activated regardless of the original extracellular signal.

The identification of the MEK1/2 signalling cascade and its role in tumour cell resistance lead to the idea that this was a possible target for antitumour therapy development. In tumour cells the MEK1/2 pathway can be activated by cell surface growth factor receptors or via downstream activating mutations in RAS and B-RAF (Beeram et al. 2005).

MEK1/2 signalling is also thought to regulate the production of vascular endothelial growth factor (VEGF) and hence angiogenesis as well as sensitizing endothelial cells (ECs) to radiation (Park et al. 2001, Byrne et al. 2005). In ECs the VEGF promoter region contains a hypoxia response element (HRE) which regulates VEGF production via hypoxia inducible factor 1α (HIF-1α) which is also a target of ERK1/2. HIF-1 activity is also known to promote radioresistance through a variety of mechanisms (Moeller et al. 2005, Williams et al. 2005).

A number of different small molecular inhibitors of MEK1/2 signalling pathways have been developed recently, with some in pre-clinical and clinical evaluations being carried out to investigate targeting and blocking the MEK1/2 pathway at different levels.

One such candidate is AZD6244 (ARRY-142886, Selumetinib), a novel orally active selective potent inhibitor of mitogen-activated protein kinase/extracellular signal-regulated kinase kinase 1/2 kinases (MAPK/ERK1/2) currently in phase II development for the treatment of non-small cell lung (NSCL) (Tzekova et al. 2008) and hepatocarcinoma cancer (Huynh et al. 2007).

### 6.1.1 Aims.

The main objective of this study was to look at the effects of combining AZD6244 with fractionated radiotherapy (RT) using Calu-6 (human lung) and HCT116 (human colon) tumour xenograft GD models. In addition we aimed to measure tumour stromal responses to the combined regimen using histological analysis as well as attempting to visualise in situ and in real-time the stromal responses using the dorsal window chamber (DWC) xenograft model.

By using these models it was hoped to try and determine some of the possible mechanisms of action of this drug in combination with RT and to determine if sequential dosing schedules produced different tumour growth delay responses.

## 6.2 Tumour xenograft responses to combined AZD6244 and RT.

The preparation of tumour cells for inoculation has been described earlier (Chapter 2.1.2.2). Briefly, Calu-6 and HCT116 cells were harvested in the exponential phase of growth and made up to inoculation concentrations of $2 \times 10^7$ cells/ml in a 1:1 mix of serum free RPMI and Matrigel™. HCT116 cells were prepared at $5 \times 10^7$ cells/ml in serum free RPMI. The cells were implanted into the dorsal skin i/d of female nude adult mice. Palpable tumours were measured at least three times a week and the data used to determine tumour growth volumes for each treatment group.

When the xenograft tumour volumes reached 240-300 $mm^3$ the mice were randomly assigned to designated treatment groups (n = 5 per group). Drug routes and volumes are listed in Chapter 2.3. Daily drug doses were split into two daily doses (bd) with an 8 hour gap between each.

- Vehicle (methocel/polysorbate)
- AZD6244 (25mg/kg oral bd) dosed for 10 days
- 10 Gy RT as fractionated 2Gy daily doses for 5 days
- 10 Gy RT as fractionated 2Gy daily doses for 5 days followed by AZD6244 (for 5 days) (sequential regimen).
- For the Calu-6 studies and extra group involved giving fractionated 10Gy RT commencing on day 1 of drug treatment (concomitant) or commencing on day 5 post drug treatments (sequential).

Average tumour volumes were recorded until the first tumour within a group reached 1,000mm$^3$. Tumour GD data was plotted using relative tumour volume to triple in size (RTV3) from the initial treatment volume (240-300 mm$^3$) and the data plotted. A two way ANOVA test was carried out on the last day when data were available for all groups.

## 6.3 Application of the DWC/IVM model to Calu-6 tumour vascular response to combined AZD6244 and RT.

The procedure for DWC attachment has been described earlier (Chapter 2.5.1). Briefly, DWCs were set up (n=6) and inoculated with Calu-6 tumour cells (~ 1x10$^6$) in a 1:1 mix of serum-free RPMI and Matrigel™ 72h post attachment. Once established tumour vasculature presented and the tumour volume approached ~60-70mm3 the DWCs were assigned into treatment groups:

- Vehicle daily for 6 days
- AZD6244 (25mg/kg oral) daily for 6 days
- 6Gy RT (2Gy daily for 3 days)
- AZD6244 daily for 6 days and 6Gy RT (2Gy daily for the first 3 days).

The DWC tumour vasculature was imaged daily using brightfield trans illumination and the microvascular density (MVD) for each treatment calculated (Chapter 2.7). AlexaBSA (1mg/kg i/v) intravital (IVM) 10 time-lapse measurements were recorded on day(s) 0, 2 and 5 for 8-10 minutes for each DWC tumour treatment (n=2).

## 6.4 Results.

Calu-6 tumours treated with AZD6244 for 10 days resulted in an increase in RTV3 (27.5 ± 3.1 days) compared to the vehicle alone treated group (13.6 ± 2.1 days). All groups receiving AZD6244 resulted in a regression of the tumour from treatment size (~ 250mm$^3$) to an average nadir volume (smallest volume reached following start of treatment) of around 117mm$^3$ occurring 24h after treatment ended. However after the drug dosing schedule was stopped the drug group alone returned to the initial treatment size ~ 7 days later and mirrored the growth rate for the RT alone group (Fig 6.1).

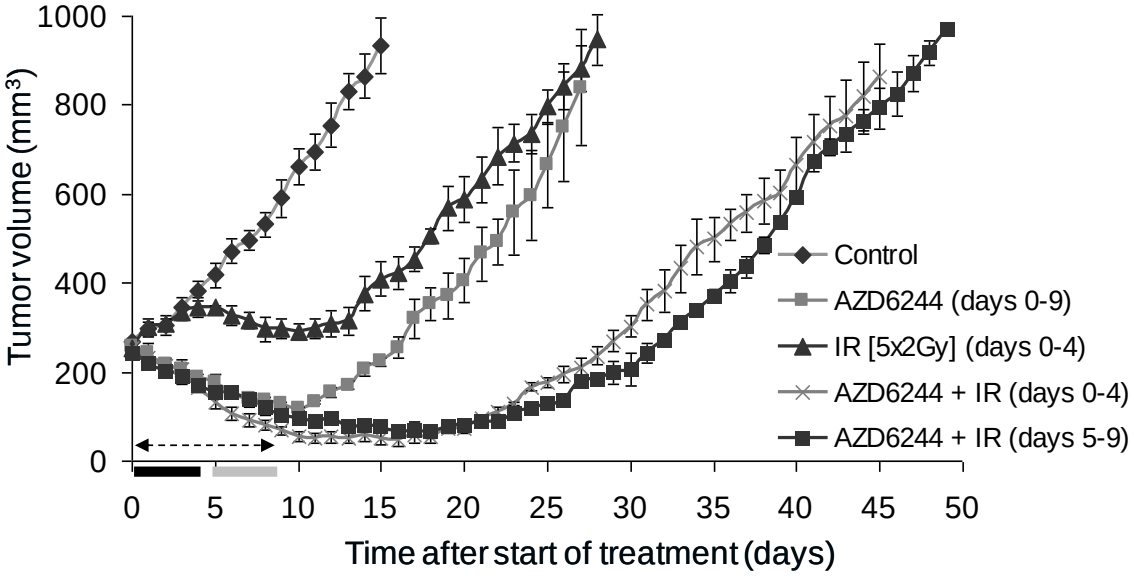


**Fig 6.1** Tumour growth delay curves for Calu-6 xenografts receiving vehicle alone, AZD6244 (25mg/kg b.i.d for 10 days alone, fractionated 10gGy radiation (IR) alone, AZD6244 + 10Gy combined on days 0-4 days and AZD6244+ 10Gy combined on days 5-9)

Fractionated RT induced a radiation GD effect with averaged RTV3 being reached 24.3 ± 2.6days. The irradiated tumours receiving 10Gy on days 0-4 regressed to 290mm$^3$ from a maximal volume of 345mm$^3$ 6 days post radiation. On day 15 there was a statistically significant interaction between RT and drug treatment (P= 0.035). Both groups receiving RT and AZD6244 reached an RTV3 around day 43 which significantly longer than either modality alone ($p < 0.05$).

AZD6244 alone for the HCT116 tumour GD study did not produce the nadir response seen in the Calu-6 tumours and did not cause regression during the course of the treatment either. The growth rate for the drug alone group mirrored the response for the RT alone group. However in the combined group treated with AZD6244 and RT an averaged nadir volume of 178mm3 occurred around day 9-10 of the dosing schedule. As was seen with the Calu-6 model the effects of the combined treatment on GD were significantly higher than that of either modality on its own ($p < 0.05$) (Fig 6.2).

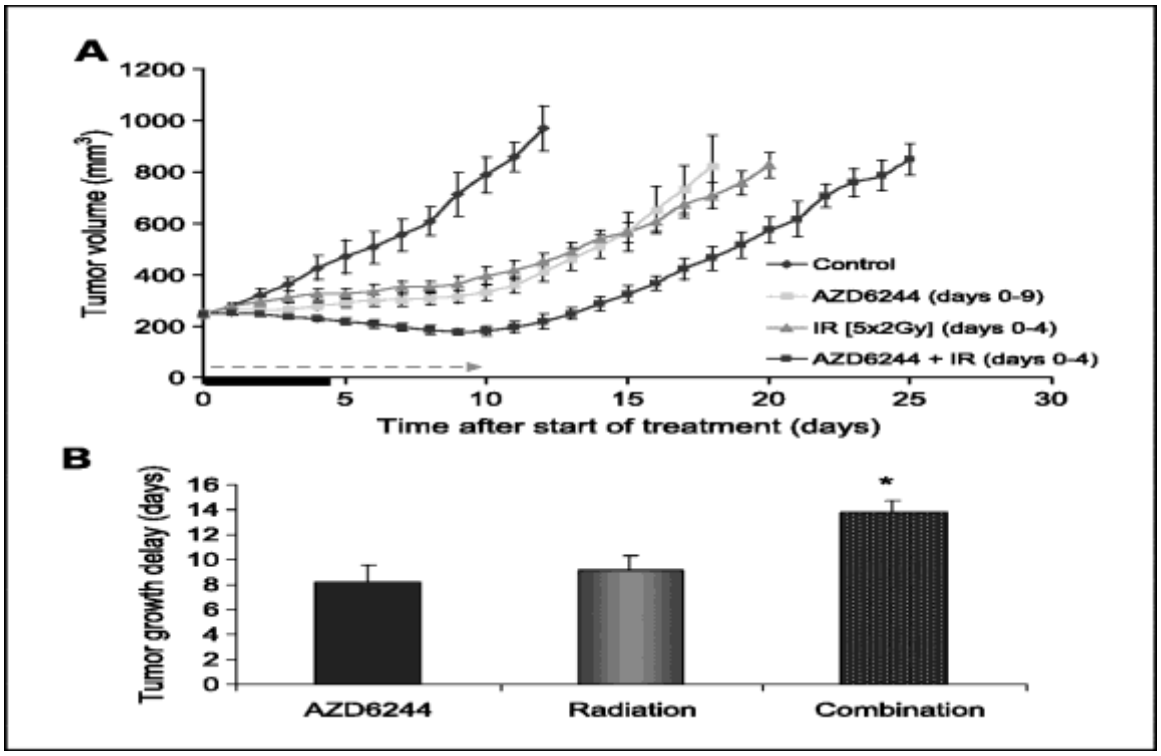


**Fig. 6.2** A**)** Effects of AZD6244 (25mg/kg twice daily for 10days) on HCT116 human colon xenografts alone and in combination with fractionated 10Gy (IR). Average tumour volumes were plotted with bars and SE until the first tumour within the group reached 1000mm$^3$. B) Tumour growth delay (GD) for HCT116 tumours treated with AZD6244 + 10Gy (IR) resulted in a significant increase in GD compared with either therapy alone (*, P <0.05 versus AZD6244 or radiation alone) Tumour growth delay ($RTV3_{treated} - RTV3_{vehicle}$). (Adapted from Shannon et al. 2009).

Combined drug and RT (symbolised as IR in the original paper by Shannon et al. 2009) therapy was significantly greater than either therapy alone (*, $p < 0.05$ versus AZD6244 or RT alone. These results show that AZD6244 combined with RT resulted in significant tumour GD for both tumour types when compared to vehicle treated control groups.

The Calu-6 DWC(n=2) tumour MVD values showed that fractionated 6Gy RT resulted in a decrease of 4.4% by day 5 compared to pre-treatment for one DWC and an increase of 12.4% for the second DWC (Fig 6.3, Table 6.1) receiving the same treatment regimen.

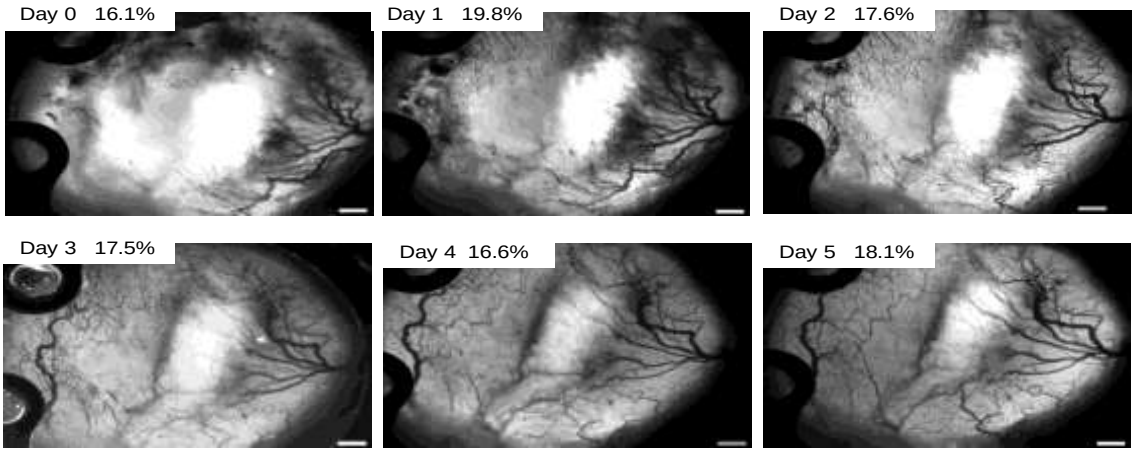


**Fig. 6.3** Brightfield images of a Calu-6 DWC (n=1) vasculature and measured MVD as a percentage of the area viewed in the DWC from day(s) 0 -5 treated with fractionated 6Gy (3x2Gy) RT for the first 3 days and vehicle daily for 6 days (Scale bar 500µm).

The effects of AZD6244 (25mg/kg) alone on measured DWC MVD (n=2) showed that after 3 doses and imaging for 5 days one DWC tumour had an increase in MVD of 6.7% whereas a second DWC tumour resulted a 17.7% decrease when compared to pre-treatment MVD measurements on day 0 (Fig 6.4, Table 6.1).

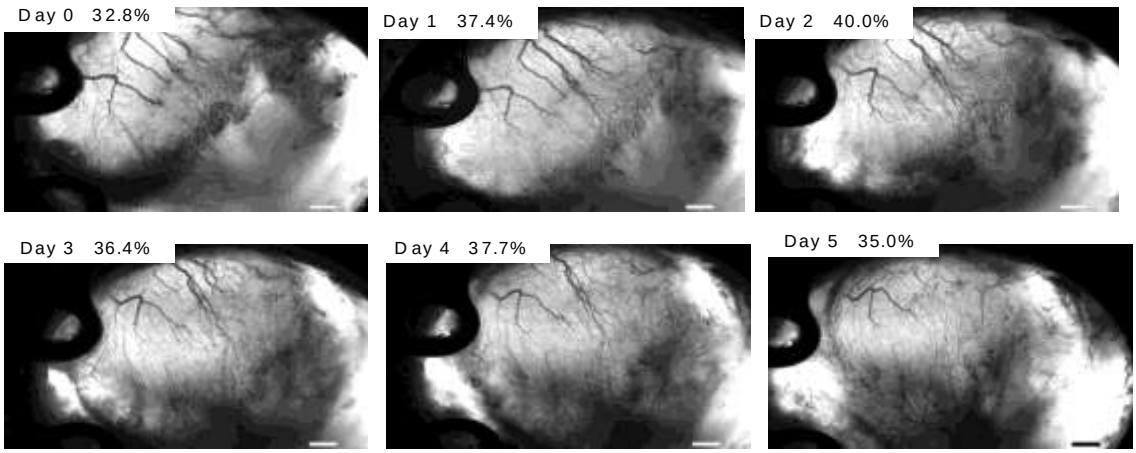


**Fig 6.4** Brightfield images of a Calu-6 DWC (n=1) vasculature and measured MVD as a percentage of the area viewed in the DWC from day(s) 0 -5 treated with AZD6244 (25mg/kg oral dosing) alone for 6 days (Scale bar 500µm).

DWC tumours treated with AZD6244 and fractionated RT combined resulted in a 64.7% reduction in MVD in one DWC and 73.1% reduction in a second DWC by day 5 compared to pre-treatment MVD measurements on day 0 (Fig. 6.5, Table 6.1).

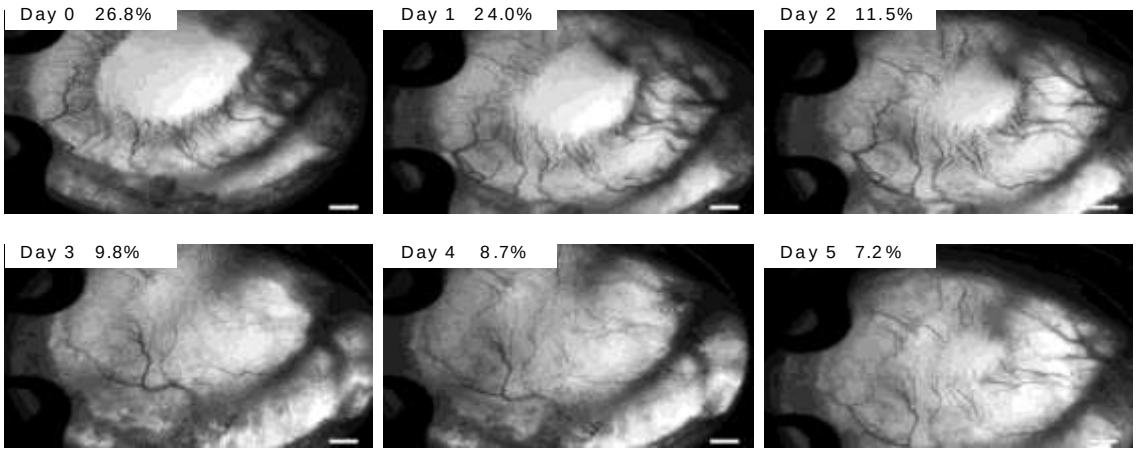


**Fig.6.5** Brightfield images of Calu-6 DWC (n=1) measured vasculature and MVD as a percentage of the area viewed in the DWC from day(s) 0 -5 treated with AZD6244 (25mg/kg oral dosing for 6days) and fractionated 6Gy RT (3x2Gy) given on the first 3 days (concurrent dosing regimen) (Scale bar 500μm).

**Table 6.1** Effects of combined AZD6244 and RT on Calu-6 DWC tumour MVD

| Treatment | DWC | MVD% Day 0 | MVD% Day 5 | MVD% change |
|---|---|---|---|---|
| **AZD6244** | 1 | 22.6 | 18.6 | -17.7 |
| **AZD6244** | 2 | 32.8 | 35.0 | +6.7 |
| **RT (6Gy)** | 3 | 13.5 | 12.9 | -4.4 |
| **RT (6Gy)** | 4 | 16.1 | 18.1 | +12.4 |
| **AZD6244 + RT (6Gy)** | 5 | 20.7 | 7.3 | -64.7 |
| **AZD6244 + RT (6Gy)** | 6 | 26.8 | 7.2 | -73.1 |

Overlaid brightfield and AlexaBSA epi-fluorescence images allowed a qualitative assessment of the Calu-6 vascular changes during a treatment regimen (Fig. 6.6).

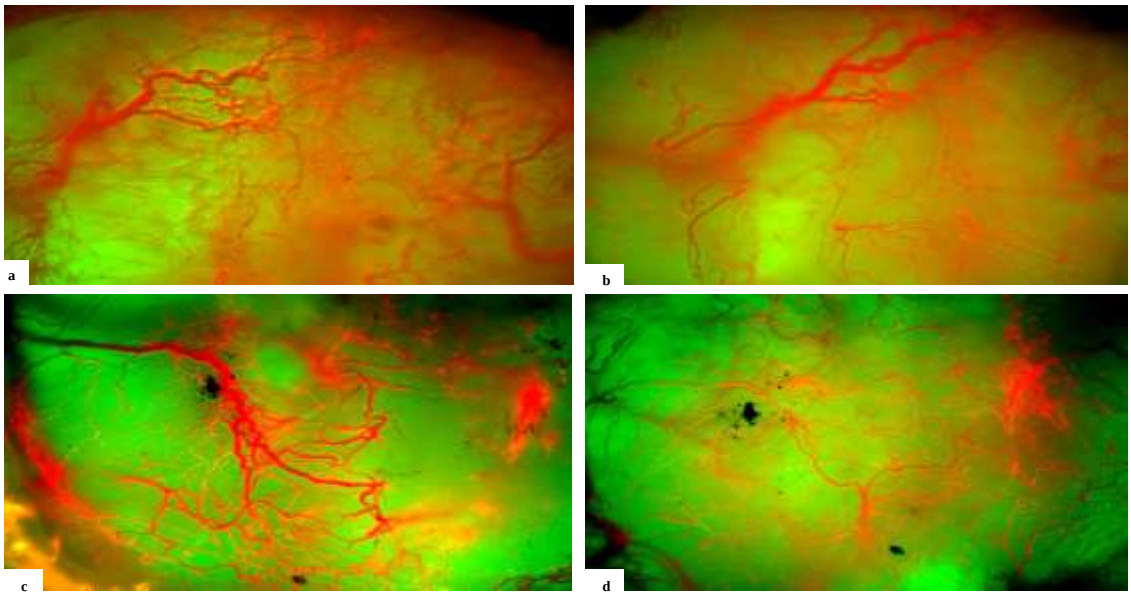


**Fig 6.6** Overlaid brightfield and AlexaBSA (1mg/kg 0.1ml i/v) epi-illuminated images showing Calu-6 DWC vasculatures (n=2) on day 0 before treatment a) n=1 and c) n=1. (b) AZD6244 (25mg/kg oral daily for 5 days) and d) day 5 post treatment with AZD6244 for 5 days combined with fractionated 6Gy beginning on day 2 as 2Gy fractions for 3 days where tumour stroma is shown in green and AlexaBSA perfused vessels in red.(Images at x40 magnification).

Time-lapse IVM measurement of the effects of AZD6244 and RT on the tumour vessel perfusion, with florescent AlexaBSA as a marker of open or perfused vessels where fluorescence measured on day 0 was assigned as 100% (Chapter 2), showed that the average change in fluorescence uptake on day 0 was 2.5 ± 0.5 fold (range 1.26-4.26) over background autofluorescence levels. The effects of AZD6244 combined with RT resulted in a 70% reduction in measured fluorescence for both DWC tumours and the drug alone treated DWC tumours resulted in a one DWC showing a 25% increase in one DWC and a 1.7% reduction in the second. It was also noted that in the drug alone treated DWCs a transient increase in AlexaBSA was seen on day2 for both DWCs, whereas fractionated RT alone caused an increase in fluorescence levels of 25% and 9.3% for two DWCs (Fig 6.7).

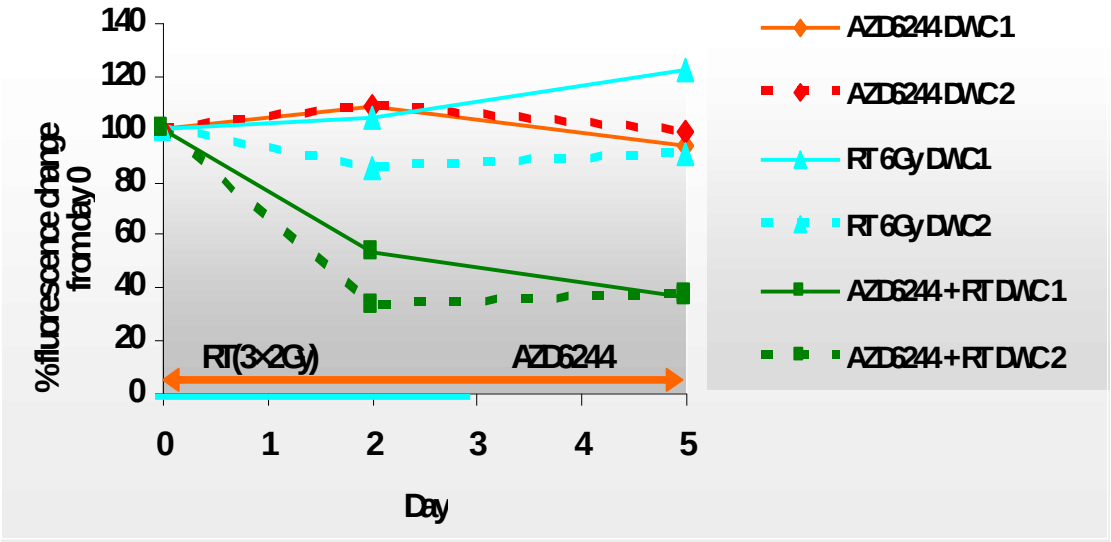


**Fig. 6.7** Calu-6 DWC AlexaBSA (1mg/ml 0.1ml i/v) vasculature fluorescence intensity responses to treatments. DWCs (n=2) treated with AZD6244 (25mg/kg bd for 3days). DWCs (n=2) treated with fractionated 6Gy radiotherapy (RT) and DWCs (n=2) treated with combined AZD6244 for 6 days and fractionated 6Gy RT beginning on day 2 (concomitant). Day 0 assigned 100% perfused with AlexaBSA. (Adapted from Shannon *et al*. 2009)

## 6.5 Discussion.

Since radiotherapy normally forms at least 50% of current antitumour strategies (Steel et al. 1997) enhancing its effectiveness even by a small percentage has the potential to markedly improve tumour response in the clinical setting. It is therefore essential that we continue to study antitumour therapy resistance using pre-clinical models if we are to optimize beneficial responses to a particular modality. In order to try and understand how tumours develop radiotherapeutic and chemotherapeutic resistance we need to address their effects on the totality of the complex biological processes that occur within the tumour stroma.

A key signalling pathways influencing cancer progression is the RAS/RAF/ mitogen-activated protein kinase (MAPK/extracellular signal-regulated kinase (ERK1/2) or

MEK1/2 signalling pathway which is important since approximately one third of human tumours have mutations in RAS, primarily the KRAS isoforms, affecting the activity of VEGF within the tumour (Park et al. 2001) and therefore the process of angiogenesis, neovascular survival (Byrne et al.2005) and vascular EC radiosensitisation (Gorski et al. 1999, Gupta et al. 2002).

In clinical trials AZD6244 has not produced optimal responses in non-small cell lung carcinomas (Tzekova et al. 2008), however MEK1/2 signalling has been shown to increase as a direct response to RT (in some tumours) when used as a monotherapy (Carter et al. 1998, Hagan et al. 2000).

These studies aimed to determine whether the novel MEK1/2 inhibitor AZD6244 could improve tumour response to fractionated RT using CALU-6 lung and HCT116 colon tumour xenografts when used in combination using concurrent or sequential dosing schedules. Additional stromal parameters measurements were assessed using tumour histological preparations (in collaboration Dr Aoife Shannon) to measure tumour MVD, vessel perfusion and levels of hypoxia.

The tumour GD data for both the Calu-6 (lung) and HCT116 (colon) xenografts showed clearly that AZD6244 had an additive effect when combined with fractionated RT for both tumour cell types compared to RT alone whether used sequentially or concurrently and that there was no benefit in using a concurrent versus a sequential dosing schedule. However the differences in the nadir volumes reached during the first 9 days of drug alone or in combination with fractionated RT for the Calu-6 tumours were greater than those seen in the HCT116 tumours.

The HCT116 drug alone treated tumours did not produce a marked tumour size reduction as seen in the Calu-6 treated groups, but did result in a small reduction in treatment volume size when combined with RT.

Apart from the fact that these are two different tumour types it also implies Calu-6 tumours may be more sensitive to AZD6244 perhaps due to different levels of either MEK1/2 signalling, different MVDs or that it has a proapototic effect in Calu-6 tumours as found by others (Davies et al. 2007). However it may be beneficial to have drugs such as AZD6244 in an antitumour regimen where it is beneficial to regress tumour growth for periods of time in order to longs maximize the benefits of additional modalities as suggested by the studies using AZD2171 (Williams et al. 2005).

Collaborative work carried out by others in the group found that AZD6244 pre-treatment of Calu-6 cells *in vitro* lead to radiosensitisation (Shannon et al. 2009), however *in vivo* tumour drug treatment for 5 days before treating with 10Gy (sequential regimen) did not significantly differ from giving the drug and RT during the first 5 days i.e. AZD6244 had not sensitized the tumours *in vivo*. This showed that there was no benefit in pre-treating tumours cells with AZD6244 before RT which conflicted with others, where an enhanced tumour cell response to RT 24h post cessation of drug was found (Hamed et al. 2008). Chung and fellow workers also found that tumour response to AZD6244 (50mg/kg) and a single 3Gy RT dose 4 hours later could potentiate an inhibitory outcome (Chung et al. 2009). Additional work carried out by the group showed that ERK (pERK), a useful marker of MEK1/2 inhibition, was inhibited when RT was administered 2 hours post drug introduction and remained inhibited throughout. In addition to these studies the group found that AZD6244 alone or in combination with and RT had no effect on the cell cycle

profile of Calu-6 cells (Shannon et al. 2009). From these studies it was becoming clearer that another mode of action must be operating in the combined treatment groups to account for the GD data.

Since the MAPK/ERK signalling pathway is known to regulate the activity of HIF-1 (Minet et al. 2000, Sang et al. 2003) and VEGF ( Park et al. 2001, Pages et al. 2000) and both have significant roles in angiogenesis, the group (principally Dr Aoife Shannon) looked at whether AZD6244 could impact on the VEGF levels in the tumours post RT treatment. We already know that VEGF is influential in conferring vascular resistance to RT in tumours (Wachsberger et al. 2003). Work by Dr Aoife Shannon showed that AZD6244 reduced the production of VEGF in Calu-6 cells *in vitro* under hypoxic conditions presumably by inhibiting MEK1/2 and HIF-1 activity. Dr Shannon also investigated VEGF, HIF-α, GLUT-1 and pERK expression and found that these were reduced in AZD6244 treated tumours compared to vehicle controls. From these studies it could be surmised that a reduced VEGF level may one of the mechanisms of action of MEK1/2 resulting in the decreased vascular ECs survival post treatment.

Additional *in vivo* studies by our group looked at the effects of Calu-6 tumours with drug alone treatment for 10 days, fractionated 10Gy alone and combined treatments to determine how these treatments impacted on tumour vessel perfusion and hypoxia.

Histological analysis of the treated tumours showed there was no significant differences in MVDs between the treatment groups ($p$ <0.05; Fig. 6.3). However there was a significant decrease in vessel perfusion, in the RT alone group and in the AZD6244 + RT group compared to the other treatment groups ($p$ <0.05) (Fig. 6.4).

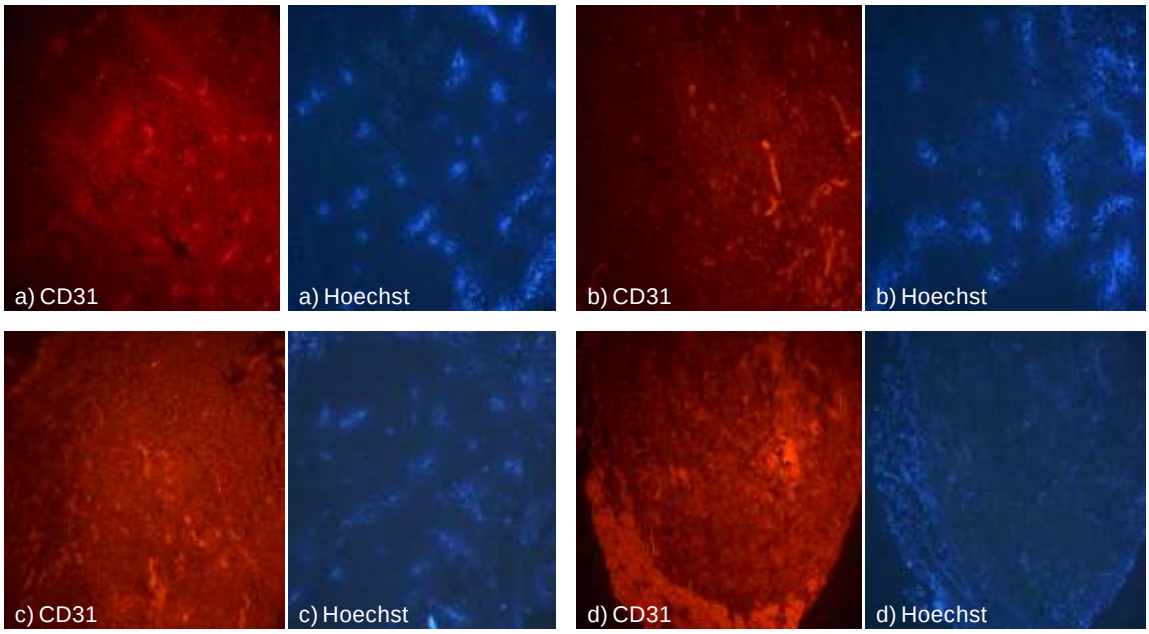


**Fig. 6.8** Endothelial cell marker (CD31) and vessel perfusion marker (Hoechst) staining for Calu-6 tumour xenografts a) vehicle alone, b) 10Gy radiation, c) AZD6244 (25mg/kg bd) and d) AZD6244 +10Gy. (Magnification x100) (Adapted, with permission from Shannon et al. 2009).

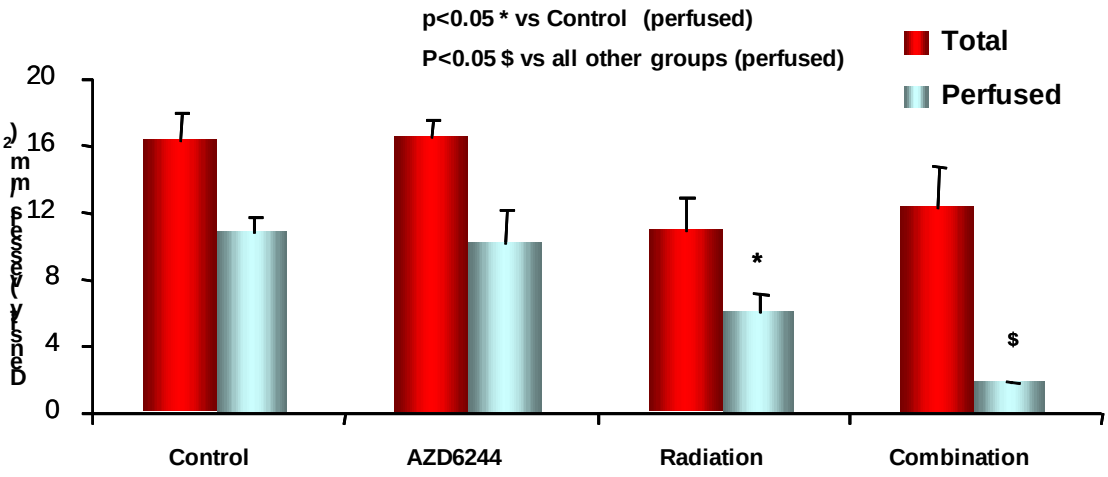


**Fig. 6.9** Microvascular density and vessel perfusion measurements of Calu-6 tumour xenografts harvested at treatment size (control), AZD6244 (25mg/kg) daily for 10 days, 10Gy (5x2Gy) and vehicle and 10Gy (5x2Gy for the first 5 days) in combination with AZD6244 for 10 days (concomitant). The total number of vessels per $mm^2$ was measured (CD31 labelled endothelial cells) and compared to the number of perfused vessels for the same area using Hoechst. (Adapted, with permission from Shannon et al. 2009).

Tumour hypoxia studies carried out by Dr Aoife Shannon showed that AZD6244 alone treated tumours had significantly less hypoxia ($p$ = 0.002) than either the RT or vehicle control tumours. This implies a possible mechanism of action for AZD6244 may be that it modifies the HIF-1 levels reducing the level of hypoxia present that resulting in the

increased GD response seen in combined drug and RT tumour schedules (Shannon et al. 2009).

In order to visualise what was happening in 'real-time' in the tumour stroma the author and co-workers employed the DWC xenograft model. When combined AZD6244 and 6Gy was applied to Calu-6 DWCs (n=2) the fluorescence intensity of AlexaBSA decreased from 100% on day 0 to ~ 30% by day 5 and the %MVDs both showed significant reductions ($p = 0.047$) compared to either modality alone.

The reduction in MVD was not as marked in the drug or radiation alone DWCs. In one drug alone treated DWC a decrease in MVD and AlexaBSA perfusion of vessels was seen, but less so in the second DWC. Perhaps some vessels were more susceptible due to vascular their heterogeneity. Although it probably implies additional DWC studies are needed. What was evident, qualitatively, was that no normalisation of vessels occurred implying that this was not one of the mechanisms of action for this drug and that the reduced hypoxia measured in the subcutaneous tumours was probably a direct result of its influence on HIF-1 activity.

However studies by Mavria et al. point to a possible different mechanism of action involving MEK1/2 signalling inhibition and its effects on tumour response to therapy. Mavria et al. proposed that blocked or non-functional MEK1/2 signalling in tumour vasculature results in a reduction in angiogenesis and this in turn reduces tumour growth via its role in up regulating Rho-kinase signalling activity which is involved in endothelial cell spreading, survival and vessel sprouting (Mavria et al. 2006).

The Rho family of GTPases is involved in a multitude of cellular events including cell cycle progression, growth, differentiation, cytoskeleton reorganization, cell motility and been shown to be elevated in several cancers (Fritz et al. 2011). Through their studies Marvia et al. found that inhibition of the ERK/MAPK reduces vascular EC survival by down regulating Rho-kinase activity which is involved in angiogenic vessel sprouting and in cytoskeletal integrity of the vessel walls. Bayless and Davies found that inhibiting Rho signalling using a Rho-kinase inhibitor Y2632 they could mediate cytoskelatal disruption of angiogenic vessels (Bayless and Davies, 2004).

Mavria et al. further proposed that inhibition of ERK/MAPK signalling influences the shape of EC cells and detachment in the extracellular matrix (ECM) (Mavria et al. 2006). Studies by Kanthou and Tozer looking at the effects of the vascular disrupting agent Combrestatin A-4 phosphate, showed that Rho-kinase activity was upregulated and that it had effects on myelin light chain (MLC) activity as well as abrogating ERK1/2 activation (Kanthou and Tozer 2002). All these findings simply highlight the complex mechanisms that exist within the tumour stroma and that by targeting one signalling pathway we may be either inducing others.

### 6.5.1 Summary.

In summary the effects of AZD6244 on the tumour cell lines Calu-6 and HCT116 when combined with RT was to significantly reduce their growths rates when maintained on AZD6244 compared to controls whether given as a concurrent or sequential schedule. The studies using the DWCs showed that the first effects the combined therapies had been to reduce MVD or close the vessels. Additional studies are warranted using the DWC model to measure the effects of AZD6244 withdrawal during a dosing regimen to determine

whether the closed or disappearing vessels re-open. It would also be interesting to use the DWC model to look at cellular recruitment during the process of angiogenesis and determine if certain antiangiogenic agents modify the vessel sprouting process in order to more fully explain their mechanisms of action.

# CHAPTER 7 - CHARACTERISING RADIATION RESPONSES IN HIF-1 DEFICIENT TUMOURS.

## 7.1 Introduction.

The low oxygen (hypoxia) mediated transcription factor hypoxia inducible factor -1 (HIF-1) has been identified in most tumours and is known to play a key role in malignant behaviour (Sharma et al. 2010). Kung et al. showed that tumour growth could be reduced post introduction of a HIF-1 inhibitor (p300/CH1 minimal binding domain) compared to untreated tumours, whilst Ravi et al. showed HIF-1 amplification increased when p53 (tumour suppressor gene) activity was modified resulting in increased angiogenesis during tumourigenesis (Kung et al. 2000, Ravi et al. 2000).

HIF-1 has been identified as a potential target by many researchers (Maxwell et al. 1997, Semenza et al. 2002, 2003). HIF-1 is also thought to have a role in the development of radioresistant tumours by increasing tumour cell apoptotic potential, proliferation rates and adenosine tri-phosphate (ATP) metabolism as well as proteomic and genomic changes. An additional mechanism of action, other than a direct influence on the tumour cells was proposed by Moeller and co-workers (Moeller et al. 2004). Moeller proposed that radiotherapy (RT) not only induced HIF-1 modulation in the tumour cells, but also had a secondary effect on the tumour vasculature endothelial cells (ECs).

We know, based on the work carried out by Gorski and co-workers investigated the effects of radiation on tumour vascular endothelial factor (VEGF) synthesis and concluded that the more radiosensitive the tumour vasculature was to radiation the less radioresistant it becomes (Gorski et al. 1999).

Camphausen and Menard further proposed that the radiation effects on vascular ECs could induce protective survival mechanisms and that these survival mechanisms influenced tumour resistance responses.

Clearly more investigation is warranted into how HIF-1 influences tumour stromal responses to radiation.

## 7.2 Aims.

These studies aimed to look at not only the effects of radiation on tumour growth delay (GD), but also its effects on tumour vascular using the standard murine xenograft GD model and applying the non-invasive dorsal window chamber (DWC) model in order to characterize the influential effects of HIF-1 post tumour irradiation.

The first objective for this part of the study was to establish the growth characteristics of the mouse hepatoma cell line Hepa1c1c7 (Hepa-1wt) which is HIF-1 competent and Hepa-1c4 which is known to be HIF-1 deficient (Maxwell et al. 1997, Dachs et al. 1997).

## 7.3 Growth characteristics of Hepa-1wt and c4 xenografts.

The preparation and establishment for tumour xenografts has been discussed earlier (Chapter 2.2, 2.2.1). Briefly, as series of studies were set up using Hepa-1wt and Hepa-1c4 tumour cells in adult female nude mice. Once the tumours had initiated growing their volumes were measured up to three times per week using callipers. The tumour volume data was then plotted to determine the growth profile characteristics for each tumour type and compared. The tumours were harvested ~1000mm$^3$ for later histological analysis by others.

### 7.3.1 Results.

The first observation was the difference in the time taken for the tumours to establish (take -rate) between the Hepa-1wt and the Hepa-c4 being ~ 7-10 days and ~18-20 days respectively post subcutaneous inoculation (Fig 7.1). Most Hepa-1wt tumours produced an accelerated rate of growth around day12 however Hepa-1c4 tumours did not begin to take until around 20 days post inoculation There time taken by the Hepa-1wt and Hepa-1c4 to reach 1000mm$^3$ was measured at an average of 28 ± 1.6 days (n=7) compared to 60.8± 10.9 days for the Hepa-1c4 tumours. However the growth rates once they had reached a tumour volume of ~200mm$^3$ were similar. These data were pooled from successive ongoing Hepa-1 studies for the two cell lines and plotted (Fig. 7.2).

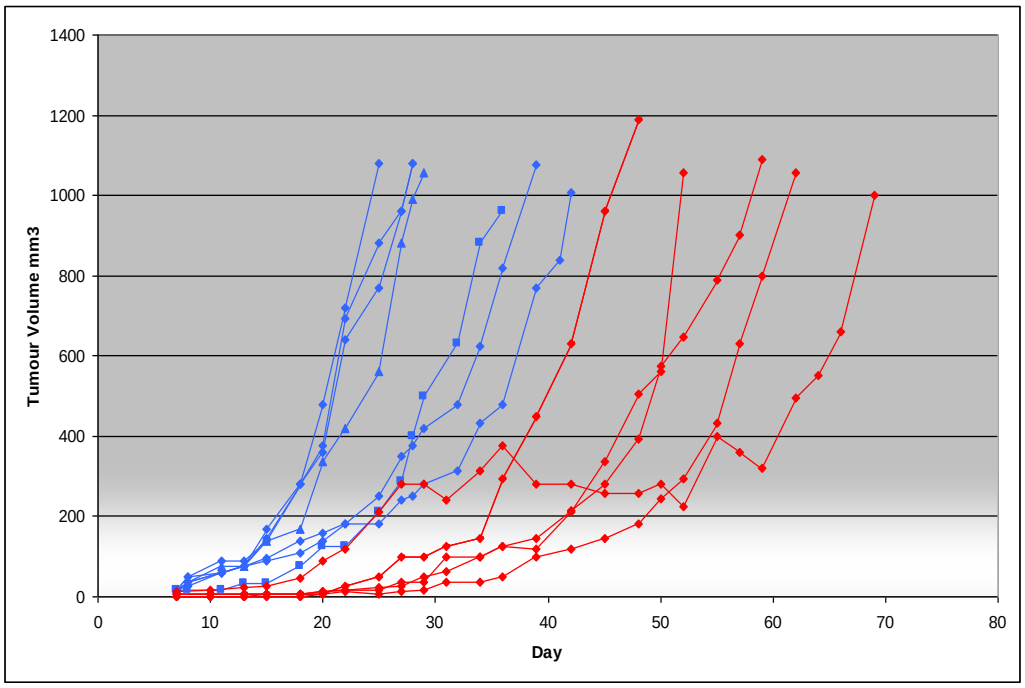


**Fig. 7.**1 Tumour volume growth curves for Hepa-1wt tumours (n=7) shown by blue growth curve lines and Hepa-1c4 tumours (n=5) shown by red growth curve lines grown as subcutaneous allografts.

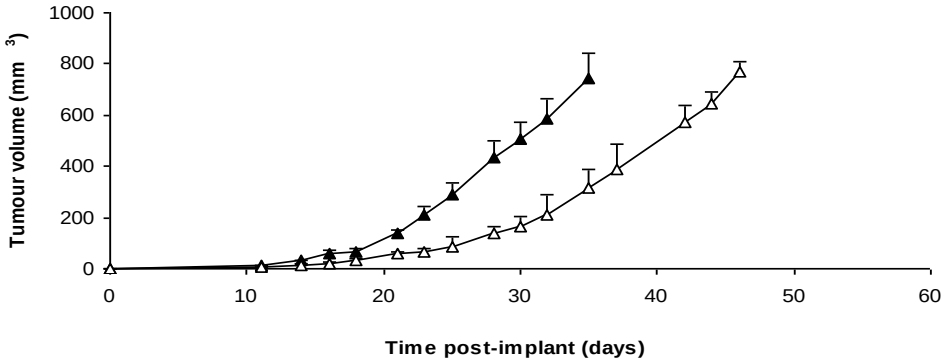


**Fig 7.2** Tumour volume growth curves for Hepa-1wt tumours (n=19) (black triangles) and Hepa-1c4 (open triangles) allografts pooled from 4 non-treatment experiments).

Through the pooling of several studies using these tumour types a reproducible characterized pattern was obtained where typically the time taken to reach a treatment size of ~ 250mm$^3$ was ~ 24 days for Hepa-1wt tumours and ~ 35 days for Hepa-1c4 tumours. A reproducible characteristic 10 day delay was seen between the two tumours, once they had established, time to reach volumes of ~1000mm$^3$.

## 7.4 Hepa-1 wt and Hepa-1 c4 response to irradiation.

The objective of this series of experiments was to characterize the effects of radiation on the tumour growth profiles obtained earlier using tumour GD analysis data. Hepa-1wt and c4 xenografts were set up as described previously (Chapter 2.2, 2.2.1). At a treatment size of 250-280mm$^3$ the tumours were randomly assigned to untreated groups (controls) and groups receiving either 10Gy, 15Gy as a single dose or 15Gy as a fractionated dose (3Gy daily for 5 days) or 20Gy irradiation (IR) as a single dose of X-rays at a rate of 2Gy per minute. The specific growth delay (SGD) was then calculated for each treatment group. The SGD was used as a measure the time taken for the tumours to reach 3 times their treatment size 250-280mm$^3$ volumes.

## 7.4 Results.

The effects of single doses of radiation on Hepa-1 wt xenografts SGD was around 1day (compared to controls) after exposure to 10Gy, 1.5 days after 15Gy and 4 days after 20Gy (Fig 7.3).

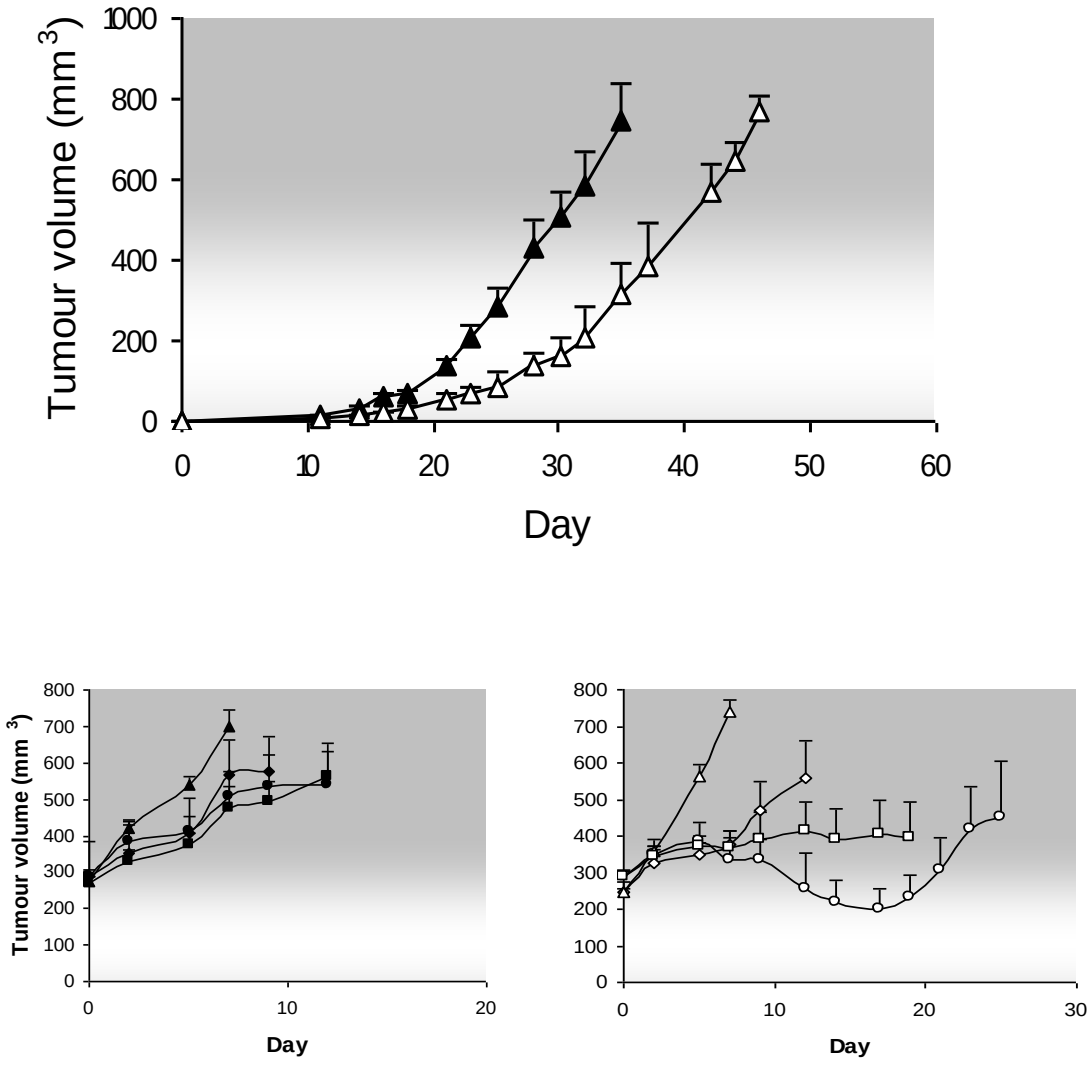


**Fig. 7.3** a) Time taken to reach 250-300mm$^3$ for Hepa-1 c4 (Δ) compared to Hepa-1 wt (▲) tumour xenografts. Data represent the mean ± SE for untreated tumours (n=19: pooled from 4 independent experiments). (b) and (c) Growth delay induced by 10 (♦, ◊), 15 (■, □) and 20 (●, ○) Gy compared with untreated (▲, Δ) Hepa-1 wt (b) and Hepa-1 c4 tumour xenografts (c). For ease of comparison, the data shown in (b) and (c) have been aligned to give a simultaneous treatment time (day 0). Each data point represents the mean of all tumours in the treatment group (n=7–13 per group) ± SE, up until the time when any tumour within the treatment group reached the designated end-point of the experiment (RTV3 i.e. 3 times treatment volume). Mean data are not shown for the remainder of the group after this point. (d) Data from (b) and (c) analyzed in terms of specific growth delay (SGD). (Taken from Williams et al. 2005).

The effect on the Hepa-1c4 SGD after single radiation doses was ~4-5 days for 10Gy, 15Gy or 20 Gy doses. The SGD for tumours receiving 15Gy as a fractionated dose of 5 x 3Gy resulted in a slightly higher SGD response in Hepa-1c4 tumours of 2.5 days compared to Hepa-1wt (1 day) (Fig. 7.4)

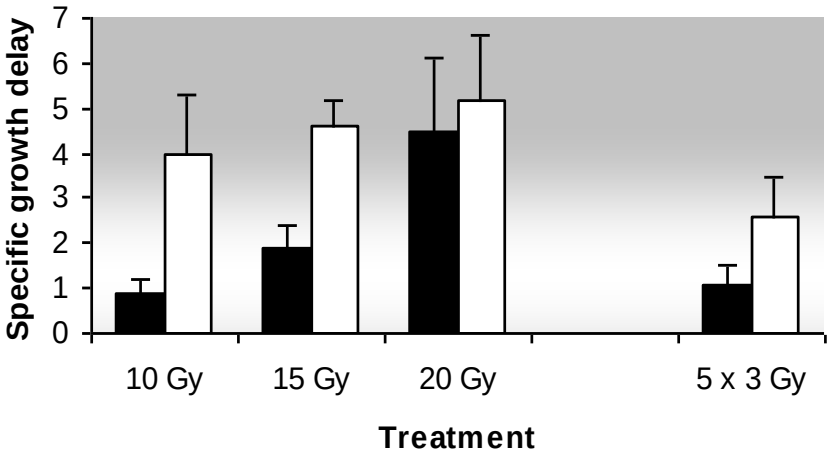


**Fig 7.4** Specific growth delay (SGD in days) data for Hepa-1wt tumours (black solid bars) and Hepa-1c4 (white solid bars) treated with 10Gy, 15Gy (as fractionated 5x3Gy doses), 15Gy and 20Gy ± SE bars. (Taken from Williams et al. 2005).

## 7.5 Hepa-1wt and Hepa-1c4 tumour vascular response to radiation using the DWC model.

The preparation and attachment of the DWC and cell inoculants has been described earlier (Chapter 2). Briefly, series of DWCs were set up in adult female nude mice and $1x10^5$ cells introduced into the chambers 72 hours later. Developing Heap-1wt and Hepa-1c4 tumour vasculature was imaged pre-irradiation with a single dose of 15Gy and daily thereafter for 7 days. These images used to determine the microvascular density measurements (MVDs) for each tumour type (Chapter 2.7). In some cases AlexaBSA (1mg/ml 0.1ml i/v) was used to determine tumour vascular blood flow within the vessels on day 7 post irradiation (Chapter 2).

### 7.5.1 Results.

A key difference between the vasculature for the DWC Hepa-1wt and the DWC Hepa-1c4 was that a more established vasculature appeared around day 10 for the Heap-1wt xenografts whereas it took around four days longer for the Hepa-1c4 vasculature to achieve the same degree of established vasculature (qualitative assessment). Hepa-1wt xenografts typically reached a volume of 60-70mm$^3$ around day 12 post inoculation whereas Hepa-1c4 xenografts took 14 days to reach the same volume. Visually the diameters of the Hepa-1wt vessels appeared larger and more robust on day 12 in comparison to the thinner less robust vessels seen on day 14 for the Hepa-1c4 tumours (Fig(s). 7.5 a) and 7.6a).

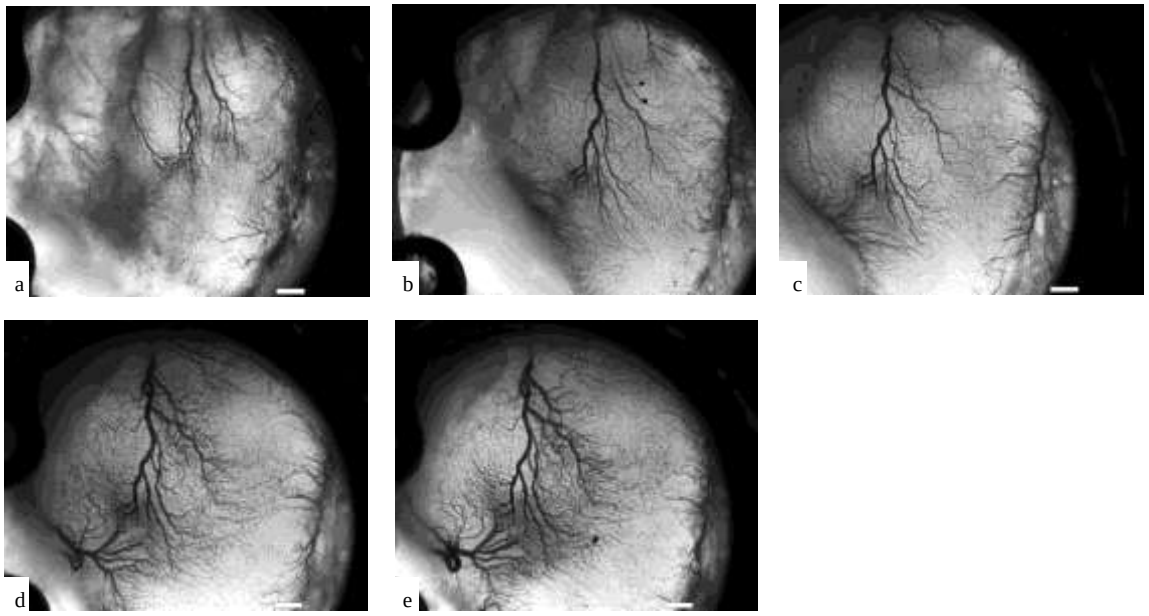


**Fig. 7.5** Brightfield images of Hepa-1wt vessels a) day 0 pre-irradiation with 15Gy b) day 1 post irradiation, c) day 3post irradiation, d) day 5 post irradiation and e) day 7 post irradiation (Scale bar 500µm).

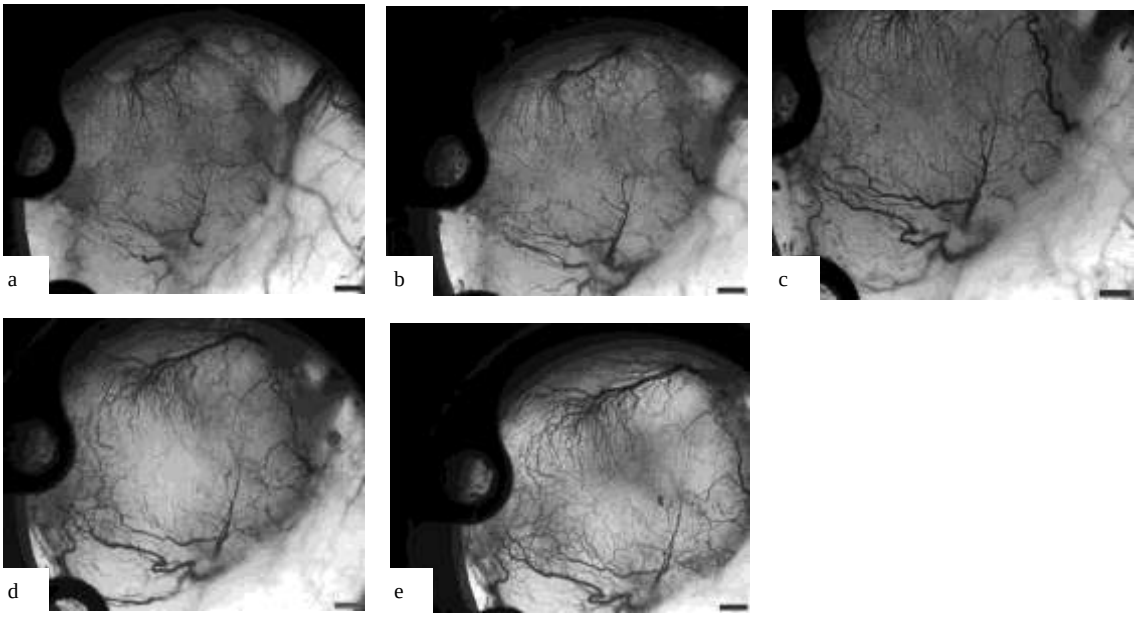


**Fig. 7.6** Brightfield images of Hepa-1c4 vessels a) day 0 pre-irradiation with 15Gy b) day 1 post irradiation, c) day 3post irradiation, d) day 5 post irradiation and e) day 7 post irradiation (Scale bar 500µm).

In one study overlaid brightfield and epi-fluorescence images using AlexaBSA showed well perfused Heap-1wt and Hepa-1c4 vessels (Fig(s). 7.7, 7.8). However by day 3 post irradiation, vessels were seen to close or disappear in the Hepa-1wt tumour as is if they were being shutdown, pruned or re-modelled. In the Hepa-1wt DWC two opposing branched vascular networks began anastamoses on day 3 resulting in fewer but larger and more distinguishable vessel (Fig 7.7 b).This was not as evident for Hepa-1c4 vessels on day 3 however there was the suggestion of it by day 7 (Fig 7.8c). On day 7 in the Hepa-1wt DWC perfused vessels appeared to initiate at the periphery of an avascular region (Fig 7.7c).

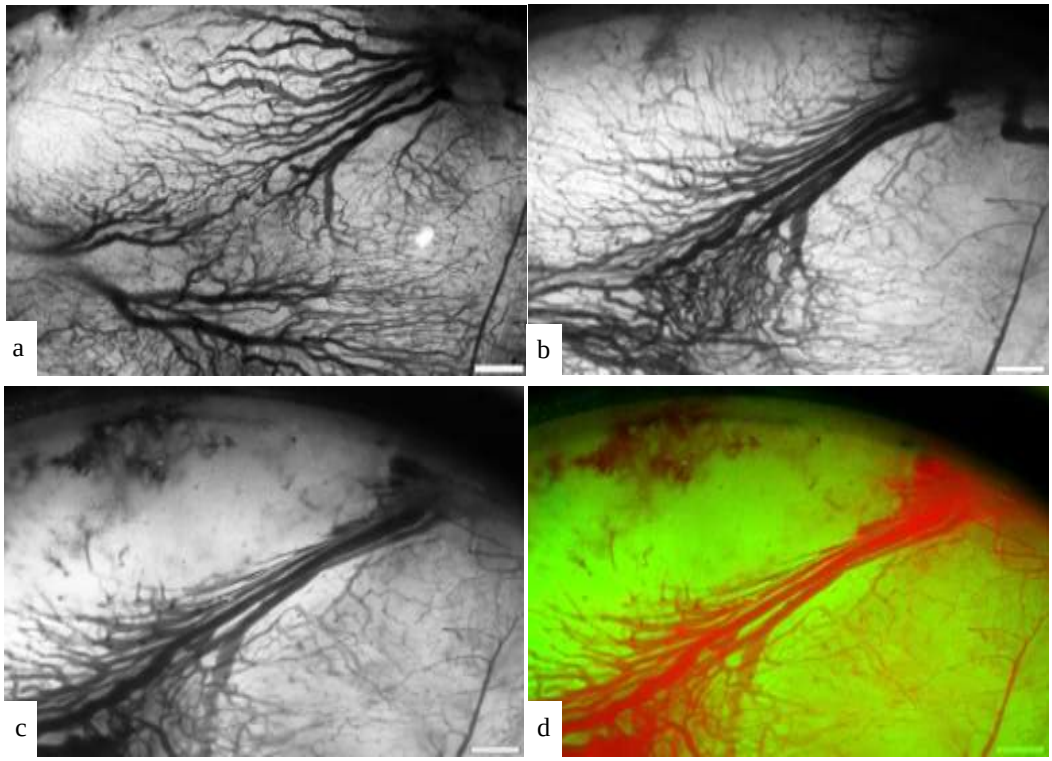


**Fig. 7.7** DWC/IVM Brightfield images of Hepa-1wt vasculature a) imaged day 0 pre 15Gy RT, b) day 3post 15Gy RT and c) day 7 post 15Gy RT. Image d) AlexaBSA perfuse epi-illuminated overlay image of brightfield image c). Perfused vessels shown in red and tumour stroma shown in green.

The re-modelling process occurring in the Hepa-1c4 DWC was not as distinct as that for the Hepa-1wt DWCs by day 7.

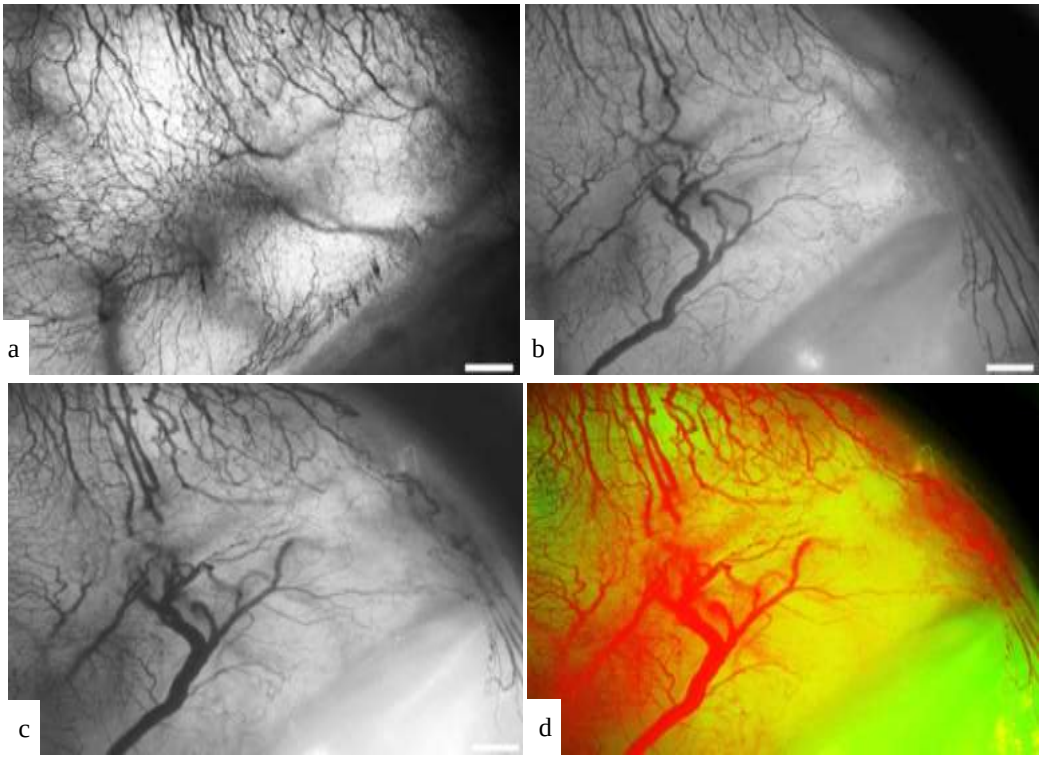


**Fig. 7.8** DWC/IVM Brightfield images of Hepa-1c4 vasculature a) imaged day 0 pre 15Gy RT, b) day 3post 15Gy RT and c) day 7 post 15Gy RT. Image d) AlexaBSA perfuse epi-illuminated overlay image of brightfield image c). Perfused vessels shown in red and tumour stroma shown in green.

Microvascular density measurements (MVDs) for the Hepa-1wt DWCs (n=3) and the Hepa-1c4 DWCs (n=3) showed that the effects of 15Gy were very pronounced on the Hepa-1c4 tumours when compared to the Hepa-1wt tumours. The MVDs for the Hepa-1wt tumours varied from a 0.7% to 5.1% reduction on day 7 post 15Gy (Fig 7.7, Table 7.1) indicating there was no marked influence. The effects of 15Gy on the Hepa-1c4 DWC vasculature was very pronounced with a reduction in MVD ranging from 26.2% to 49.8% (Fig. 7.8, Table 7.1).

**Table 7.1 Summarised effects of 15Gy on Hepa-1wt and Hepa-1c4 DWC MVD.**

| Tumour Hepa-1 | DWC | MVD% Day 1 | MVD% Day 3 | MVD% Day 5 | MVD% Day 7 | % Change in MVD from Day 0 |
|---|---|---|---|---|---|---|
| **Wt** | 1 | 30.4 | 38.2 | 33.7 | 29.2 | -4.0 |
| **wt** | 2 | 21.5 | 19.5 | 20.1 | 20.4 | -5.1 |
| **wt** | 3 | 26.2 | 24.4 | 23.5 | 26.0 | -0.7 |
| **c4** | 4 | 27.1 | 28.6 | 26.4 | 20.0 | -26.2 |
| **c4** | 5 | 10.6 | 7.1 | 6.0 | 4.7 | -55.6 |
| **c4** | 6 | 27.3 | 15.0 | 18.0 | 13.7 | -49.8 |

## 7.6 Discussion.

This work forms part of ongoing studies by our group looking at the effects of HIF-1 activity in response to radiation using HIF-1 deficient Hepa-1c4 and proficient Hepa-1wt tumour cell lines. Since radiation forms such a large part of current antitumour regimens in the clinic, and radioresistance presents in many tumours, a great deal of interest has focused on how these tumours manage to survive radiotherapy (RT) even at high doses. One area that has been studied for many years has been tumour hypoxia and the signalling mechanisms it induces post radiation treatment.

HIF-1, under hypoxic conditions, induces various factors such as VEGF via its actions on hypoxia response elements (HREs) after binding to its cognate DNA sequence (Semenza, 2003). VEGF induces angiogenesis in response to hypoxia, but also protects endothelial cells (ECs) from the cytotoxic effects of irradiation and consequently increase tumour radioresistance (Gorski et al. 1999, Moeller et al. 2004).

Previous studies, carried out comparing the radioresponsiveness of the tumour cell lines *in vitro,* where survival post radiation was measured using clonogenic survival data, showed that there was little difference in response between the two tumour cell lines regardless of the amount of radiation received 5Gy-20Gy (Williams et al. 2005). In addition it was found by co-workers that the expression of p21 protein post radiation (associated with cell cycle arrest) was similar in both cell types. After the group had established there was little difference between HIF-1 competent or deficient tumour cell lines in vitro, implying HIF-1 was not conferring a direct cellular effect the group investigated the effects in *vivo* using murine xenograft models.

Xenograft tumour growth delay (GD) studies clearly showed that the HIF-1 deficient Hepa-1c4 tumours grew at a much slower rate than the Hepa-1wt tumours confirming earlier studies carried out by the group where increased responsiveness to RT *in vivo* using Chinese hamster ovary (CHO) proficient and deficient tumour xenografts (Williams et al. 2002).

The response to varying doses of RT showed that the HIF-1wt cells were less resistant to RT as the dose was increased and that 10Gy resulted in the same measured GD response as seen for 20Gy in the Hepa-1c4 tumours. Additional work by the group using the radiosensitizing drug Misonidazole showed that the GD for the Hepa-1wt tumours could be increased to that seen with Hepa-1c4 tumours and that Misonidazole has little or no effect on the Hepa-1c4 RT response (Williams et al. 2005).

Additional studies using the DWC/IVM model warrant measuring the vessel perfusion characteristics of 15Gy Hepa-1wt and Hepa-1c4 in combination with Misonidazole as well as measuring the MVDs of the tumours harvested from earlier DWC/IVM 15Gy studies and in order to determine the in situ effects of stromal radiosensitisation.

Applying the DWC/IVM model to the microvasculature of the two tumour types showed that a similar pattern of growth to that seen for the tumour GD xenografts studies, in that the time taken to achieve a 50-60mm$^3$ volume for DWC Hepa-1wt was on average 4-5 days quicker than that seen for Hepa-1c4 DWC xenografts. The Hepa-1c4 vasculature, although having similar MVD values at the same tumour volume as the Hepa-1wt, produced visually thinner and more branched vessels i.e. the vessels did not appear as robust as those visualized in the Hepa-1wt DWCs. AlexaBSA introduction showed that the vessels remained perfused after 7 days post 15Gy RT, but that the MVD of the HEPA-1c4 decreased drastically (Table 7.1). The smaller less developed vessels seen in the Hepa-1wt DWCs seemed to be being 'pruned' (or remodelled) resulting in the development of larger vessels (Fig 7.7). Since vascular volume seemed to have increased it will be necessary to revisit these results using software that can measure tumour vessel width.

However care has to be taken when interpreting two dimensional (2D) data rather than the more accurate 3dimensional (3D) currently being developed using photoacoustic mapping (PAM). By using 3D reconstruction it would be possible to see what, if any, additional branching is present underneath the vessels that might be contributing to the enlarged vessels.

The vascular re-modelling seen in this work is in agreement with the recent findings where it has been proposed that placental growth factor (PlGF) as well as VEGF promotes vascular normalisation by recruiting pericytes to vessels making them functionally more normal (Hedlund et al. 2009).

There are probably many other processes that are activated within the tumour stroma that contribute to vessel normalisation other than the accepted VEGF family responses so far reported in pre-clinical and clinical studies.

Observations by the author, using RT in DWC/IVM model studies (and in additional combined modality studies), resulted in a transient AlexaBSA time-lapse perfusion increase 24-48h post delivery of RT in several DWCs (data not included). An induced stroma tissue inflammatory response may account for the qualitative observation of stronger Hepa-1wt vasculature appearance during RT treatment resulting in an influx of immune cells to cope with the induced damage. It is widely accepted that sites of inflammation are characterized by significant changes in the metabolic supply and demand and that these could result in inflammation-associated tissue hypoxia occurring in a number of disease states (Dehne and Brune, 2009). In order to determine if radiation alone is causing an increase in vessel volume it will be necessary to return to these images and apply the CAIMEN software package described earlier (Chapter 1).

On going DWC xenograft studies are currently being carried out to determine what types of cells are being recruited into the stromal tissue in response therapy regimens using mouse cells that constitutively express green fluorescent protein (GFP) with a view to studying bone marrow progenitor cell (BMPC) recruitment.

Knowing that HIF-1-driven transcription factor activity plays a major role in compensating for loss of oxygen, it becomes evident that modulation of HIF-1 activity could be a potent mechanism for treating not only solid tumours, but also a wide range of hypoxia-related pathologies.

By decreasing HIF-1 activity in tumours pre RT it may be possible to reduce angiogenic stimulation and increase the effect of RT. However we need to be aware that removing or lowering one angiogenic contributory factor may allow secondary ‘backup’ processes to become active. It may be necessary to consider targeting the backup processes before using primary antitumour therapies. What is clearly evident is that the ‘whole’ of the tumour stroma needs to be considered when looking at chemoradiation regimens.

**REFERENCES:**


Adjei, A. A. (2001). Blocking oncogenic Ras signaling for cancer therapy. J Natl Cancer Inst, 93, 1062–1074.

Aebersold DM, Burri P, Beer KT, Laissue J, Djonov V, Greiner RH, Semenza GL. Expression of hypoxia-inducible factor-1alpha: a novel predictive and prognostic parameter in the radiotherapy of oropharyngeal cancer. Cancer Res 2001; 61: 2911-2916.

Albert MJ, et al. Inhibition of poly (ADP-ribose) polymerase enhances cell death and improves tumor growth delay in irradiated lung cancer models. Clin. Cancer Res. 2007; 13, 3033.

Algire GH, Chalkey HW. Vascular reactions of normal and malignant tissues in vivo. I. Vascular reactions of mice to wounds and to normal and neoplastic transplants. J Natl Cancer Inst 6: 73-85, 1945.

Algire GH, Legallais FY. Recent developments in the transparent-chamber technique as adapted to the mouse. J Natl Cancer Inst 1949; 10: 225-253, incl 228 pl.

Ali M, Telfer BA, McCrudden C, O'Rourke M, Thomas HD, Kamjoo M, Kyle S, Robson T, Shaw C, Hirst DG, Curtin NJ, Williams KJ. Vasoactivity of AG014699, a clinically active small molecule inhibitor of poly (ADP-ribose) polymerase: a contributory factor to chemopotentiation in vivo? Clin Cancer Res 2009; 15: 6106-6112.

Amoh Y, Katsuoka K, Hoffman RM. Color-coded fluorescent protein imaging of angiogenesis: the AngioMouse models. Curr Pharm Des 2008; 14: 3810-3819.

Bajou K, Masson V, Gerard RD, Schmitt PM, Albert V, Praus M, Lund LR, Frandsen TL, Brunner N, Dano K, Fusenig NE, Weidle U, Carmeliet G, Loskutoff D, Collen D, Carmeliet P, Foidart JM, Noel A. The plasminogen activator inhibitor PAI-1 controls in vivo tumor vascularization by interaction with proteases, not vitronectin. Implications for antiangiogenic strategies. J Cell Biol 2001; 152: 777-784.

Batchelor TT, Sorensen AG, Tomaso ED, Zhang WT, Duda DG, Cohen KS, Kozak KR, Cahill DP, Chen PJ, Zhu M, Ancukiewicz M, Mrugala MM, Plotkin S, Drappatz J, Louis DN, Ivy P, Scadden DT, Benner T, Loeffler JS, Wen PY and Jain RK. AZD2171, a Pan-VEGF receptor tyrosine kinas inhibitor, normalizes tumor vasculature and alleviates edema in glioblastoma patients. Cancer Cell 2007; 11:83-95.

Batchelor TT, Duda DG, di Tomaso E, Ancukiewicz M, Plotkin SR, Gerstner E, Eichler AF, Drappatz J, Hochberg FH, Benner T, Louis DN, Cohen KS, Chea H, Exarhopoulos A, Loeffler JS, Moses MA, Ivy P, Sorensen AG, Wen PY, Jain RK. Phase II study of cediranib, an oral pan-vascular endothelial growth factor receptor tyrosine kinase inhibitor, in patients with recurrent glioblastoma. J Clin Oncol 28: 2817–2823, 2010.

Batra S, Matsumoto S, Hyodo F, Mitchell J, Krishna MC. MRI assessment of angiogenesis inhibitor sunitinib's influence on tumor oxygenation to identify an optimal chemoradiotherapeutic window. Int J Radiat Oncol Biol Phys 75: S43, 2009.

Baudelet C, Gallez B. Effect of anesthesia on the signal intensity in tumors using BOLD-MRI: comparison with flow measurements by Laser Doppler flowmetry and oxygen measurements by luminescence-based probes. Magn Reson Imaging 2004; 22: 905-912.

Baumann M, Krause M. The impact of tumour biology on cancer treatment and multidisciplinary strategies. Medical Radiology 2009: 323-334.

Bayless KJ and Davis GE, Microtubule depolymerization rapidly collapses capillary tube networks in vitro and angiogenic vessels in vivo through the small GTPase Rho, *J. Biol. Chem.* **279** (2004), pp. 11686–11695

Bedford JS and Dewey WC. Historical and current highlights in radiation biology: has anything important been learned by irradiating cells? Radiat Res 2002, 158, 251-291.

Beeram M, Patnaik A, Rowinsky EK. Raf: a strategic target for therapeutic development against cancer. J Clin Oncol 2005; 23:6771–90.

Benchaou M, Lehmann W, Slosman DO, Becker M, Lemoine R, Rufenacht D, Donath A. The role of FDG-PET in the preoperative assessment of N-staging in head and neck cancer. Acta Otolaryngol 1996; 116: 332-335.

Bergers G, Benjamin LE. Tumorigenesis and the angiogenic switch. Nat Rev Cancer 2003; 3: 401-410.

Berk DA, Yuan F, Leunig M, Jain RK. Fluorescence photobleaching with spatial Fourier analysis: measurement of diffusion in light-scattering media. Biophys J 1993; 65: 2428-2436.

Benjamin LE, Golijanin D, Itin A, Pode D, Keshet E. Selective ablation of immature blood vessels in established human tumors follows vascular endothelial growth factor withdrawal. J Clin Invest 103: 159–165, 1999.

Bernsen HJ, Rijken PF, Peters JP, Bakker JH, Boerman RH, Wesseling P, van der Kogel AJ. Suramin treatment of human glioma xenografts: effects on tumor vasculature and oxygenation status. J Neurooncol 44: 129–136, 1999.

Bibby MC. Orthotopic models of cancer for preclinical drug evaluation: advantages and disadvantages. Eur J Cancer 2004; 40: 852-857.

Byrski T, Huzarski T, Dent R et al. Response to neoadjuvant therapy with cisplatin in BRCA1- positive breast cancer patients. Breast Cancer Res. Treat. (2008)

Bryant HE, Schultz N, Thomas HD, et al. Specific killing of BRCA2-deficient tumours with inhibitors of poly(ADP-ribose) polymerase. Nature 2005; 434:913–7.

Biedermann KA, Sun JR, Giaccia AJ, Tosto LM and Brown JM (1991) *scid* mutation in mice confers hypersensitivity to ionizing radiation and a deficiency in DNA double-strand break repair. Proc Natl Acad Sci USA, 88, 1394–1397.

Birkel A, Loges N, Mugnaioli E, Branscheid R, Koll D, Frank S, Panthofer M, Tremel W. Interaction of alkaline metal cations with oxidic surfaces: effect on the morphology of SnO2 nanoparticles. Langmuir 2010; 26: 3590-3595.

Birner P, Schindl M, Obermair A, Breitenecker G, Oberhuber G. Expression of hypoxia-inducible factor 1alpha in epithelial ovarian tumors: its impact on prognosis and on response to chemotherapy. Clin Cancer Res 2001; 7: 1661-1668.

Bos JL, ras ongogenes in human cancer: a review. Cancer Research, 1989; 49: 4682-4689.

Bos R, van Diest PJ, van der Groep P, Greijer AE, Hermsen MA, Heijnen I, Meijer GA, Baak JP, Pinedo HM, van der Wall E, Shvarts A. Protein expression of B-cell lymphoma gene 6 (BCL-6) in invasive breast cancer is associated with cyclin D1 and hypoxia-inducible factor-1alpha (HIF-1alpha). Oncogene 2003; 22: 8948-8951.

Broxmeyer, H.E., S. Cooper, Z.H. Li, L. Lu, H.Y. Song, B.S. Kwon, R.E. Warren, and D.B. Donner. 1995. Myeloid progenitor cell regulatory effects of vascular endothelial cell growth factor. Int J Hematol. 62:203-15.

Brizel DM, Scully SP, Harrelson JM, Layfield LJ, Bean JM, Prosnitz LR, Dewhirst MW. Tumour oxygenation predicts for the likelihood of distant metastases in human soft tissue sarcoma. Cancer Res 1996; 56: 941-943.

Brizel DM, Sibley GS, Prosnitz LR, Scher RL, Dewhirst MW. Tumour hypoxia adversely affects the prognosis of carcinoma of the head and neck. Int J Radiat Oncol Biol Phys 1997; 38: 285-289.

Brower V. Evidence of efficacy: researchers investigating markers for angiogenesis inhibitors. J Natl Cancer Inst 2003; 95: 1425-1427.

Brunet A, Roux D, Lenormand P, Dowd S, Keyse S, Pouyssegur J. Nuclear translocation of p42/p44 mitogen-activated protein kinase is required for growth factor-induced gene expression and cell cycle entry. EMBO J 1999; 18:664–74.

Budach W, Taghian A, Freeman J, Gioioso D, and Suit HD. Impact of stromal sensitivity on radiation response of tumors. J Natl Cancer Inst 1993; 85: 988-993.

Bullitt E, Lin NU, Smith JK, Zeng D, Winer EP, Carey LA, Lin W, Ewend MG. Blood vessel morphologic changes depicted with MR angiography during treatment of brain metastases: a feasibility study. Radiology 245: 824–830, 2007.

Bussink J, Kaanders JH, Rijken PF, Raleigh JA, Van der Kogel AJ. Changes in blood perfusion and hypoxia after irradiation of a human squamous cell carcinoma xenograft tumor line. Radiat Res 2000; 153: 398-404.

Buysschaert I, Carmeliet P Dewerchin M. Clinical and fundamental aspects of angiogenesis and anti-angiogenesis. Acta Clin Belg. 2007 May-Jun; 62(3):162-9.

Byrne AM, Bouchier-Hayes DJ, Harmey JH. Angiogenic and cell survival functions of vascular endothelial growth factor (VEGF). J Cell Mol Med 2005; 9:777–94.

Calabrese CR, Almassy R, Barton S, Batey MA, Calvert AH, Canan-Koch S, Durkacz BW, Hostomsky Z, Kumpf RA, Kyle S, Li J, Maegley K, Newell DR, Notarianni E, Stratford IJ, Skalitzky D, Thomas HD, Wang LZ, Webber SE, Williams KJ, Curtin NJ. Anticancer chemosensitization and radiosensitization by the novel poly (ADP-ribose) polymerase-1 inhibitor AG14361. J Natl Cancer Inst 2004; 96: 56-67.

Camphausen K, Menard C. Angiogenesis inhibitors and radiotherapy of primary tumours. Expert Opin Biol Ther 2002; 2: 477-481.

Carmeliet P and Jain KJ. Principles and mechanisms of vessel normalization for cancer and other angiogenic diseases. Nature Reviews Drug Discovery (2011) 10, 417-427.|

Cao H, Chang V, Hernandez R, Heagy MD. Matrix screening of substituted N-aryl-1, 8-naphthalimides reveals new dual fluorescent dyes and unusually bright pyridine derivatives. J Org Chem 2005; 70: 4929-4934.

Cao C, Albert JM, Geng L, Ivy PS, Sandler A, Johnson DH, et al. Vascular endothelial growth factor tyrosine kinase inhibitor AZD2171 and fractionated radiotherapy in mouse models of lung cancer. Cancer Res 2006; 66:11409–15.

Carmeliet P, Jain RK. Angiogenesis in cancer and other diseases. Nature 2000; 407: 249-257.

Carter S, Auer KL, Reardon DB, et al. Inhibition of the mitogen activated protein (MAP) kinase cascade potentiates cell killing by low dose ionizing radiation in A431 human squamous carcinoma cells. Oncogene 1998; 16:2787–96.

Cengel KA, Voong KR, Chandrasekaran S, Maggiorella L, Brunner TB, Stanbridge E, Kao GD, McKenna WG, Bernhard EJ. Oncogenic K-Ras signals through epidermal growth factor receptor and wild-type H-Ras to promote radiation survival in pancreatic and colorectal carcinoma cells. Neoplasia. 2007; 9: 341 – 348.

Chen BK, Kung HC, Tsai TY, Chang WC. Essential role of mitogen-activated protein kinase pathway and c-Jun induction in epidermal growth factor-induced gene expression of human 12-lipoxygenase. Mol Pharmacol 2000; 57: 153-161.

Chen BP, Uematsu N, Kobayashi J, Lerenthal Y, Krempler A, Yajima H, Lobrich M, Shiloh Y, Chen DJ. Ataxia telangiectasia mutated (ATM) is essential for DNAPKcs phosphorylations at the Thr-2609 cluster upon DNA double strand break. Journal of Biological Chemistry 2007; 282: 6582 – 6587

Choquet P, Calon A, Breton E, Beck F, Domon-Dell C, Freund JN, Constantinesco A. Multiple-contrast X-ray micro-CT visualization of colon malformations and tumours in situ in living mice. C R Biol 2007; 330: 821-827.

Choueiri TK, Plantade A, Elson P, et al: Efficacy of sunitinib and Sorafenib in metastatic papilarry and chromophobe renal cell carcinoma. J Clin Oncol 2008 26:127-131,

Chung EJ, Brown AP, Asano H, Mandler M, Burgan WE, Carter D, Camphausen K, Citrin D. In vitro and in vivo radiosensitization with AZD6244 (ARRY-142886), an inhibitor of mitogen-activated protein kinase/extracellular signal-regulated kinase 1/2 kinase. Clin Cancer Res 2009; 15: 3050-3057.

Claes A, Leenders W. Vessel normalization by VEGF inhibition. A complex story. Cancer Biol Ther 2008; 7: 1014-1016

Clauss, M., M. Gerlach, H. Gerlach, J. Brett, F. Wang, P.C. Familetti, Y.-C.E. Pan, J.V. Olander, D.T. Connolly, and D. Stern. Vascular permeability factor: a tumor-derived polypeptide that induces endothelial cell and monocyte procoagulant activity and promotes monocyte migration. J. Exp.Med (1990). 172:1535-1545.

Cobleigh MA, Langmuir VK, Sledge GW, et al. A phase I/II dose-escalation trial of bevacizumab in previously treated metastatic breast cancer. Semin Oncol. 2003; 30 117–24.

Cohen-Jonathan E, Evans SM, Koch CJ, Muschel RJ, McKenna WG, Wu J, Bernhard EJ. The farnesyltransferase inhibitor L744, 832 reduces hypoxia in tumors expressing activated H-ras. Cancer Res 61: 2289–2293, 2001.

Condeelis J, Segall JE. Intravital imaging of cell movement in tumours. Nat Rev Cancer 2003; 3: 921-930.

Connolly DT, Heuvelman DM, Nelson R, Olander JV, Eppley BL, Delfino JJ, Siegel NR,

Curtin N. Therapeutic potential of drugs to modulate DNA repair in cancer. Expert Opin Ther Targets 2007; 11: 783-799.

Curtin NJ. PARP inhibitors for cancer therapy. Expert Rev Mol Med 2005; 7: 1-20.

Dachs GU, Patterson AV, Firth JD, Ratcliffe PJ, Townsend KM, Stratford IJ, Harris AL. Targeting gene expression to hypoxic tumor cells. Nat Med 1997; 3: 515-520.

Dachs GU, Tupper J, Tozer GM. From bench to bedside for gene-directed enzyme prodrug therapy of cancer. Anticancer Drugs 2005; 16: 349-359.

Davies BR, Logie A, McKay JS, et al. AZD6244 (ARRY-142886), a potent inhibitor of mitogen-activated protein kinase/extracellular signal-regulated kinase kinase 1/2 kinases: mechanism of action in vivo, pharmacokinetic/pharmacodynamic relationship, and potential for combination in preclinical models. Mol Cancer Ther 2007; 6:2209–19.

Delmas C, End D, Rochaix P, Favre G, Toulas C, Cohen-Jonathan E. The farnesyltransferase inhibitor R115777 reduces hypoxia and matrix metalloproteinase 2 expression in human glioma xenograft. Clin Cancer Res 9: 6062–6068, 2003.

Dendy PP, Wardman P. Hypoxia in biology and medicine: the legacy of L H Gray. Br J Radiol 2006; 79: 545-549.

Dehne N and Brüne B. HIF-1 in the inflammatory microenvironment Exp Cell Res 2009; 315 11; 1791-1797

Devoisselle JM, Begu S, Tourne-Peteilh C, Desmettre T, Mordon S. In vivo behaviour of long-circulating liposomes in blood vessels in hamster inflammation and septic shock models-use of intravital fluorescence microscopy. Luminescence 2001; 16: 73-78.

Dewhirst MW, Shan S, Cao Y, Moeller B, Yuan F, Li CY. Intravital fluorescence facilitates measurement of multiple physiologic functions and gene expression in tumors of live animals. Dis Markers 2002; 18: 293-311.

Dings RP, Loren M, Heun H, McNiel E, Griffioen AW, Mayo KH, Griffin RJ. Scheduling of radiation with angiogenesis inhibitors anginex and Avastin improves therapeutic outcome via vessel normalization. Clin Cancer Res 13: 3395–3402, 2007.

Dittmann K, Mayer C, Fehrenbacher B, Schaller M, Raju U, Milas L, Chen DJ, Kehlbach R, Rodemann HP.Radiation-induced epidermal growth factor receptor nuclear import is linked to activation of DNA-dependent protein kinase. Journal of Biological Chemistry . 2005a; 280: 31182 – 31189.

Dittmann K, Mayer C, Rodemann HP. Inhibition of radiation-induced EGFR nuclear import by C225 (Cetuximab) suppresses DNA-PK activity. Radiotherapy & Oncology . 2005 ; 76: 157 – 161.

Ellis LM, Hicklin DJ. VEGF-targeted therapy: Mechanisms of anti-tumour activity. Nat Rev Cancer 8 2008*:* 579–591.

Dings PM, Loren M, Heun H, MvNiel E, Griffioen A, Mayo H, Griffin RJ. Scheduling of Radiation with Angiogenesis Inhibitors Anginex and Avastin Improves Therapeutic Outcome via Vessel Normalization. Clin Cancer Res (2007); 13(11) 3395-3402.

Donawho K, et al. ABT-888, an orally active poly (ADP-ribose) polymerase inhibitor that potentiates DNA-damaging agents in preclinical tumor models; Clin. Cancer Res.2007 13, 2728 (2007)

Dungey FA, Loser DA, Chalmers AJ. Replication-dependent radiosensitization of human glioma cells by inhibition of poly(ADP-ribose) polymerase: mechanisms and therapeutic potential. Int J Radiat Oncol Biol Phys 2008;72:1188–97.

Endrich B, Asaishi K, Gotz A, Messmer K. Technical report--a new chamber technique for microvascular studies in unanesthetized hamsters. Res Exp Med (Berl) 1980; 177: 125-134.

Eniu A. Integrating biological agents into systemic therapy of breast cancer: Trastuzumab, lapatinib, bevacizumab. J BUON. 2007;12:S119–26.

Erlichman C, Adjei AA, Alberts SR, Sloan JA, Goldberg RM, Pitot HC, Rubin J, Atherton PJ, Klee GG, Humphrey R. Phase I study of the matrix metalloproteinase inhibitor, BAY 12-9566. Ann Oncol 2001; 12: 389-395.

Farmer H, McCabe N, Lord CJ, et al. Targeting the DNA repair defect in BRCA mutant cells as a therapeutic strategy. Nature 2005; 434:917–21.

Ferrara N. VEGF as a therapeutic target in cancer. Oncology 2005; 69 Suppl 3: 11-16.

Ferrera, N. and Kerbel, R. S. Angiogenesis as a therapeutic target. Nature 2005, 438, 967-974

Fiedler W, Schuch G, Loges S. Prognostic implication of expression of Angiopoietin-2 in acute myeloid leukemia. Leuk Res 2008; 32: 843-844.

Fischer C, Mazzone M, Jonckx B, Carmeliet P FLT1 and its ligands VEGFB and PlGF: drug targets for anti-angiogenic therapy? Nat Rev Cancer (2008) 8:942–956.

Folkman J. Tumor angiogenesis: therapeutic implications. N Engl J Med 1971; 285: 1182-1186.

Folkman J. The role of angiogenesis in tumor growth. Semin Cancer Biol 1992; 3: 65-71.

Folkman J, Merler E, Abernathy C, Williams G. Isolation of a tumor factor responsible for angiogenesis. J Exp Med 1971; 133: 275-288.

Franco M, Man S, Chen L, Emmenegger U, Shaked Y, Cheung AM, et al. Targeted anti-vascular endothelial growth factor receptor-2 therapy leads to short-term and long-term impairment of vascular function and increase in tumour hypoxia. Cancer Res 2006; 66:3639–48.

Fremin C, Meloche S. From basic research to clinical development of MEK1/2 inhibitors for cancer therapy. J Hematol Oncol 2010; 3: 8.

Fritz JM, Dwyer-Nield LD and Malkinson AM. Stimulation of neoplastic mouse lung cell proliferation by alveolar macrophage-derived, insulin-like growth factor-1 can be blocked by inhibiting MEK and PI3K activation. Molecular Cancer 2011 10: 76

Fukumura D, Ushiyama A, Duda DG, Xu L, Tam J, Krishna V, Chatterjee K, Garkavtsev I, Jain RK. Paracrine regulation of angiogenesis and adipocyte differentiation during in vivo adipogenesis. Circ Res 2003; 93: e88-97.

Fukumura D, Xavier R, Sugiura T, Chen Y, Park EC, Lu N, Selig M, Nielsen G, Taksir T, Jain RK, Seed B. Tumor induction of VEGF promoter activity in stromal cells. Cell 1998; 94: 715-725.

Fukumura D, Xu L, Chen Y, Gohongi T, Seed B, Jain RK. Hypoxia and acidosis independently up-regulate vascular endothelial growth factor transcription in brain tumors in vivo. Cancer Res 2001; 61: 6020-6024.

Fukumura D, Duda DG, Munn LL and Jain RK. Tumor microvasculature and microenvironment: novel insights through intravital imaging in pre-clinical models. Microcirculation 2010 17: 206-225.

Gangarosa LM, Sizemore N, Graves-Deal R, Oldham SM, Der CJ, Coffey RJ. A raf-independent epidermal growth factor receptor autocrine loop is necessary for Ras transformation of rat intestinal epithelial cells. Journal of Biological Chemistry 1997; 272: 18926 – 18931.

Garcia-Barros M, Lacorazza D, Petrie H, Haimovitz-Friedman A, Cardon-Cardo C, Nimer S, Fuks Z, Kolesnick R. Host acid sphingomyelinase regulates microvascular function not tumor immunity. Cancer Res 2004; 64: 8285-8291.

Garcia-Barros M, Paris F, Cordon-Cardo C, Lyden D, Rafii S, Haimovitz-Friedman A, Fuks Z, Kolesnick R. Tumor response to radiotherapy regulated by endothelial cell apoptosis. Science 2003; 300: 1155-1159.

Gatenby RA, Gillies RJ. Why do cancers have high aerobic glycolysis? Nat Rev Cancer 2004; 4: 891-899.

Gee S, Quinlan F, Ozharar S, Delfyett PJ. Ultralow-noise mode-locked optical pulse trains from an external cavity laser based on a slab coupled optical waveguide amplifier (SCOWA). Opt Lett 2005; 30: 2742-2744.

Geng L, Donnelly E, McMahon G, Lin PC, Sierra-Rivera E, Oshinka H, Hallahan DE. Inhibition of vascular endothelial growth factor receptor signalling leads to reversal of tumor resistance to radiotherapy. Cancer Res 2001 61; 2413-2419.

Gerber H. B., Dixit V., Ferrara N. Vascular endothelial growth factor induces expression of the antiapoptotic proteins Bcl-2 and A1 in vascular endothelial cells. J. Biol. Chem. (1998); 273*:* 13313-13316

Gerweck LE, Vijayappa S, Kurimasa A, Ogawa K, Chen DJ. Tumor cell radiosensitivity is a major determinant of tumor response to radiation. Cancer Res 2006

Gitler MS, Monks A, Sausville EA. Preclinical models for defining efficacy of drug combinations: mapping the road to the clinic. Mol Cancer Ther 2003; 2: 929-932.

Golding SE, Rosenberg E, Neill S, Dent P, Povirk LF, Valerie K. Extracellular signal-related kinase positively regulates ataxia telangiectasia mutated, homologous recombination repair, and the DNA damage response. Cancer Res 2007; 67:1046–53.

Gorkhale, PC, McRae D, Monia BP, Bagg A, Rahman A, Dritschillo A and Kasid U. Antisense raf oligodeoxyribonucleotide is a radiosensitizer in vivo. Antisense Nucleic Acid Drug Dev. 1999; 9: 191-201.

Gorski DH, Beckett MA, Jaskowiak NT, Calvin DP, Mauceri HJ, Salloum RM, Seetharam S, Koons A, Hari DM, Kufe DW, Weichselbaum RR. Blockage of the vascular endothelial growth factor stress response increases the antitumor effects of ionizing radiation. Cancer Res 1999; 59: 3374-3378.

Graff B, Bjornaes I and Rofstad EK. Microvascular Permeability of Human Melanoma Xenografts to Macromolecules: Relationships to Tumor Volumetric Growth Rate, Tumor Angiogenesis, and VEGF Expression. Microvasc Res. 2001; 61 (2) 187-198.

Grassme, H, A. Cremesti, R. Kolesnick, and E. Gulbins. 2003. Ceramide-mediated clustering is required for CD95-DISC formation. Oncogene. 22:5457–5470.

Gray LH. Conditions which affect the biologic damage resulting from exposure to radiation. Acta radiol 1954; 41: 63-83.

Gray LH. Radiobiologic basis of oxygen as a modifying factor in radiation therapy. Am J Roentgenol Radium Ther Nucl Med 1961; 85: 803-815.

Gray R, Bhattacharya S, Bowden C, Miller K, Comis RL. Independent review of E2100: A phase III trial of bevacizumab plus paclitaxel versus paclitaxel in women with metastatic breast cancer. J Clin Oncol. 2009;27 :4966–72.

Greenblatt MS, P. Tumour Angiogenesis: Transfilter diffusion studies in the hamster by the transparent chamber technique. Journal of the National Cancer Institute 1968; 41.
Griffin RJ, Molema G, Dings RP. Angiogenesis treatment, new concepts on the horizon. Angiogenesis 2006; 9: 67-72.

Griffiths JR, McSheehy PM, Robinson SP, Troy H, Chung YL, Leek RD, Williams KJ, Stratford IJ, Harris AL, Stubbs M. Metabolic changes detected by in vivo magnetic resonance studies of HEPA-1 wild-type tumors and tumors deficient in hypoxia-inducible factor-1beta (HIF-1beta): evidence of an anabolic role for the HIF-1 pathway. Cancer Res 2002; 62: 688-695.

Griffon-Etienne G, Boucher Y, Brekken C, Suit HD, Jain RK. Taxane-induced apoptosis decompresses blood vessels and lowers interstitial fluid pressure in solid tumors: clinical implications. Cancer Res 1999; 59: 3776-3782.

Guo H, Renaut RA, Chen K, Reiman E. FDG-PET parametric imaging by total variation minimization. Comput Med Imaging Graph 2009; 33: 295-303.

Gupta VK, Jaskowiak NT, Beckett MA, et al. Vascular endothelial growth factor enhances endothelial cell survival and tumor radioresistance. Cancer J 2002;8:47–54.

Hagan M, Wang L, Hanley JR, Park JS, and Dent P. Ionizing radiation-induced mitogen-activated protein (MAP) kinase activation in DU145 prostate carcinoma cells: MAP kinase inhibition enhances radiation-induced cell killing and G2/M-phase arrest. Radiat Res 2000; 153:371–83.

Hagedorn M, Zilberberg L, Lozano RM, Cuevas P, Canron X, Redondo-Horcajo M, Gimenez-Gallego G, Bikfalvi A. A short peptide domain of platelet factor 4 blocks angiogenic key events induced by FGF-2. Faseb J 2001; 15: 550-552.

Hak S, Reitan NK, Haraldseth O, de Lange Davies C. Intravital microscopy in window chambers: a unique tool to study tumor angiogenesis and delivery of nanoparticles. Angiogenesis 2010; 13: 113-130.

Hakem R. DNA-damage repair; the good, the bad, and the ugly. EMBO J 2008; 27: 589-605.

Halder SK, Beauchamp RD, Datta PK. Smad7 induces tumorigenicity by blocking TGF-beta-induced growth inhibition and apoptosis. Exp Cell Res 2005; 307: 231-246.

Hamed H, Hawkins W, Mitchell C, Gilfor D, Zhang G, Pei XY, Dai Y, Hagan MP, Roberts JD, Yacoub A, Grant S, Dent P. Transient exposure of carcinoma cells to RAS/MEK inhibitors and UCN-01 causes cell death in vitro and in vivo. Mol Cancer Ther 2008; 7: 616-629.

Hanahan D, Weinberg RA. The hallmarks of cancer. Cell 2000; 100: 57-70.

Harrison RM. Second cancers following radiotherapy: a suggested common dosimetry framework for therapeutic and concomitant exposures. Br J Radiol 2004; 77: 986-990.

Harris AL: Hypoxia–a key regulatory factor in tumour growth. Nat Rev Cancer 2002, 2:38-47.

He, Y., Kozaki, K., Karpanen, T., Koshikawa, K., Yla-Herttuala, S., Takahashi, T. and Alitalo, K. Suppression of tumor lymphangiogenesis and lymph node metastasis by blocking vascular endothelial growth factor receptor 3 signalling. J. Natl. Cancer Inst. (2002). 94, 819-825.

Hedlund EM, Hosaka K, Zhong Z, Cao R, Cao Y. Malignant cell-derived PlGF promotes normalization and remodeling of the tumor vasculature. Proc Natl Acad Sci USA 2009; 106: 17505-17510.

Helmlinger G, Yuan F, Dellian M, Jain RK. Interstitial pH and pO2 gradients in solid tumors in vivo: high-resolution measurements reveal a lack of correlation. Nat Med 1997; 3: 177-182.

Herbert Hurwitz, M.D., Louis Fehrenbacher, M.D., William Novotny, M.D. et al. Bevacizumab plus Irinotecan, Fluorouracil, and Leucovorin for Metastatic Colorectal Cancer. NEJM 2004: 350; 23; 2335 - 2342.

Hickey MM, Simon MC. Regulation of angiogenesis by hypoxia and hypoxia-inducible factors. Curr Top Dev Biol 2006; 76: 217-257.

Hiratsuka S, Watanabe A, Aburatani H, Maru Y Tumour-mediated upregulation of chemoattractants and recruitment of myeloid cells predetermines lung metastasis. Nat Cell Biol (2006) 8:1369–1375.

Hirst DG, Joiner B, Hirst VK. Is oxygen the limiting substrate for the expansion of cords around blood vessels in tumours? Adv Exp Med Biol 1994; 345: 431-436.

Hirst DG, Kennovin GD, Flitney FW. The radiosensitizer nicotinamide inhibits arterial vasoconstriction. Br J Radiol 1994; 67: 795-799.

Hockel M, Schlenger K, Mitze M, Schaffer U, Vaupel P. Hypoxia and Radiation Response in Human Tumors. Semin Radiat Oncol 1996; 6: 3-9.

Hoffman RM. Recent advances on in vivo imaging with fluorescent proteins. Methods Cell Biol 2008; 85: 485-495.

Hoffman RM, Yang M. Whole-body imaging with fluorescent proteins. Nat Protoc 2006; 1: 1429-1438.

Huang Q, Shan S, Braun R.D, Lanzen J, Anyrhambatla G, Kong G, Borelli, M, Corry, P, Dewhirst, M.W, Li, C.Y. Non-invasive visualization of tumors in rodent dorsal skin window chambers: a novel model for evaluating anti-cancer therapies. Nat. Biotech. 17 1999: 1033–1035.

Huynh H, Soo KC, Chow PK, Tran E: Targeted inhibition of the extracellular signal-regulated kinase kinase pathway with AZD6244 (ARRY-142886) in the treatment of hepatocellular carcinoma. Mol Cancer Ther 2007, 6:138-146.

Ide A, Baker, N.H. & Warren, S.L. Vascularization of the Brown Pearce rabbit epithelioma transplant as seen in the transparent ear chamber. Am. J. Roentgenol 1939; 42: 891-899.

Iga AM, Sarkar S, Sales KM, Winslet MC, and Seifalian AM. Quantitating therapeutic disruption of tumor blood flow with intravital video microscopy. Cancer Res 2006; 66: 11517-11519.

Iruela-Arispe ML, Lombardo M, Krutzsch HC, Lawler J, Roberts DD. Inhibition of angiogenesis by thrombospondin-1 is mediated by 2 independent regions within the type 1 repeats. Circulation 1999; 100: 1423-1431.

Jain RK. Normalizing tumor vasculature with anti-angiogenic therapy: a new paradigm for combination therapy. *Nat Med* 7: 987–989, 2001.

Jain RK, Munn LL, Fukumura D. Dissecting tumour pathophysiology using intravital microscopy. Nat Rev 2002; 2 266-276.

Jain RK. Molecular regulation of vessel maturation. Nat Med 2003; 9: 685-693.

Jain RK. Normalization of tumor vasculature: an emerging concept in antiangiogenic therapy. Science 2005; 307: 58-62

Fukumura D and Jain RK. Tumor microvasculature and microenvironment: Targets for anti-angiogenesis and normalization. Microvascular Research 2007; 74 72–84.

Janssens GO, M.D, Terhaard CH, Doornaert PA et al. Toxicity Profile and Compliance to Accelerated Radiotherapy Plus Carbogen and Nicotinamide for Clinical Stage T2–4 Laryngeal Cancer: Results of a Phase III Randomized Trials. International Journal of Radiation Oncology*Biology*Physics 2011 (in press).

Jekunen A, Kairemo K. Inhibition of angiogenesis at endothelial cell level. Microsc Res Tech 2003; 60: 85-97.

Jiang BH, Liu LZ. PI3K/PTEN signalling in tumorigenesis and angiogenesis. Biochim Biophys Acta. 2008;1784:150–158.

Kaanders JH, Pop LA, Marres HA et al. ARCON: experience in 215 patients with advanced head-and-neck cancer. Int J Radiat Oncol Biol Phys 2002; 52: 769–778.

Kanthou C, Tozer GM. The tumor vascular targeting agent combretastatin A-4-phosphate induces reorganization of the actin cytoskeleton and early membrane blebbing in human endothelial cells. Blood 2002; 99: 2060-2069.

Kanthou C, Tozer GM. Microtubule depolymerizing vascular disrupting agents: novel therapeutic agents for oncology and other pathologies. Int J Exp Pathol 2009; 90: 284-294.

Ke,Q and Costa M. Hypoxia-Inducible Factor-1(HIF-1). Mol Pharmacol 70: 1469-1480.

Kasid U, Pfeifer A, Brennan T, Beckett, M Weichselbaum, R Dritschilo A and Mark GE. Effect of antisense c-raf-1 on tumorigenicity and radiation sensitivity of human squamous carcinoma. Science (Wash. DC) 1989, 243: 1354-1356.

Kelland LR. Of mice and men: values and liabilities of the athymic nude mouse model in anticancer drug development. Eur J Cancer 2004; 40: 827-836.

Kerger H, Torres Filho IP, Rivas M, Winslow RM, Intaglietta M. Systemic and subcutaneous microvascular oxygen tension in conscious Syrian golden hamsters. Am J Physiol 1995; 268: H802-810.

Kiessling F, Huppert J, Palmowski M. Functional and molecular ultrasound imaging: concepts and contrast agents. Curr Med Chem 2009; 16: 627-642.

Kiessling I, Bzyl J, Kiessling F. Molecular ultrasound imaging and its potential for paediatric radiology. Pediatr Radiol 2010.

Kimbro KS and Simons JW. Hypoxia-inducible factor-1 in human breast and prostate cancer Endocrine-Related Cancer 2006 13 739-749

Koch CJ, Kruuv J, Frey HE. Variation in radiation response of mammalian cells as a function of oxygen tension. Radiat Res 1973; 53: 33-42.

Koh, B.G. Darnay and G. Powis, Hypoxic-associated factor, a novel E3-ubiquitin ligase, binds and ubiquitinates hypoxia-inducible factor-1α, leading to its oxygen-independent degradation, Mol. Cell. Biol. 28 (2008), 7081–7095

Kolesnick RN, Goni FM, and Alonso A. Compartmentalization of ceramide signalling. Physical foundations and biological effects. J Cell Physiol 2000; 184:285-300.

Kong G, Braun RD, Dewhirst MW. Characterization of the Effect of Hyperthermia on Nanoparticle Extravasation from Tumor Vasculature. Cancer Research 2001; 61: 3027-3032.

Kraus RM, Stallings HW, 3rd, Yeager RC, Gavin TP. Circulating plasma VEGF response to exercise in sedentary and endurance-trained men. J Appl Physiol 2004; 96: 1445-1450.

Kuhnle GE, Groh J, Leipfinger FH, Kuebler WM, Goetz AE. Quantitative analysis of network architecture, and microhemodynamics in arteriolar vessel trees of the ventilated rabbit lung. Int J Microcirc Clin Exp 1993; 12: 313-324.

Kuhnle GE, Leipfinger FH, Goetz AE. Measurement of microhemodynamics in the ventilated rabbit lung by intravital fluorescence microscopy. J Appl Physiol 1993; 74: 1462-1471.

Kung AL, Wang S, Klco JM, Kaelin WG, Livingston DM. Suppression of tumor growth through disruption of hypoxia-inducible transcription. Nat Med 2000; 6: 1335-1340.

Kuszyk BS, Corl FM, Franano FN, Bluemke DA, Hofmann LV, Fortman BJ, Fishman EK. Tumor transport physiology: implications for imaging and imaging-guided therapy. AJR Am J Roentgenol 2001; 177: 747-753.

Laderoute KR, Alarcon RM, Brody MD, Calaoagan JM, Chen EY, Knapp AM, Yun Z, Denko NC, Giaccia AJ. Opposing effects of hypoxia on expression of the angiogenic inhibitor thrombospondin 1 and the angiogenic inducer vascular endothelial growth factor. Clin Cancer Res 2000; 6: 2941-2950.

Leach MO, Brindle KM, Evelhoch JL, Griffiths JR, Horsman MR, Jackson A, Jayson GC, Judson IR, Knopp MV, Maxwell RJ, McIntyre D, Padhani AR, Price P, Rathbone R, Rustin GJ, Tofts PS, Tozer GM, Vennart W, Waterton JC, Williams SR, Workman P. The assessment of antiangiogenic and antivascular therapies in early-stage clinical trials using magnetic resonance imaging: issues and recommendations. Br J Cancer 2005; 92: 1599-1610.

Lee GC, Heijn M, di Tomaso E, Griffon-Etienne G, Ancukiewicz M, Koike MC, Park KR, Ferrara N, Jain RK, Suit HD and Boucher Y. Anti-vascular endothelial growth factor treatment augments tumor radiation response under normoxic or hypoxic conditions, Cancer Res 2000, 60, 5565–5570.

Lehmann W, Benchaou M, Slosman DO, Townsend D, Ryser JE, Widmann JJ, Rufenacht D, Lacroix JS, Donath A. [Positron emission tomography (PET) in the preoperative evaluation of cervical lymph node metastasis of ORL cancer]. Schweiz Rundsch Med Prax 1993; 82: 1457-1461.

Lehr HA, Leunig M, Menger MD, Nolte D, Messmer K. Dorsal skinfold chamber technique for intravital microscopy in nude mice. Am J Pathol 1993; 143: 1055-1062.

Leimgruber RM, Feder J. Tumor vascular permeability factor stimulates endothelial cell growth and angiogenesis. J Clin Invest (1989) 84:1470–1478.

Leung DY, Jain N, Leo HL. New concepts in the pathogenesis of atopic dermatitis. Curr Opin Immunol 2003; 15: 634-638.

Leung, D.W, Cachianes, G, Kuang, W.J, Goeddel, D.V, Ferrara, N. Vascular endothelial growth factor is a secreted angiogenic mitogen. Science (1989), 246, 1306– 1309.

Li C. Novel mechanism of inhibition by the P2 receptor antagonist PPADS of ATP-activated current in dorsal root ganglion neurons. J Neurophysiol 2000; 83: 2533-2541.

Li H-CWaP-C. Proteins Expressed on Tumor Endothelial Cells as Potential Targets for Anti-Angiogenic Therapy. Journal of Cancer Molecules 2010; 4: 17-22.

Loges S, Roncal C, Carmeliet P. Development of targeted angiogenic medicine. J Thromb Haemost 2009; 7: 21-33.

Lovett J, Ricci S, Mazzaferro V, et al. Sorafenib improves survival in advanced hepatocellular carcinoma: results of a phase III randomized placebo-controlled trial (SHARP trial. J Clin Oncol 2007; 25 2007 ASCO annual meeting proceedings part I):LBA1

Lunt SJ, Kalliomaki TM, Brown A, Yang VX, Milosevic M, Hill RP. Interstitial fluid pressure, vascularity and metastasis in ectopic, orthotopic and spontaneous tumours. BMC Cancer 2008; 8: 2

Lunt SJ, Gray C, Reyes-Aldasoro CC, Matcher SJ and Tozer GM. Application of intravital microscopyin studies of tumor microcirculation.
J Biomed Opt 2011; 15: 011113.

Ma J, Pulfer S, Li S, Chu J, Reed K, Gallo JM. Pharmacodynamic-mediated reduction of temozolomide tumor concentrations by the angiogenesis inhibitor TNP-470. Cancer Res 61: 5491–5498, 2001.

McCubrey JA, Steelman LS, Abrams SL et al. Roles of the RAF/MEK/ERK and PI3K/PTEN/AKT pathways in malignant transformation and drug resistance. Adv Enzyme Regul 2006; 46:249 –279.

Makale MT, Chen PC, and Gough DA. Peter C. Variants of the tissue-sensor array window chamber. Am J Physiol Heart Circ Physiol. 2005 289: H57–H65.

Mandriota SJ, Turner KJ, Davies DR *et al*. HIF activation identifies early lesions in VHL kidneys:evidence for site-specific tumor suppressor function in the nephron. *Cancer Cell* 2002; 1:459–468.

Martin GR, Jain RK. Fluorescence ratio imaging measurement of pH gradients: calibration and application in normal and tumor tissues. Microvasc Res 1993; 46: 216-230.

Mauceri HJ, Hanna NN, Beckett MA, Gorski DH, Staba MJ, Stellato KA, Bigelow K, Heimann R, Gately S, Dhanabal M, Soff GA, Sukhatme VP, Kufe DW, Weichselbaum RR. Combined effects of angiostatin and ionizing radiation in antitumour therapy. Nature 1998; 394: 287-291.

Mavria G, Vercoulen Y, Yeo M, Paterson H, Karasarides M, Marais R, Bird D, Marshall CJ. ERK-MAPK signalling opposes Rho-kinase to promote endothelial cell survival and sprouting during angiogenesis. Cancer Cell 2006; 9, 33–44.

Mayer RJ. Two steps forward in the treatment of colorectal cancer. N Engl J Med. 2004; 350 2406–8

Maxwell PH, Dachs GU, Gleadle JM, Nicholls LG, Harris AL, Stratford IJ, Hankinson O, Pugh CW, Ratcliffe PJ. Hypoxia-inducible factor-1 modulates gene expression in solid tumors and influences both angiogenesis and tumor growth. Proc Natl Acad Sci U S A 1997; 94: 8104-8109.

Maxwell PH, Wiesener MS, Chang GW, Clifford SC, Vaux EC, Cockman ME, Wykoff CC, Pugh CW, Maher ER, Ratcliffe PJ. The tumour suppressor protein VHL targets hypoxia-inducible factors for oxygen-dependent proteolysis. Nature 1999; 399: 271-275.

McDonald DM and Baluk P. Significance of blood vessel leakiness in cancer. Cancer Res 2002 Sep 15; 62(18):5381-5.

McKenna WG, Weiss MC, Endlich B, Ling CC, Bakanauskas VJ, Kelsten ML and Muschel RJ. (1990). Cancer Res., 50, 97–102.

Menger MD, Lehr HA. Scope and perspectives of intravital microscopy--bridge over from in vitro to in vivo. Immunol Today 1993; 14: 519-522.

Miknyoczki S, Chang H, Grobelny J et al. The selective poly(ADP-ribose) polymerase-1(2) inhibitor, CEP-8983, increases the sensitivity of chemoresistant tumor cells to temozolomide and irinotecan but does not potentiate myelotoxicity**.** Mol Cancer Ther August 2007 6; 2290-2302.

Minchinton AI, Tannock IF. Drug penetration in solid tumours. Nat Rev Cancer 2006; 6: 583-592.

Minet E, Arnould T, Michel G, Roland I, Mottet D, Raes M, Remacle J, Michiels C. ERK activation upon hypoxia: involvement in HIF-1 activation. FEBS Lett 2000; 468: 53-58.

Minet E, Michel G, Remacle J, Michiels C. Role of HIF-1 as a transcription factor involved in embryonic development, cancer progression and apoptosis (review). Int J Mol Med 2000; 5: 253-259.

Moeller BJ, Cao Y, Li CY, Dewhirst MW. Radiation activates HIF-1 to regulate vascular radiosensitivity in tumors: role of reoxygenation, free radicals, and stress granules. Cancer Cell 2004; 5: 429-441.

Moeller BJ, Dreher MR, Rabbani ZN, et al. Pleiotropic effects of HIF-1 blockade on tumor radiosensitivity. Cancer Cell 2005; 8: 99–110

Moeller BJ, Pasqualini R, Arap W. Ceramide-mediated apoptosis following ionizing radiation in human prostate cancer cells: PKC alpha joins the fray. Cancer Biol Ther 2009; 8: 64-65.

Molina S, Castet V, Fournier-Wirth C, Pichard-Garcia L, Avner R, Harats D, Roitelman J, Barbaras R, Graber P, Ghersa P, Smolarsky M, Funaro A, Malavasi F, Larrey D, Coste J, Fabre JM, Sa-Cunha A, Maurel P. The low-density lipoprotein receptor plays a role in the infection of primary human hepatocytes by hepatitis C virus. J Hepatol 2007; 46: 411-419.

de Murcia G, de Murcia JM. Poly (ADP-ribose) polymerase: a molecular nick-sensor. Trends Biochem Sci. 1994;19:172–176.

Nagy JA, Feng D, Vasile E, Wong WH, Shih SC, Dvorak AM, Dvorak HF. Permeability properties of tumor surrogate blood vessels induced by VEGF-A. Lab Invest 2006; 86:767-780.

Nickerson MM, Song J, Meisner JK, Bajikar S, Burke CW, Shuptrine CW, Owens GK, Skalak TC, Price RJ. Bone marrow-derived cell-specific chemokine (C-C motif) receptor-2 expression is required for arteriolar remodeling. Arterioscler Thromb Vasc Biol 2009; 29: 1794-1801.

Nicoli S, Ribatti D, Cotelli F, Presta M. Mammalian tumor xenografts induce neovascularization in zebrafish embryos. Cancer Res 2007; 67: 2927-2931.

Nussenbaum F, Herman IM. Tumor angiogenesis: insights and innovations. J Oncol 2010; 2010: 132641.

O'Reilly MS, Boehm T, Shing Y, Fukai N, Vasios G, Lane WS, Flynn E, Birkhead JR, Olsen BR, Folkman J. Endostatin: an endogenous inhibitor of angiogenesis and tumor growth. Cell 1997; 88: 277-285.

O'Reilly MS, Holmgren L, Shing Y, Chen C, Rosenthal RA, Moses M, Lane WS, Cao Y, Sage EH, Folkman J. Angiostatin: a novel angiogenesis inhibitor that mediates the suppression of metastases by a Lewis lung carcinoma. Cell 1994; 79: 315-328.

O'Rourke JF, Dachs GU, Gleadle JM, Maxwell PH, Pugh CW, Stratford IJ, Wood SM, Ratcliffe PJ. Hypoxia response elements. Oncol Res 1997; 9: 327-332.

Pages G, Milanini J, Richard DE, Berra E, Gothie E, Vinals F, Pouyssegur J. Signalling angiogenesis via p42/p44 MAP kinase cascade. Ann N Y Acad Sci 2000; 902: 187-200.

Palmowski M, Huppert J, Ladewig G, Hauff P, Reinhardt M, Mueller MM, Woenne EC, Jenne JW, Maurer M, Kauffmann GW, Semmler W, Kiessling F. Molecular profiling of angiogenesis with targeted ultrasound imaging: early assessment of antiangiogenic therapy effects. Mol Cancer Ther 2008; 7: 101-109.

Papenfuss HD, Gross JF, Intaglietta M, Treese FA. A transparent access chamber for the rat dorsal skin fold. Microvasc Res 1979; 18: 311-318.

Park H. Aromatic hydrocarbon nuclear translocator as a common component for the hypoxia- and dioxin-induced gene expression. Mol Cells 1999; 9: 172-178.

Park JS, Qiao L, Su ZZ, Hinman D, Willoughby K, McKinstry R, Yacoub A, Duigou GJ, Young CS, Grant S, Hagan MP, Ellis E, Fisher PB, Dent P. Ionizing radiation modulates vascular endothelial growth factor (VEGF) expression through multiple mitogen activated protein kinase dependent pathways. Oncogene 2001; 20: 3266-3280.

Peralta-Leal A, Rodríguez-Vargas JM et al. PARP inhibitors: New partners in the therapy of cancer and inflammatory diseases. Free Radical Biology and Medicine. 2009; 47 (1) 13-26

Phillips GD, Stone AM, Jones BD, Schultz JC, Whitehead RA and Knighton DR. Vascular endothelial growth factor (rhVEGF165) stimulates direct angiogenesis in the rabbit cornea In Vivo (1994); 8: 961–965

Pickhardt PJ, Taylor AJ, Johnson GL, Fleming LA, Jones DA, Pfau PR, Reichelderfer M. Building a CT colonography program: necessary ingredients for reimbursement and clinical success. Radiology 2005; 235: 17-20.

Plate KH, Breier G, Millauer B, Ullrich A and Risau W. Up-regulation of vascular endothelial growth factor and its cognate receptors in a rat glioma model of tumour angiogenesis. Cancer Res. (1993) 53: 5822–5827

Plate KH, Breier G, Weich HA, Mennel HD, Risau W. Vascular endothelial growth factor and glioma angiogenesis: coordinate induction of VEGF receptors, distribution of VEGF protein and possible in vivo regulatory mechanisms. Int J Cancer (1994) 59: 520–529

Pries AR, Hopfner M, le Noble F, Dewhirst MW, Secomb TW. The shunt problem: control of functional shunting in normal and tumour vasculature. Nat Rev Cancer 2010 Aug;10 (8):587-93.

Plummer R, Middleton M, Wilson R, et al. Final clinical, pharmacokinetic and pharmacodynamic results of the phase I study of the novel poly(ADP-ribose) polymerase (PARP) inhibitor, AG014699, in combination with temozolomide. Clin Cancer Res 2005. 11:9099S.

Plummer ER and Calvert H. Targeting poly (ADP-ribose) polymerase: a two-armed strategy for cancer therapy. Clin Cancer Res. 2007 13; 6252-6.

Qayum N, Muschel RJ, Im JH, Balathasan L, Koch CJ, Patel S, McKenna WG, Bernhard EJ. Tumor vascular changes mediated by inhibition of oncogenic signalling. Cancer Res 69: 6347–6354, 2009.

Rajan A, Gutierrez M, Kummar S et al. A phase I combination study of AZD2281 and cisplatin plus gemcitabine in adults with solid tumors. Ann Oncol 2009; 20 (Suppl 3): iii42–iii44

Rajeswari MR, Jain A, Sharma A, Singh D, Jagannathan NR, Sharma U, Degaonkar MN. Evaluation of skin tumors by magnetic resonance imaging. Lab Invest 2003; 83: 1279-1283.

Rapisarda A, Uranchimeg, B, Scudiero, D.A, Selby, M, Sausville, E.A, Shoemaker, R.H., and Melillo, G. 2002. Identification of small molecule inhibitors of hypoxia-inducible factor 1 transcriptional activation pathway. Cancer Res. 62*:* 4316-4324

Ratcliffe PJ, Ebert BL, Firth JD, Gleadle JM, Maxwell PH, Nagao M, O'Rourke JF, Pugh CW, Wood SM. Oxygen regulated gene expression: erythropoietin as a model system. Kidney Int 1997; 51: 514-526.
Ravi R, Mookerjee B, Bhujwalla ZM, Sutter CH, Artemov D, Zeng Q, Dillehay LE, Madan A, Semenza GL, Bedi A. Regulation of tumor angiogenesis by p53-induced degradation of hypoxia-inducible factor 1alpha. Genes Dev 2000; 14: 34-44.

Ren G, Liu Z, Miao Z, Liu H, Subbarayan M, Chin FT, Zhang L, Gambhir SS, Cheng Z. PET of malignant melanoma using 18F-labeled metallopeptides. J Nucl Med 2009; 50: 1865-1872.

Robinson SP, Howe FA, Stubbs M, Griffiths JR. Effects of nicotinamide and carbogen on tumour oxygenation, blood flow, energetics and blood glucose levels. Br J Cancer 2000; 82: 2007-2014.

Rottenberg S, Jaspers JE, Kersbergen A et al. High sensitivity of BRCA1-deficient mammary tumors to the PARP inhibitor AZD2281 alone and in combination with platinum drugs. Proc Natl Acad Sci 2008; 105: 17079–17084.

Ruddock MW, BurnsD M, Murphy LE, O'Rourke MG, Hirst DG. The effect of nicotinamide on spontaneous and induced activity in smooth and skeletal muscle. Radiother Oncol
2000; 56:253–7.

Samowitz WS, Curtin K, Schaffer D, Robertson M, Leppert M, Slattery ML. Relationship of Ki-ras mutations in colon cancers to tumor location, stage, and survival: a population-based study. Cancer Epidemiol Biomarkers Prev 2000; 9: 1193–7.

Sandison JC. A new method for the microscopic study of living growing tissues by the introduction of a transparent chamber in the rabbit's ear. Anat. Rec. 1924; 28: 281-287.

Sang N, Stiehl DP, Bohensky J, Leshchinsky I, Srinivas V, and Caro J. MAPK signalling up-regulates the activity of hypoxia-inducible factors by its effects on p300. J Biol Chem 2003; 278: 14013-14019.

Schultze A, Decker S, Otten J, Horst AK, Vohwinkel G, Schuch G, Bokemeyer C, Loges S, Fiedler W. TAE226-mediated inhibition of focal adhesion kinase interferes with tumor angiogenesis and vasculogenesis. Invest New Drugs 2010; 28: 825-833.

Schwabe GC, Hoffmann K, Loges NT, Birker D, Rossier C, de Santi MM, Olbrich H, Fliegauf M, Failly M, Liebers U, Collura M, Gaedicke G, Mundlos S, Wahn U, Blouin JL, Niggemann B, Omran H, Antonarakis SE, Bartoloni L. Primary ciliary dyskinesia associated with normal axoneme ultrastructure is caused by DNAH11 mutations. Hum Mutat 2008; 29: 289-298.

Schwartz DL, Powis G, Thitai-Kumar A, He Y, Bankson J, Williams R, Lemos R, Oh J, Volgin A, Soghomonyan S, Nishii R, Alauddin M, Mukhopadhay U, Peng Z, Bornmann W, Gelovani J. The selective hypoxia inducible factor-1 inhibitor PX-478 provides in vivo radiosensitization through tumor stromal effects. Mol Cancer Ther. 2009 Apr; 8(4):947-58
Seddon B, Kelland LR, Workman P. Bioreductive prodrugs for cancer therapy. Methods Mol Med 2004; 90: 515-542.

Segers J, Di Fazio V, Ansiaux R, Martinive P, Feron O, Wallemacq P, Gallez B. Potentiation of cyclophosphamide chemotherapy using the anti-angiogenic drug thalidomide: importance of optimal scheduling to exploit the "normalization" window of the tumor vasculature. Cancer Lett 244: 129–135, 2006.

Seitz G, Warmann SW, Fuchs J, Mau-Holzmann UA, Ruck P, Heitmann H, Hoffman RM, Mahrt J, Muller GA, Wessels JT. Visualization of xenotransplanted human rhabdomyosarcoma after transfection with red fluorescent protein. J Pediatr Surg 2006; 41: 1369-1376.

Semenza GL. Involvement of hypoxia-inducible factor 1 in human cancer. Intern Med 2002; 41: 79-83.

Semenza GL. HIF-1 and tumor progression: pathophysiology and therapeutics. Trends Mol Med 2002; 8: S62-67.

Semenza GL. Targeting HIF-1 for cancer therapy. Nat Rev Cancer 2003; 3: 721-732.

Semenza GL. Intratumoral hypoxia, radiation resistance, and HIF-1. Cancer Cell 2004; 5: 405-406.

Senger, D.R., Peruzzi, C.A., Feder, J., and Dvorak, H.F. A highly conserved vascular permeability factor secreted by a variety of human and rodent tumor cell lines. Cancer Res. (1986). 46; 5629-5632.

Shaner NC, Patterson GH, Davidson MW. Advances in fluorescent protein technology. J Cell Sci 2007; 120: 4247-4260.

Shannon AM, Telfer BA, Smith PD, Babur M, Logie A, Wilkinson RW, Debray C, Stratford IJ, Williams KJ, Wedge SR. The mitogen-activated protein/extracellular signal-regulated kinase kinase 1/2 inhibitor AZD6244 (ARRY-142886) enhances the radiation responsiveness of lung and colorectal tumor xenografts. Clin Cancer Res 2009; 15: 6619-6629.

Sharma V, Dixit D, Koul N, Mehta VS, Sen E. Ras regulates interleukin-1beta-induced HIF-1alpha transcriptional activity in glioblastoma. J Mol Med 2010.

Sharouni SY, Kal HB, Batterman JJ, and Schramel FMNH. Sequential *Versus* Concurrent Chemo-radiotherapy in Inoperable Stage III Non-small Cell Lung Cancer. Anticancer Research 2006 26: 495-506

Simpson-Herren L, Wheeler GP. Howard Earle Skipper: in memoriam (1915-2006). Cancer Res 2006; 66: 12035-12036.

Sizemore N, Cox AD, Barnard JA, Oldham SM, Reynolds ER, Der CJ, Coffey RJ. Pharmacological inhibition of Rastransformed epithelial cell growth is linked to down-regulation of epidermal growth factor-related peptides. Gastroenterology 1999 117: 567 – 576.

Skipper HE. Thoughts on cancer chemotherapy and combination modality therapy (1974). Jama 1974; 230: 1033-1035.

Sklar MD. The ras oncogenes increase the intrinsic resistance of NIH 3T3 cells to ionizing radiation. Science 1988; 239: 645–7.

Sonveaux P, Kaz AM, Snyder SA, Richardson RA, Cardenas-Navia LI, Braun RD, Pawloski JR, Tozer GM, Bonaventura J, McMahon TJ, Stamler JS, Dewhirst MW. Oxygen regulation of tumor perfusion by S-nitrosohemoglobin reveals a pressor activity of nitric oxide. Circ Res 2005; 96: 1119-1126.

Srinivas V, Zhang LP, Zhu XH, and Caro J (1999) Characterization of an oxygen/ redox-dependent degradation domain of hypoxia-inducible factor alpha (HIFalpha) proteins. Biochem Biophys Res Commun 260**:**557–561.

Steel G (1997) (ed.) *The role of radiotherapy in the management of cancer*. Edward Arnold London

Steinhausen M, Hill E, Parekh N. Intravital microscopical studies of the tubular urine flow in the conscious rat. Pflügers Archiv European Journal of Physiology 1976; 362: 261-264.

Stylianopoulos T, Poh MZ, Insin N, Bawendi MG, Fukumura D, Munn LL, Jain RK. Diffusion of particles in the extracellular matrix: the effect of repulsive electrostatic interactions. Biophys J 2010; 99: 1342-1349.

Su, J.L., Yang, P.C., Shih, J.Y., Yang, C.Y., Wei, L.H., Hsieh, C.Y., Chou, C.H., Jeng, Y.M., Wang, M.Y., Chang, K.J. The VEGF-C/Flt-4 axis promotes invasion and metastasis of cancer cells. Cancer Cell 9(2006), 209–223.

Szabó C, Dawson VL Role of poly (ADP-ribose) synthetase activation in inflammation and reperfusion injury. Trends Pharmacol Sci 1998a. 19: 287-298.

Tang N, Du G, Wang N, Liu C, Hang H, Liang W. Improving penetration in tumors with nanoassemblies of phospholipids and doxorubicin. J Natl Cancer Inst 2007; 99:1004–15.

Tannock IF. Oxygen diffusion and the distribution of cellular radiosensitivity in tumours. Br J Radiol 1972; 45: 515-524.

Tannock IF, Lee CM, Tunggal JK, Cowan DS, Egorin MJ. Limited penetration of anticancer drugs through tumor tissue: a potential cause of resistance of solid tumors to chemotherapy. Clin Cancer Res 2002; 8: 878-884.

Teicher BA. Malignant cells, directors of the malignant process: role of transforming growth factor-beta. Cancer Metastasis Rev 2001; 20: 133-143.

Teicher BA, Herman TS, Menon K. Enhancement of fractionated radiation therapy by an experimental concentrated perflubron emulsion (Oxygent) in the Lewis lung carcinoma. Biomater Artif Cells Immobilization Biotechnol 1992; 20: 899-902.

Teicher BA, Holden SA, Ara G, Dupuis NP, Liu F, Yuan J, Ikebe M, Kakeji Y. Influence of an anti-angiogenic treatment on 9L gliosarcoma: oxygenation and response to cytotoxic therapy. Int J Cancer 1995; 61: 732-737.

Teicher BA A systems approach to cancer therapy. (1996). (Antioncogenics + standard cytotoxics—mechanism(s) of interaction). Cancer Metastasis Rev 15: 247-272

Teng LS, Jin KT, He KF, Wang HH, Cao J, Yu, DC. Advances in combination of antiangiogenic agents targeting VEGF-binding and conventional chemotherapy and radiation for cancer treatment. .J Chin Med Assoc. 2010 Jun; 73(6):281-8.

Tentori L, Portarena I, and Graziani G. Potential clinical applications of poly (ADP-ribose) polymerase (PARP) inhibitors. Pharmacol Res 2002 45:73–85.

Thomlinson RH. Tumour anoxia and the response to radiation. Sci Basis Med Annu Rev 1965: 74-90.

Tian, H., McKnight, S.L., Russell, D.W., 1997. Endothelial PAS domain protein I (EPAS1), a transcription factor selectively expressed in endothelial
cells. Genes Dev. 11, 72_82.

Tillmanns H, Ikeda S, Hansen H, Sarma JS, Fauvel JM, Bing RJ. Microcirculation in the ventricle of the dog and turtle. Circ Res 1974; 34: 561-569.

Tillmanns H, Steinhausen M, Leinberger H, Thederan H, Kubler W. Pressure measurements in the terminal vascular bed of the epimyocardium of rats and cats. Circ Res 1981; 49: 1202-1211.

Tong RT, Boucher Y, Kozin SV, et al: Vascular normalization by vascular endothelial growth factor receptor 2 blockade induces a pressure gradient across the vasculature and improves drug penetration in tumors. Cancer Res 2004 64:3731-3736.

Toulany M, Dittmann K, Baumann M, Rodemann HP. 2005a. Radiosensitization of Ras-mutated human tumor cells in vitro by the specific EGF receptor antagonist BIBX1382BS. Radiotherapy & Oncology 74:117 – 129.

Toulany M, Dittmann K, Kruger M, Baumann M, Rodemann HP. 2005b. Radioresistance of K-Ras mutated human tumor cells is mediated through EGFR-dependent activation of PI3K-AKT pathway. Radiotherapy & Oncology 76:143 – 150.

Toulany M, Kasten-Pisula U, Brammer I, Wang S, Chen J, Dittmann K, Baumann M, Dikomey E, RodemannHP. 2006. Blockage of epidermal growth factor receptorphosphatidylinositol 3-kinase-AKT signalling increases radiosensitivity of K-RAS mutated human tumor cells in vitro by affecting DNA repair. Clinical Cancer Research 12: 4119 –4126.

Toulany M, Baumann M, Rodemann HP. 2007. Stimulated PI3K-AKT signalling mediated through ligand or radiationinduced EGFR depends indirectly, but not directly, on constitutive K-Ras activity. Molecular Cancer Research 5:863 – 872.

Tozer GM, Ameer-Beg SM, Baker J, Barber PR, Hill SA, Hodgkiss RJ, Locke R, Prise VE, Wilson I, Vojnovic B. Intravital imaging of tumour vascular networks using multi-photon fluorescence microscopy. Adv Drug Deliv Rev 2005; 57: 135-152.

Tozer GM, Kanthou C, Baguley BC. Disrupting tumour blood vessels. Nat Rev Cancer 2005; 5: 423-435.

Tozer GM, Kanthou C, Lewis G, Prise VE, Vojnovic B, Hill SA. Tumour vascular disrupting agents: combating treatment resistance. Br J Radiol 2008; 81 Spec No 1: S12-20.

Tozer GM, Kanthou C, Parkins CS, Hill SA. The biology of the combretastatins as tumour vascular targeting agents. Int J Exp Pathol 2002; 83: 21-38.

Tunggal JK, Cowan DS, Shaikh H, Tannock IF. Penetration of anticancer drugs through solid tissue: a factor that limits the effectiveness of chemotherapy for solid tumors. Clin Cancer Res 1999; 5: 1583-1586.

Tzekova V, Cebotaru C, Ciuleanu TE, Damjanov D, Ganchev V, Kanarev V, Stella PJ, Sanders N, Pover G, Hainsworth JD: Efficacy and safety of AZD6244 (ARRY-142886) as second/third-line treatment of patients (pts) with advanced non-small cell lung cancer (NSCLC). J Clin Oncol (abstract) 2008, 26:8029.

Ueno M, Ban S, Nakanoma T, Tsukamoto T, Nonaka S, Hirata R, Iida M, Deguchi N. Hypercalcemia in a patient with renal cell carcinoma producing parathyroid hormone-related protein and interleukin-6. Int J Urol 2000; 7: 239-242.

Underhill C, Toulmonde1M, Bonnefoi H. A review of PARP inhibitors: from bench to bedside. Annals of Oncology 2011: 22: 268–279.
Unterberg A, Wahl M, Baethmann A. Effects of bradykinin on permeability and diameter of pial vessels in vivo. J Cereb Blood Flow Metab 1984; 4: 574-585.

Van Trappen PO, Steele D, Lowe DG, Baithun S, Beasley N, Thiele W, Weich H, Krishnan J, Shepherd JH, Pepper MS, Jackson DG, Sleeman JP, Jacobs IJ. Expression of vascular endothelial growth factor (VEGF)-C and VEGF-D, and their receptor VEGFR-3, during different stages of cervical carcinogenesis. J Pathol.( 2003); 201:544–554

Vajkoczy P, Menger MD, Simpson E, Messmer K. Angiogenesis and vascularization of murine pancreatic islet isografts. Transplantation 1995; 60: 123-127.

Vajkoczy P, Schilling L, Ullrich A, Schmiedek P, Menger MD. Characterization of angiogenesis and microcirculation of high-grade glioma: an intravital multifluorescence microscopic approach in the athymic nude mouse. J Cereb Blood Flow Metab 1998; 18: 510-520.

Vaupel P. Hypoxia and aggressive tumor phenotype: implications for therapy and prognosis. Oncologist 2008; 13 Suppl 3: 21-26.

Venkitaraman AR. Targeting the molecular defect in BRCA-deficient tumors for cancer therapy. Cancer cell (2009), 16, No. 2; 89-9

Wachsberger P, Burd R, Dicker AP. Tumor response to ionizing radiation combined with antiangiogenesis or vascular targeting agents: exploring mechanisms of interaction. Clin Cancer Res 2003; 9: 1957-1971.

Wang X, Ohnishi K, Takahashi A, Ohnishi T. Poly ADP-ribosylation is required for p53-dependent signal transduction induced by radiation. Oncogene 1998, 17, 2819-2825.

Warbey VS, Ferner RE, Dunn JT, Calonje E, O'Doherty MJ. [18F]FDG PET/CT in the diagnosis of malignant peripheral nerve sheath tumours in neurofibromatosis type-1. Eur J Nucl Med Mol Imaging 2009; 36: 751-757.

Warren BS, P. The growth of the blood supply to melanoma transplants in the hamster cheek pouch. Laboratory Investigations 1966; 15.

Wedge SR, Kendrew J, Hennequin LF, Valentine PJ, Barry ST, Brave SR, Smith NR, James NH, Dukes M, Curwen JO, Chester R, Jackson JA, Boffey SJ, Kilburn LL, Barnett S, Richmond GH, Wadsworth PF, Walker M, Bigley AL, Taylor ST, Cooper L, Beck S, Jurgensmeier JM, Ogilvie DJ. AZD2171: a highly potent, orally bioavailable, vascular endothelial growth factor receptor-2 tyrosine kinase inhibitor for the treatment of cancer. Cancer Res 2005; 65: 4389-4400.

Weidner N. New paradigm for vessel intravasation by tumor cells. Am J Pathol 2002; 160: 1937-1939.

Wildiers H, Guetens G, De Boeck G, Verbeken E, Landuyt E, Landuyt W, de Bruijn EA and van Oosterom, AT. Effect of antivascular endothelial growth factor treatment on the intratumoral uptake of CPT-11. Br J Cancer 88(2003): 1979-1986.

Willett CG, Boucher Y, di Tomaso E, Duda DG, Munn LL, et al. Direct evidence that the VEGF-specific antibody bevacizumab has antivascular effects in human rectal cancer. Nat Med 10 (2004): 145–147

Williams KJ, Telfer BA, Airley RE, Peters HP, Sheridan MR, van der Kogel AJ, Harris AL, Stratford IJ. A protective role for HIF-1 in response to redox manipulation and glucose deprivation: implications for tumorigenesis. Oncogene 2002; 21: 282-290.

Williams, K. J., B. A. Telfer, et al. "ZD6474, a potent inhibitor of vascular endothelial growth factor signalling, combined with radiotherapy: schedule-dependent enhancement of antitumor activity." Clin Cancer Res 2004: 10(24): 8587-8593.

Williams KJ, Telfer BA, Shannon AM, Babur M, Stratford IJ, Wedge SR. Combining radiotherapy with AZD2171, a potent inhibitor of vascular endothelial growth factor signalling: pathophysiologic effects and therapeutic benefit. Mol Cancer Ther 2007; 6: 599-606.

Williams KJ, Telfer BA, Shannon AM, Babur M, Stratford IJ, Wedge SR. Inhibition of vascular endothelial growth factor signalling using cediranib (RECENTIN; AZD2171) enhances radiation response and causes substantial physiological changes in lung tumour xenografts. Br J Radiol 2008; 81 Spec No 1: S21-27.

Williams KJ, Telfer BA, Stratford IJ, Wedge SR. ZD1839 ('Iressa'), a specific oral epidermal growth factor receptor-tyrosine kinase inhibitor, potentiates radiotherapy in a human colorectal cancer xenograft model. Br J Cancer 2002; 86: 1157-1161.

Williams KJ, Telfer BA, Xenaki D, Sheridan MR, Desbaillets I, Peters HJ, Honess D, Harris AL, Dachs GU, van der Kogel A, Stratford IJ. Enhanced response to radiotherapy in tumours deficient in the function of hypoxia-inducible factor-1. Radiother Oncol 2005; 75: 89-98.

Willis R. Pathology of Tumours. London: Butterworth & Co 1976.

Winkler F, Kozin SV, Tong RT, et al: Kinetics of vascular normalization by VEGFR2 blockade governs tumor response to radiation. Cancer Cell (2004) 6:553-563.

Witte D, Thomas A, Ali N, Carlson N, Younes M. Expression of the vascular endothelial growth factor receptor-3 (VEGFR-3) and its ligand VEGF-C in human colorectal adenocarcinoma. Anticancer Res. 2002; 22:1463–1466

Wong CM, Chun AC, Kok KH, Zhou Y, Fung PC, Kung HF, Jeang KT, Jin DY. Characterization of human and mouse peroxiredoxin IV: evidence for inhibition by Prx-IV of epidermal growth factor- and p53-induced reactive oxygen species. Antioxid Redox Signal 2000; 2: 507-518.

Wong HK, Lahdenranta J, Kamoun WS, Chan AW, McClatchey AI, Plotkin SR, Jain RK, di Tomaso E. Anti-vascular endothelial growth factor therapies as a novel therapeutic approach to treating neurofibromatosis-related tumors. Cancer Res 70: 3483–3493, 2010.

Workman P, Aboagye EO, Balkwill F, Balmain A, Bruder G, Chaplin DJ, Double JA, Everitt J, Farningham DA, Glennie MJ, Kelland LR, Robinson V, Stratford IJ, Tozer GM, Watson S, Wedge SR, Eccles SA. Guidelines for the welfare and use of animals in cancer research. Br J Cancer 2010; 102: 1555-1577.

Wouters, B.G. & Brown, J.M. (1997). Cells at intermediate oxygen levels can be more important than the "hypoxic fraction" in determining tumor response to fractionated radiotherapy. *Radiat Res*, **147,** 541-50.

Xu K, Tang B, Huang H, Yang G, Chen Z, Li P, An L. Strong red fluorescent probes suitable for detecting hydrogen peroxide generated by mice peritoneal macrophages. Chem Commun (Camb) 2005: 5974-5976.

Yamaguchi N, Anand-Apte B, Lee, M, Sasaki T, Fukai N, Shapiro R, Que I, Lowik C, Timpl R, and Olsen BR. Endostatin inhibits VEGF-induced endothelial cell migration and tumor growth independently of zinc binding. EMBO J., 18: 4414–4423, 1999.

Yang JC, Haworth L, Sherry RM, et al. A randomized trial of bevacizumab, an anti–vascular endothelial growth factor antibody, for metastatic renal cancer. N Engl J Med. 2003 349:427–34.

Yang L, Li Y. Quantum dots as fluorescent labels for quantitative detection of Salmonella typhimurium in chicken carcass wash water. J Food Prot 2005; 68: 1241-1245.

Yang M, Baranov E, Jiang P, Sun FX, Li XM, Li L, Hasegawa S, Bouvet M, Al-Tuwaijri M, Chishima T, Shimada H, Moossa AR, Penman S, Hoffman RM. Whole-body optical imaging of green fluorescent protein-expressing tumors and metastases. Proc Natl Acad Sci U S A 2000; 97: 1206-1211.

Yeo EJ, Chun YS, Park JW. New anticancer strategies targeting HIF-1. Biochem Pharmacol 2004; 68: 1061-1069.

Yewalkar N, Deore V, Padgaonkar A, Manohar S, Sahu B, Kumar P, Jalota-Badhwar A, Joshi KS, Sharma S, Kumar S. Development of novel inhibitors targeting HIF-1alpha towards anticancer drug discovery. Bioorg Med Chem Lett 2010; 20: 6426-6429.

Yoon S, Seger R. The extracellular signal-regulated kinase: multiple substrates regulate diverse cellular functions. Growth Factors 2006; 24:21–44.

Yuan F, Chen Y, Dellian M, Safabakhsh N, Ferrara N and Jain RK. Time-dependent vascular regression and permeability changes in established human tumor xenografts induced by an anti-vascular endothelial growth factor/vascular permeability factor antibody, Proc. Natl. Acad. Sci. (1996), USA 93**,** 14765–14770.

Zhou Q, Guo P, Gallo JM. Impact of angiogenesis inhibition by sunitinib on tumor distribution of temozolomide. Clin Cancer Res 14: 1540–1549, 2008.

Zhou Q, Gallo JM. Differential effect of sunitinib on the distribution of temozolomide in an orthotopic glioma model. Neuro-Oncology 11: 301–310, 2009.

Zips D, Eicheler W, Geyer P, Hessel F, Dorfler A, Thames HD, et al. Enhanced susceptibility of irradiated tumour vessels to vascular endothelial growth factor receptor tyrosine kinase inhibition. Cancer Res 2005; 65:5374–9.

Zheng A, Shan D, Wang B. A Redox-Sensitive Resin Linker for the Solid Phase Synthesis of C-Terminal Modified Peptides. J Org Chem 1999; 64: 156-161.

Znati CA, Rosenstein M, Boucher Y, Epperly MW, Bloomer WD, Jain RK. Effect of radiation on interstitial fluid pressure and oxygenation in a human tumor xenograft. Cancer Res 1996; 56: 964-968.

Znati CA, Rosenstein M, McKee TD, Brown E, Turner D, Bloomer WD, Watkins S, Jain RK, Boucher Y. Irradiation reduces interstitial fluid transport and increases the collagen content in tumors. Clin Cancer Res 2003; 9: 5508-5513.

## APPENDIX 1 AUTHOR ASSOCIATED PUBLISHED PAPERS.

Ali M, Telfer BA, McCrudden C, O'Rourke M, Thomas HD, Kamjoo M, Kyle S, Robson T, Shaw C, Hirst DG, Curtin NJ, Williams KJ. Vasoactivity of AG014699, a clinically active small molecule inhibitor of poly (ADP-ribose) polymerase: a contributory factor to chemopotentiation in vivo? Clin Cancer Res 2009; 15: 6106-6112.

Chinje EC, Williams KJ, Telfer BA, Wood PJ, van der Kogel AJ, Stratford IJ. 17beta-Oestradiol treatment modulates nitric oxide synthase activity in MDA231 tumour with implications on growth and radiation response. Br J Cancer 2002; 86: 136-142.

Cowen RL, Patterson AV, Telfer BA, Airley RE, Hobbs S, Phillips RM, Jaffar M, Stratford IJ, Williams KJ. Viral delivery of P450 reductase recapitulates the ability of constitutive overexpression of reductase enzymes to potentiate the activity of mitomycin C in human breast cancer xenografts. Mol Cancer Ther 2003; 2: 901-909.

Cowen RL, Williams KJ, Chinje EC, Jaffar M, Sheppard FC, Telfer BA, Wind NS, Stratford IJ. Hypoxia targeted gene therapy to increase the efficacy of tirapazamine as an adjuvant to radiotherapy: reversing tumor radioresistance and effecting cure. Cancer Res 2004; 64: 1396-1402.

de Caestecker MP, Bottomley M, Telfer BA, Hutchinson IV, Vose BM, Ballardie FW. Detection of abnormal peripheral blood mononuclear cell cytokine networks in human IgA nephropathy. Kidney Int 1993; 44: 1298-1308.

de Caestecker MP, Telfer BA, Hutchinson IV, Ballardie FW. The detection of intracytoplasmic interleukin-1 alpha, interleukin-1 beta and tumour necrosis factor alpha expression in human monocytes using two colour immunofluorescence flow cytometry. J Immunol Methods 1992; 154: 11-20.

Friswell MK, Gika H, Stratford IJ, Theodoridis G, Telfer B, Wilson ID, McBain AJ. Site and strain-specific variation in gut microbiota profiles and metabolism in experimental mice. PLoS One 2010; 5: e8584.

Lunt SJ, Cawthorne C, Ali M, Telfer BA, Babur M, Smigova A, Julyan PJ, Price PM, Stratford IJ, Bloomer WD, Papadopoulou MV, Williams KJ. The hypoxia-selective cytotoxin NLCQ-1 (NSC 709257) controls metastatic disease when used as an adjuvant to radiotherapy. Br J Cancer 2010; 103: 201-208.

Lunt SJ, Telfer BA, Fitzmaurice RJ, Stratford IJ, Williams KJ. Tirapazamine administered as a neoadjuvant to radiotherapy reduces metastatic dissemination. Clin Cancer Res 2005; 11: 4212-4216.

Matzow T, Cowen RL, Williams KJ, Telfer BA, Flint PJ, Southgate TD, Saunders MP. Hypoxia-targeted over-expression of carboxylesterase as a means of increasing tumour sensitivity to irinotecan (CPT-11). J Gene Med 2007; 9: 244-252.

Patterson AV, Williams KJ, Cowen RL, Jaffar M, Telfer BA, Saunders M, Airley R, Honess D, van der Kogel AJ, Wolf CR, Stratford IJ. Oxygen-sensitive enzyme-prodrug gene therapy for the eradication of radiation-resistant solid tumours. Gene Ther 2002; 9: 946-954.

Reinoso RF, Telfer BA, Brennan BS, Rowland M. Uptake of teicoplanin by isolated rat hepatocytes: comparison with in vivo hepatic distribution. Drug Metab Dispos 2001; 29: 453-459.

Reinoso RF, Telfer BA, Rowland M. Tissue water content in rats measured by desiccation. J Pharmacol Toxicol Methods 1997; 38: 87-92.

Reinoso RF, Telfer BA, Rowland M. In vitro studies of teicoplanin binding to rat tissues and erythrocytes. Eur J Pharm Sci 1998; 6: 145-152.

Reinoso RF, Telfer BA, Rowland M. Use of a single-pass in situ perfused rat hindlimb to study tissue distribution kinetics. Method development and experiences with Evans blue. J Pharmacol Toxicol Methods 2000; 43: 191-198.

Rice L, Waters CE, Eccles J, Garside H, Sommer P, Kay P, Blackhall FH, Zeef L, Telfer B, Stratford I, Clarke R, Singh D, Stevens A, White A, Ray DW. Identification and functional analysis of SKA2 interaction with the glucocorticoid receptor. J Endocrinol 2008; 198: 499-509.

Shannon AM, Telfer BA, Smith PD, Babur M, Logie A, Wilkinson RW, Debray C, Stratford IJ, Williams KJ, Wedge SR. The mitogen-activated protein/extracellular signal-regulated kinase kinase 1/2 inhibitor AZD6244 (ARRY-142886) enhances the radiation responsiveness of lung and colorectal tumor xenografts. Clin Cancer Res 2009; 15: 6619-6629.

Sommer P, Cowen RL, Berry A, Cookson A, Telfer BA, Williams KJ, Stratford IJ, Kay P, White A, Ray DW. Glucocorticoid receptor over-expression promotes human small cell lung cancer apoptosis in vivo and thereby slows tumor growth. Endocr Relat Cancer 2010; 17: 203-213.

Williams KJ, Albertella MR, Fitzpatrick B, Loadman PM, Shnyder SD, Chinje EC, Telfer BA, Dunk CR, Harris PA, Stratford IJ. In vivo activation of the hypoxia-targeted cytotoxin AQ4N in human tumor xenografts. Mol Cancer Ther 2009; 8: 3266-3275.

Williams KJ, Telfer BA, Brave S, Kendrew J, Whittaker L, Stratford IJ, Wedge SR. ZD6474, a potent inhibitor of vascular endothelial growth factor signalling, combined with radiotherapy: schedule-dependent enhancement of antitumor activity. Clin Cancer Res 2004; 10: 8587-8593.

Williams KJ, Telfer BA, Shannon AM, Babur M, Stratford IJ, Wedge SR. Combining radiotherapy with AZD2171, a potent inhibitor of vascular endothelial growth factor signalling: pathophysiologic effects and therapeutic benefit. Mol Cancer Ther 2007; 6: 599-606.

Williams KJ, Telfer BA, Shannon AM, Babur M, Stratford IJ, Wedge SR. Inhibition of vascular endothelial growth factor signalling using cediranib (RECENTIN; AZD2171) enhances radiation response and causes substantial physiological changes in lung tumour xenografts. Br J Radiol 2008; 81 Spec No 1: S21-27.

Williams KJ, Telfer BA, Stratford IJ, Wedge SR. ZD1839 ('Iressa'), a specific oral epidermal growth factor receptor-tyrosine kinase inhibitor, potentiates radiotherapy in a human colorectal cancer xenograft model. Br J Cancer 2002; 86: 1157-1161.

Williams KJ, Telfer BA, Xenaki D, Sheridan MR, Desbaillets I, Peters HJ, Honess D, Harris AL, Dachs GU, van der Kogel A, Stratford IJ. Enhanced response to radiotherapy in tumours deficient in the function of hypoxia-inducible factor-1. Radiother Oncol 2005; 75: 89-98.

# APPENDIX II ORIGINAL PUBLISHED PAPERS RELEVANT TO THIS THESIS.